University of Alberta

Development and Applications of a Semi-analytical Approximate Thermal Simulator

by

Vahid Dehdari

A thesis submitted to the Faculty of Graduate Studies and Research
in partial fulfillment of requirements for degree of

Doctor of Philosophy

in

Mining Engineering

Department of Civil and Environmental Engineering

Spring 2014
Edmonton, Alberta

Abstract

Oil sand reservoirs play an important role in the economy of Canada due to their significant recoverable reserves. Due to the high viscosity of the oil in these reservoirs, conventional methods cannot be used for production. The steam-assisted gravity drainage (SAGD) method is an efficient way of producing oil from these reservoirs. Predicting oil production and steam injection rates is required for planning and managing a SAGD operation. This can be done by simulating the fluid flow with flow simulation codes, but this is very time consuming. The run time for a 3D heterogeneous model with one well pair can exceed 2 days. Another important task in SAGD operation is the optimization of the trajectory of the wells; the production forecasts for different well positions would require running the flow simulator multiple times, but that is too expensive. Yet another task is to quantify the uncertainty in steam requirements and bitumen production due to multiple realizations of the geological properties. Another task is to rank the multiple realizations from poor performing to good performing. This ranking could be used to help select a subset of realizations for more careful analysis. Finally, forecasting the location of the steam chamber at different time steps is a very important task for considering geomechanical effects. For these reasons, an approximate model that reasonably predicts oil production and steam injection rates with low computational effort would be valuable. In this dissertation, a reliable SAGD approximate simulator for predicting SAGD performance with 3D heterogeneous models of geologic properties is developed. This approximate simulator can handle different types of operating strategies. The approach is an approximate solution using a semi analytical model based on relevant theories including Butler's SAGD theory. The proxy is much faster than the full simulator and it gives accurate estimated oil production and steam injection rates at different time steps. Theoretical and numerical research has been undertaken to develop the proxy, implement it in fast code, demonstrate the accuracy of prediction and apply to realistic examples.

Acknowledgements

I would like to express my sincerest gratitude to Dr. Clayton V. Deutsch. He is the best advisor that anyone would ever wish for. I thank him for his brilliant ideas, for his tolerance, for his kindness and for all the time he spent with me. I admire his integrity, ingenuity and diligence as a researcher and as a person.

I wish to express my sincere appreciation and gratitude to Dr. Dean S. Oliver, Professor of the Center for Integrated Petroleum Research (CIPR) for his invaluable assistance, guidance, and support which built a strong base for my knowledge.

A special note of gratitude goes to the department of civil and environmental engineering staff, Alice Da Silva, Anne Jones, Arlene Figley, Lorraine Grahn and Trina Cattral, for their daily contribution is essential to the success of the student's school.

I thank ConocoPhillips for providing me an internship opportunity from which I gained deep insight to the theory and applications of SAGD approximate simulator. During my internship with ConocoPhillips, Jose Walter Vanegas was a wonderful mentor who taught me a great deal from introduction and industrial applications of advanced technologies developed in academia to things an engineer needs to know in operations.

I acknowledge the financial support of the member companies of the Center for Computational Geostatistics (CCG). Special gratitude is extended to Computer Modeling Group (CMG) for generously providing multiple STARS licenses.

Many thanks to my friends, Mahshid Babakhani, Ryan Barnett, Miguel Cuba, Maryam Hadavand, Mehdi Rezvandehy, Samaneh Sadeghi, Diogo Silva, Yevgeniy Zagayevskiy for their continuous support and encouragement to finish my doctoral studies. I would also like to thank them all for the splendid shared moments.

Special thanks to my parents and siblings, for all their prayers and words of encouragement. This dissertation is dedicated to my wife Nazanin for her companionship, understanding and unconditional love.

Table of Contents

List of Figures

List of Tables

List of Symbols

Symbol	Definition	First Use
T_s	Steam temperature	7
ξ	Distance	7
T_r	Reservoir temperature	7
q	Rate of oil drainage	7
k	Permeability	7
$\Delta\rho$	Difference between oil density and steam density	7
g	Earth's gravity	7
θ	Angle of element respect to horizontal direction	7
μ	Dynamic viscosity	7
ν	Kinematic viscosity	7
U	Velocity	7
α	Thermal diffusivity	7
m	Dimensionless parameter in Eq. 1.5, etc.	8
γ	Heat penetration depth	8
ϕ	Porosity	8
ΔS_o	Recoverable oil saturation	8
h	Height of reservoir	8
t	Time	10
Q	Cumulative oil	11
Q_{cp}	Cumulative heat to the steam chamber and produced oil	12
v_{ch}	Total chamber volume at time t	12
c_r	Rock compressibility	12

List of Abbreviations

Abbrv.	Definition	First Use
SAGD	Steam-assisted gravity drainage	1
DA	Drainage area	2
NPV	Net present value	2
NCB	Net continues bitumen	2
CSOR	Cumulative steam oil ratio	5
EVF	Effective volume factor	17
GIF	Geomechanical impact factor	19
SAP	Solvent-aided process	22
SSR	Solvent steam ratio	22
SOR	Steam oil ratio	22
OOIP	Original oil in place	23
F_{GC}	Fraction of globally connected cells	24
F_{LC}	Fraction of locally connected cells	24
CHV	Connected hydrocarbon volume	24
TOF	Time of flight	25
MCS	Monte Carlo simulation	26
ISOR	Instantaneous steam oil ratio	41
SQP	Sequential Quadratic Programming	43
DE	Differential Evolution	43
KKT	Karush-Kuhn-Tucker	44
WOR	Water oil ratio	50
VHC	Volumetric heat capacity	84

Chapter 1

Introduction

Canada has the third largest oil reserves in the world and 97% of these reserves are in the oil sands (Upstream Dialogue, 2012); oil sand reservoirs play an important role in the economy of Canada. Canada's oil sands are found in three main deposits – the Athabasca, Peace River and Cold Lake deposits in Alberta and Saskatchewan. The oil sands are at the surface near Fort McMurray but deeper underground in other areas. The current estimate of crude oil reserves is 170 billion barrels (Government of Alberta, 2011). Only 20% of these reserves are close to the surface and can be mined. More than 80% of these reserves are to be recovered by in-situ methods, but conventional production methods cannot be used for oil production due to the very high viscosity of the bitumen. For this reason, thermal recovery mechanisms such as cyclic steam injection or steam-assisted gravity drainage (SAGD) are being implemented as efficient ways of producing oil. SAGD is perhaps the most common method for producing heavy oil. In this method, two horizontal wells are drilled parallel to each other. The bottom well is the production well and it should be drilled close to the bottom of the reservoir because any oil below this well cannot be produced. The top well is the injection well and it is commonly drilled 5-10 meters above the production well so that the bitumen between these wells can be quickly recovered and so that heated bitumen will drain by gravity to this pressure sink. Steam from the injection well will rise upward and the heated bitumen will drain to the producer. The length of each well pair is often around 1 kilometer to permit efficient steam distribution and minimize the number of wells. The heating by injected steam and drainage of bitumen by gravity gives this approach its name. During steam assisted gravity drainage (SAGD), the steam chamber moves upwards during a rising period and then it will move horizontally during a spreading period

after the lighter steam reaches the impermeable top of the reservoir. Fig. 1.1 shows a schematic illustration of this process.

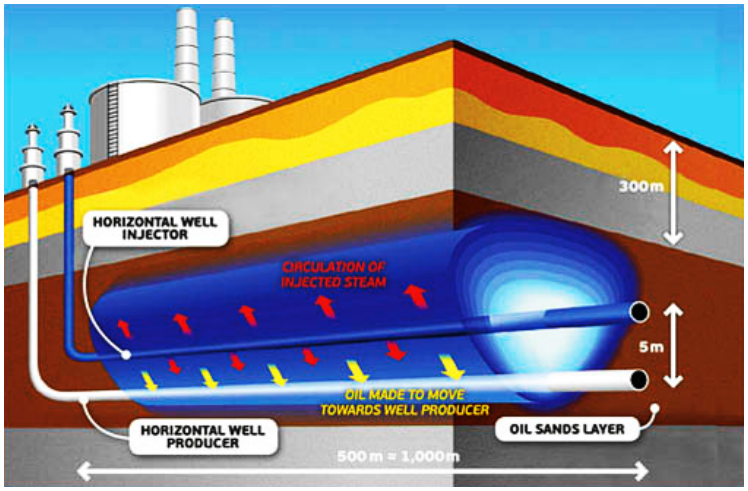

Figure 1.1: Development of steam chamber by injecting steam in SAGD process (source: www.ifpenergiesnouvelles.com)

Producible bitumen is found over leases or project development areas and its pay thickness may exceed 100 m (Energy Resources Conservation Board, 2012). Multiple drainage areas (DAs) each containing multiple well pairs are designed to develop areas. The number of wells per DA (based on the well spacing) depends on the geological properties of that DA and economic parameters; often, operators are drilling five to twenty well pairs that are separated approximately 100 m (Energy Resources Conservation Board, 2012). The ultimate goal is to maximize the net present value (NPV). A larger number of wells can produce more resources during early production, but the cost of drilling will be high. The optimal number of wells can be found by maximizing NPV that can be calculated if the production is forecast with a flow simulator. Fig. 1.2 shows the location of a surface pad and five wells on a DA. This figure also shows four different steps of producing bitumen. These steps are steam injection, heating bitumen, moving bitumen downward due to the gravity drainage and separating oil and produced water at the surface.

All well pairs in a drainage area are tied to the same surface facility. Fig. 1.3 shows some DAs over areas that contain significant resources, that is, a high amount of net continuous bitumen (NCB).

The location of the surface pads for each DA depends on the location of roads, rivers, lakes, swamps and other surface features. The geological properties and

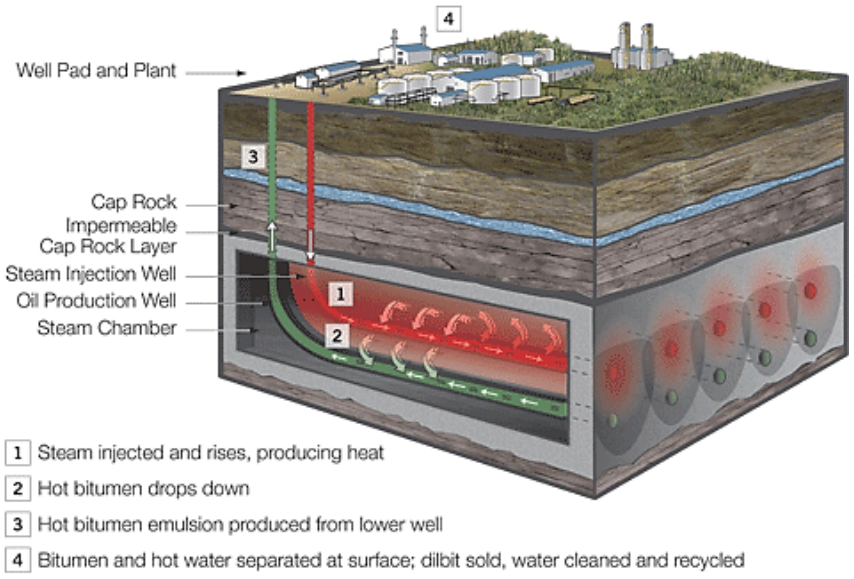

Figure 1.2: Location of surface pad and different wells on a DA (source: www.connacheroil.com)

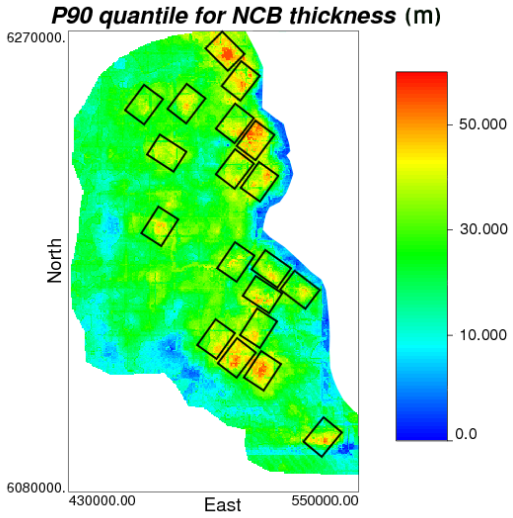

Figure 1.3: DAs location in a field. The East and North coordinates have the units of meters. The units of the color bar are meters of reservoir thickness (Dehdari, 2011).

the interaction between steam chambers of different DAs are also considered for selecting the location of surface pads. Based on pressure differences and steam chamber interaction between different DAs, the sequence and location of drilling the wells could be changed. Differential pressure between adjacent wells should be minimized to avoid steam loss due to the pressure difference. For example, it is undesirable to have new wells immediately adjacent to a depleted steam chamber with low pressure. The starting time of steam injection in adjacent DAs should be optimized to minimize this pressure difference.

Companies want to optimize the number of DAs, their locations, the surface pad locations, well spacing, detailed well trajectories and other operating parameters such as the injected steam pressure.

The conventional approach for developing these reservoirs is based on collecting geological and geophysical data by drilling exploratory wells, then building 3D reservoir models using geostatistical methods and after that running flow simulations on selected realizations to establish a robust reservoir management plan. Considering uncertainty in the flow simulator is very time consuming due to simulation run time. Usually a chosen P50 (or median) model is used for sensitivity studies and optimization with the flow simulator. Yet, the optimization of DA locations, well spacing, and operating conditions should consider the geological uncertainty represented by multiple geological models to be truly robust and optimal.

Regarding heterogeneity and uncertainty, usually there are shale barriers at different positions in these reservoirs. Steam cannot pass a thick shale barrier. Also, if there is a shale barrier between the injector and producer wells, oil cannot drain to the producer. For these reasons, optimizing the injector and producer well trajectory is important. Robust well spacing and well placement optimization should be done by considering uncertainty in the reservoir properties. Running different models with trajectories chosen by trial and error is very time consuming and it is unlikely that optimal locations would be found. A proxy model that can approximately predict flow would be a useful supplement for commercial flow simulators in some situations. A proxy would implement simplified flow equations or analytical solutions. Such a proxy based on computing the time dependent analytical equations can be calibrated for reliable prediction from heterogeneous reservoir models with realistic operating conditions.

In this dissertation, a numerical implementation of Butler theory (Butler, 1987a,

1991) has been used for quickly predicting SAGD performance.

Butler's theory is based on computing the steam interface location and oil production rate at different time steps. This method applies to 2D sections. For considering 3D models, the interaction between different slices will be neglected, and the amount of oil production and steam injection can be summed together for the cumulative oil production and steam injection. Fig. 1.4 shows how Butler's model could be used to convert a 3D model to different 2D sections. The left side of Fig. 1.4 shows a 3D section of a SAGD model that shows location of producer on the left with a red line. Black arrows show the direction of steam chamber rise on 2D sections. The blue surfaces show the bottom and top of the reservoir. The right side of this figure shows the spreading of the steam chamber on one 2D section. The orange circle shows the location of the producer. The blue lines on each side show the location of steam interface at different time steps.

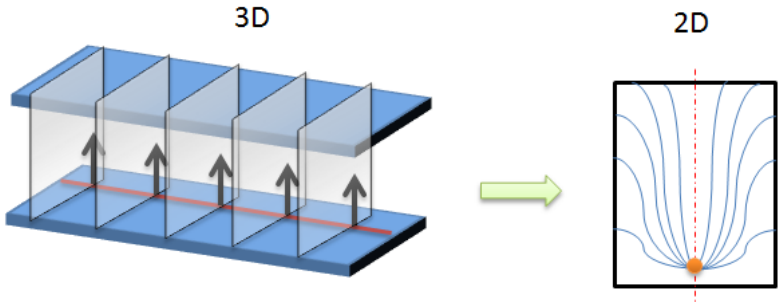

Figure 1.4: 3D section of a SAGD model in Butler theory. Red line in the left shows producer trajectory. Well direction assumed to be from left to right. Distance between completions is about 25 m. Pay zone is between two blue plates and height of pay zone is about 70 m. Black arrows show direction of steam chamber rising from different completions along 2D sections. Orange circle on the right shows the location of producer completion and blue curves show the locations of steam interface at different time steps.

Butler's model assumes three different periods for producing oil: a rising period, a spreading period and a confinement period. During the rising period, steam moves toward the top of the reservoir and after contacting the impermeable top of the reservoir, the steam starts spreading laterally. After reaching the reservoir boundary or the adjacent well pair, it moves downward through the reservoir.

Butler developed a method for predicting the amount of steam required and as a result the cumulative steam oil ratio (CSOR). The CSOR is considered to be an

important parameter in SAGD performance assessment. It is the ratio of cumulative injected steam to the cumulative produced oil. An estimate of the CSOR can be calculated by calculating the total heat losses to the reservoir, overburden, steam chamber and produced oil. This provides the volume of steam injected.

Butler's theory for estimating the amount of oil production and steam injection is approximate and the final cumulative oil production or steam injection using this model can be up to 150% different than simulator results due to ignoring heterogeneity or steam injection constraints. Fig. 1.5 shows a comparison between cumulative oil production and cumulative steam injection of predicted by the original Butler theory and from a full physics flow simulator for a 2D heterogeneous model. Depending on the operating strategies of the simulation model, larger differences between results can be observed. For this reason, an optimized modified formalism is required for improved accuracy.

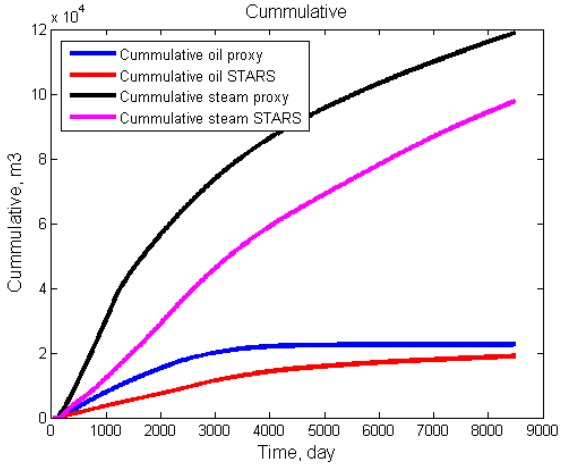

Figure 1.5: Comparison between results of Butler model and simulator (STARS) for a 2D heterogeneous model. Notice the large difference.

1.1 Butler's Original Theory for Forecasting Oil Production Rate

The model assumes vertical continuity between the producing well and the overburden. As a result, the steam chamber will contact the top of the reservoir immediately. Then, the steam chamber spreads sideways until reaching lateral confinement. Finally, after confinement, the steam front moves downward (Butler, 1987a, 1991). Using this theory, the steam interface could be divided into different smaller seg-

ments. Then, the location, heat penetration rate and also the oil production from each segment can be computed at each time step. The Darcy equation could be applied on a small segment of the interface as is shown in Fig. 1.6. This segment has steam temperature of T_s and at the distance ξ temperature is equal to the reservoir temperature which is T_r.

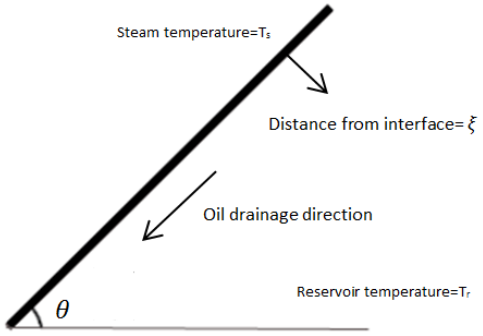

Figure 1.6: Small vertical section through interface

Based on Darcy's law, the flow within an element with width of $d\xi$ can be written as Eq. 1.1:

$$dq_o = \frac{k\Delta\rho g \sin\theta}{\mu} d\xi = \frac{kg\sin\theta}{\nu} d\xi \tag{1.1}$$

In this equation q_o is rate of oil drainage (m^3/s), g is earth's gravity $(9.81 m/s^2)$, k is permeability m^2, θ is angle of element respect to horizontal direction and ν is kinematic viscosity (m^2/s) which is dynamic viscosity μ $(Kg/(m.s))$ divided by $\Delta\rho$ which is difference between oil density and steam density (Kg/m^3). For unheated reservoir with temperature T_r, the corresponding equation is:

$$dq_r = \frac{kg\sin\theta}{\nu_r} d\xi \tag{1.2}$$

As a result, the difference between dq_o and dq_r can be written by dq. After integrating dq, Eq. 1.3 can be obtained:

$$q = kg\sin\theta \int_0^\infty \frac{d\xi}{\nu} = kg\sin\theta \int_0^\infty (\frac{1}{\nu} - \frac{1}{\nu_r}) d\xi. \tag{1.3}$$

Butler showed this integral can be computed by defining viscosity as a function of distance from interface. He obtained the following relation between temperature and distance from the interface:

$$\frac{T - T_r}{T_s - T_r} = \exp\frac{-U\xi}{\alpha} \tag{1.4}$$

In this equation U is velocity (m/s) and α is thermal diffusivity (m^3/s) and T_s is steam temperature. By differentiating Eq. 1.4, $d\xi$ can be obtained then we can write:

$$\int_0^{\infty}(\frac{1}{\nu}-\frac{1}{\nu_r})d\xi=\frac{\alpha}{U}\int_{T_r}^{T_s}(\frac{1}{\nu}-\frac{1}{\nu_r})\frac{dT}{T-T_r}=\frac{\alpha}{U}\frac{1}{m\nu_s} \tag{1.5}$$

where in Eq. 1.5, m is equal to the Eq. 1.6:

$$m=[\nu_s\int_{T_r}^{T_s}(\frac{1}{\nu}-\frac{1}{\nu_r})\frac{dT}{T-T_r}]^{-1} \tag{1.6}$$

The relationship between viscosity and the distance from the interface can be obtained from this temperature distribution. Butler showed that the following relation between viscosity and temperature is valid:

$$\frac{\nu_s}{\nu}=(\frac{T-T_r}{T_s-T_r})^m \tag{1.7}$$

The parameter m can be computed by solving Eq. 1.6 (Butler, 1987a). By combining Eq. 1.3 and Eq. 1.5 the oil drainage flow at a point on the interface as a function of velocity U and the angle θ can be obtained:

$$q=\frac{kg\alpha\sin\theta}{m\nu_s U}=\frac{\gamma kg\sin\theta}{m\nu_s} \tag{1.8}$$

In Eq. 1.8, γ is the heat penetration depth and it is equal to α/U for the steady state temperature distribution given by Eq. 1.4.

By combining Eq. 1.8 and a material balance equation, Eq. 1.9 for oil production rate can be obtained:

$$q=\sqrt{\frac{2\phi\Delta S_o kg\alpha h}{m\nu_s}} \tag{1.9}$$

In Eq. 1.9, ϕ is porosity, ΔS_o is recoverable oil saturation and h is height of reservoir. In this model, Butler assumed that the steam interface spreads horizontally to infinity and there is no confinement or no-flow boundary. Also, as seen in Fig. 1.7, the steam interfaces at different time steps do not start at the producing well.

Butler introduced the TANDRAIN model to connect the steam interface curves to the production wells and consider the effect of confinement (Fig. 1.8). Based on this model, he changed factor 2 in Eq. 1.9 with 1.5:

$$q=\sqrt{\frac{1.5\phi\Delta S_o kg\alpha h}{m\nu_s}} \tag{1.10}$$

For finding the steam interface location, the initial steam interface should be discretized by different segments above the well. By changing time, the steam

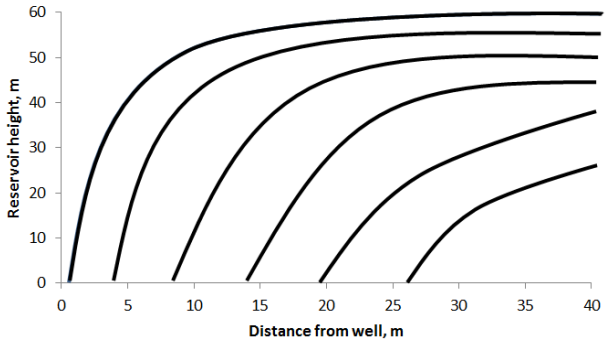

Figure 1.7: Interface curves using original theory

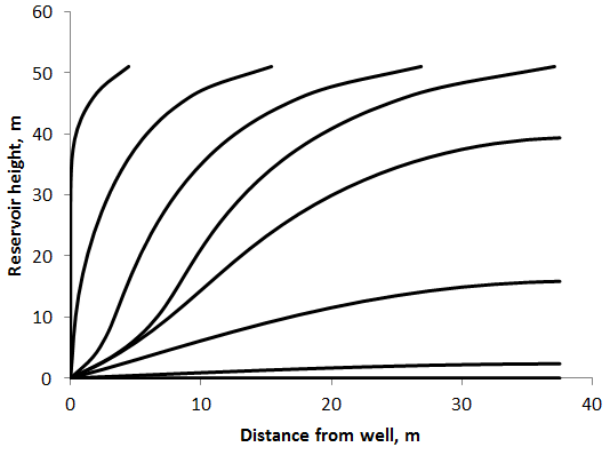

Figure 1.8: Interface curves using TANDRAIN theory

interface location can be obtained from the material balance equation assuming that the average flow of oil depleting the top section is equal to the flow calculated for each top element. Butler showed that Eq. 1.11 can be used for finding the interface location before confinement:

$$(\frac{\partial x}{\partial t}) = \frac{-(\frac{\partial q}{\partial y})}{\phi \Delta S_o} \tag{1.11}$$

Also, he showed that when the reservoir is not infinite, that is, there is coalescence (contacting steam chambers of adjacent wells) or a reservoir boundary, the steam interface direction should be changed and it moves downward when it reaches the boundary. In this case, the x location of each segment of the steam interface is the same as before but the y location can be obtained from Eq. 1.12.

$$(\frac{\partial y}{\partial t}) = \frac{(\frac{\partial q}{\partial x})}{\phi \Delta S_o} \tag{1.12}$$

As a result, when adjacent wells exist, half of the spacing between them can be considered as the location of a no-flow boundary.

Butler obtained a rate of heat accumulation ahead of the interface by writing the differential heat equation and considering conduction and the heat that is left behind the interface. Then, if the temperature gradient varies linearly, the heat penetration rate can be obtained using Eq. 1.13:

$$\frac{d\gamma}{dt} = \frac{2}{\pi}(\frac{\alpha}{\gamma} - U) \tag{1.13}$$

In this equation, α is thermal diffusivity (m^2/d) and γ is the heat penetration (m).

Assuming a fracture above the well, that is, a continuous instantaneous connection to the top of the reservoir is not realistic. For these reasons, Butler proposed another period called the rising period (Butler, 1987b, 1991). The steam interface moves gradually to the top of the reservoir. The interface will spread sideways after contacting impermeable zones.

Butler assumed that the rising steam chamber is cone shaped with the center of the cone at the producer. Based on the observed shape of rising steam chambers from experimental data, the sides of this chamber are straight lines with an angle of 58° from the horizontal. Fig. 1.9 shows the shape of the steam chamber in Butler's model.

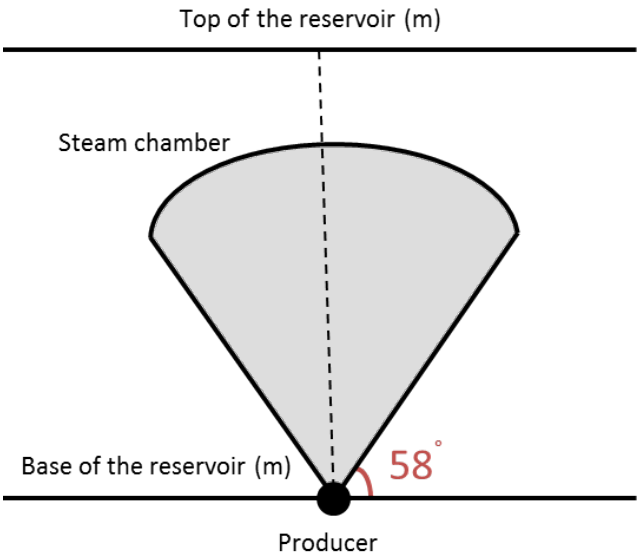

Figure 1.9: Cone shape Butler rising model with angle of 58 degree from the horizontal direction

He considered a homogeneous model and computed the amount of hydrocarbon volume in the chamber at differential time dt and set it equal to Eq. 1.10. Then by integrating the equation, the height of the steam chamber as a function of time can be obtained. By setting this height in the volumetric equation, an equation for computing the cumulative oil production at different time steps during the rising period can be obtained. Then, by differentiating this equation respect to time, the flow rate at different time steps for the rising period can be obtained. Eqs. 1.14–1.16 are for computing the height of the steam chamber, cumulative oil of rising chamber and flow rate of rising chamber at different times:

$$h = 2(\frac{kg\alpha}{m\nu_s\phi\Delta S_o})^{1/3}t^{2/3} \tag{1.14}$$

$$Q = 2.25(\frac{kg\alpha}{m\nu_s})^{2/3}(\phi\Delta S_o)^{1/3}t^{4/3} \tag{1.15}$$

$$q = 3(\frac{kg\alpha}{m\nu_s})^{2/3}(\phi\Delta S_o)^{1/3}t^{1/3} \tag{1.16}$$

To find the time of changing from rising to spreading, Butler (1991) proposed the time when the oil production rate versus recovery for both rising and spreading periods intersect. Fig. 1.10 shows this time. At this time, both rising and spreading rates, in addition to their cumulative productions are the same. As a result, the oil production profile would be continuous without any abrupt change.

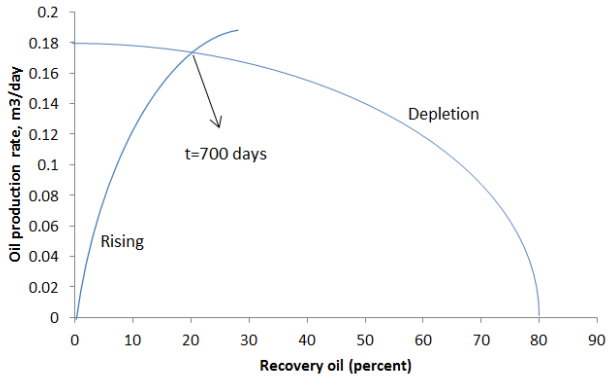

Figure 1.10: Finding the time for changing from rising to spreading period

1.2 Butler's Original Theory for Forecasting Steam Injection Rate

The amount of steam injection and the cumulative steam oil ratio (CSOR) are very important for assessing the efficiency of SAGD operations. Butler (1987b) introduced an approximate method for estimating steam injection rate at different time steps. He suggested that the cumulative steam injection can be computed from the total heat loss to different parts of the reservoir during steam injection. This heat loss can be converted to the total mass of injected steam using the steam latent heat. The total heat loss is computed as the sum of the following (Butler, 1991):

1. Cumulative heat to the steam chamber and produced oil from T_r to T_s:

$$Q_{cp} = v_{ch} c_r \rho_r (T_s - T_r) + Q c_o \rho_o (T_m - T_r) \tag{1.17}$$

2. Cumulative heat loss to over burden above the steam chamber:

$$Q_o = (4/3) k_{ob} (T_s - T_r) A \sqrt{t/\pi \alpha_{ob}} \tag{1.18}$$

3. Cumulative heat to the reservoir:

$$Q_r = w(\sum_{i=1}^{n} l_i \gamma_i)(T_s - T_r) \tag{1.19}$$

In these equations, v_{ch} is the total chamber volume at time t, $c_r \rho_r$ is the volumetric heat capacity of the chamber excluding drainage condensate and including residual oil and connate water saturation at the start of production, $c_o \rho_o$ is volumetric heat capacity of oil, Q is cumulative oil production at time t, T_m is mixing

temperature which is $T_r + (\frac{m}{m+1})(T_s - T_r)$, w is width of reservoir, k_{ob} and α_{ob} are thermal conductivity and thermal diffusivity of overburden, A is the area of hot zone at time t, l_i is the length of segment i and γ_i is heat penetration of segment i.

The total heat loss is calculated by combining these heat losses. The total mass of steam consumption at time t can also be calculated.

$$m_{\text{steam}} = \frac{\text{Total heat transferred}}{\text{Enthalpy of steam}} = \frac{Q_{cp} + Q_o + Q_r}{\lambda} \tag{1.20}$$

Finally, using the steam density, the cumulative steam injection (cold water equivalent) can be computed.

In Butler's model, the interaction between different 2D vertical slices will be ignored, and the amount of oil and steam production can be summed together for the cumulative oil production and steam injection. The following procedure can be used for finding the steam interface position and calculating the produced oil and injected steam volumes:

1. Assume a small non-zero value for γ set initial $\theta = 90^\circ$ and initialize steam interface position vertically above the producer.

2. Repeat this step for all time steps

   - Find oil rate q using Eq. 1.8 for spreading period
   - Find interface velocity from Eq. 1.11 before confinement or Eq. 1.12 after confinement
   - Find new steam interface position based on the velocity of each segment
   - Find new θ for each segment of steam interface
   - Find new γ from Eq. 1.13 for each segment
   - Compute total heat loss for finding steam injection rate
   - Find oil production rate using both rising and spreading periods equations (before transition) or only spreading period equation (after transitions)

3. Check for reaching transition time between rising and spreading periods

For each time step, steps 2-3 should be repeated for finding oil production and steam injection rates. Before the end of rising period, heat loss to the overburden is

zero, because steam is not connected to the top of the reservoir. But after finding transition time between rising and spreading periods, heat loss to the overburden should be computed using Eq. 1.18 and step 2 should be repeated for the next time step.

1.3 Review of Modifications to the Butler's Original Theory

Reis (1992) assumed an inverted triangular shape for the steam chamber. In his model, the temperature profile in the oil declines exponentially with increasing distance from the steam/oil interface, but unlike Butler's model, Reis assumed that the temperature decline is independent of interface position. As a result, he found a similar equation to the Butler Eq. 1.4:

$$\frac{T - T_r}{T_s - T_r} = \exp^{-aU\xi/\alpha} \tag{1.21}$$

The only difference between his equation and Butler's equation is related to the constant a. In this equation a is an empirical constant equal to 0.4.

As a result, he found the following equation for predicting the oil drainage rate:

$$q = \sqrt{\frac{\phi \Delta S_o k g \alpha h}{2am\nu_s}} \tag{1.22}$$

All parameters in Eq. 1.22 are defined above. He mentioned that experimental oil rates reported are slightly lower than what Butler's method predicts.

Also he obtained Eq. 1.23 for computing the steam oil ratio. This equation is obtained by dividing the total steam injection rate by the oil production rate. The total steam injection rate has been computed from an energy balance equation.

$$SOR = \frac{M_R \Delta T}{\rho_w L_s x_s \phi \Delta S_o}[1 + \frac{4\alpha t}{H^2 a} + \frac{4}{H}\sqrt{\frac{\alpha t}{\pi}}] \tag{1.23}$$

In Eq. 1.23, M_R is formation heat capacity, $\Delta T = T_s - T_r$ is difference between steam and reservoir temperatures, ρ_w is water density, L_s is latent heat of steam, x_s is steam quality, α is thermal diffusivity and H is the thickness of formation.

Akin (2005) developed a mathematical model for gravity drainage in heavy oil reservoirs during steam injection. His model was based on the inverted triangular shape of steam chamber which he observed in experimental experiments. In this model, he considered dependency of temperature and asphaltene on the viscosity of heavy oil. He showed that neither Butler's model nor Reis's model included the effect

of steam distillation and asphaltene deposition. Asphaltene deposition can decrease viscosity and as a result the production rate can be increased during asphaltene deposition. As a result, he developed the following equation for predicting the oil drainage rate:

$$q = \sqrt{\frac{\phi \Delta S_o k g h w_s}{2 m \nu_s}} \tag{1.24}$$

In this equation w_s is the steam zone half-width (m) and other parameters are similar to the Butler model.

By considering different examples he compared oil and steam rates to previous models. His results did not show any significant improvement relative to the other models. He simply assumed that a linear geometry can be assumed for the steam chamber instead of an s-shaped curve. Neither this model, nor Butler's model can estimate oil production and steam injection rates for heterogeneous cases.

Nukhaev et al. (2006) proposed a new analytical model for SAGD performance. They also modeled the initial stage of oil production before the steam chamber reaches the producer. Their model accounts for mass and heat transfer during the production and they found significant correlation between the production rate and the dynamics of steam chamber evolution. Based on these assumptions, they showed that the following equations can be used for predicting the oil production rate before the end of the rising period:

$$q_{po} = \frac{q_p - q_{p1}}{1 + \tau} \tag{1.25}$$

where q_{p1} is the minimum production rate during the rising period:

$$q_{p1} = \frac{c_1 \lambda \Delta T_o}{L \rho_w} \tag{1.26}$$

and c_1 is a constant equal to $4\sqrt{c^2 + 1}$ and c is model constant equal to 1.5.

Also, oil production during the spreading period can be computed using the following equation:

$$q_{po} = \frac{q_p - q_{p2}}{1 + \tau} \exp^{-\frac{t - t_f}{(1+\tau) t_\lambda}} \tag{1.27}$$

where q_{p2} is the minimum production rate during spreading period:

$$q_{p2} = \frac{4 c h_s \lambda \Delta T_o}{l_a L \rho_w} \tag{1.28}$$

In Eq. 1.27, t_λ and τ can be defined as:

$$t_\lambda = \frac{l_a h_s L \rho_w \phi \Delta S_o}{4 \lambda \Delta T_o} \tag{1.29}$$

where l_a is a constant equal to 0.5 and

$$\tau = \frac{\bar{\rho}c\Delta T_o}{L\rho_w\phi\Delta S_o} \tag{1.30}$$

Also, the steam chamber height can be computed using Eq. 1.31:

$$h_s = h_p(q_{po}/q_m)^2 \tag{1.31}$$

where

$$q_m = \sqrt{\frac{4.C.K.g.a.\phi.\Delta S_o.h_p}{m.\nu_s}} \tag{1.32}$$

where $\Delta T_0 = T_s - T_r$ is the difference between steam temperature and reservoir temperature. Also, the maximum value of the drainage rate q_m can be estimated using Eq. 1.32 which is the same as Butler's model. It is expressed as a function of steam chamber height instead of time.

In these equations q_{po} is the oil production rate, C is the model constant equal to 0.625, h_s is the steam chamber height, λ is thermal conductivity, L is the specific heat of steam condensation, T_s is steam temperature, T_r is reservoir temperature, ρ_w is density of water and q_m is maximum value of drainage rate, t_f is the time when the steam chamber reaches top of the reservoir, $\bar{\rho}c$ is the average heat capacity of steam condensation, a is thermal diffusivity of reservoir and h_p is the distance between top of reservoir and the production well.

Edmunds and Peterson (2007) proposed an analytical model to estimate cumulative steam oil ratio (CSOR) of SAGD or other steam-based bitumen recovery such as cyclic steam injection using a time-average effective temperature for steam zone. This model is a simplification and generalization of Reis's model (Reis, 1992). Eq. 1.33 shows the formula for the proposed model:

$$\text{CSOR} = [\frac{\Delta T}{H_{lv}\phi\Delta S_o}][c_{ir} + \frac{\sqrt{k_o c_{ov} t}}{h\eta_s}] \tag{1.33}$$

In the above equation H_{lv} is the latent heat of condensation of steam, c_{ir} is the initial reservoir volumetric heat capacity, c_{ov} is overburden volumetric heat capacity, k_o is overburden thermal conductivity, h is the height of reservoir above producer and η_s is effective sweep efficiency.

This model accounts for more than the previous models and also can be used for other thermal recovery methods such as cyclic steam injection. For estimating the steam injection rate, they considered the effect of underburden heat loss, which

is assumed to be equal to the one third of overburden heat loss. Considering underburden heat loss can improve CSOR estimation, but as they mentioned in the paper, this model cannot account for the effect of excessive steam loss due to the presence of a thief zone at the top or bottom of the reservoir. They investigated efficiency of this model with several examples and claimed that the match between the CSOR of a simulator and their model is better than the other models. The results for cyclic steam injection were not close.

Vanegas et al. (2008) added different options to the Butler SAGD model for considering heterogeneity of reservoir parameters. They also calibrated the proxy results to match closer to the simulator results. The options they added to the model are:

1. Considering reservoir heterogeneity in two ways:

   - The arithmetic average of porosity, permeability, water saturation and diffusivity coefficient were calculated along the steam interface weighed by the distance from the producer. This introduces model heterogeneity.
   - An effective volume factor was calculated to consider shale barriers. During production at a specific time step, if the permeability is very low the steam cannot pass through that shale barrier and the amount of oil production should be calibrated. They defined an effective volume factor as the ratio of vertically connected porous volume to the overall pore volume and multiplied this factor by the amount of oil production at that time step for finding the discounted oil production rate. In this equation nb_h is the number of blocks in the horizontal direction of the reservoir vertical section and nb_{vsi} is number of blocks below the first shale in the vertical direction at the ith block of horizontal direction.

   $$\text{EVF} = \frac{\sum_{i=1}^{nb_h} \sum_{j=1}^{nb_{vsi}} \text{VP}_{ij}}{\text{Total VP}} \tag{1.34}$$

2. Calculate the average oil relative permeability for computing the effective oil permeability instead of absolute permeability. They assumed an initial value for oil relative permeability at the first time step and multiplied it by the average permeability. For subsequent time steps, they computed the fraction of water and then computed the corresponding value of oil relative permeabil-

ity from a relative permeability table or the Wyllie and Gardner correlation (Ahmed, 2006).

3. They showed that different parameters in the proxy could be calibrated in order to get a better match between results of proxy and reservoir simulator. They selected four parameters for calibrating the proxy results:

   - a parameter for oil production rates during rising period
   - a parameter for oil production rates during spreading period
   - a parameter for average permeability
   - a parameter for CSOR

They used a simulated annealing technique to minimize the mismatch between the predictions of the proxy and the simulator.

The first two parameters shift the oil production rates during different time periods. Calibrating permeability accounts for geomechanical effects, that is, the potential increase in permeability over time. Due to the heating of the reservoir, permeability can be increased gradually. Also, the calibration factor for CSOR shifts CSOR linearly to match the results with simulator results.

This calibration can give unrealistic results and in some cases finding a good fit between the simulator and proxy is impossible. For example, the optimization algorithm could decrease the permeability to decrease the steam front velocity. It may then cause the steam front to stop before confinement at the last time step. Then, by multiplying rates in the rising and spreading periods, a good fit between the simulator results and the proxy can be obtained, but there are no physics behind changing these rates and it may cause unrealistic results for other cases or operating strategies. Also, this proxy cannot identify connected hydrocarbon volumes efficiently and assumes all the oil in the reservoir can be produced. Moreover, this proxy does not capture heterogeneity in a correct or efficient manner.

Azad and Chalaturnyk (2010) considered geomechanical effects in changing effective porosity and effective permeability in Butler's model. They mentioned that changes in porosity and permeability can be modeled using Eqs. 1.35–1.36:

$$\frac{k}{k_i} = (1 + \varepsilon_v/\phi_o)^3/(1 + \varepsilon_v) \tag{1.35}$$

$$\phi = (\phi_i + \varepsilon_v)/(1 + \varepsilon_v) \tag{1.36}$$

In these equations, k_o and ϕ_o are the initial permeability and porosity. Also ε_v is the shear-induced volumetric strain. Using these formulas, they considered geomechanical effects for improving Butler's model. There are different methods for computing effective porosity and permeability in the Butler model and considering different averaging methods can give completely different ranges of effective properties. In this case, considering geomechanical effects in changing porosity and permeability does not improve the proxy results significantly. The method for computing effective properties is more important than using geomechanical effects. Also, there are other important effects such as heterogeneity that can change the results significantly. In addition to that, they did not compare their proxy results with simulator results to show the accuracy of their method. Also, they did not compare proxy results before and after considering geomechanical effects. Finally it seems that their results are similar to the Reis model that they used for comparison.

Azad and Chalaturnyk (2013) considered a similar proxy model for the history matching. They showed that the stress ratio $q^{'}/p^{'}$ geomechanical impact factor (GIF) can be used as an indicator for the reservoir stress. This factor can consider the effect of in-situ stress and injection pressure in calculating the porosity and permeability of oil sand reservoirs. $q^{'}$ and $p^{'}$ can be calculated from the following equations:

$$q^{'} = \frac{\sigma_1^{'} - \sigma_3^{'}}{2} \tag{1.37}$$

$$p^{'} = \frac{\sigma_1^{'} + \sigma_3^{'}}{2} \tag{1.38}$$

where $\sigma_1^{'}$ and $\sigma_3^{'}$ are the maximum effective stress and the minimum effective stress, respectively.

They considered two case studies of the UTF pilot test (phase A and B) for checking reliability and level of uncertainty of such models. The final match between the proxy results and the field data was close.

Sharma and Gates (2011) proposed considering convection heat transfer mechanism at the edge of a the SAGD steam chamber when the water saturation is greater than the irreducible water saturation. Butler's original theory only considers the conduction mechanism during the SAGD operation. For the first time, Farouq-Ali (1997) discussed limitations of the Butler's original theory about the heat transfer mechanisms and neglecting the convection as an important mechanism during the SAGD operation. Later, Ito et al. (1998) showed that for some cases effect of

the convection and conduction mechanisms are equally important. As Sharma and Gates (2011) showed, the water mobility is many times greater than the bitumen mobility. They showed that enhancement of the heat transfer rate by convection may not necessary cause increasing the oil production rate. When the water saturation is greater than the connate water saturation, apparent thermal diffusivity can be calculated from the following equation:

$$\alpha^* = \frac{K_{TH}}{\rho_{os}c_p - \rho_c c_{pc}\frac{k_{rwro/\mu_w}}{k_{rw_{\text{int}}}/\mu_{w_{\text{int}}}}(\frac{S_w - S_{wc}}{1-S_{wc}-S_{or}})^b} \tag{1.39}$$

where K_{TH} is the thermal conductivity, ρ_{os} is the density of the oil sands, ρ_c is the density of condensate at the steam temperature, c_p is the volumetric heat capacity of the oil sands, c_{pc} is the volumetric heat capacity of the condensate, k_{rwro} is the relative permeability of water at the residual oil saturation, $k_{rw_{\text{int}}}$ is the relative permeability of water at the steam chamber interface, μ_w is the dynamic viscosity of the water, $\mu_{w_{\text{int}}}$ is the dynamic viscosity of water at the steam chamber interface, and b is the Corey coefficient.

In this case, if $S_w = S_{wc}$, then $\alpha^* = \alpha$, and when $S_w > S_{wc}$, then $\alpha^* > \alpha$.

They mentioned that for the case that $S_w > S_{wc}$, temperature distribution can be computed from the equation Eq. 1.40 by Newton's method for α^* versus ξ:

$$\alpha^*[1 - \frac{\rho_c c_{pc}}{\rho_{os}c_p}\frac{k_{rwro/\mu_w}}{k_{rw_{\text{int}}}/\mu_{w_{\text{int}}}}\exp(-b\frac{U_x}{\alpha^*}\xi)] = \alpha \tag{1.40}$$

where U_x is the interface velocity measured in the horizontal direction, ξ is the distance measured from the steam chamber edge in the direction normal to it, and α is the conduction thermal diffusivity.

After finding the temperature distribution, the convective and conductive heat fluxes can be calculated from the following equations:

$$Q_{\text{conv}} = V_c c_{pc}\rho_c(T - T_r) \tag{1.41}$$

$$Q_{\text{cond}} = -K_{TH}\frac{\partial_T}{\partial_x} \tag{1.42}$$

where V_c is the condensate convective velocity normal to the steam edge and can be computer from the following equation:

$$V_c = U_x\frac{k_{rw/\mu_w}}{k_{rw_{\text{int}}}/\mu_{w_{\text{int}}}} \tag{1.43}$$

where k_{rw} is the relative permeability of water.

Miura and Wang (2012) proposed an analytical model for predicting CSOR. They derived this model using material /energy balance and gravity-drainage theories. The steam injection volume can be computed from the total heat loss to the reservoir as Butler proposed. In developing this model, they also used Butler's formula for computing the average residual oil saturation in the steam chamber by changing time Butler (1991). Eq. 1.44 shows the CSOR model they developed.

$$\text{CSOR} = \frac{\Delta T(t)}{\Delta H(t)\phi(s_{oi} - \frac{b-1}{b}(\frac{v_s\phi h_s(t)}{bkgt})^{1/(b-1)})} \times (c_{vr} + \frac{\sqrt{k_t C_{vo} t}}{\beta h_s(t)}) \tag{1.44}$$

In this equation b is the exponent in the Cardwell and Parsons (1949) equation for the relative permeability. Also ΔH is the difference between enthalpy of steam at the chamber temperature and enthalpy of the condensate at the producing temperature.

They modified heat loss to the overburden by considering the coalescence effect as Butler suggested (Butler, 1991). Eq. 1.45 can be used for computing CSOR for the time that two adjacent wells existed next to the each other, and coalescence is happening. The proposed equation is:

$$\text{CSOR} = \frac{H_{\text{after}}}{\Delta H(t) O_{\text{after}}} \tag{1.45}$$

where

$$\begin{aligned} H_{\text{after}} =& \dot{A}t\Delta T\{C_{vr}(\beta h_s)[1 - n(\frac{t-t_1}{t})^2] + \sqrt{k_t C_{vo} t} - n\sqrt{k_t C_{vo}(t-t_1)}\} \\ &+ n\dot{A}t_1\Delta T\sqrt{k_t C_{vo}(t-t_1)} \end{aligned} \tag{1.46}$$

$$O_{\text{after}} = \dot{A}t(\beta h_s)\phi\Delta S_o[1 - n(\frac{t-t_1}{t})^2] \tag{1.47}$$

In this equation n is the chamber coalescence factor, and $\dot{A}$ is the rate of heating overburden. $n = 1$ means the chamber coalesces with two adjacent chambers and $n = 0.5$ means it coalesces with only one chamber. Also t_1 is the time that steam chamber takes to reach the neighboring chamber. H_{after} is the cumulative heat consumption after the coalescence and O_{after} is the cumulative oil production after the coalescence. They did not improve the old models significantly and just added simple options to the Butler model. As an example, they added estimation of residual oil saturation, which was discussed earlier by Butler (Butler, 1991), to the model to make it more complicated. The results that they showed in the paper were not significantly better than other models and all of models gave close results. Also for computing steam injection rate, they did not consider the effect of heat loss to

the reservoir. It can cause underestimation of the cumulative heat loss and lowers the estimated CSOR significantly.

Gupta and Gittins (2012) developed a semi-analytical mathematical model based on the Butler's theory by considering a solvent-aided process (SAP). They introduced a small amount of hydrocarbon solvent as an additive to the injected steam. They computed the solvent mole fraction in the vapor phase from the the interface temperature. Liquid-phase mole fraction can be computed using the equilibrium factor. Finally, a volume-fraction liquid concentration can be obtained from these values. This process reduces the heat requirement for the SAGD process. Proxy can help to optimize amount of the required solvent for this process. Using this proxy, the solvent steam ratio (SSR) and steam oil ratio (SOR) have been predicted for a few light-alkane solvents. Also, they showed that for computing the cumulative heat loss to the steam chamber and overburden, T_c which is the average temperature in the steam chamber should be used instead of T_s in the Eqs. 1.17–1.18. As another change, T_i which is the arithmetic average between the steam saturation and the draining interface temperatures should be used instead of the T_s in the Eq. 1.19 for computing the cumulative heat loss to the reservoir.

Hampton et al. (2013) considered effect of thermal conductivity and permeability heterogeneity on the SAGD performance. They considered numerical simulation results of the several heterogeneous models and based on those results modified the Butler's equations for better prediction of SAGD performance by the proxy model. they noticed that variation in permeability more significantly impacted the steam chamber than corresponding thermal conductivity variations. They also noticed that upscaling heterogenic values for input into the proxy analytical model will result in an underestimated flow rate due to the inability to fully account for the impact of shale barriers during the SAGD process.

1.4 Methods for Ranking of Reservoir Realizations

Simulating reservoir behavior is an important step in production optimization. For making a simulation model, a static model of geological properties should be generated first. Geostatistical methods can be used for this purpose. Most traditional methods are based on variograms and simulation to generate realizations. It is common to generate 100 realizations. Uncertainty in different modeling parameters can lead to increased uncertainty in the production results after flow simulation. The

best method for quantifying this uncertainty is to run all of the realizations through the flow simulator. This is very time consuming given the time to run the simulator. For this reason, the number of static models should be reduced while still trying to represent the uncertainty. This can be done by ranking the realizations. Ranking summarizes the multivariate distribution of facies, porosity, permeability and water saturation by a scalar. The ranked realizations can be divided into different groups and then one realization from each group can represent uncertainty of that group. Most of the time, realizations are classified into three different groups for identifying the low ($P10$), medium ($P50$) and high ($P90$) quality realizations. Then, these three realizations can be used for flow simulation. Some of the simple ranking measures are based on static methods and some are based on dynamic performance based on a fast flow modeling. The ranking parameter should be highly correlated with the production performance of reservoir.

Static methods can be divided into the following sub methods: a) Volumetric methods, b) Statistical methods, c) Global connectivity, and d) Local connectivity. The volumetric method is based on calculating original oil in place (OOIP) and ranking realizations based on this parameter. This method is the simplest method, but usually has a low correlation coefficient with the real ranking index. The equation for this method is

$$\text{OOIP} = \sum_{z=1}^{n_z} \sum_{y=1}^{n_y} \sum_{x=1}^{n_x} V_{(x,y,z)}(1 - S_{w_{(x,y,z)}})\phi_{(x,y,z)}. \tag{1.48}$$

In this equation V is volume, and n_x, n_y, and n_z are number of grids in different directions.

This equation can be improved by considering only net cells. In the case of considering net cells, the formula for computing OOIP is:

$$\text{OOIP}_{\text{net}} = C \sum_{z=1}^{n_z} \sum_{y=1}^{n_y} \sum_{x=1}^{n_x} V_{(x,y,z)}(1 - S_{w_{(x,y,z)}})\phi_{(x,y,z)} i_{(x,y,z)} \tag{1.49}$$

In this equation, i is a categorical variable and its value is 0 if cell has porosity or permeability less than the cutoff value, otherwise it is equal to 1.

In the SAGD process, the amount of oil production depends on the connection of the steam chamber to the surrounding reservoir. This connectivity can be global or local. Global connectivity indicates the proportion of net reservoir connected within a specified drainage volume. A cell is connected globally when it is net

(porosity and permeability is greater than cutoff, $i_{\text{net}} = 1$) and connected to one or more neighboring net cells ($i_{GC} = 1$). Global connectivity is a good ranking measurement in homogeneous reservoirs. The fraction of globally connected cells can be defined as:

$$\text{F}_{\text{GC}} = \frac{\sum_{z=1}^{n_z} \sum_{y=1}^{n_y} \sum_{x=1}^{n_x} i_{\text{net}_{(x,y,z)}} i_{\text{GC}_{(x,y,z)}}}{V} \tag{1.50}$$

Local connectivity depends on the ability of the steam chamber to reach and recover bitumen within local windows. Usually global connectivity is not the same as local connectivity. In the SAGD process, the steam can spread in a certain window, not to all parts of the reservoir. Global connectivity will consider all parts of the reservoir, but local connectivity can consider a window around the producer and injector. Global connectivity can be large, but local connectivity can be much smaller. In this case, the formula for calculating local connectivity is:

$$\text{F}_{\text{LC}} = \frac{\sum_{z=1}^{n_z} \sum_{y=1}^{n_y} \sum_{x=1}^{n_x} i_{\text{net}_{(x,y,z)}} i_{\text{LC}_{(x,y,z)}}}{V} \tag{1.51}$$

McLennan and Deutsch (2005) used these methods for ranking realizations. They ranked realizations from the McMurray formation based on the cells connectivity and then calibrated results using flow simulator results. They obtained a correlation coefficient of 0.9 between global connectivity and cumulative oil production. This correlation coefficient was close to 1.0 when local connectivity has been considered instead of global connectivity. Similar to the local connectivity, connected hydrocarbon volume (CHV) can be computed based on the following formula:

$$\text{CHV} = \sum_{y=1}^{n_y} \sum_{x=1}^{n_x} i_{\text{net}_{(x,y)}} (1 - S_{w_{(x,y)}}) \phi_{(x,y)} \tag{1.52}$$

In this formula, i_{net} is an indicator of connectivity defined as 1 if cell is connected to the well and as 0 otherwise. This can be calculated on different xy slices and then summed over all slices. Again a window could be defined around the wells. Also, the connectivity calculation could be modified in two ways: 1- Limit within a maximum distance from the well, and 2- Consider only connected cells to the production well. Also, a direct line of sight to the production well can be considered. Then all of connected net cells along these lines can be considered for calculating connected hydrocarbon volume. Fig. 1.11 shows net (red) and non-net (blue) cells along line of sights in a window around production well. The local connectivity is much smaller than global connectivity.

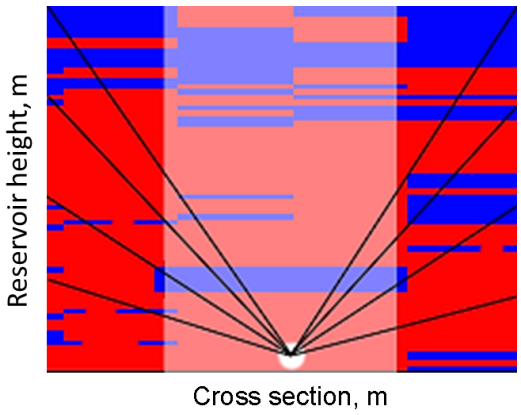

Figure 1.11: Line of sights in a window around production well. Red shows net and blue shows non-net grid cells.

All connected cells outside of the window are ignored. Fenik et al. (2009) used this method for ranking realizations. They compared connected hydrocarbon volumes for different models with different simulator outputs and found a good correlation between CHV and simulator results.

The new version of CHV (Wilde and Deutsch, 2012) can also consider different production steps during production. If steam reaches a shale barrier, it moves along it to reach to the end of the barrier. In this case, a second step of production can begin. Because steam is light, it prefers to move vertically and a rising period can be started and after that steam spreads to the other sides of the reservoir. More steps imply a longer production time.

There are some dynamic methods for ranking. In these methods, the flow equations may be simplified for faster simulation. This simplification may reduce the correlation with real production results, but the correlation can be higher than volumetric, statistical or connectivity methods. Examples of these methods are random-walk, time-of-flight (TOF) , tracer, streamline setups and proxy. These methods are slower than static methods.

The true ranking method is based on the running full model with the flow simulator for calculating cumulative oil production, cumulative steam production and NPV. An equation for a single ranking measure related to NPV is:

$$\text{NPV} = \sum_{i=1}^{N_t} \frac{\nu_o Q_{oi} - \nu_w Q_{wi}}{(1+r)^{t_i}} \tag{1.53}$$

In this formula, i is time step index, N_t is total number of time steps, r is

discount rate, t_i is cumulative time since start of production, ν_o and ν_w are price of oil and cost of steam injection, Q_{oi} and Q_{wi} are total oil and steam production over the time step Δt_i.

Zanon et al. (2005), created a full analytically space of uncertainty and showed how ranking can helps to sample more efficiently than MCS. They used a Kolmogorov-Smirnov test for measuring closeness of ranked realizations and MCS. They ranked realizations based on the NPV.

Vanegas et al. (2009) used a proxy based on the Butler's SAGD theory for ranking realizations. They considered a synthetic 3D well pad with 8 well pairs as a case study. They ranked realizations based on the cumulative oil production, but they did not compare results with a reservoir simulator.

1.5 Research Plan

This research will be directed toward developing and applying a novel semi-analytical model for predicting SAGD performance. Existing theories do not accurately predict flow performance in many circumstances. The steam interface moves too fast and the shape of the rising chamber is unrealistic. For this reason, some important production aspects should be considered in the formulation of the proxy for this research.

A new rising model should be developed that mimics the latest experimental and flow simulation results. Butler's rising model assumes forming a cone shape steam chamber above the producer and its height will increase gradually, but in reality the shape of steam chamber during rising is close to a trapezoid and its size will increase gradually until it reaches the top of the reservoir, then the spreading period will start.

Existing proxy models consider that production is from a homogeneous reservoir model. It is unrealistic to assume a single value for each reservoir parameters such as porosity, permeability, water saturation and PVT properties. In this work different research avenues should be explored to account for heterogeneity. One idea is to compute representative average properties along the steam interface at different time steps. On the other hand, the idea of CHV (connected hydrocarbon volume) can be adapted as a preprocessing step before running the proxy to restrict calculations to the connected net cells. The use of heterogeneous models may cause unrealistic peaks and variations in oil and steam profiles. In practice, flow is diffusive, yet the

proposed proxy models may respond instantaneously to local variations in reservoir properties. Perhaps effective properties could be used to provide stable results. These effective properties could be obtained by appropriate averages of porosity, water saturation and permeability of connected net cells.

Additional research should be devoted to establishing a realistic shape and location of the steam chamber as a function of time. The cumulative oil production will be limited to the amount of producible oil within the steam chamber.

Another important area of research will be to develop and integrate injection well constraints in the proxy calculations for considering different operating strategies. There is often a maximum allowable steam injection rate. The steam rate is important because of heat losses and cumulative steam oil ratio. The heat loss to the overburden depends on a suitable rising model and contact with the overburden. Some operators consider dropping steam injection pressure during production (at certain time steps or after exceeding ISOR limit). Using a realistic trigger to drop pressure may be an important development for cases with a thief zone at the top of the reservoir.

The effect of thief zones may be significant. Top gas and top water can cause significant heat loss to the overburden. Also, some of the injected steam can be lost to the thief zone and not contact the reservoir. As a result, the CSOR will increase significantly. This effect will be considered in the developed proxy by understanding the effects with flow simulation.

Considering the coalescence effect of steam chambers may be important for correctly predicting the amount of heat loss to the overburden. Coalescence will occur when the adjacent steam chambers come in contact with each other. After coalescence, the heat loss to the overburden would be decreased. This should be studied in the development of the novel proxy model.

Considering other aspects such as average relative permeability for flow of oil, wells with deviated trajectory, effect of shale barriers around wells and steam cross over between adjacent slices are very important for forecasting the SAGD performance of realistic models. All of these effects should be studied in the development of the novel proxy model.

The results of the proxy can be calibrated to a limited number of flow simulation results using an efficient optimization algorithm. This should provide a better match between the results of the simulator and proxy. Manually calibrating

the proxy would likely be tedious and time consuming. An optimization algorithm would permit this calibration to be done automatically. Sequential Quadratic Programming (SQP) can be used for this reason. The objective function will be the mismatch between the bitumen production and steam injection results of the proxy and simulator. The calibration parameters must be reasonable to make the proxy as predictive as possible.

After developing a reliable proxy, it should be used for different applications such as ranking of reservoir realizations, transferring realizations uncertainty and well trajectory optimization. Running all of realization through the flow simulator is very time consuming. Running them with a proxy should provide a very good solution. The proxy could also be used for well trajectory optimization by changing location of perforations to maximize a well-defined objective function.

Sensitivity analysis on the proxy parameters will be undertaken. Demonstrating the range of applicability of the proxy will be considered to identify the most important proxy parameters and situations where the proxy can be used for estimating SAGD performance. Some of input parameters in the proxy are uncertain. Research should be undertaken to establish the most sensitive parameters and to account for their uncertainty.

In the next Chapter, all of these modifications are explained with details. By applying these modifications, new proxy can be used for forecasting SAGD performance of realistic reservoir models.

1.6 Dissertation Outline

Chapter 2 presents the proposed semi-analytical model for predicting SAGD performance. Butler's original theory is not efficient for predicting performance in presence of heterogeneity and/or steam injection constraints. This Chapter considers modifications and options to Butler's model for improving predicting performance.

Chapter 3 considers the first application of the proxy which is forecasting the SAGD performance. In this Chapter, several 2D and 3D models are tested. 2D models are synthetic, but 3D models are realistic history matched models. In this Chapter, different heterogeneous models with different operating strategies are tested for assessing the proxy performance.

Chapter 4 considers the second application of the proxy which is a new method for forecasting steam chamber location. Butler's original theory is not efficient for

forecasting the steam chamber location of heterogeneous models. In this Chapter, a new method by combining the CHV and proxy results is presented. Different 2D examples are considered for assessing the performance of the new method.

Chapter 5 considers the third application of the proxy which is transferring uncertainty and ranking of reservoir realizations. This Chapter shows a comparison between results of the proxy and other methods such as the reservoir simulator and the CHV tool.

Chapter 6 considers the fourth application of the proxy which is the well trajectory optimization. In this Chapter, the producer and injector trajectories are optimized using the differential evolution (DE) method which is an efficient optimization algorithm. Proxy is used for computing the objective function instead of the flow simulator.

Chapter 7 shows an illustrative case study based on a synthetic 3D example with 3 well pairs. This Chapter proposed a new work flow for SAGD reservoir management and results are compared with the traditional work flow.

Finally, **Chapter 8** summarizes the methodology presented in this dissertation and shows the conclusions of different Chapters. Future work is discussed at the end of this Chapter.

Chapter 2

Methodology

This work develops a semi-analytical model for predicting SAGD performance. Butler's original theory is not efficient for predicting performance in presence of heterogeneity and/or steam injection constraints. The steam interface in Butler's original theory moves faster than predicted by high resolution reservoir simulation. Also, the shape of the rising chamber in Butler's theory is different from simulation results and does not accurately predict oil production and steam injection rates during this period. The difference between the end time of the rising period between the simulator and the proxy causes erroneous prediction of steam injection rates at later times due to the difference in calculation of heat loss to the overburden. As another disadvantage, Butler's theory does not consider the effect of an upper thief zone on forecasting steam injection rates. For these reasons, some modifications are necessary for improving both oil and steam predictions. After finding a reliable proxy, it can be used for different applications.

For the first step, Butler's theory should be modified for improving prediction of both oil production and steam injection rates. In this Chapter, modifications and options to Butler's model are developed. Sections 2.1 to 2.12 show these modifications.

2.1 Develop a New Rising Model

In this work, a new rising model for estimating oil production and steam injection rates is developed. The current models assume that steam contacts the top of the reservoir immediately and as a result, heat loss to the overburden is overestimated. For correcting this assumption, a rising period must be considered where the rise of steam is modeled explicitly.

Butler's rising model assumes there is a cone shape steam chamber above the producer and its height will increase gradually. By running different homogeneous cases, results showed that shape of steam chamber depends highly on the reservoir properties such as porosity, horizontal permeability and vertical permeability. High porosity and permeability cause the cone shaped steam chamber to spread horizontally very fast. It seems that vertical to horizontal permeability anisotropy ratio is very important in changing the shape of the steam chamber. If this ratio is one, the shape of steam chamber is very close to the shape of Butler's rising model, but by decreasing this ratio, the rising time will increase and the shape of the steam chamber would be close to an ellipse. Steam is very light and moves upward. Only barriers with very low permeability can stop the upward movement of the steam chamber. Fig. 2.1 shows cross section of steam temperature for three different cases with different permeability anisotropy ratios.

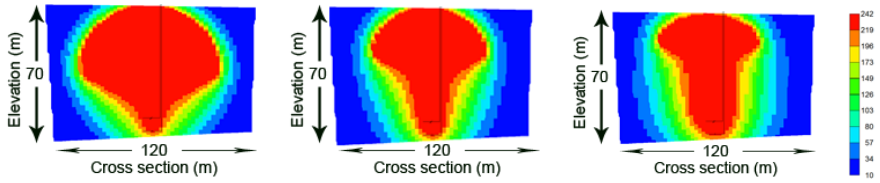

(a) Kh=1200, kv=1200 after 6 years (b) Kh=1200, kv=800 after 6 years (c) Kh=1200, kv=400 after 6 years

Figure 2.1: Shape of steam chamber for homogeneous models with different horizontal and vertical permeabilities

As Fig. 2.1 shows, the shape of the steam chamber is cone shaped only if the permeability anisotropy ratio is 1. Decreasing the vertical to horizontal permeability ratio, the shape would be close to an ellipse and even if the vertical permeability is low, steam prefers to rise instead of spread before it reaches to the top of the reservoir.

In reality, vertical permeability is always less than the horizontal permeability due to small scale orientations of grains and shale laminae that are relatively flat and horizontal. Fig. 2.2 shows the steam temperature for finding the shape of the steam chamber for nine wells in a 2D heterogeneous model and well spacing of 120 m. The shape of the steam chambers for different wells are close to an ellipse instead of a cone. There are barriers with low permeability above the well which stops the rising period (wells 1 and 5 in Fig. 2.2), but the shape of the steam chambers are close to elliptical.

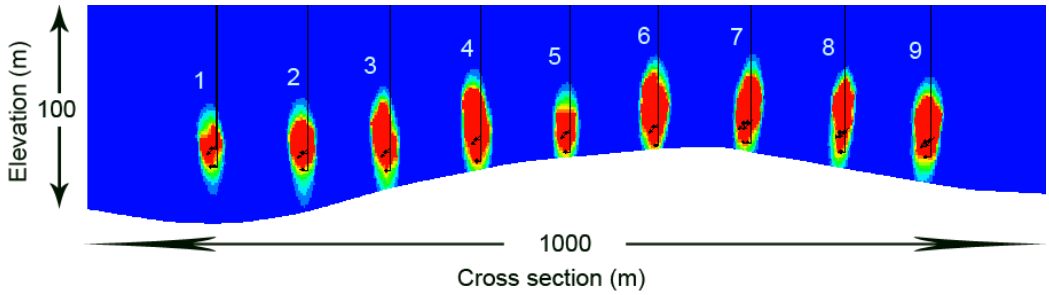

Figure 2.2: Steam temperature for finding the shape of the steam chamber for different wells in a 2D drainage area with heterogeneous porosity and permeability and a thief zone on the top after 1460 days

The shape of the steam chamber for heterogeneous cases is not exactly elliptical because both ends of the ellipse are not rounded. Also, the chamber is not exactly trapezoidal due to the heterogeneity in the models.

The chamber shape is assumed to be close to trapezoidal with an angle of 58° from horizontal. A correction factor β can be used for calibrating the results with the simulator in order to match the simulator and also correct the ratio between height and width of the steam chamber. The size of the chamber will grow with time until its height reaches the top of the reservoir. Then, the spreading period will begin. This is closer to flow simulation results than Butler's rising model which only fits homogeneous cases.

Fig. 2.3 shows the shape of the steam chamber in the new model. In Fig. 2.3, the height of the steam chamber is h and the half width of steam chamber is w.

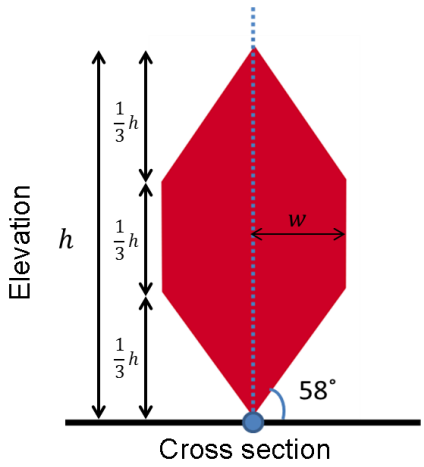

Figure 2.3: Shape of steam chamber in the model

For developing a new rising model, the amount of oil production at each time step during spreading and rising periods are assumed to be the same. Based on the amount of oil during the spreading period, the height of rising chamber can be computed by assuming a trapezoid shape for the steam chamber. Butler assumed the same assumption for developing his rising model. Knowledge of the width and height of the steam chamber at each time step permits the exact shape of steam chamber to be plotted, as shown in Fig. 2.3.

At each time step $\tan(32) = w/(\frac{1}{3}h)$ and as a result $w = 1/3\tan(32) \simeq 0.2h$. A correction factor β can be used to calibrate the shape of the steam chamber with simulation. The range of the parameter β is between 0.5 and 1.5.

The initial value for β is 1. As a result, $w = 0.2\beta h$. Also $\frac{dw}{dh} = 0.2\beta$. Then

$$\frac{dw}{dt} = 0.2\beta\frac{dh}{dt} \tag{2.1}$$

The area of the trapezoid is equal to the average length of the two bases multiplied by the height of trapezoid. As a result, the cumulative oil production is equal to:

$$Q = \int_0^t q dt = \frac{2}{3}hw\phi\Delta S_o \tag{2.2}$$

The oil rate at different time steps can be obtained by differentiating Eq. 2.2 respect to the time:

$$\begin{aligned} q &= \frac{2}{3}\phi\Delta S_o(w\frac{dh}{dt} + h\frac{dw}{dt}) = \frac{2}{3}\phi\Delta S_o(w\frac{dh}{dt} + h\frac{dw}{dh}\frac{dh}{dt}) \\ &= \frac{4}{15}\beta\phi\Delta S_o h\frac{dh}{dt} \end{aligned} \tag{2.3}$$

By equating Eq. 2.3 with Eq. 1.10 the following is obtained:

$$q = \frac{4}{15}\beta\phi\Delta S_o h\frac{dh}{dt} = \sqrt{\frac{1.5\phi\Delta S_o kg\alpha h}{m\nu_s}} \tag{2.4}$$

For finding h, Eq. 2.4 should be integrated with respect to time.

$$\int_0^h h^{1/2}dh = \frac{3.75}{\beta}\sqrt{\frac{1.5kg\alpha}{m\nu_s\phi\Delta S_o}}\int_0^t dt \tag{2.5}$$

As a result, the height of the steam chamber h can be obtained:

$$h = 3.62\beta^{-2/3}(\frac{kg\alpha}{m\nu_s\phi\Delta S_o})^{1/3}t^{2/3} \tag{2.6}$$

The half width of the steam chamber is equal to $w = 0.2\beta h$.

Assuming $\beta = 1$, and comparing Eq. 2.6 with Eq. 1.14, the rate of increasing height in the new model is computed to be about 1.8 times that of Butler's rising model. The new model proposed here matches the simulator results more closely.

By substituting Eq. 2.6 into Eq. 2.5, the cumulative oil production at each time step can be obtained:

$$Q(t) = 2\beta^{-1/3}(\frac{kg\alpha}{m\nu_s})^{2/3}(\phi\Delta S_o)^{1/3}t^{4/3} \tag{2.7}$$

Finally by differentiating Eq. 2.7 respect to the time, oil rate can be computed:

$$q(t) = 2.66\beta^{-1/3}(\frac{kg\alpha}{m\nu_s})^{2/3}(\phi\Delta S_o)^{1/3}t^{1/3} \tag{2.8}$$

These equations are useful when the model is homogeneous. In this case, if the volume behind the steam chamber in both rising and spreading periods are the same, the cumulative oil of both periods are the same too. As a result, the predictions of both periods can be coupled easily, but in heterogeneous cases, the porosity, water saturation and even residual oil saturation at different grid locations are not the same. As a result, coupling both periods is difficult and the cumulative oil production and oil production rate at the coupling time step are not the same leading to a sharp peak in the oil production profile. To solve this problem, it has been assumed that amount of oil rate at each time step for both periods are the same. As a result, at each time step the oil rate and cumulative oil production are the same for both models. At first, amount of cumulative oil in rising period for different heights should be computed, then based on the amount of oil in the spreading period, the height of the steam chamber in the rising period can be estimated. As a result, heat loss to the overburden can be estimated. This is an estimated rising model used only for finding the height of the steam chamber at different time steps. There is no heat loss to the overburden before contacting the top of the reservoir. After the end of rising period, heat loss to the overburden can be computed using Butler's original theory.

The steam chamber volume at the end of rising period for both Butler's model and the new model can be obtained by computing volume of their geometries. Fig. 2.4 shows the approximate area of each chamber at the end of rising period in a model with 80 m well spacing with reservoir height of 70 m.

The chamber area in Butler's rising model is about 2.4 times the new model. For the case of 80 m well spacing, which is very common, at the end of the rising

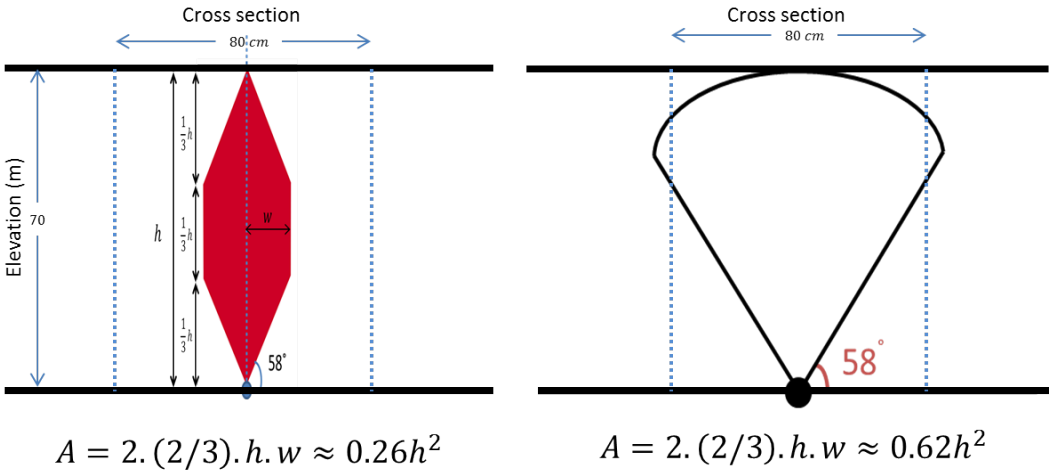

Figure 2.4: The area of the new rising model (left) and Butler's rising model (right) at the end of rising period in a model with 80 m well spacing and reservoir height of 70 m.

period, Butler's model contacts the horizontal boundaries of the model which is unrealistic. Butler's rising model also underestimates the amount of heat loss to the overburden. In the case of Butler's model, the steam moves equally in the vertical and horizontal directions, but in the new rising model, steam prefers to move in the vertical direction. At the end of the rising period, Butler's model contacts a large area of the overburden compared to the new model which is unrealistic. In the new rising model, this area is much smaller and gradually increases during the spreading period which is more realistic.

2.2 Considering Reservoir Heterogeneity for Forecasting Oil Production Rates

Butler's model is efficient for estimating oil production from homogeneous reservoir models. In this work, reservoir heterogeneity has been considered in three different ways. The first one is in computing average properties along the steam interface at different time steps. Porosity and water saturation averages can be computed using arithmetic average of the grid values that the steam interface passes through. The values will be weighted based on the distance from producing well. A larger weight should be given to the closer cells. The same approach can be used for finding the average permeability, but instead of the arithmetic average, a harmonic average should be used due to the vertically movement of flow in series through the grid

blocks. These average values can be used for estimating the new location of the steam interface at different time steps.

The second way to include the effect of heterogeneity on the oil production is to account for impermeable shale barriers. Steam cannot pass through a shale barrier and moves toward other parts of the reservoir. If these shale barriers are connected, the steam cannot move through them and all of the oil above them cannot be produced. For this reason, a CHV (connected hydrocarbon volume) tool can be used for finding connected net grids (Wilde and Deutsch, 2012). The proxy only allows production from connected net grid cells. This tool can also identifies steps and angles and distances maps. When there is a laminated shale barrier, steam cannot pass through it and moves toward other parts of the reservoir. If these shale barriers are connected to the each other, steam cannot move above of them and all of oils above these areas cannot be produced. Net grid cells are determined by setting a threshold for porosity and permeability that are important for flow. If a gird cell has porosity or permeability smaller than these thresholds, steam cannot pass through it. Different production steps, angles and distances based on line of sight to the producer are also computed. If steam along the line of sight reaches to a shale barrier, it moves along it until it reaches the end of the barrier. At the end of barrier, a second step of production will begin. Because steam is light, it prefers to move upward and a new rising period will be started. More steps mean longer production time. As a result, this tool can compute the angle between the original location of the bitumen and the production well respect to the vertical direction. A larger angle means longer time for bitumen to be produced. Also, the distance from a grid cell to the producer based on the step and angle of grids can be computed. In this case, the total length of the flow path is the sum of the lengths of each flow step and length of each flow step can be computed based on the angles. Fig. 2.5 shows result of CHV for a 2D model.

Fig. 2.5(a) shows connected net grids in a 2D slice of a reservoir. In this figure, connected net grid cells are red, and non-net grid cells are blue. Although there are shale barriers at the middle right of the reservoir, the steam can move to the upper part through the other side of the reservoir. The steam cannot pass through the top of the reservoir due to the low permeability of the rock above the reservoir. Also Figs. 2.5(b)–2.5(d) show steps, angles and distances maps, respectively.

If the average permeability in some parts of the reservoir is higher than other

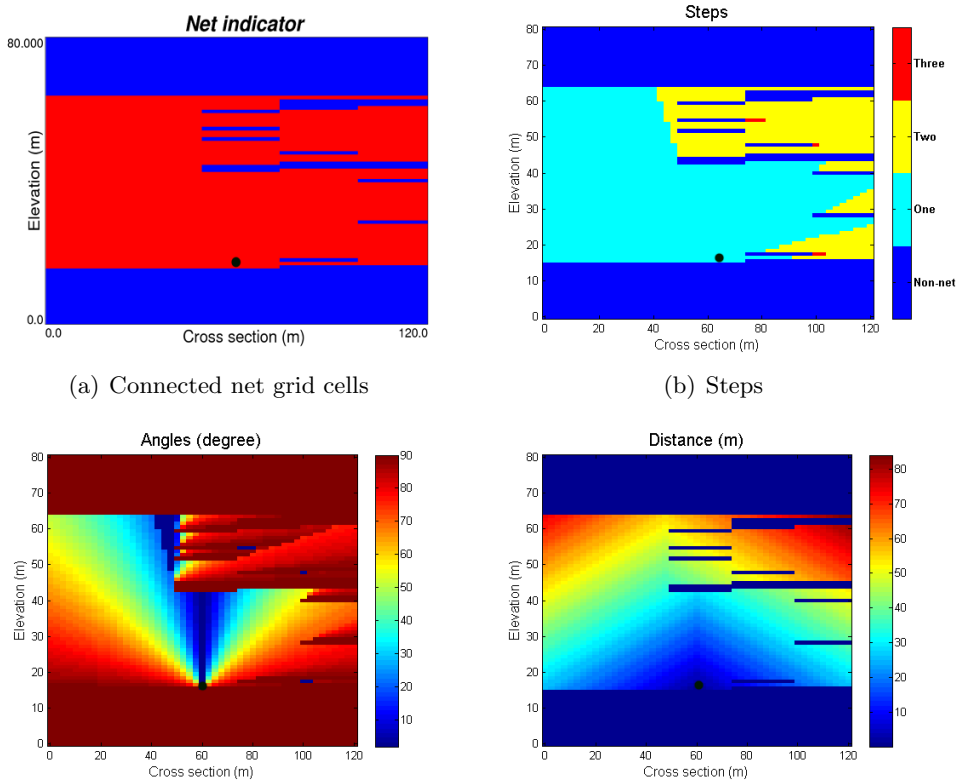

(a) Connected net grid cells

(b) Steps

(c) Angles

(d) Distances

Figure 2.5: CHV results which are connected net grid cells, production steps, angle between the original location of the bitumen and the production well and distance from a grid cell to the producer based on the step and angle of grids

parts, the steam interface moves faster and causes a peak in the oil production and steam injection rates which are not seen in reality. In this case, a third way for computing average properties has been considered. In this case, instead of computing average properties at different time steps, effective values of these properties can be computed. For this reason, arithmetic average of connected net grids for porosity and water saturation can be computed for finding effective porosity and effective water saturation. Also, the geometric average of permeability for connected net grids can be computed for finding effective permeability. These constant effective parameters can be used for proxy computations at different time steps.

2.3 Volumetric Computation of Produced Oil Behind the Steam Chamber

Butler's equations were developed for homogeneous models and give an unrealistically high recovery. Although Butler's model can predict the location of the s-shaped steam chamber by changing the time, an inverted triangular shape of steam chamber is used for volume calculations with a correction factor to approximate the s-shape of steam chamber. In this work, the s-shaped locations of the steam chamber at different time steps have been estimated using Butler's theory and the cumulative oil production has been computed based on the amount of producible oil behind the steam chamber. No geometric correction is required. Fig. 2.6 shows the area behind the steam chamber which contains both producible (red) and non-producible (blue) grid cells. The producible grid cells are identified with the CHV tool based on line of sight and considering steps and angles of production. The cumulative oil production at this time step is equal to the summation of the oil in all red grids behind the shaded area. In this figure, the steam interface has been shown by a black s-shaped curve and the black circle shows the location of the producer.

2.4 Consider Thief Zone Effect on the Steam Injection Rate

Sometimes a thief zone may exist at the top of the reservoir. This thief zone is permeable and contains water and gas. Top gas and top water can cause increased heat loss to the overburden. As a result, the steam injection rate will increase significantly. Considering this effect is important in estimating steam injection rates

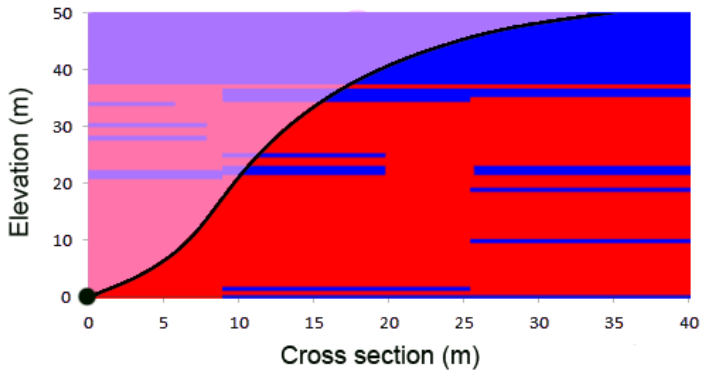

Figure 2.6: Producible oil behind the steam chamber

and the CSOR. Butler's model underestimates the steam injection rate in this case. In this work, the effect of the thief zone has been considered by modifying the thermal diffusivity of the overburden. Fig. 2.7 shows the water saturation of a 2D cross sectional slices of a model with a thief zone at the top of the reservoir.

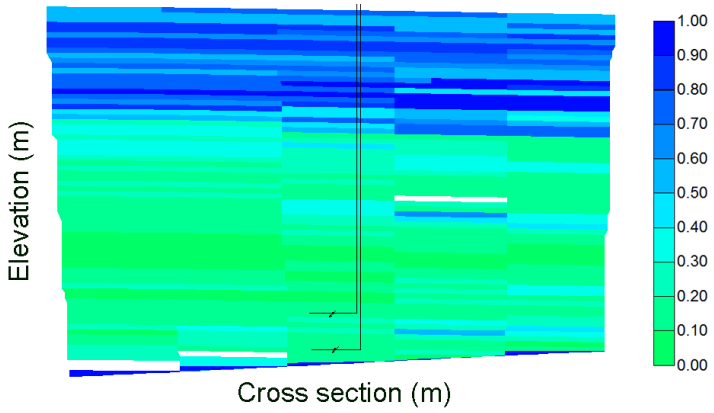

Figure 2.7: Thief zone on the top of the reservoir. XZ slice of water saturation. Wells are along y direction and grid sizes in x and z directions are 2.5 m and 1 m, respectively

Fig. 2.7 shows high water saturation in the upper thief zone. The new overburden thermal diffusivity can be computed from the average properties in the thief zone:

$$\alpha = \frac{k}{\rho c} = \frac{k_w s_w \phi + k_o s_o \phi + k_r (1-\phi)}{(\rho c)_w s_w \phi + (\rho c)_o s_o \phi + (\rho c)_r (1-\phi)} \tag{2.9}$$

In Eq. 2.9, k_w, k_o and k_r are thermal conductivity of water, oil and rock, respectively. Also $(\rho c)_w$, $(\rho c)_o$ and $(\rho c)_r$ are volumetric heat capacity of water, oil and rock, respectively.

The bulk oil weight is computed for the grid cells to identify the thief zone. Bulk oil weight is the ratio of oil weight to the total weight of the grid cell. The start of the thief zone is when the bulk oil weight is below a threshold for some vertical distance. Bulk oil weight can be computed from Eq. 2.10:

$$\text{BOW} = \frac{\rho_o \phi (1 - s_w)}{\rho_o \phi (1 - s_w) + \rho_w \phi s_w + \rho_m (1 - \phi)} \tag{2.10}$$

where ρ is density and o, w and m stand for oil, water and matrix, respectively. Using this formula, the bulk oil weight for all of grids can be computed easily. After separating thief zone from pay zone, the arithmetic average of porosity, oil saturation and water saturation in the thief zone can be computed easily.

In this case, the new thermal diffusivity is higher than the initial overburden thermal diffusivity and the heat loss to the overburden will increase which is close to reality.

As discussed before, when there is mobile water in the reservoir (same as thief zone), the convection heat transfer mechanism can be as important as the conduction heat transfer mechanism (Sharma and Gates, 2011). In this case convective heat transfer should be considered using Eq. 1.41. Apparent thermal diffusivity can be computed using Eq. 1.39 instead of the method explained above. As explained by Sharma and Gates (2011), enhancement of the heat transfer rate by convection may not necessary cause increasing the oil production rate, but in this case, it causes increasing the steam injection rate as a result of increasing cumulative heat loss to the overburden. Considering the convective heat loss to the overburden has an important role in the modeling of the thief zone effect on increasing the steam injection rate.

2.5 Set Injector Constraints on the Proxy

There are two types of constraints set on the steam injector: 1- Maximum bottom hole pressure (BHP) and 2- Maximum injection rate. If the injected steam rate is below the maximum available steam, BHP stays at its maximum value, otherwise BHP should be decreased to keep the steam injection rate at the maximum value. Butler's theory has been modified to consider these constraints. In this case, the proposed proxy computes the total heat loss at each time step and then computes the steam injection rate that is compared to the injection rate constraints. The total heat loss depends on the steam temperature (or pressure) and there should

be a balance between total heat loss and available steam. If the steam injection rate is below the maximum limit, the steam injection pressure will not be changed, otherwise, steam injection pressure should be decreased to keep the steam injection rate below the maximum value. In this manner, the steam injection pressure and steam injection temperature at different time steps can be obtained and compared with simulator results. If the steam pressure is above the maximum limit, it should be dropped. In this case, new PVT properties should be computed based on the new pressure and the steam injection rate will decrease. Both of these constraints can be set on the proxy at the same time. One of the reasons that Butler's model predict steam rate much higher than the simulator is related to the neglecting these constraints.

2.6 Production Trigger for Dropping Pressure

The ability of the proxy to handle variable steam injection pressure during the simulation leads to the possibility of setting triggers on the proxy for dropping steam injection pressure. Three types of trigger are used in practice and can be set in the proxy:

1. Pressure trigger
2. ISOR trigger
3. Blow-down trigger

Using the pressure trigger, the proxy can drop the pressure n times, each time for x months, after a certain date. n and x are arbitrary values set for each reservoir. Setting such a trigger is important in controlling the steam injection rate especially if a thief zone is present. Steam entering into the thief zone can increase CSOR significantly which has a strong negative economic impact.

Also using an instantaneous steam oil ratio (ISOR) will limit, steam injection pressure for a certain amount of time (e.g. 6 months) to keep the ISOR below a set maximum limit.

Finally, setting a blow-down trigger can be useful for controlling the amount of steam injection at the end of the well pair productive life. Blow-down trigger starts after a certain amount of oil recovery (e.g. 55%). At this time, steam injection should be stopped, but oil production will continue for a time. In this case, the

steam injection rate is zero and the CSOR will decrease significantly. Neglecting this operating strategy may overstate the CSOR significantly.

2.7 Consider Coalescence Effect

Considering the coalescence effect of steam chambers may be important for correctly predicting the amount of heat loss to the overburden. Coalescence will occur when adjacent steam chambers come in contact with each other. After coalescence, the heat loss to the overburden would be decreased because the hot zone ceases to expand. Fig. 2.8 shows a schematic illustration of the effect of coalescence.

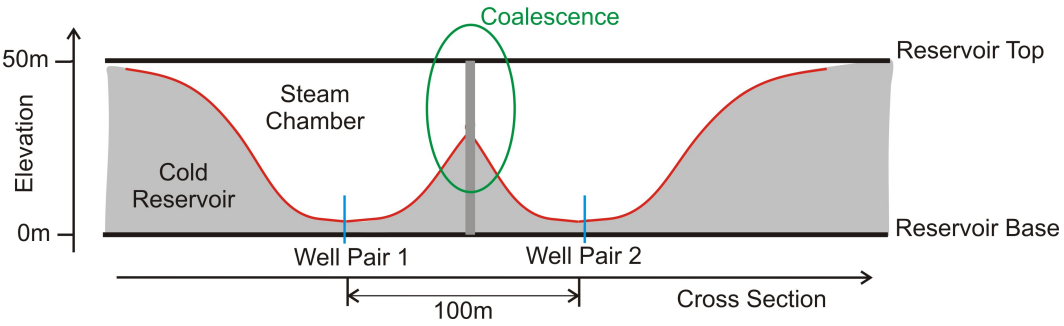

Figure 2.8: Coalescence effect. Two well pairs are adjacent to each other. The red curves show the interface of steam chambers at a particular time.

In this figure, two well pairs are adjacent to each other. The red curves show the interface of steam chambers at a particular time. As the steam chambers of both wells reach to each other, coalescence starts and rate of heat loss to the overburden starts to decrease. Location of coalescence plane depends on many parameters such as the steam front velocities on both sides, reservoir heterogeneity and the operating strategy is applied for SAGD operation. Usually coalescence plane is not located at the mid-distance between wells, but for simplicity the mid-distance between wells can be selected as a plane where the steam chambers contact each other. The heat loss to the overburden before confinement can be computed using the following equation (Butler, 1991):

$$Q_o = \frac{4}{3} k_{ob}(T_s - T_r) A \sqrt{\frac{t}{\pi \alpha_{ob}}} = \frac{4}{3} \frac{k_{ob}(T_s - T_r)\dot{A}}{\sqrt{\pi \alpha_{ob}}} t^{3/2} \tag{2.11}$$

In Eq. 2.11, $\dot{A}$ is the rate of heating overburden $\dot{A} = A/t$ for $0 \leq t \leq t_c$ where t_c is coalescence time.

After coalescence, Eq. 2.11 overestimates heat loss to the overburden, because at this time, heated area stops growing. The heat can be computed by setting time equal to $t' = t - t_c$. As a result, heat beyond $\dot{A}t_c$ is equal to:

$$Q_c = \frac{4}{3}\frac{k_{ob}(T_s - T_r)\dot{A}}{\sqrt{\pi\alpha_{ob}}}t'^{3/2} = \frac{4}{3}\frac{k_{ob}(T_s - T_r)\dot{A}}{\sqrt{\pi\alpha_{ob}}}(t - t_c)^{3/2} \tag{2.12}$$

where $\dot{A} = A/t_c$ for $t \geq t_c$.

Thus, the cumulative heat loss to the overburden at times greater than t_c can be computed by subtracting Eq. 2.12 form Eq. 2.11 (Butler, 1991):

$$Q_c = \frac{4}{3}\frac{k_o(T_s - T_r)\dot{A}}{\sqrt{\pi\alpha}}[t^{3/2} - (t - t_c)^{3/2}] \tag{2.13}$$

In this case $\dot{A} = A/t_c$ for $t \geq t_c$.

2.8 Automatic Calibration of Proxy Results

Calibration can be done to adjust some of proxy parameters to improve the match to flow simulation. Manually calibration is very tedious and time consuming. An optimization algorithm will be used for automatic optimization. Two optimization methods have been considered. The first one is the Sequential Quadratic Programming (SQP) which is a gradient based method (Dehdari and Oliver, 2012; Dehdari et al., 2012) and the second one is Differential Evolution (DE) which is an evolutionary algorithm. SQP is suitable for solving nonlinear optimization problem with continuous and differentiable objective functions and inequality constraints. DE is an efficient method for solving integer optimization problems. SQP can be used for solving calibration problem and DE can be used for solving problems such as well trajectory optimization (see later). Some background on these two optimization methods can be seen in the next two sections.

2.8.1 Sequential Quadratic Programming (SQP)

Suppose an objective or cost function, $f(x)$, subject to constraints $c_i(x) \geq 0$ for $i = 1, 2, \ldots, q$ should be minimized.

$$\text{minimize } f(x) \tag{2.14a}$$

$$\text{Subject to : } c_i(x) \geq 0 \qquad \text{for } i = 1, 2, \ldots, q \tag{2.14b}$$

$f(x)$ can be a linear or nonlinear function of the control variables. $c_i(x)$ are constraints which are functions of x and can be nonlinear. $f(x)$ and $c_i(x) \geq 0$ are

assumed to be continuous and have continuous second partial derivatives, and the feasible region of this problem is assumed to be nonempty. The solution of this problem can be found by writing the Karush-Kuhn-Tucker (KKT) conditions and solving this system of equations (Antoniou and Lu, 2007; Nocedal and Wright, 2006):

$$\begin{aligned} \nabla_x \mathcal{L}(x, \mu) &= 0 \\ c_j(x) &\geq 0 \qquad \text{for } j = 1, 2, \ldots, q \\ \mu &\geq 0 \\ \mu_j c_j(x) &= 0 \qquad \text{for } j = 1, 2, \ldots, q. \end{aligned} \tag{2.15}$$

In the above equations $\mathcal{L}(x, \mu)$ is the Lagrangian of the problem, defined as

$$\mathcal{L}(x, \mu) = f(x) - \sum_{j=1}^{q} \mu_j c_j(x) \tag{2.16}$$

where μ is the vector of Lagrange multipliers. Also KKT conditions are first order necessary conditions for finding an optimal solution of a nonlinear optimization problem.

For solving this system of equations, a Taylor series expansion for each of these conditions can be written to obtain a new system of linear equations which has KKT conditions of the following optimization problem:

$$\text{minimize } \frac{1}{2}\delta^T \mathbf{Y}_k \delta + \delta^T \mathbf{g}_k \tag{2.17a}$$

$$A_k \delta \geq -\mathbf{C}_k \qquad \text{for } k = 1, 2, \ldots, q \tag{2.17b}$$

In this optimization problem, $\mathbf{Y}_k$ is the Hessian of the Lagrangian, $\mathbf{g}_k$ is the gradient of the Lagrangian with respect to the control variables, A_k is the Jacobian of the constraints and C_k is a matrix of constraints at x_k where k is the iteration index. Using this method, the nonlinear optimization problem is converted to a quadratic optimization problem. As a result, only a quadratic optimization problem must be solved at each iteration. This is the reason that this method is called sequential quadratic programming. By solving this problem, the search direction δ of the original optimization problem, can be computed. This inequality quadratic optimization problem can be solved by converting it to equality optimization problem by considering only active constraints. After that, this equality constraint optimization problem can be solved by converting it to an unconstrained optimization problem using the variable elimination method (Antoniou and Lu, 2007). Optimized values

from the unconstrained optimization problem can be computed easily by solving for variables that make the derivatives equal to zero. The initial solution can be updated using the following formula:

$$x_{k+1} = x_k + \alpha_k \delta_x \tag{2.18}$$

The solution is updated in the search direction while staying in the feasible region. The following one-variable multi-dimensional optimization problem is solved to find α:

$$\phi(\alpha) = f(x_k + \alpha\delta_x) - \sum_{j=1}^{q} (\mu_{k+1})_j \, c_j(x_k + \alpha\delta_x) \tag{2.19}$$

Solving the line search problem is possible using different methods such as Strong Wolfe conditions (Oliver et al., 2008). For solving this problem, values of Lagrange multipliers should be computed, which can be found by solving the following equation that is based on linearizing the first KKT condition.

$$\mu_{k+1} = (\mathbf{A}_{ak}\mathbf{A}_{ak}^T)^{-1}\mathbf{A}_{ak}(\mathbf{Y}_k\delta_x + \mathbf{g}_k) \tag{2.20}$$

In Eq. 2.20 the rows of $\mathbf{A}_{ak}$ are those rows of A_k satisfying the equality $\mathbf{A}_k\delta_x + \mathbf{C}_k = 0$ and μ_{k+1} denotes the associated Lagrange multiplier vector. Also, the Lagrange multipliers of other inequality constraints, which are not active, are equal to zero.

After finding the search direction and step length, the initial solution can be updated. This procedure should be terminated when the difference between the objective function in two iterations is less than the stopping criteria. Fig. 2.9 shows a flowchart for finding the optimal solution using SQP optimization algorithm.

Convergence of SQP algorithm is very fast, but it may be trapped in a local minima or maxima (Dehdari and Oliver, 2012; Dehdari et al., 2012).

2.8.2 Differential Evolution (DE)

This method has been introduced by Storn and Price (Storn and Price, 1997). Differential evolution is a population based method. Convergence of population based methods are slower than gradient based methods, but as an advantage, the objective function can be non-differentiable, non-continuous, non-linear, noisy, flat or multi-dimensional. Also, it can find multiple local or global optimums and it will not be trapped in local minima or maxima.

Assume a parameter vector D with real parameters and the size of the population is NP. In this case a vector of parameters is $x_{i,G} = [x_{1,i,G}, x_{2,i,G}, \ldots, x_{D,i,G}]$ where $i = 1, 2, \ldots, NP$ and G is generation number.

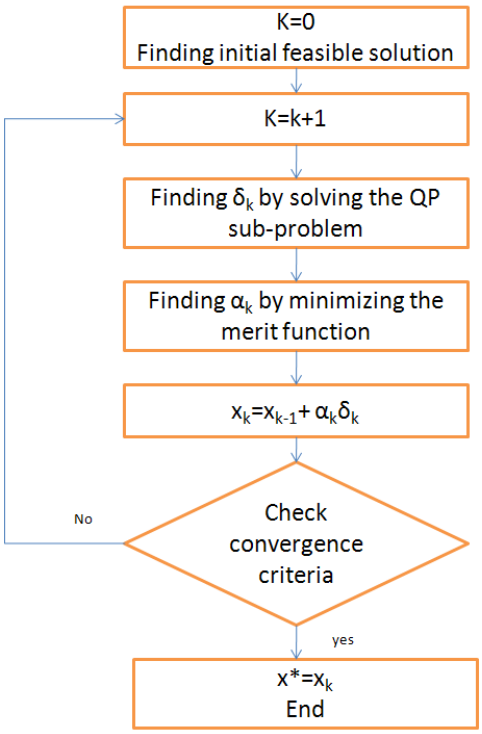

Figure 2.9: Flow chart of SQP

The first step is to generate initial parameter values that can be picked randomly from a uniform distribution between lower and upper values of each parameter. The number of parameters is constant during optimization.

The second step is mutation that generates a new parameter vector based on the other three vectors. Eq. 2.21 can be used for generating a new parameter vector $\nu_{i,G+1}$ which is called a donor vector

$$\nu_{i,G+1} = x_{r1,G} + F(x_{r2,G} - x_{r3,G}) \tag{2.21}$$

where r_1, r_2 and r_3 are random indexes which should be selected from NP population randomly. In the above formula, F is a mutation factor and its value is a constant between 0 and 2 and it can control the amplification of the differential variation.

The third step is crossover for increasing the diversity of the perturbed parameter vectors. For this reason, a trial vector $u_{i,G+1}$ can be obtained from elements of the target vector $x_{i,G}$ and the donor vector $\nu_{i,G+1}$. Assume the trial vector has the form of $u_{i,G+1} = [u_{1i,G+1}, u_{2i,G+1}, \ldots, u_{Di,G+1}]$. The trial vector can be obtained from

Eq. 2.22:

$$u_{ji,G+1} = \begin{cases} \nu_{ji,G+1} & \text{if } (rand_j \leq CR) \text{ or } (j = I_{rand}) \\ x_{ji,G} & \text{if } (rand_j > CR) \text{ and } (j \neq I_{rand}) \end{cases} \quad \text{j=1,2,...,D} \qquad (2.22)$$

In this formula, $rand_j$ is the jth evaluation of uniform random number between 0 and 1. Also CR is crossover constant between 0 and 1. It is an arbitrary value and can be selected by the user. Also I_{rand} is randomly chosen index less than D to guarantee that $u_{i,G+1}$ gets at least one parameter from $\nu_{i,G+1}$, and $\nu_{i,G+1}$ is not equal to $x_{i,G}$.

The last step is called selection. In this step, the trial vector $u_{i,G+1}$ should be compared with the target vector $x_{i,G}$. The objective function for each of them should be computed and the one with the lower objective function should be selected for the next generation $x_{i,G+1}$. Fig. 2.10 shows the flow chart of differential evolution technique.

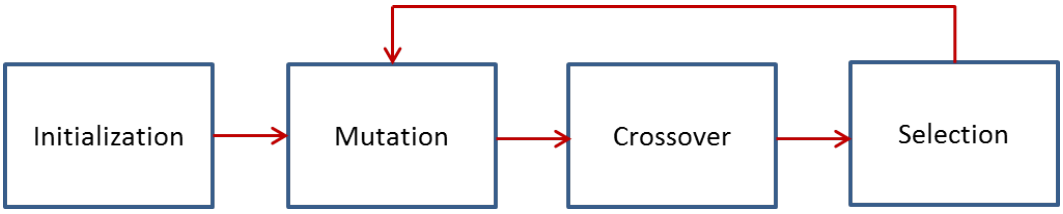

Figure 2.10: Flow chart of differential evolution

The process of mutation, crossover and selection should be continued until a stopping criteria met.

2.8.3 Objective Function and Calibration Parameters

In this work, five different calibration parameters have been selected for calibration and an arbitrary lower and upper bound can be selected for each of them. Three of them are for calibrating the oil production results and two of them are for calibrating the steam injection results. Selecting the calibration parameters is important. Reasonable parameters should be selected for calibration; otherwise calibration can give unrealistic results. For improving estimated oil production rates, three calibration parameters which are the steam interface velocity at different production stages i.e. rising, spreading and confinement are selected. If the steam interface moves too fast, it reaches to the boundary in the early time steps. Also, if it moves very slow, the amount of oil production would be too small. For this reason, calibrating the steam

front velocity is important. For calibrating the estimated steam injection rates two selected parameters are the overburden thermal diffusivity and reservoir volumetric heat capacity to modify heat losses to the overburden and reservoir respectively. As a result they may overestimate or underestimate heat losses to the overburden and reservoir. By calibrating these five parameters, a better match between results of the simulator and the proxy can be obtained. Also, the objective function is the mismatch between the proxy and simulator results and has two terms. The first term is the squared mismatch between cumulative oil production and the second term is the squared mismatch between cumulative steam injection. The objective value is the summation of both terms.

$$\text{Obj} = \sum_{t=1}^{n_t} [Q_{op}(t) - Q_{os}(t)]^2 + \sum_{t=1}^{n_t} [Q_{wp}(t) - Q_{ws}(t)]^2 \tag{2.23}$$

where $Q_{op}(t)$ is proxy cumulative oil production at time t, $Q_{os}(t)$ is simulator cumulative oil production at time t, $Q_{wp}(t)$ is proxy cumulative steam injection at time t and $Q_{ws}(t)$ is simulator cumulative steam injection at time t.

Optimization can be done in one stage or two stages. One stage optimization means optimizing all of calibration parameters at once; however, the steam calibration parameters are independent of the oil calibration parameters. For this reason, optimization can be done in two stages. In this case, the oil production parameters are calibrated first and then by keeping them constant, the steam injection calibration parameters should be optimized.

Values of cumulative steam injections are larger than values of cumulative oil productions, as a result, the second part of objective function would be larger than the first part and the optimization algorithm tries to minimize steam mismatch more than the oil mismatch. For this reason, one over squared value of initial CSOR can be selected as a weight for second term:

$$\text{Obj} = \sum_{t=1}^{n_t} [Q_{op}(t) - Q_{os}(t)]^2 + \frac{1}{\text{CSOR}^2} \sum_{t=1}^{n_t} [Q_{wp}(t) - Q_{ws}(t)]^2 \tag{2.24}$$

Using this objective function, both oil production and steam injection would be close to each other. Of course, this is not particularly important since the components of the objective function are essentially independent.

Also instead of optimizing cumulative values, rates can be optimized too. If the objective function is defined based on the rates and there is a peak in the oil or steam profiles, the optimization algorithm tries to remove that peak at the expense of the

overall fit. In this case, minimizing the mismatch between cumulative production and injection is preferred.

2.9 Average Relative Permeability for Flow of Oil

Based on Butler's theory, at each time step, the amount of oil production from each segment of the steam front can be computed using Eq. 1.8. In that equation, permeability is absolute permeability, but because the oil rate should be computed, it is more reasonable to multiply this absolute permeability by oil relative permeability for finding the oil effective permeability which is $k_o = kk_{ro}$. Butler showed that approximately 40% relative permeability is a reasonable estimation for modifying the absolute permeability. But he showed that average oil relative permeability can be computed from fraction of water at each time step (Butler and Dargie, 1994). The oil rate is proportional to k_{ro}/ν_o or k_{ro}/μ_o. Also, the water rate is proportional to k_{rw}/μ_w. As a result, the fraction of water can be computed as:

$$f_w = \frac{q_w}{q_w + q_o} = \frac{\frac{k_{rw}}{\mu_w}}{\frac{k_{rw}}{\mu_w} + \frac{k_{ro}}{\mu_o}} = \frac{1}{1 + \frac{\mu_w}{\mu_o}\frac{k_{ro}}{k_{rw}}} \tag{2.25}$$

Also, using the Wyllie and Gardner correlation in clean sands, the oil and water relative permeabilities can be approximated by cubic function of mobile saturations (Ahmed, 2006):

$$k_{ro} = S_o^{*^3} \tag{2.26}$$

$$k_{rw} = (1 - S_o^*)^3 = (1 - k_{ro}^{1/3})^3 \tag{2.27}$$

where in above equations S_o^* is equal to:

$$S_o^* = \frac{S_o - S_{or}}{1 - S_{wi} - S_{or}} \tag{2.28}$$

By combining Eq. 2.25 and Eq. 2.27, the fraction of water can be computed:

$$f_w = \frac{q_w}{q_w + q_o} = \frac{\frac{k_{rw}}{\mu_w}}{\frac{k_{rw}}{\mu_w} + \frac{k_{ro}}{\mu_o}} = \frac{1}{1 + \frac{\mu_w}{\mu_o}\frac{k_{ro}}{(1-k_{ro}^{1/3})^3}} \tag{2.29}$$

By solving this equation for k_{ro}:

$$k_{ro} = \frac{1}{[1 + [\frac{\mu_o}{\mu_w}(\frac{1}{f_w} - 1)]^{-1/3}]^3} \tag{2.30}$$

For finding average oil relative permeability at each time step, the fraction of water at that time step should be computed. Eq. 2.31 can be used for finding the

fraction of water:

$$f_w = \frac{q_w}{q_w + q_o} = \frac{1}{1 + \frac{q_o}{q_w}} = \frac{1}{1 + \frac{1}{\text{WOR}}} \tag{2.31}$$

where in Eq. 2.31, WOR is water oil ratio. The water to steam ratio at each time step is assumed equal to 1. For this reason, WOR is equal to the instantaneous steam oil ration (ISOR) at each time step. As a result, using ISOR at each time step, the average oil relative permeability can be computed.

2.10 Other Modifications

Butler's original theory only considered the location of the producer, but the location of the injector is also very important. In this case, estimating performance of a 3D model with deviated trajectory could be possible and locations of both producer and injector are designed by the engineer.

The proxy considers the location of both of producer and injector. If a shale barrier exists around the injector, it would change the injection of steam into the reservoir. Shale barriers between the producer and injector are very important. If a shale barrier exists between the producer and injector, there would not be any communication between them and oil would not be produced from that slice. For this reason, the proposed proxy will check for shale barriers for approximately five meters above the producer with angle of 64 degrees. This angle has been selected based on the angle of the steam chamber during the rising period. Fig. 2.11 shows checking the existence of shale barriers inside the red area. As Fig. 2.11 shows, one

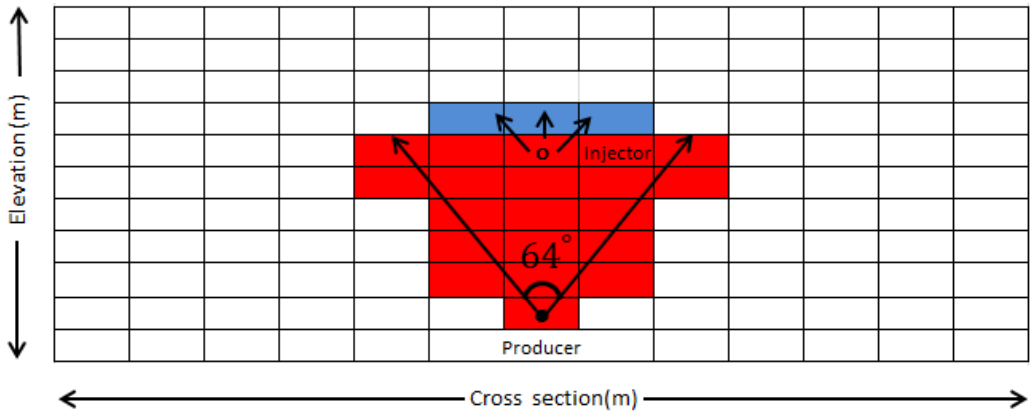

Figure 2.11: Consider effect of shale barriers between producer and injector

meter above and one meter below of injector (blue area) should be considered for

checking existence of shale barriers around the injector.

If a shale barrier stops production on one slice, steam may cross from an adjacent slice. In this case, if steam cannot be injected into one slice or there is no communication between the producer and injector in that slice, but one of adjacent slices is able to inject steam or produce the bitumen, we assume that oil of that non-producible slice could be produced by the adjacent one.

2.11 Consider Multiple Well-pairs in a DA

The proposed proxy is designed to compute the performance of multiple well pairs in a DA simultaneously. In this case, the producer and injector trajectories and the boundary of each well should be defined. The proxy saves the results of each well and DA separately. Fig. 2.12 shows a small DA with five well pairs.

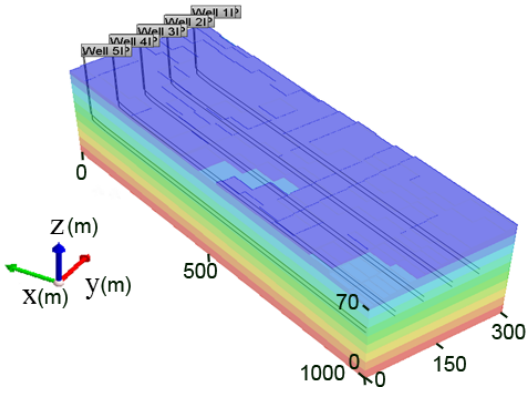

Figure 2.12: multiple well-pairs in a DA

This is very useful for uncertainty roll-up and ranking of reservoir realizations using multiple wells in a DA.

2.12 Use Multiple Thermal Rock Types

Different thermal rock types can be recognized from shale volume in each grid cell. The shale volume can be computed from the effective porosity. Each thermal rock type has a separate set of thermal properties. Defining different thermal rock types is important to match the simulator and it also has an effect on computing heat loss to the overburden when a thief zone is present at the top of the reservoir. The

following equation can be used for computing shale volume (Paradigm Ltd., 2012):

$$V_{\text{shale}} = 0.8969 - 3.3681\phi + 2.7129\phi^2 \tag{2.32}$$

By setting different thresholds for shale percentages, different thermal rocks can be identified. Shale percentage is between zero and 100. Depends on the number of thermal rock types, increments of successive thresholds can be equal.

2.13 Summary

In this Chapter, several options for improving the prediction of both oil production and steam injection rates have been considered. Some of these option are developing a new rising model, considering reservoir heterogeneity for forecasting oil production rates, considering thief zone effect on the steam injection rate, setting injector constraints for different operating strategies, considering coalescence effect and calibrating the proxy parameters for finding a better match between the proxy and simulator results.

In the next Chapter, several 2D and 3D examples are considered for testing the developed proxy and comparing the proxy results with the simulator results. The 2D examples are synthetic models, but the 3D examples are realistic history matched models. Proxy results should be matched with the production data of realistic models. If a model is history matched, the proxy results should be closed to the simulator that means proxy results honor the production data too. Flow simulation results are approximate due to the assumptions used for modeling the flow behavior. Although commercial flow simulators cannot consider all complexities and nonlinearities of flow equations, they forecast results with proven accuracy. Geostatistical models are uncertain and different from the true reservoir. For this reason, history matching can be used for finding a match between the flow simulator results and production data by changing reservoir properties. Although the simulator results are approximate, if the geostatistical model is close to the true model, the flow simulation results should be close to the production data. Due to the complexity of commercial simulators, they are very slow. For this reason, they cannot be used for different applications such as ranking or well trajectory optimization. The proxy can be used as a substitute for the commercial flow simulator for running reservoir models multiple times. In this case, uncertainty in reservoir parameters can be considered without extensive use of the flow simulator.

Chapter 3

Forecasting SAGD Performance

For testing proxy efficiency, SAGD performance of several 2D and 3D models have been tested. At first, different 2D models have been considered in Section 3.1 for assessing the proxy performance for each 2D slice. For all of the examples, oil production, steam injection (both rates and cumulative), CSOR and steam pressure have been compared. The STARS (Computer Modeling Group Ltd., 2012) flow simulator has proven forecasting capability over decades and 100s of billions of dollars of investment (Alberta Energy Regulator, 2013 and before). Comparing the proposed proxy to this simulator is a worthwhile verification of its performance forecasting ability.

Different synthetic 2D and realistic history matched 3D models with different operating strategies are tested in Sections 3.1 to 3.2 for assessing the proxy forecasting ability. Then, Section 3.3 shows a comparison between the proxy and simulator run time.

3.1 Synthetic 2D Examples

For testing the capability of the proxy, 100 2D realizations based on a realistic model in the Alberta oil sands have been generated. Each model has a grid dimension of $1 \times 49 \times 83$. The grid size in the x, y and z directions are 25 m, 2.5 m and 1 m, respectively. A stratigraphic pinchout exists at the bottom of the reservoir. Top water and top gas exists above the pay zone. Five different facies and seven different thermal rock types are considered. Each facies has a separate relative permeability curve.

In all of these models, permeability at the top part of the reservoir is significantly less than in the pay zone. Gas is present in the top five meters of the model and

there is no gas in the pay zone or in the lower thief zone. There is little oil in the thief zone and the average porosity in the thief zone is less than the average of porosity in the pay zone. In all of these examples, the producer has been drilled above the pinchout elevation and it is in the middle of the 2D section.

3.1.1 Geostatistical Modeling of Realizations

A vertical trend has been modeled. The horizontal extent of the model is small and there is no trend in that direction. In this case, 1D vertical trend can be computed by moving average of data along vertical direction. A moving window of 5 m was chosen because the results are stable and not overly smoothed. Fig. 3.1 shows the vertical trend for different facies proportions. Different facies are defined based on the rock qualities. Grid cells with higher porosity and permeability have better rock quality. In this example, there are five facies in the model. Facies 1 has the best rock quality (sand) and facies 5 has the worst (shale).

As shown in Fig. 3.1, the probabilities of facies 1 and 2 in the lower half of the reservoir are higher than in the upper half. Also, the probabilities of facies 3, 4 and 5 in the upper half of the reservoir are higher than the lower half. Facies 3, 4 and 5 are low quality facies present in the thief zone.

The range of facies continuity for each facies in the vertical and horizontal directions can be assessed with the variogram. Variogram models are based on the variogram of all data in the base case realistic model. In generating realizations, isotropic continuity has been assumed in all horizontal directions. Fig. 3.2 shows the horizontal variograms for each facies.

Fig. 3.3 also shows the variogram in the vertical direction for all facies. As expected, the vertical ranges are much shorter than the horizontal ranges.

Sequential indicator simulation has been used for generating the 2D facies models (Deutsch and Journel, 1992). Then, porosity is modeled by-facies using sequential Gaussian simulation (Deutsch and Journel, 1992) and then results of different facies have been merged together based on the facies realizations. The same procedure has been used for generating permeability and water saturation realizations, but collocated cokriging method has been used for modeling them using the generated porosity realizations to enforce reasonable correlation between all variables (Deutsch and Journel, 1992).

Fig. 3.4 shows different properties of one of the generated realizations in the

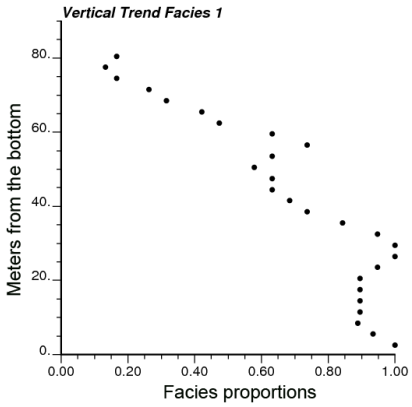

(a) Facies 1

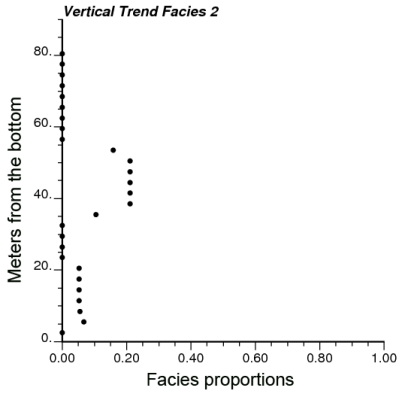

(b) Facies 2

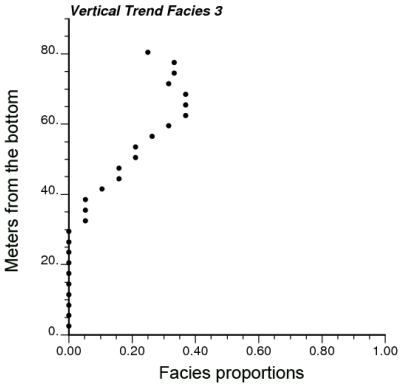

(c) Facies 3

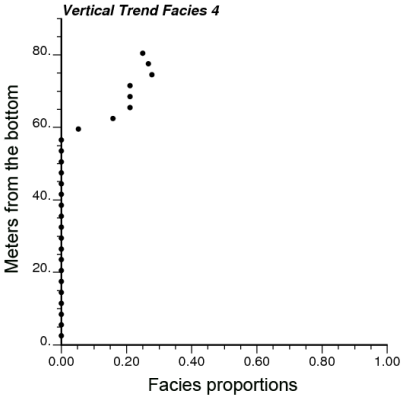

(d) Facies 4

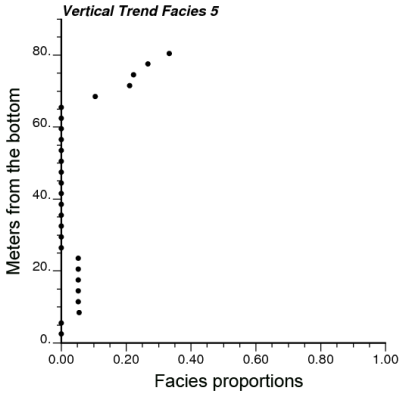

(e) Facies 5

Figure 3.1: Vertical trend of simulation models

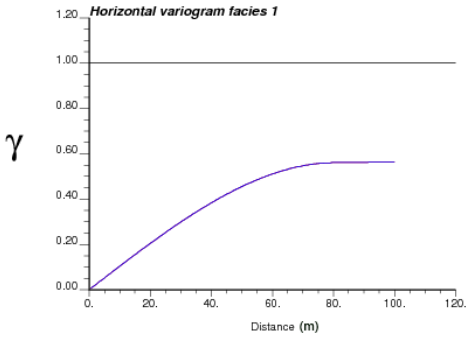

(a) Horizontal facies 1

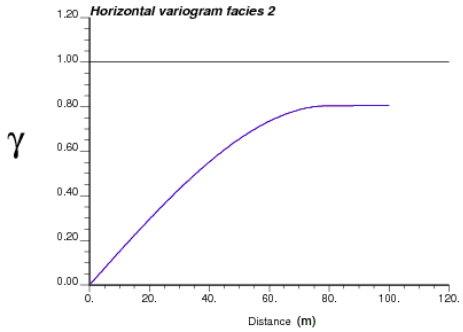

(b) Horizontal facies 2

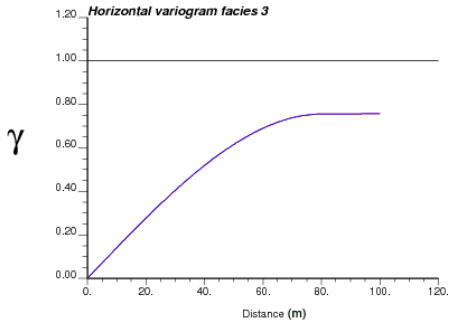

(c) Horizontal facies 3

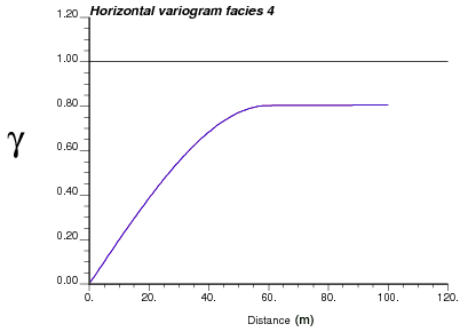

(d) Horizontal facies 4

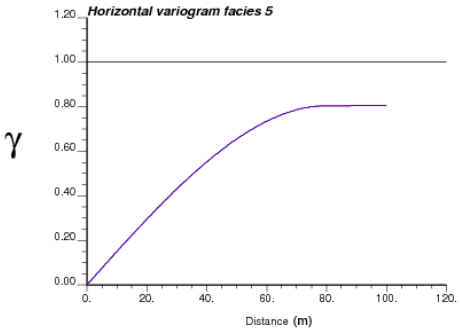

(e) Horizontal facies 5

Figure 3.2: Horizontal variograms for modeling different facies

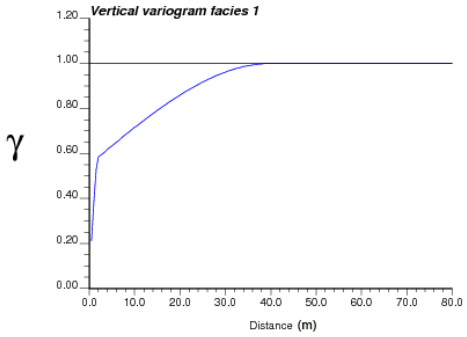

(a) Vertical facies 1

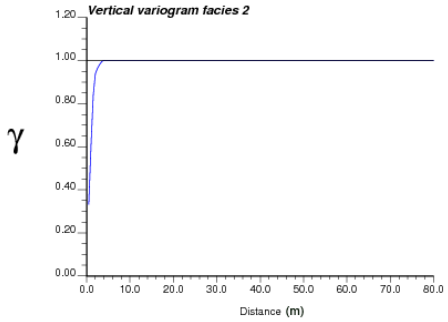

(b) Vertical facies 2

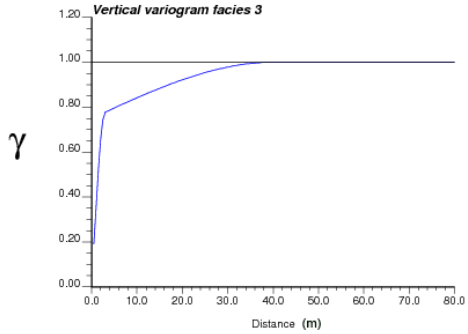

(c) Vertical facies 3

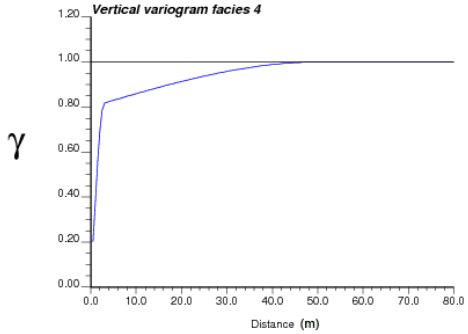

(d) Vertical facies 4

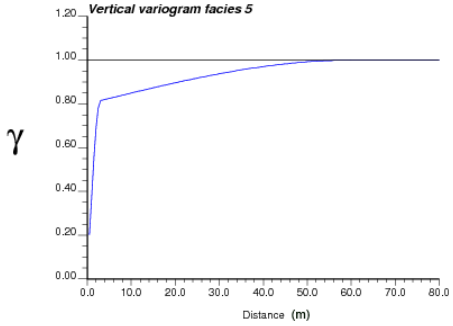

(e) Vertical facies 5

Figure 3.3: Vertical variograms for modeling different facies

yz plane after importing them to the simulation model. The realization appears reasonable because it is similar to the realistic models. permeability at the top part of the reservoir is significantly less than in the pay zone. Gas is present in the top five meters of the model and there is no gas in the pay zone or in the lower thief zone. There is little oil in the thief zone and the average porosity in the thief zone is less than the average of porosity in the pay zone.

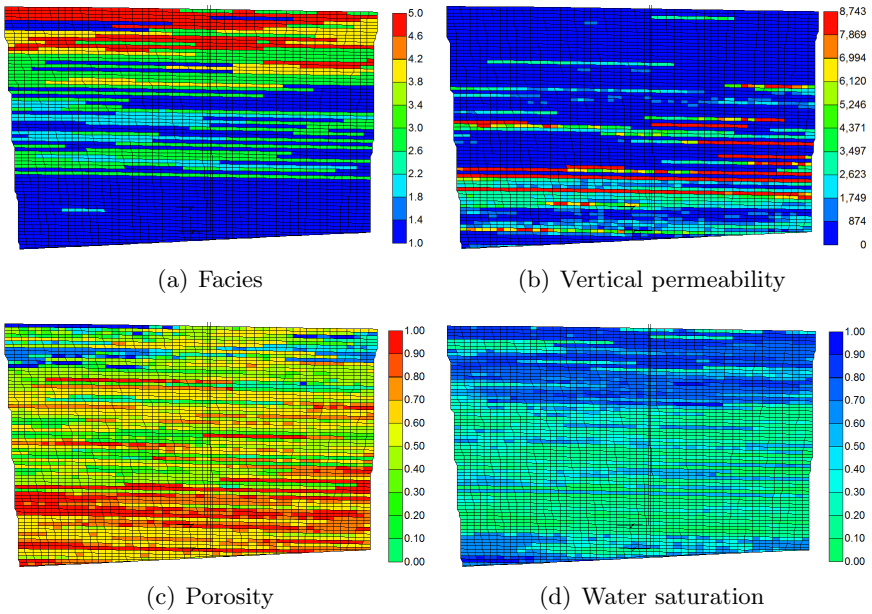

(a) Facies (b) Vertical permeability

(c) Porosity (d) Water saturation

Figure 3.4: Different properties of one of the generated realizations in yz plane – grid sizes in horizontal and vertical directions are 2.5 m and 1 m respectively

This procedure was repeated to generate 100 different realizations. The realizations have been ranked by CHV and then six of them ($P15$, $P30$, $P45$, $P60$, $P75$ and $P90$) based on the connectivity of grids to the producer have been selected for testing their SAGD performance with proxy. These six realizations were run with the STARS simulator (Computer Modeling Group Ltd., 2012) by assuming unlimited steam availability. The maximum bottom hole pressure for all of these cases is 3500 kpa. Fig. 3.5 shows the cumulative oil production and cumulative steam injection of these models for 23 years of production. There is a significant range of uncertainty between the models.

The proxy was applied to compute the performance at each time step.

1. Oil production rate and cumulative oil production

2. Steam injection rate and cumulative steam injection

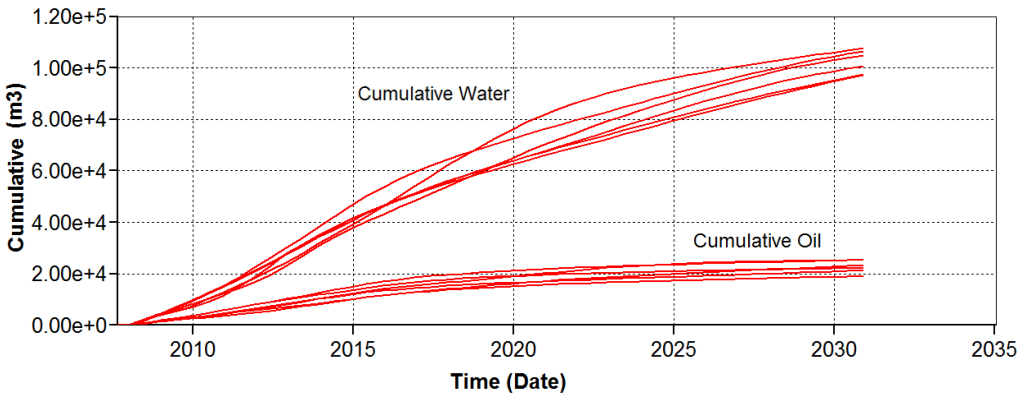

Figure 3.5: Uncertainty in the performance of generated realizations

3. Cumulative steam oil ratio (CSOR)

4. Steam temperature at injector completion

5. Steam pressure at injector completion

6. Steam interface position

Different operating strategies have been considered for testing the proxy flexibility. These operating strategies are:

1. Unlimited steam availability for injection

2. Limited steam availability for injection (set $Q_{inj,max}$)

3. Limited bottom-hole pressure (set $BHP_{inj,max}$)

4. Pressure trigger for consecutive pressure drops

5. ISOR trigger for dropping pressure after exceeding ISOR from a certain limit

6. Tapered pressure operating strategy

In all of these cases, only constraints on the injector changed. Injector constraints are 1- Maximum steam injection rate 2- Maximum bottom-hole pressure. The net cells were determined by a threshold of 5% for porosity and 20 md for permeability. The latest version of CHV (Wilde and Deutsch, 2012) was applied to obtain the different production steps and angles during the production.

In the next sections, SAGD performance of all of these 6 models have been tested by the proxy and results are compared with the simulator results. For some of these

models, above operating strategies have been applied for testing the proxy flexibility in changing the steam injection pressure by changing the operating strategy.

It is desirable to compare proxy results with the production data, but because these models are synthetic models and production data is not available, the proxy performance is compared with the reservoir simulator.

3.1.2 Synthetic 2D Model 1 with Different Operating Strategies

Unlimited Steam Availability

This first example considers unlimited steam availability case with 3 steps of production. Fig. 3.6 shows results of the first example.

Figs. 3.6(a)–3.6(b) show different steps and angle of steam interface during production. Blue color in Fig. 3.6(a) shows non-net grids with very low porosity and permeability. Also, the dark blue color in Fig. 3.6(b) shows rising periods at the start of different steps. Sometimes one step may have several starting points at different locations of the reservoir. In this example, step 2 has several starting points. Fig. 3.6(c) shows comparison between oil production rates and steam injection rates of the proxy and simulator. There are local differences which are unavoidable due to the complexity of reservoir simulator models. Fig. 3.6(d) shows comparison between cumulative oil production and cumulative steam injection of proxy and simulator. The cumulative oil production of the proxy is about 4% higher than simulator. Also, the cumulative steam injection of the proxy is less than 1% higher than the simulator which is within a reasonable tolerance. Figs. 3.6(e)–3.6(f) show a comparison between the CSOR and steam injection pressure of the proxy and simulator. The simulator CSOR is about 3% higher than the proxy which is also within a reasonable tolerance. The match between the steam pressure of the proxy and simulator is perfect due to the unlimited steam availability for injection. In this case, the steam injection pressure does not need to drop during the simulation.

Thief Zone Effect on the Steam Injection Rate

Thief zones contain cold water and as a result steam that enters the thief zone loses its heat very fast and is not heating bitumen. The heat loss to the overburden should use the rock properties of the thief zone instead of the overburden. As developed above, the thief zone can be separated from the pay zone by computing the bulk oil weight. Then, the average porosity and water saturation can be computed from the

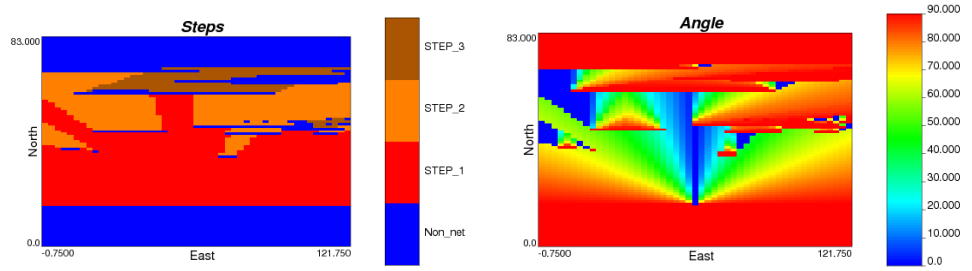

(a) Steps

(b) Angles

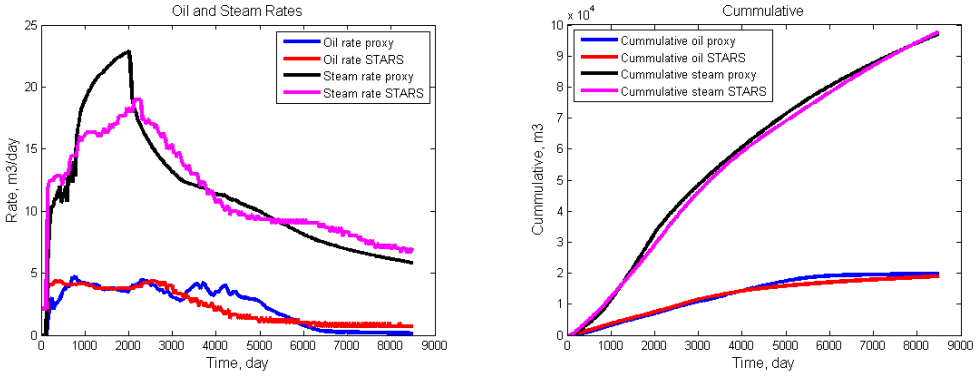

(c) Oil and steam rates

(d) Oil and steam cumulates

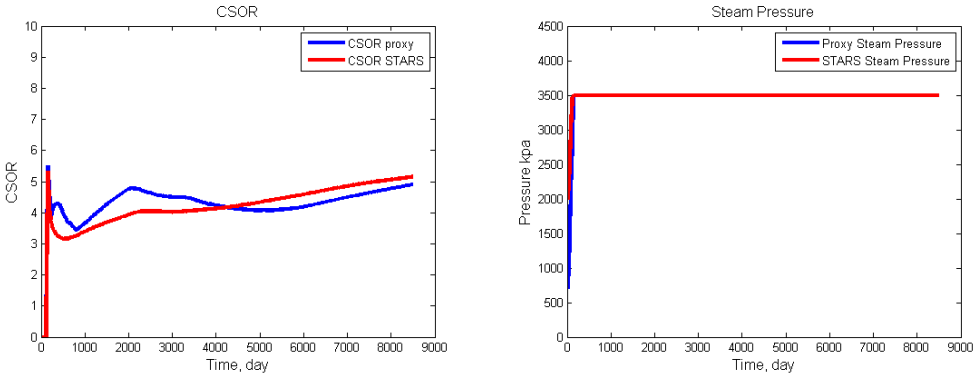

(e) Cumulative steam oil ratio

(f) Steam pressure

Figure 3.6: Comparison between results of proxy and simulator for model 1

grid cells inside the thief zone. The thermal diffusivity can then be calculated as:

$$\alpha = \frac{k}{\rho c} = \frac{k_w s_w \phi + k_o s_o \phi + k_r (1-\phi)}{(\rho c)_w s_w \phi + (\rho c)_o s_o \phi + (\rho c)_r (1-\phi)} \tag{3.1}$$

Fig. 3.7 shows bitumen and steam injection results for the first model without considering the effect of the thief zone.

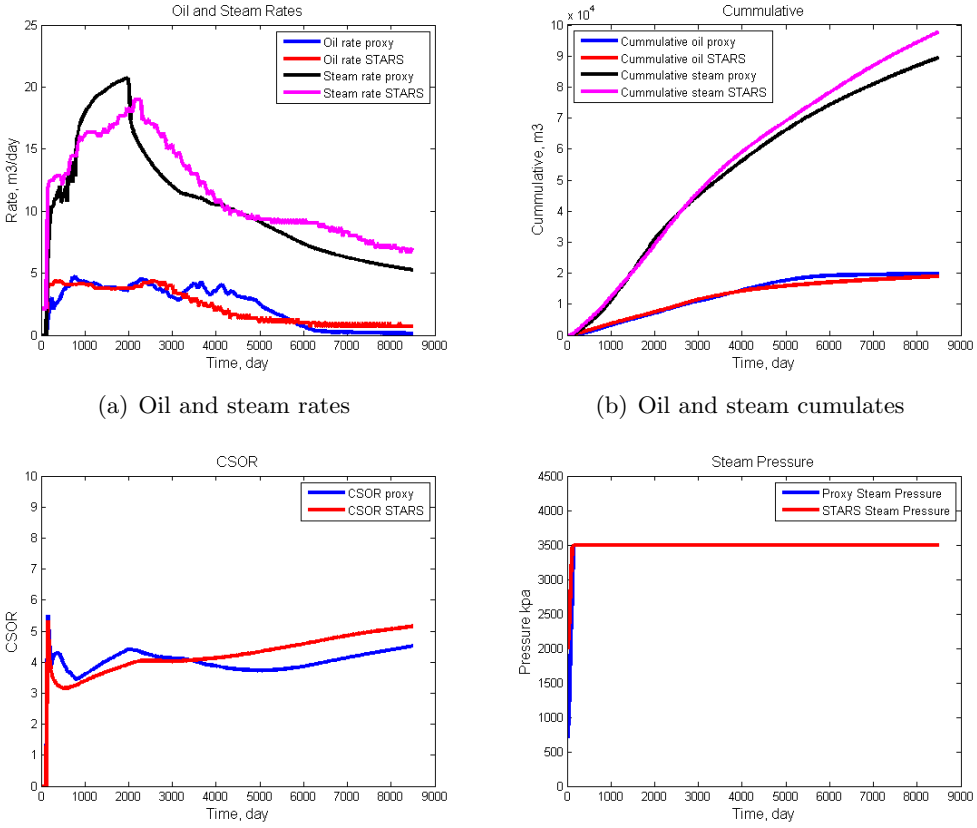

(a) Oil and steam rates

(b) Oil and steam cumulates

(c) Cumulative steam oil ratio

(d) Steam pressure

Figure 3.7: Comparison between the proxy and simulator for model 1 without considering thief zone effect on the steam injection rates

Fig. 3.7 shows that the predicted cumulative steam injection is less than the simulator. In this case, the cumulative oil production of the proxy is still about right, that is, 4% higher than the simulator, but the cumulative steam injection of the proxy is about 8% lower than simulator. As a result, the estimated CSOR of the proxy is about 12% less than the results of the simulator, which is becoming significant. Without considering effect of thief zone, the overburden thermal diffusivity is 0.11, but after separating thief zone, averaging properties and also computing new overburden thermal diffusivity, the new value of thermal diffusivity is about 0.2 which is significantly higher than the original value. As a result, heat loss to the

overburden will increase and effect of thief zone can be captured using this method. New results have been shown in the Figs. 3.6(c)–3.6(f)

Comparison between Butler Rising Model and New Rising Model

In the base case (Fig. 3.6), new rising model has been used instead of Butler's rising model for estimating the steam injection rate. Fig. 3.8 shows the results of first example using Butler's rising model instead of new rising model.

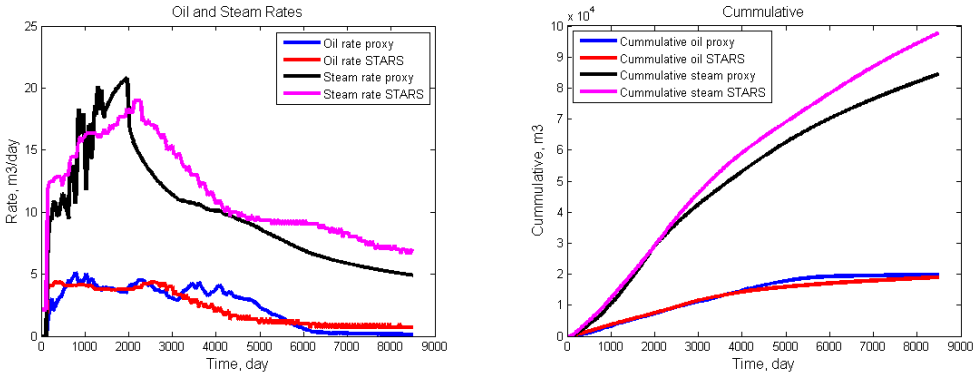

(a) Oil and steam rates

(b) Oil and steam cumulates

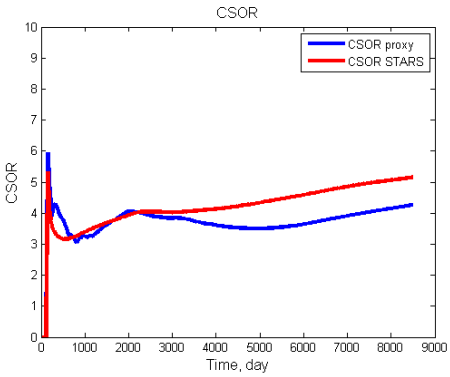

(c) Cumulative steam oil ratio

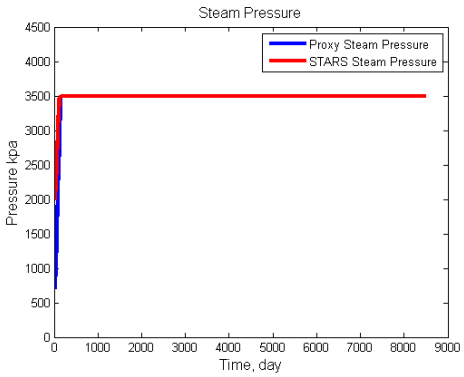

(d) Steam pressure

Figure 3.8: Comparison between results of proxy and simulator for model 1 using Butler rising model instead of the new rising model

The rate of steam rise of Butler's rising model is slower than the new rising model and may underestimate cumulative steam injection due to the wrong estimation of end of rising time. The rate of increasing height of the new model is about 1.8 times that of Butler's rising model and end of rising in new model is close to the simulation results which is at about 500 days. Figs. 3.8(a)–3.8(b) shows decreasing steam injection rate compare to the Figs. 3.6(c)–3.6(d) where the new rising model was used. Butler's rising model reduces steam injection of proxy is about 13% less

than the simulator results which is significant. Oil production is the same as before, because estimating cumulative heat loss affects the steam injection rate not the oil production rate. In the current proxy, the steam pressure will change based on the constraints on the injector and in this case we assumed that unlimited steam is available for injecting into the reservoir, as a results, as Fig. 3.8(d) shows that the steam injection pressure is constant and did not drop during the simulation. Also Fig. 3.8(c) shows that the proxy CSOR is about 17% less than the simulator CSOR. Thus, ignoring the thief zone effect can cause a significant error in the estimations.

Naïve Butler Model

Figs. 3.6(a)–3.6(d) show the results of the new proxy by adding all of new options. In this example, results of naïve Butler model without those options have been considered for comparison. Fig. 3.9 shows the new proxy results using Butler's original model.

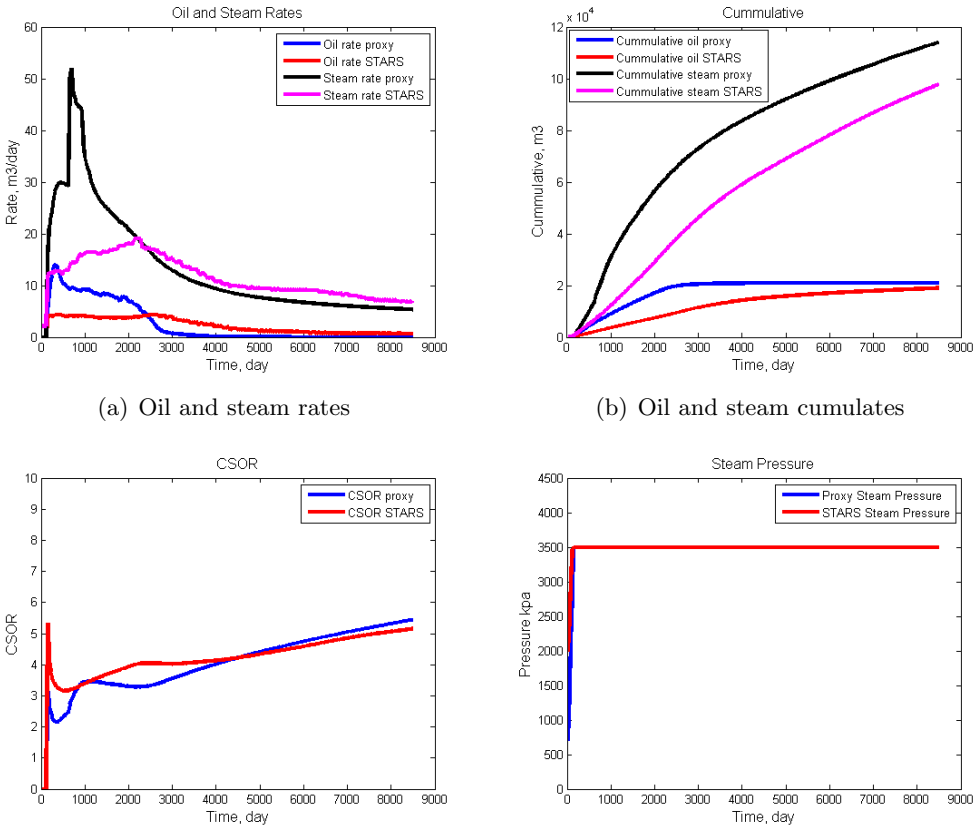

(a) Oil and steam rates

(b) Oil and steam cumulates

(c) Cumulative steam oil ratio

(d) Steam pressure

Figure 3.9: Comparison between results of proxy and simulator for model 1 using naïve Butler model

In this case, all of new options such as new rising model, relative permeability computation, effect of thief zone on estimating overburden thermal diffusivity and identifying the pay zone and neglecting oils in the non-connected grids to the producer have been deactivated. Without considering these effects, as Figs. 3.9(a)–3.9(b) show, both oil production rates and steam injection rates are higher than the simulator. By neglecting the relative permeability effect, the average permeability would be very high and the steam interface in the proxy moves very fast and sweeps all of oil in the reservoir (even thief zone) after about 3000 days. In this case, the cumulative oil production of the proxy is about 10% more than simulator and final cumulative steam injection of proxy is about 17% more than the simulator. The estimate of the CSOR as shown in Fig. 3.9(c) is only about 6% higher than the simulator which is due to overestimating both oil production and steam injection rates. Although the final CSOR is close to the simulator results, but these results are not good for computing NPV or transferring uncertainty. In Butler's original theory, different operating strategies cannot be tested, because this method only works with unlimited steam availability.

In the last example, there was no limitation for steam injection rate and we assumed that unlimited steam is available for injecting into the reservoir. Sometimes, there is a limit for available amount of steam for injection. For this reason, different constraints should be set on the injector. These constraints are maximum allowable steam injection rate and maximum allowable bottom-hole pressure. These constraints can lead to completely different results. This is shown in the following examples.

Operating Strategy 1 – Limited Steam Injection Rate

The maximum steam injection rate has been set to 10 m^3/day and maximum bottom-hole pressure has been set at 3500 kpa to see how the proxy changes the pressure. Fig. 3.10 shows a comparison between results of the proxy and simulator for this example.

As Fig. 3.10 shows, the cumulative steam injection is very close to the simulator and except the last three years, steam is injected at maximum allowable rate. There should a balance between computed steam injection rate (based on the total heat loss) and the available steam at each time step. If computed steam injection rate is above the limit, the proxy decreases the steam pressure to keep the balance between

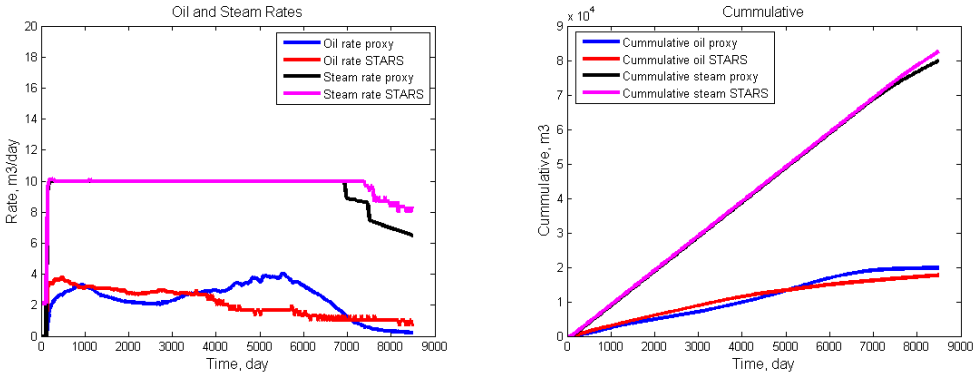

(a) Oil and steam rates

(b) Oil and steam cumulates

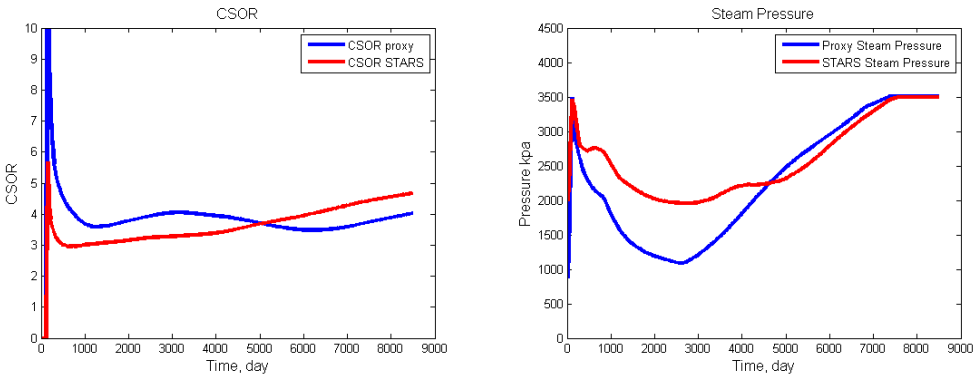

(c) Cumulative steam oil ratio

(d) Steam pressure

Figure 3.10: Comparison between results of proxy and simulator for model 1 by limiting steam injection rate

computed steam injection rate and available steam for injection, but if the computed steam injection rate is below the limit, the proxy increases the steam pressure to keep this balance. In this case, steam pressure cannot be higher than the maximum bottom-hole pressure which is 3500 kpa. If steam pressure is equal or above the 3500 kpa and the computed steam injection rate is below the limit, the steam pressure cannot be increased anymore.

As Fig. 3.10 shows, the steam injection pressure of the proxy and the simulator do not match completely, but at least trends are the same and the proxy identified that steam injection pressure should be decreased or increased. It seems that the proxy dropped the pressure more than the simulator. This could be due to the difference in the methods that the proxy and simulator are using for computing PVT properties, steam pressure and etc. For example, the proxy is using correlations for computing steam injection pressure, but the simulator is using a steam table which is more accurate. In this case, the match between the steam rates is close but the match between the oil rates is less than satisfactory. Also, final cumulative oil production of the proxy is about 11% more than the simulator result and the final cumulative steam injection of proxy is about 3% less than the simulator result. Finally, the final CSOR of the proxy is about 13% less than the simulator result.

Operating Strategy 2 – Limited Bottom-hole Pressure

Again model 1 has been used, but in this case, the maximum steam injection rate is kept constant equal to 100 m^3/day and the maximum bottom-hole pressure has been set for the injector. The maximum bottom-hole pressure has been changed from 3500 kpa to 2300 kpa after 3000 days. The pressure changes in the simulator will not happen suddenly. For example it may take 6 months to reach to the new steam injection pressure. The same approach was used in the proxy during pressure changes. Fig. 3.11 shows comparison between the results of the proxy and the simulator for this example.

As Fig. 3.11 shows, the steam injection pressures are matched very closely and other results are reasonable. The final cumulative steam injection and cumulative oil production are very close to the each other and rates are also very close. It seems that the proxy steam front during the rising period moved a little slower than the simulator and also the proxy steam injection rate during spreading was a little higher than the simulator. The final CSOR values are very close. In this case, the

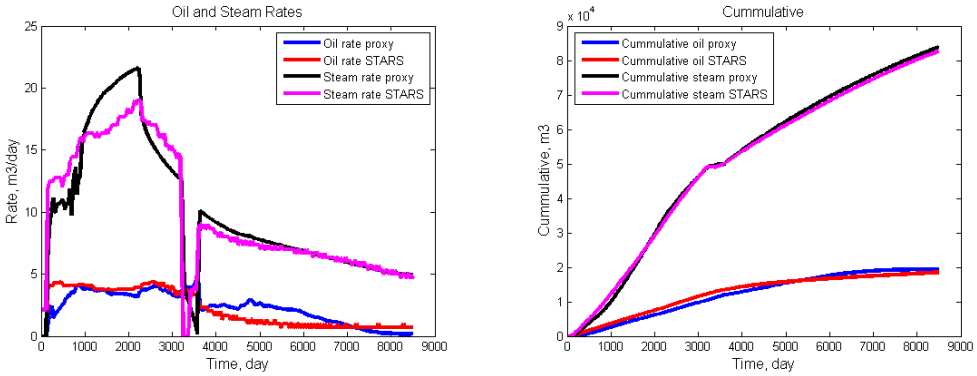

(a) Oil and steam rates

(b) Oil and steam cumulates

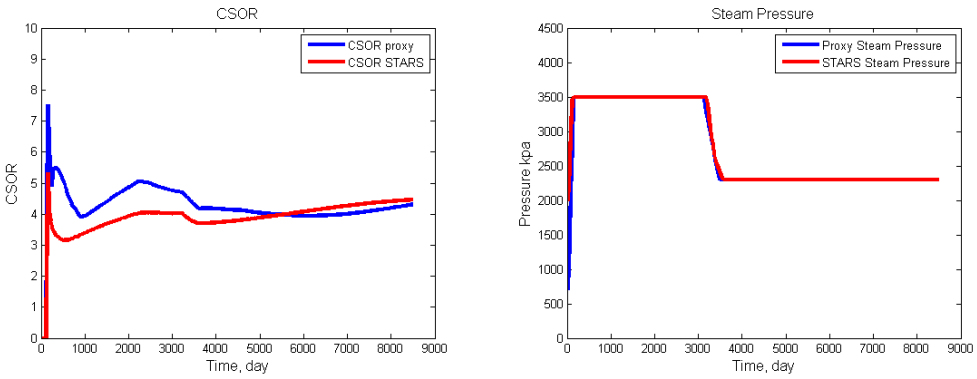

(c) Cumulative steam oil ratio

(d) Steam pressure

Figure 3.11: Comparison between results of proxy and simulator for model 1 by changing bottom hole pressure

final cumulative oil production of the proxy is about 4% more than simulator result and final cumulative steam injection of proxy is about 1% more than the simulator result. Also the final CSOR of the proxy is about 3% less than the simulator result. These results are very close given the many modeling assumptions and the precision required in the final forecasts.

Operating Strategy 3 – Pressure Trigger

For this operating strategy, the pressure trigger has been set on the first model. The trigger starts working at 700 days and drop pressure $n = 19$ times by 100 kpa for 6 months. The pressure trigger is very important for dropping the pressure to avoid steam entering the thief zone. The pressure trigger causes a significant decrease in the final cumulative steam injection compared to the base case (unlimited steam availability), but the final cumulative oil production would be close to the base case. Fig. 3.12 shows a comparison between the results of the proxy and simulator for this example.

As Fig. 3.12 shows, the steam injection pressures are completely matched and cumulative results are close to the each other. Again, the proxy steam front during rising period moved slower than the simulator. Also the proxy steam injection rate during spreading is a little higher than the simulator. Except for the first couple of years, the CSOR forecasts are very close. The mismatch between CSOR in the first years is related to the slower movement of the proxy steam front compared to the simulator. The final cumulative oil production of the proxy is about 7% more than the simulator result and the final cumulative steam injection of the proxy is about 2% more than the simulator result. As a result, the final CSOR of the proxy is about 5% less than the simulator result. For a fast proxy these differences seem to be reasonable.

Operating Strategy 4 – ISOR Trigger

In this case, the ISOR trigger has been tested on the first model. ISOR trigger will start working at 400 days and drop pressure $n = 19$ times by 100 kpa for 6 month if the ISOR exceed a certain limit which is 3.5 in this case. The ISOR trigger causes significant decrease in the final cumulative steam injection compared to the base case, but the final cumulative oil production remains close to the base case. This is the most difficult type of operating strategy and finding a good match between

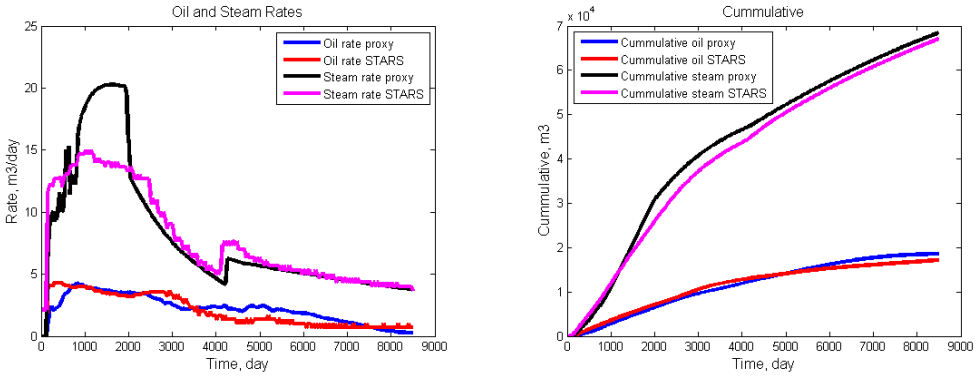

(a) Oil and steam rates

(b) Oil and steam cumulates

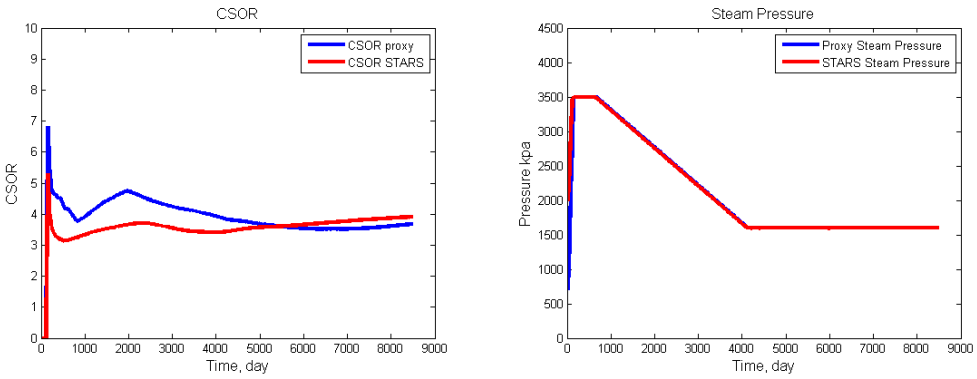

(c) Cumulative steam oil ratio

(d) Steam pressure

Figure 3.12: Comparison between results of proxy and simulator for model 1 using pressure trigger

results of the proxy and simulator is very difficult. Fig. 3.13 shows the results of this case.

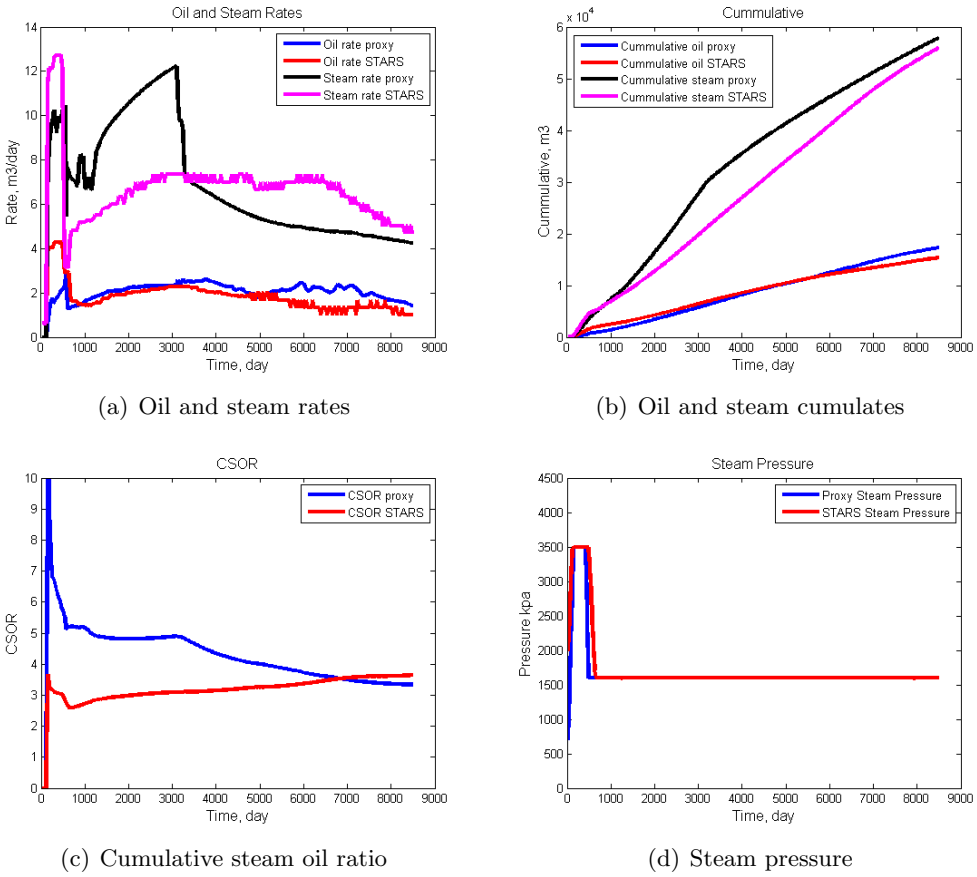

(a) Oil and steam rates

(b) Oil and steam cumulates

(c) Cumulative steam oil ratio

(d) Steam pressure

Figure 3.13: Comparison between results of proxy and simulator for model 1 using ISOR trigger

As Fig. 3.13 shows, the final cumulative steam injection of the proxy is close to the simulator, but the match between the steam injection rates does not appear satisfactorily close. This is due to overestimating the steam injection rate before 3000 days and underestimating the steam injection rate after that time. The cumulative oil production of the proxy is close to the simulator. The final CSOR values are close to the each other. The final cumulative oil production of the proxy is about 12% more than the simulator result and the final cumulative steam injection of the proxy is about 4% more than the simulator result. Also the final CSOR of the proxy is about 8% less than the simulator result.

In this case, the trigger dropped the pressure very fast to avoid contacting the steam with the thief zone, but in the case of the proxy, steam contacted the thief

zone faster leading to greater heat loss to the overburden. This led to a higher steam injection rate compared to the simulator. There are also some shale barriers in the middle of the reservoir that slow the steam rise to, the top of the thief zone and as a result cumulative steam is significantly less than the proxy. Fig. 3.14 shows grids with very low vertical permeability (less than 100 md) in the reservoir.

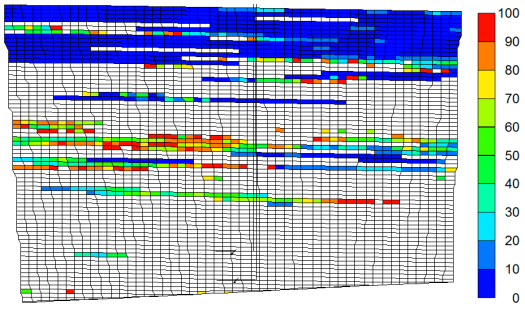

Figure 3.14: Grid cells with vertical permeability of less than 100 md in yz plane – grid sizes in horizontal and vertical directions are 2.5 m and 1 m respectively

As Fig. 3.14 shows, in the middle of the reservoir, vertical permeability is very low. Normally, injected steam with 3500 kpa can go through these low permeability zones without any problem (same as base case of model 1), but not in this case because steam pressure drops to a low 1600 kpa. As a result, oil above these areas is not produced and the heat loss to the overburden is reduced significantly. Fig. 3.15 shows ternary diagram and also reservoir temperature at the end of the simulation.

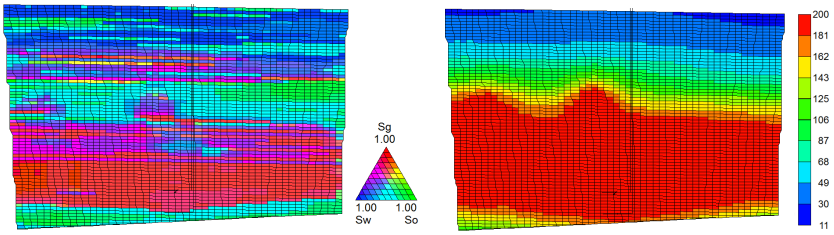

(a) Ternary diagram (b) Reservoir temperature

Figure 3.15: Ternary diagram and reservoir temperature at the end of the simulation in yz plane – grid sizes in horizontal and vertical directions are 2.5 m and 1 m respectively

As Fig. 3.15(a) shows, the location of the steam chamber can be identified when the percentage of gas saturation is high. The steam has not reached the thief zone at the top of the reservoir. For these reasons, the match between the proxy and simulator is not that good.

3.1.3 Synthetic 2D Model 2 with Different Operating Strategies

Unlimited Steam Availability

Fig. 3.16 shows a comparison between the proxy and simulator results for the second model. All of the operating strategies are the same as the first model presented above. The only difference is the heterogeneity of these models.

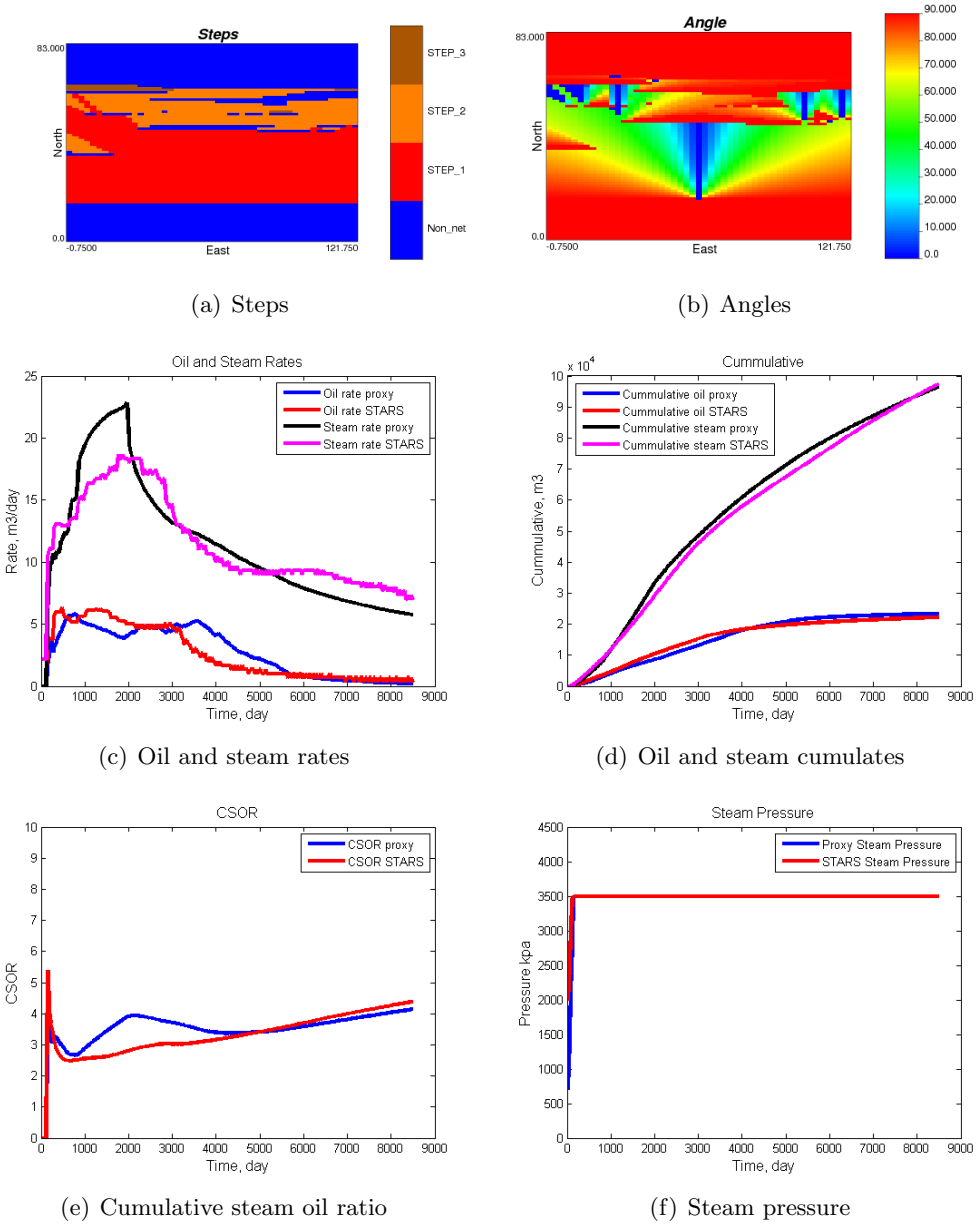

(a) Steps

(b) Angles

(c) Oil and steam rates

(d) Oil and steam cumulates

(e) Cumulative steam oil ratio

(f) Steam pressure

Figure 3.16: Comparison between results of proxy and simulator for model 2

As Fig. 3.16(a) shows, three steps of production can be observed, but the third step is only for a small number of grid cells which are close to the top. As a result,

oil of these grids will only be produced after a long time. Different rising periods can be recognized in Fig. 3.16(b) with a dark blue color. As Figs. 3.16(c)–3.16(e) show, a good match between the results of the simulator and proxy can be observed. Final cumulative oil production of the proxy is about 4% more than simulator result and the final cumulative steam injection of the proxy is about 1% less than the simulator result. There is a little mismatch between steam injection rates of the simulator and proxy and it seems that steam injection rates in the proxy are overestimated for the spreading period before starting the confinement. This could be due to the existence of a large barrier above the well pair. In this case, the simulator heat loss to the overburden would be zero for a longer time and as a result, the proxy heat loss to the overburden and also steam injection rate would be more than the simulator, because the proxy does not consider the effect of the barriers in the same manner. The final CSOR of the proxy is about 5% less than the simulator result which is a reasonable difference for proxy. Due to the unlimited steam availability, as Fig. 3.16(f) shows, the steam injection pressure did not drop during the simulation.

Tapered Pressure Operating Strategy

In this case, model 2 has been used to check the tapered pressure operating strategy. In this case after 3000 days, the pressure is dropped by 100 *kpa* per year. This operating strategy is similar to the pressure trigger. Fig. 3.17 shows the results of the tapered pressure operating strategy.

As Fig. 3.17 shows, the cumulative steam injection drops in the last years due to dropping pressure. Similar to the trigger case, this operating strategy decreased cumulative steam injection significantly. It seems that the final cumulative steam injection of the proxy is higher than the simulator which is due to the higher steam injection rate of the proxy compared to simulator in the last two years. The rates, CSOR and steam injection pressures are very close. The final cumulative oil production of the proxy is about 6% more than the simulator result and the final cumulative steam injection of the proxy is about 7% more than the simulator result. As a result, the final CSOR of proxy is about 1% more than the simulator result.

3.1.4 Synthetic 2D Model 3 with Unlimited Steam Availability

Fig. 3.18 shows the third model with a different heterogeneity for reservoir parameters.

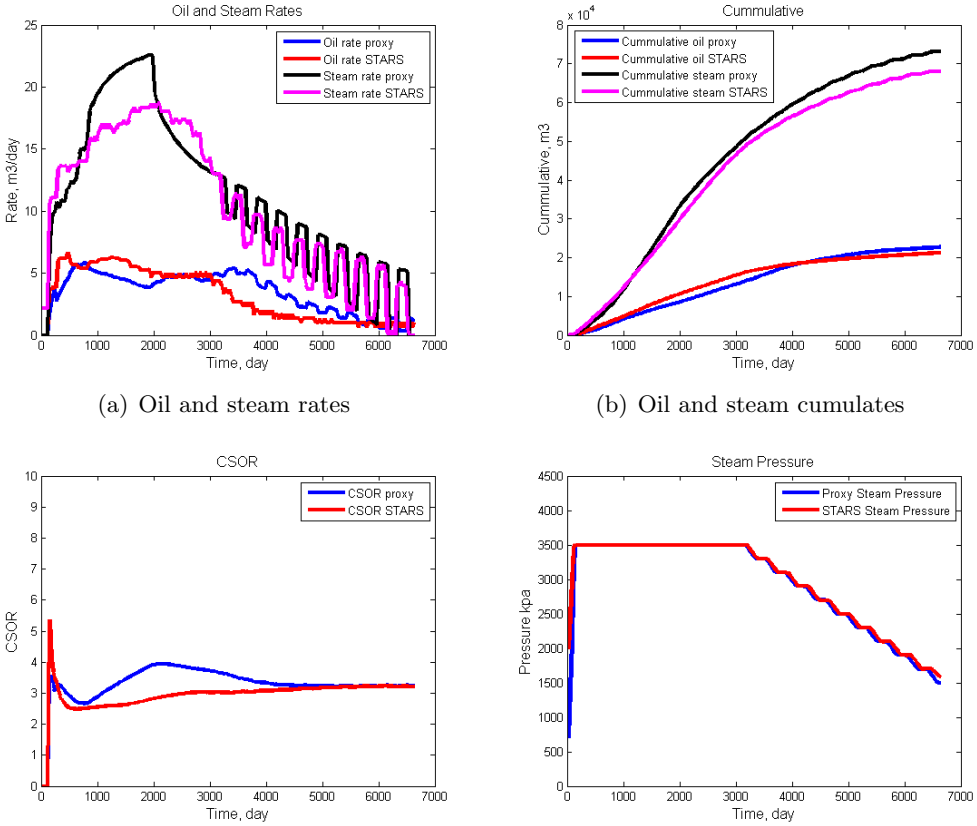

(a) Oil and steam rates

(b) Oil and steam cumulates

(c) Cumulative steam oil ratio

(d) Steam pressure

Figure 3.17: Results of model 2 using tapered pressure operating strategy

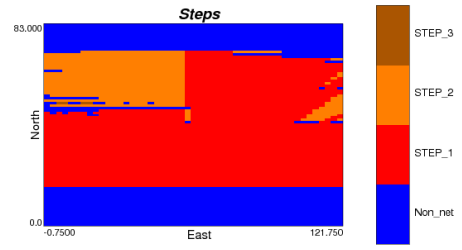

(a) Steps

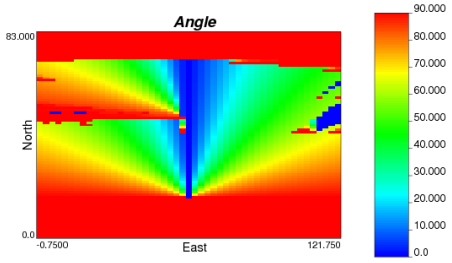

(b) Angles

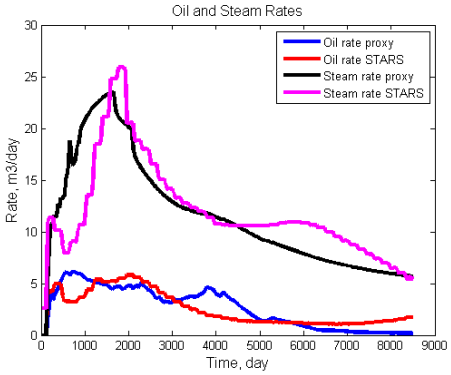

(c) Oil and steam rates

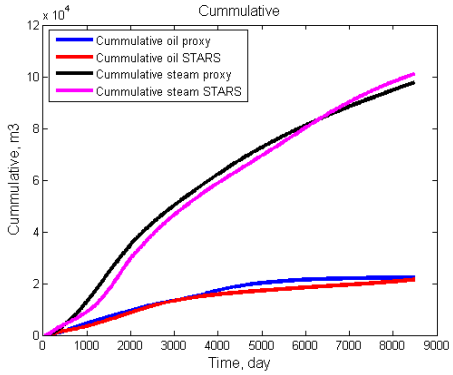

(d) Oil and steam cumulates

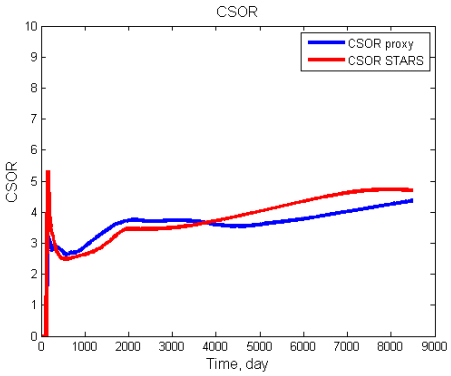

(e) Cumulative steam oil ratio

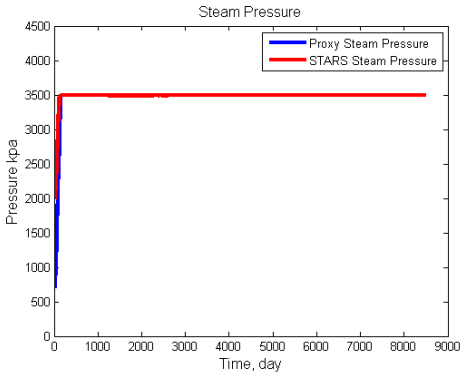

(f) Steam pressure

Figure 3.18: Comparison between results of proxy and simulator for model 3

Fig. 3.18(a) shows two steps of production. Starting points of these two steps have been shown by a dark blue color in Fig. 3.18(b). The existence of large barriers above the wells at low elevations cause differences between steam front velocities, heat losses and steam injection rates between the proxy and simulator. In this case, the cumulative steam results of the simulator and proxy cross each other. As a result, before steam contacts the barrier, the steam injection rate of the simulator would be lower than the proxy which is due to the delay in the heat loss to the overburden, but after that, the steam injection rate will increase significantly because steam at the same time covers a large area of overburden. Also at the time that steam contacts the barrier, the oil production rate of the simulator decreases because a temporary spreading period will start and oil production rates during the spreading period is lower than the rising period. As a result, the oil production rate decreases up to the time that steam passes the barrier and starts another rising period. Then, the oil production rate of the simulator will increase. As Figs. 3.18(c)–3.18(e) show, there is a good match between results of the simulator and proxy. The final cumulative oil production of the proxy is about 3% less than the simulator result and the final cumulative steam injection of the proxy is about 2% less than the simulator result. Thus, the final CSOR of the proxy is about 6% less than the simulator result. Steam injection rates of the proxy and simulator did not match completely and it seems this it is due to the faster steam chamber movement in the proxy during the rising and spreading periods compare to the simulator. Again, due to the unlimited steam availability, the steam injection pressure did not drop as shown in Fig. 3.18(f).

3.1.5 Synthetic 2D Model 4 with Unlimited Steam Availability

Fig. 3.19 shows results for the fourth model. Fig. 3.19(a) shows three steps of production. Again, the starting points of these two steps have been shown by dark blue color in Fig. 3.19(b).

As Figs. 3.19(c)–3.19(e) show, the match between the cumulative oil production of the proxy and simulator is close although there are local variations due to heterogeneity in the reservoir. The final cumulative oil production of the proxy is about 2% less than the simulator result. The match between the steam injection (both rates and cumulative) of the simulator and proxy are not as close as expected. Again this is due to the existence of large barriers at different elevations above the wells. These barriers cause a decrease in the oil and steam rates of the simulator. In

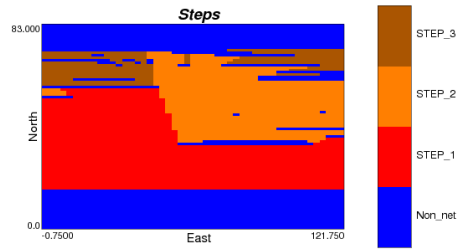

(a) Steps

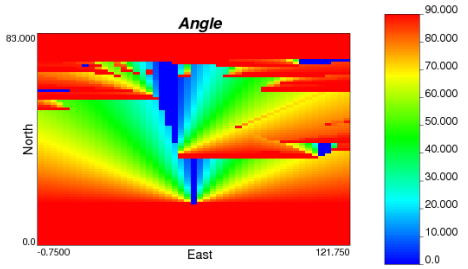

(b) Angles

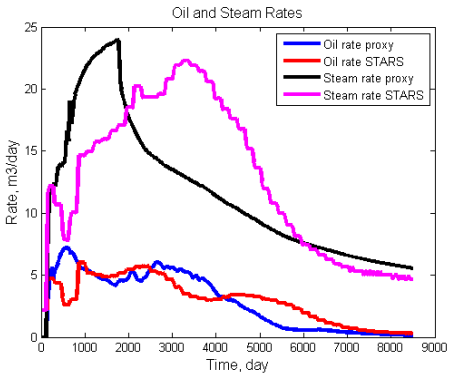

(c) Oil and steam rates

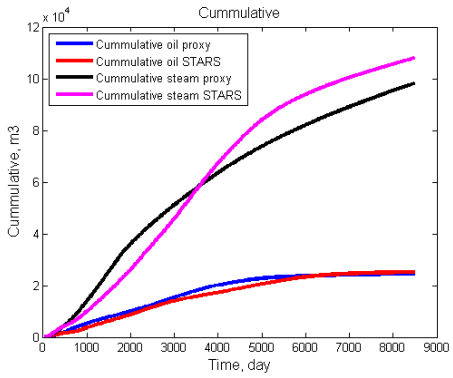

(d) Oil and steam cumulates

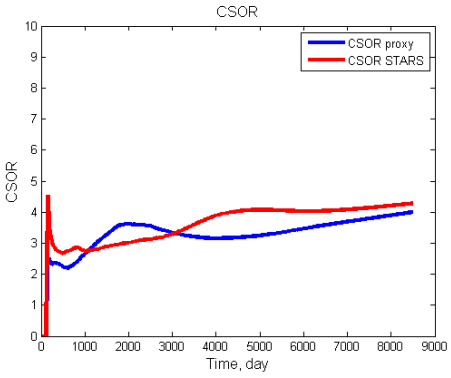

(e) Cumulative steam oil ratio

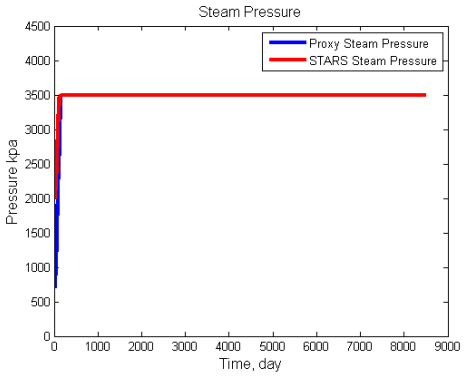

(f) Steam pressure

Figure 3.19: Comparison between results of proxy and simulator for model 4

this case, the rising period of the simulator ends with a delay, but because the proxy only considers rising, spreading and confinement periods, these types of barriers do not have any effect on the proxy results. The final cumulative steam injection of the proxy is about 8% less than the simulator. The final CSOR of proxy is about 6% less than the simulator result. Again, due to the unlimited steam availability, the steam injection pressure did not drop as seen in Fig. 3.19(f).

3.1.6 Synthetic 2D Model 5 with Unlimited Steam Availability

Fig. 3.20 shows the fifth model with another model of heterogeneity. This example is very similar to the fourth example and there is a large barrier at a low elevation above the well that causes differences in forecasts from the proxy and simulator. Again three steps of production can be identified in the Fig. 3.20(a), but the third step is very short and just related to a small number of grid cells.

As Figs. 3.20(c)–3.20(e) show, the match between the oil production rates and steam injection rates are not particularly close. That large barrier caused differences between the oil and steam rates at different periods of production. Although the final cumulative oil production of both proxy and simulator are close, the rates are different. The final cumulative oil production of the proxy is about 2% less than simulator result and the final cumulative steam injection of the proxy is about 6% less than the simulator result. Again in this example, the CSOR results are close; the proxy is about 4% less than the simulator.

3.1.7 Synthetic 2D Model 6 with Unlimited Steam Availability

Fig. 3.21 shows the sixth model which has two steps of production. There are two steps of production and there is a large barrier on one side of the reservoir at low elevation and another one at high elevation. As Fig. 3.21(b) shows, the large barrier at low elevation does not have any effect on the rising period. The smaller barrier at a high elevation (close to the thief zone) is not horizontally continuous and it does not have a significant effect on the results.

the barrier close to the thief zone causes a slight delay is the end of the rising period in the simulator. The difference in the steam front velocities of the proxy and simulator during the spreading and confinement and also the delay at the end of rising period caused some difference in the results. The final cumulative oil production of the proxy is about 5% less than the simulator and the final cumulative

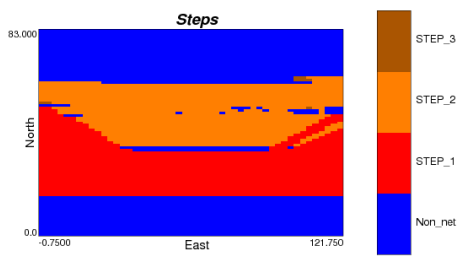

(a) Steps

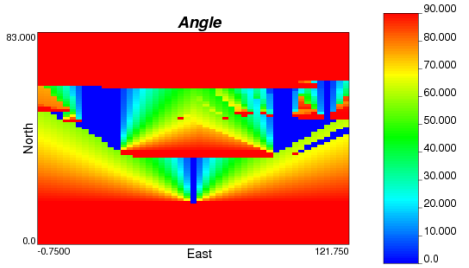

(b) Angles

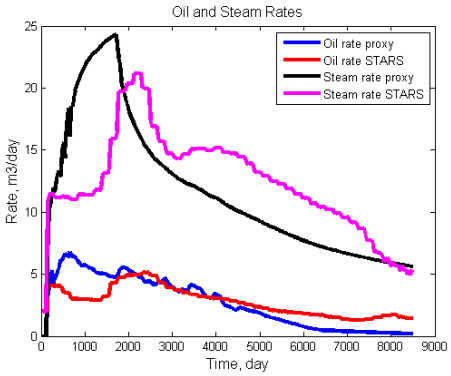

(c) Oil and steam rates

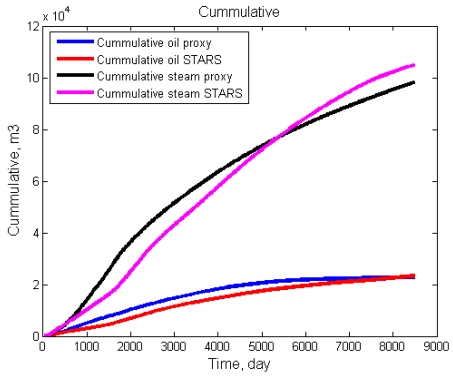

(d) Oil and steam cumulates

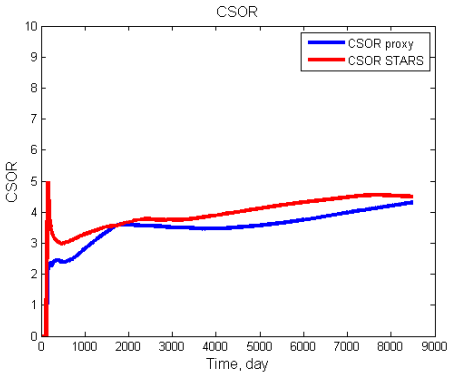

(e) Cumulative steam oil ratio

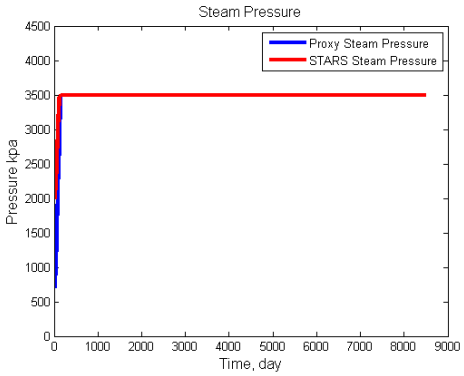

(f) Steam pressure

Figure 3.20: Comparison between results of proxy and simulator for model 5

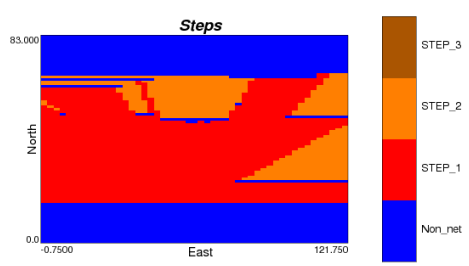

(a) Steps

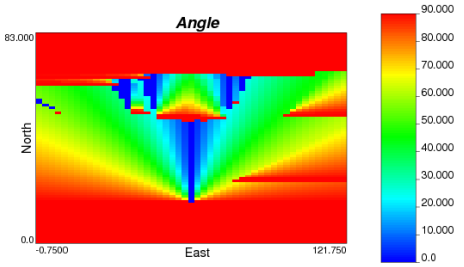

(b) Angles

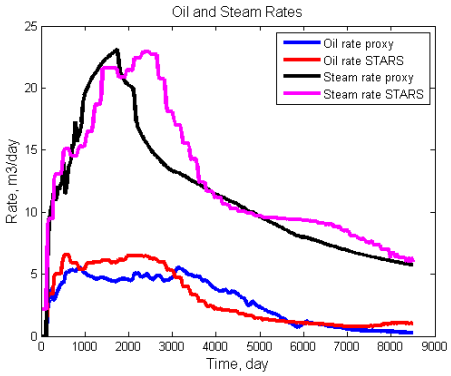

(c) Oil and steam rates

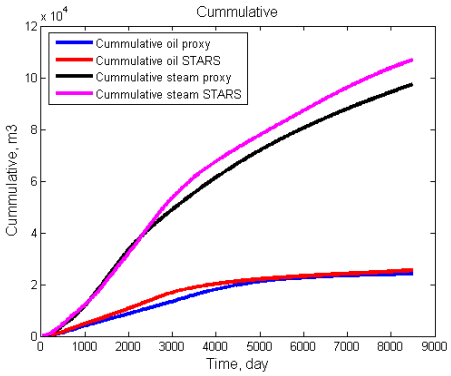

(d) Oil and steam cumulates

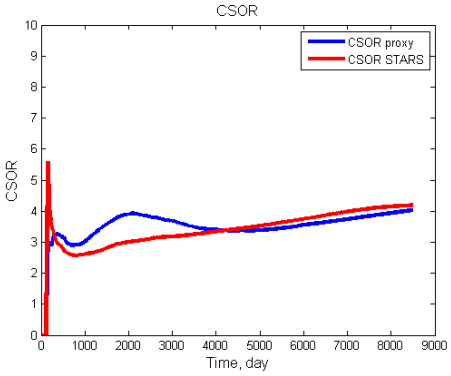

(e) Cumulative steam oil ratio

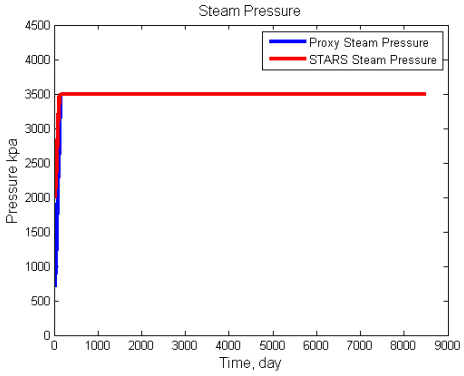

(f) Steam pressure

Figure 3.21: Comparison between results of proxy and simulator for model 6

steam injection of the proxy is about 8% less than the simulator. Also, the final CSOR of the proxy is about 3% less than the simulator. These differences are very minor.

In the last example, matches between results of simulator and proxy were not perfect, but optimization methods can be used to automatically calibrate results. For calibration, the SQP method has been used to calibrate the calibration parameters automatically (Dehdari and Oliver, 2012; Dehdari et al., 2012). Five different parameters have been selected for calibration. Three of them are for calibrating oil production results, and two of them are for calibrating steam injection results. The oil calibration parameters are the steam interface velocity multiplier for rising, spreading and confinement periods. The steam calibration parameters are the overburden thermal diffusivity multiplier and another multiplier for the volumetric heat capacity of steam chamber.

The objective function for calibration is the mismatch between the results of the proxy and simulator. All parameters can be calibrated at the same time and objective function can be set equal to mismatch between CSOR of proxy and simulator, or mismatch between cumulative oil and steam of them. Also, these parameters can be calibrated in two stages. In the first stage, only steam front velocities are calibrated by selecting objective function as mismatch between cumulative oil of proxy and simulator, and then in the second stage, the remaining two parameters related to the steam injection results can be matched by selecting objective function as mismatch between cumulative steam injection, or CSOR of proxy and simulator. Calibrating the oil parameters can change the steam results significantly, but calibrating steam results has a minor effect on the oil production rates in the case of limited steam availability. As a result, selecting the objective function and number of stages in the optimization depends highly on the case that should be optimized.

In the next examples, results of model six have been calibrated with two methods 1- Calibrate all parameters at the same time by selecting objective function as mismatch between cumulative oil and cumulative steam of proxy and simulator 2- Calibrate parameters in two stages, that is, first calibrating the oil parameters and then calibrating the steam parameters.

Calibrating All Parameters at the Same Time without Giving Weights to the Objective Function

In the first calibration example, all of parameters have been calibrated at the same time. Fig. 3.22 shows the results of simultaneous calibration of all of parameters at the same time.

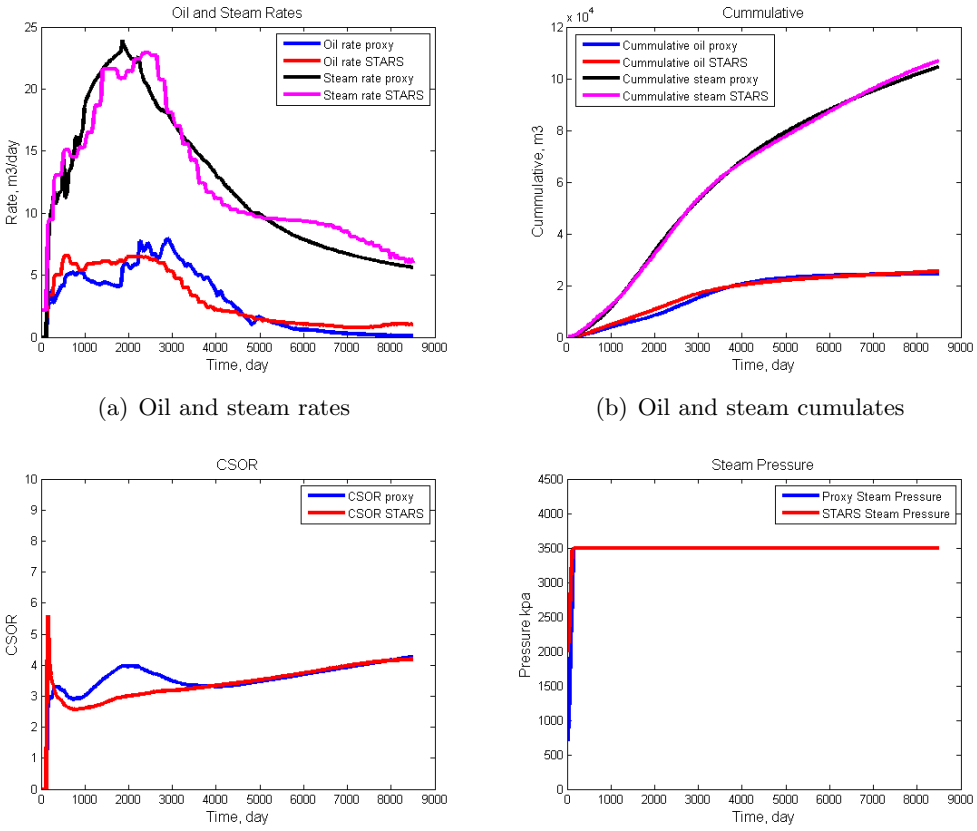

(a) Oil and steam rates

(b) Oil and steam cumulates

(c) Cumulative steam oil ratio

(d) Steam pressure

Figure 3.22: Simultaneous calibration of parameters of model 6 – no weights

In calibration, the effect of heterogeneity can be captured in the proxy model by changing the steam front velocities at different production periods. As shown in Fig. 3.21(a), it seems that the simulator steam front during confinement period moved faster than the proxy and it caused decreasing steam injection rates of proxy compare to the simulator. As a result, a higher velocity for proxy steam front velocity is expected after calibration. The match between the results of the simulator and proxy during rising and spreading periods were satisfactory, for this reason, we do not expect any changes for these periods. As Fig. 3.22 shows, the match between the results after calibration are better than before calibration. In this case, the final

cumulative oil production of the proxy is about 3% less than the simulator and the final cumulative steam injection of the proxy is less than 1% more than the simulator. Thus, the final CSOR of the proxy is about 2% more than the simulator. It can be interesting to look at the values of calibrated parameters to see if changes are reasonable or not. Table. 3.1 shows initial and final values of calibrated parameters.

Table 3.1: Values of calibration parameters using SQP method as optimization algorithm – all parameters at the same time – no weight

	V_r **mult.**	V_s **mult.**	V_c **mult.**	α_{ob} **mult.**	VHC **mult.**
Initial	1.0	1.0	1.0	1.0	1.0
Final	0.976	0.938	1.483	1.0	0.744

As Table. 3.1 shows, the rising and spreading velocity multipliers are very close to 1.0, but confinement velocity multiplier increased to increase the front velocity to match the steam injection rates of the proxy with the simulator. This is what we expected even before calibration. The thermal diffusivity multiplier did not change and the volumetric heat capacity has been decreased a little bit to find a better match between results of simulator and proxy. SQP is a very fast and robust gradient based algorithm for optimizing parameters. For this 2D case, the total calibration time using time step size of 10 days was about 1 minute, which is very fast. Fig. 3.23 shows the change in the objective function versus the number of proxy runs for finding an optimal solution using SQP optimization algorithm.

As Fig. 3.23 shows, the initial objective function was $1.89E+7$ and after two iterations and about 20 runs, the objective function decreased to $1.53E+7$. Because each run of proxy takes less than 1 second, for this 2D example with time step size of 10 days, 20 runs means less than 20 seconds. In the next 50 proxy runs, the objective function decreased slowly and the final objective function after 69 runs was $1.24E+6$.

Calibrating All Parameters at the Same Time by Giving Weights to the Objective Function

In the last example, the same weight was given to the oil mismatch and steam mismatch. Because values of cumulative steam injection are much larger than the cumulative oil production, the mismatch of the steam results would be larger than the mismatch of oil rates. Weights can be given to the oil mismatch and steam

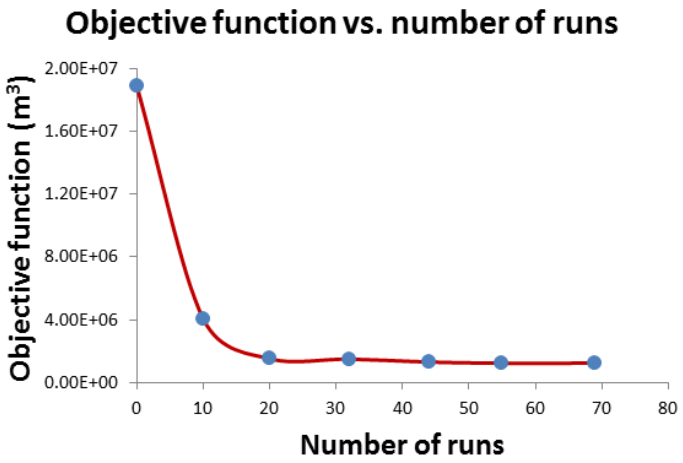

Figure 3.23: Objective function vs. number of proxy runs – calibrating all parameters at the same time – no weight

mismatch in the objective function to make both of them equally important. As Eq. 2.24 shows, a weight equal to one over square of final simulator CSOR can be given to the steam part of the objective function to make both parts approximately equally important. In this case, a better match for oil rates can be expected. Fig. 3.24 shows results of one step optimization by selecting weight for the objective function.

As Fig. 3.24 shows, the match between the oil rate of the simulator and proxy is much better than before. Also, the cumulative oil and steam matches between results of simulator and proxy are satisfactory, but the match between the steam rates is not as good as before. The final cumulative oil production of the proxy is about 3% less than the simulator and the final cumulative steam injection of the proxy is less than 1% more than the simulator. The final CSOR of the proxy is about 2% more than the simulator. The final mismatch between the results for both cases are essentially the same, but in the case of using weight, the match between the oil rates is very good, and the match between the steam rates is not as good as the case of no weight. Table. 3.2 shows the different results of the calibration parameters.

The steam front velocity during confinement increased, but this time the steam front velocity during spreading increased too. Also, the change in the steam calibration parameters are smaller than before and they seems more realistic.

The CSOR could be selected as objective function too, but in this case, the

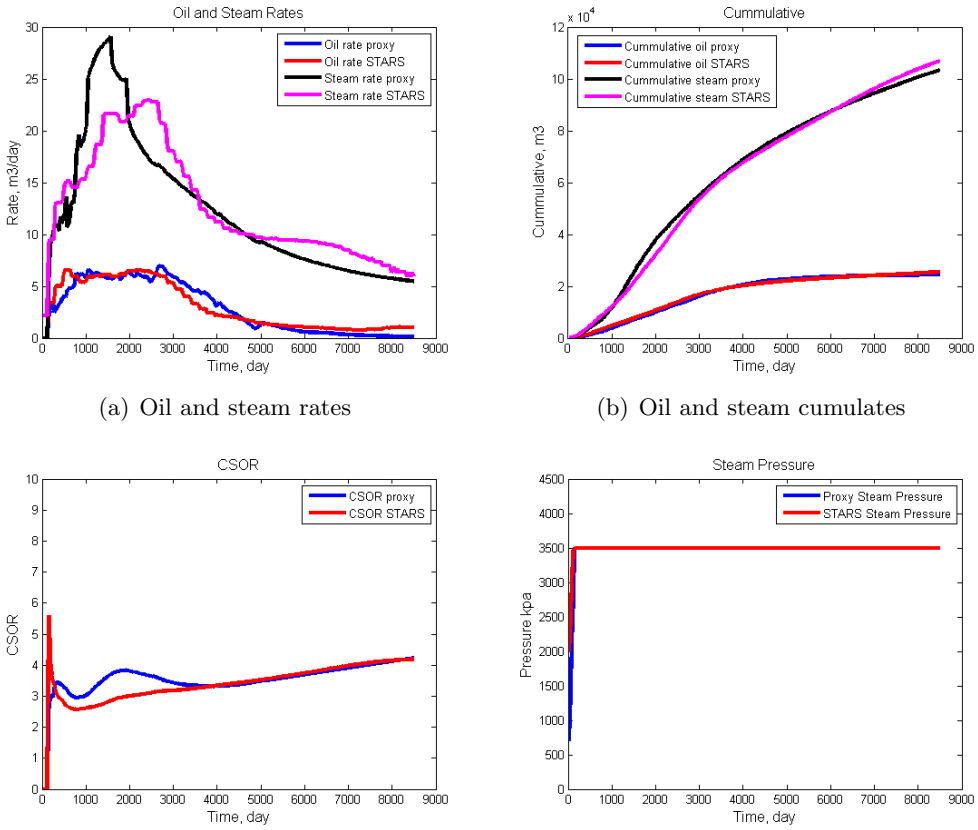

(a) Oil and steam rates

(b) Oil and steam cumulates

(c) Cumulative steam oil ratio

(d) Steam pressure

Figure 3.24: Simultaneous calibration of parameters of model 6 – use weight

Table 3.2: Values of calibration parameters using SQP method as optimization algorithm – all parameters at the same time – use weight

	V_r **mult.**	V_s **mult.**	V_c **mult.**	α_{ob} **mult.**	VHC **mult.**
Initial	1.0	1.0	1.0	1.0	1.0
Final	0.90	1.32	1.29	1.03	0.90

match between the CSOR of the simulator and proxy could be very good, but both the oil and steam predictions could be be overestimated or underestimated which is not a good result. For this reason, selecting a weight for the objective function is preferred.

Calibrate Only Oil Parameters

Most of the time, there is no need to calibrate the steam parameters since calibrating the oil parameters provides a good match of the steam injection results. Fig. 3.25 shows the results of calibrating the oil parameters with both components in the objective function.

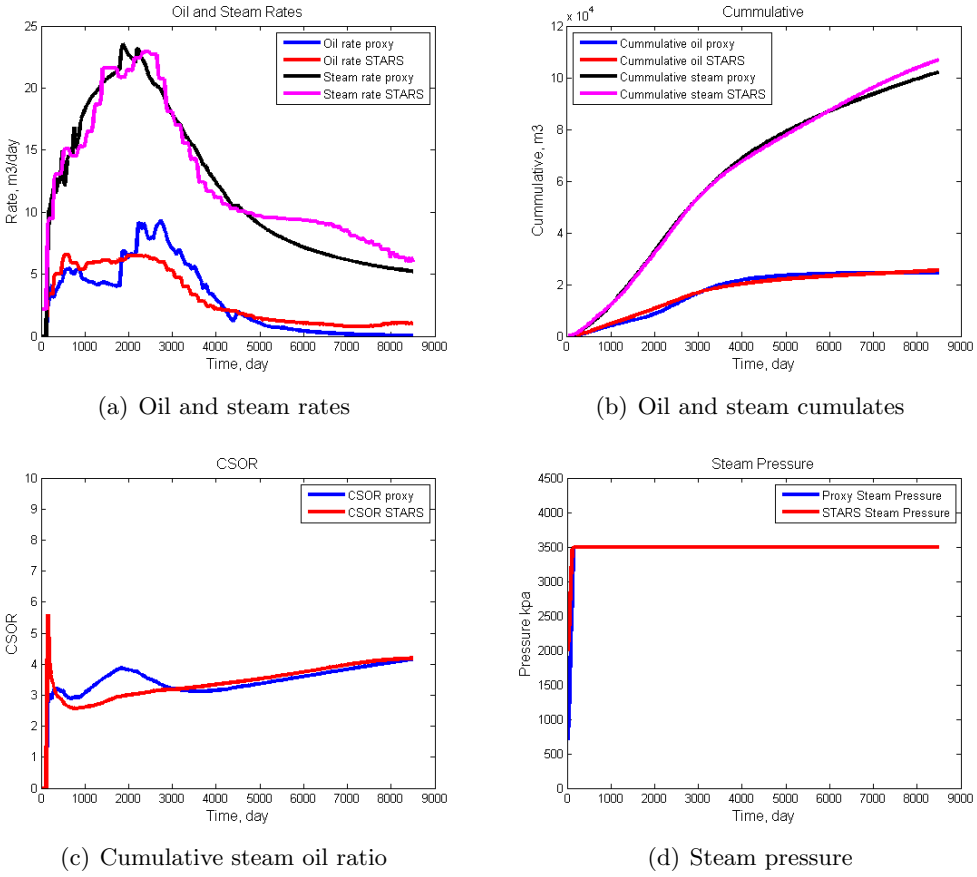

(a) Oil and steam rates

(b) Oil and steam cumulates

(c) Cumulative steam oil ratio

(d) Steam pressure

Figure 3.25: Calibrating only oil parameters of model 6

As Fig. 3.25 shows, calibrating the oil parameters provides a very good match. The cumulative steam injection could be improved slightly by considering those calibration parameters.

Table. 3.3 shows the value of calibration parameters before and after calibration.

Table 3.3: Calibrating oil parameters using SQP method as optimization algorithm

	V_r **mult.**	V_s **mult.**	V_c **mult.**	α_{ob} **mult.**	VHC **mult.**
Initial	1.0	1.0	1.0	1.0	1.0
Final	1.04	0.91	1.78	1.0	1.0

As can be seen in Table. 3.3, the rising and spreading velocity multipliers are still close to the 1.0, but the confinement velocity multiplier increased (even more than the previous cases) to increases the front velocity at this stage and find a better match between the results of both cumulative oil and cumulative steam. The match between the oil rates of the simulator and proxy are not very close, but as you can see matches between cumulative and CSOR are very good and values of the calibrated parameters are reasonable.

Fig. 3.26 shows the change to the objective function versus the number of proxy runs during optimization.

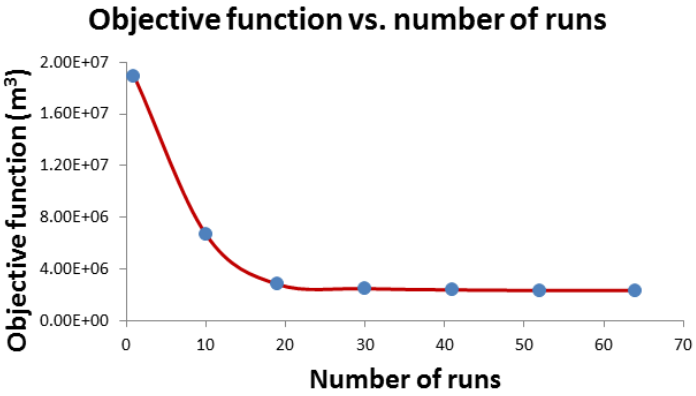

Figure 3.26: Objective function vs. number of proxy runs – calibrate only oil parameters

Again in this case, the optimal values have been found in about 20 runs (less than 20 seconds) which is very fast.

Calibration by Two Stages Optimizations

For the last calibration case, a two stage calibration has been tested. First, the oil parameters should be calibrated and then the steam parameters. The weights are also important in this case to balance the fitting of the oil production versus steam injection. We expect to find a good match between oil rates of proxy and

simulator because those parameters are fit first. Fig. 3.27 shows results of two stage calibration.

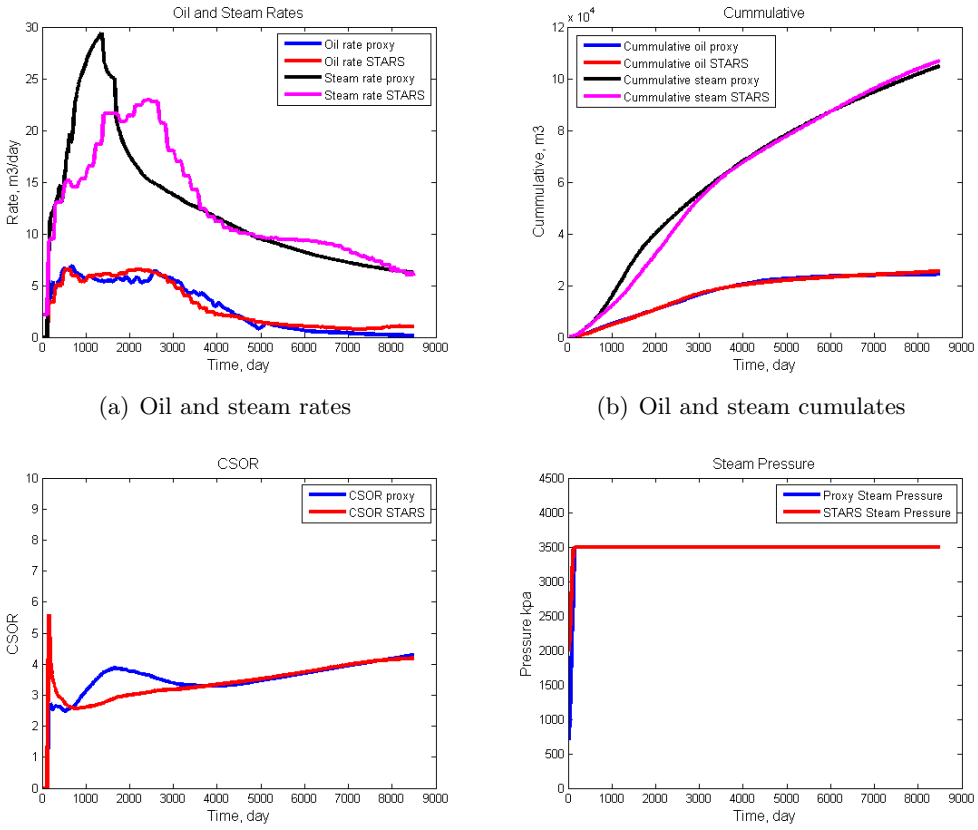

(a) Oil and steam rates

(b) Oil and steam cumulates

(c) Cumulative steam oil ratio

(d) Steam pressure

Figure 3.27: Two stages calibration of parameters of model 6

As Fig. 3.27 shows, after calibration cumulative results are much better than before calibration, but steam injection rates are not matched completely during the spreading and confinement periods and local differences can be observed. In this case, a very good match between the oil rates of proxy and simulator has been found. In this case, the final cumulative oil production of the proxy is about 4% less than the simulator and the final cumulative steam injection of the proxy is about 2% less than the simulator. Thus, the final CSOR of the proxy is about 2% more than the simulator. Table. 3.4 shows calibrated values of calibration parameters.

In this case, the calibration objective function and matches are very similar to the calibration results of one stage calibration using weights in the objective function, but the final calibrated values are completely different. The steam front velocity

Table 3.4: Calibrating parameters using SQP method as optimization algorithm – Two stage calibration

	V_r **mult.**	V_s **mult.**	V_c **mult.**	α_{ob} **mult.**	VHC **mult.**
Initial	1.0	1.0	1.0	1.0	1.0
Final	1.34	1.28	1.17	0.76	0.4

during the rising, spreading and confinement increased, and both steam parameters have decreased. In this case, the volumetric heat capacity decreased significantly, which does not seem realistic. Fig. 3.28 shows the change of objective function versus the number of proxy runs.

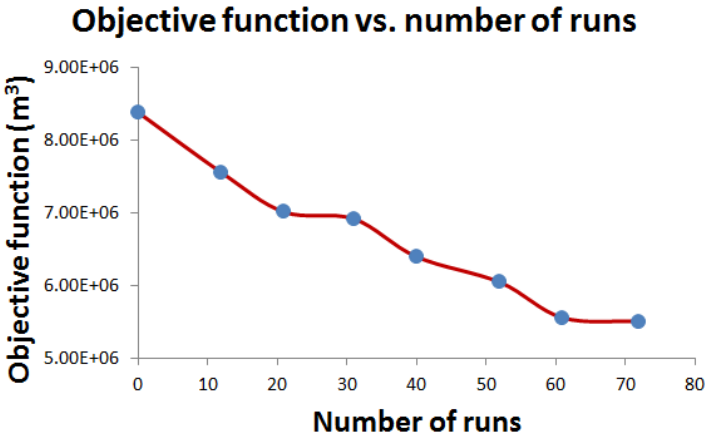

Figure 3.28: Objective function vs. number of proxy runs – two stages optimizations

In the case of two stage calibration, the rate of convergence is slower than the one stage calibration.

The most realistic results appear to be obtained by calibrating all of parameters at the same time and using a weight in the objective function.

3.2 Realistic 3D History Matched Models with Different Operating Strategies

In the previous sections, several 2D examples with different operating strategies have been tested by the proxy. Results showed satisfactory performance of the proxy in forecasting simulator behavior for different operating strategies. Depending on the model size, the simulator run time of a 2D model can be 20 minutes with a single CPU. This run time is based on the runs on a machine with Intel® Core™ *i*7

CPU @2.80 GHz. When multiple 2D slices merge together to form a 3D model, the simulator run time will increase significantly even using multiple processors. Average simulator run time for a 3D model with 36 slices along the well (each 25 m) and well spacing of 80 m on that machine is about 40 hours which is very time consuming in the case that several models need to be run for transferring uncertainty, ranking of realizations or well trajectory optimization. In this case, approximate simulation of reservoir model using the proxy instead of using the flow simulator can be very helpful. As we showed before, proxy performance for 2D models were satisfactory, as a result we expect to find satisfactory results for 3D cases too. As we discussed before, for 3D models, the interaction between adjacent slices can be considered for the case that one slice is not able to inject steam or produce bitumen, but adjacent slices are producing; there may be cross-over between adjacent slices. The amount of oil production and steam injection of different slices should be summed together for finding the cumulative oil production and steam injection.

For testing different operating strategies such as the maximum steam injection rate, the total amount of available steam at each time step should be divided by the number of 2D slices in the model, and the same amount of available steam for each slice to inject into the reservoir should be assumed. If the predicted steam injection rate for each slice is above the limit for that slice, steam injection pressure should be dropped for that slice. The final steam injection pressure can be obtained by averaging steam injection pressures of different slices at each time step.

In this section, two realistic 3D models for testing proxy efficiency have been selected. These two models are located in Alberta and they belong to two different DAs. Grid dimensions for the first and second models are $51 \times 55 \times 90$ and $50 \times 54 \times 75$ respectively. Also, the grid sizes along i, j and k directions for both of models are $2.5 \times 25 \times 1$. Wells in both models are along the j direction and the length of the wells is approximately 1 km. Five facies and seven different thermal rock types are used in the models. These models are history matched models and simulation results are matched with the production data. Simulation time for the first model is 7770 days and for the second one is 5550 days.

The proxy time step size was set to 15 days. As a result, the proxy run time for these models is less than 15 seconds. Correlations have been used for calculating PVT and rock properties. All of the proxy results are uncalibrated results.

Two different operating strategies for each model have been tested. The first

operating strategy is based on injecting steam with pressure of 4000 *kpa* for the first 120 days during the start-up period, then dropping the pressure to 3500 *kpa* for 330 days. After 450 days, the pressure trigger starts working and drops pressure 100 *kpa*/*year*. After 55% recovery of bitumen in the pay zone, a blow-down trigger stops injecting steam into the reservoir. The second operating strategy is based on injecting steam with pressure of 4000 *kpa* for the first 120 days during the start-up period, then dropping pressure to 3500 *kpa* for 1080 days and then dropping pressure to 2200 *kpa* for the rest of simulation. The blow-down trigger stops injecting steam into the reservoir.

3.2.1 Realistic 3D Model 1 with Operating Strategy 1

Fig. 3.29 shows a comparison between the proxy and simulator results for the first model with the first operating strategy.

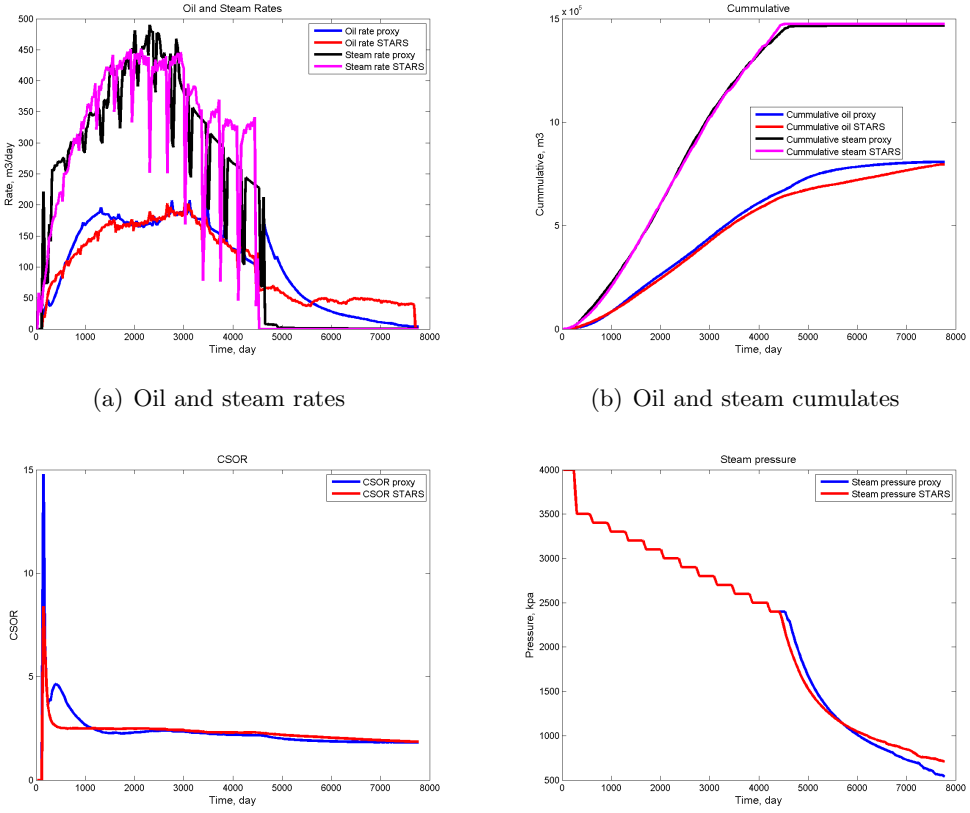

(a) Oil and steam rates

(b) Oil and steam cumulates

(c) Cumulative steam oil ratio

(d) Steam pressure

Figure 3.29: Comparison between results of proxy and simulator for model 1 with the first operating strategy

As Fig. 3.29 shows, the match between rates is reasonable. The trends of the

proxy and simulator rates (both oil and steam) are the same, except after blowdown where there is more mismatch in the oil rates. The match between the final cumulative oil production and final cumulative steam injection of the proxy and simulator are very close to each other. In this case, the final cumulative oil production of the proxy is about 2% higher than the simulator and the final cumulative steam injection of the proxy is about 1% less than the simulator. As a result, the final CSOR of the proxy is about 2% less than the simulator. Some mismatch can be observed between the CSOR results before 1000 days due to the low proxy oil production rates, but after that time CSOR values are very close to the each other. As Fig. 3.29(d) shows, there is good match between steam pressure of proxy and simulator.

For 3D models, the results of all 2D slices are summed together, for this reason, the oil and steam profiles for the 3D models are much smoother than the 2D models. In the case of 2D models, the heterogeneity has a large effect on changing the shape of the production and injection profiles and most of the times, more than one peak can be observed in the profiles. But in the case of 3D models, because all of results of 2D sections should be summed together, most of the time profiles are smoother and only one peak can be observed in the oil and steam profiles.

3.2.2 Realistic 3D Model 2 with Operating Strategy 1

Fig. 3.30 shows a comparison between proxy and simulator results for the second model with the first operating strategy.

As Fig. 3.30 shows, the match between rates is very good and the trends of the proxy and simulator rates (both oil and steam) are the same. The final cumulative oil production is very close, but the final cumulative steam injection is different. In this case, the final cumulative oil production of the proxy is about 1% less than the simulator and the final cumulative steam injection of the proxy is about 7% less than the simulator. As a result, the final CSOR of the proxy is about 6% less than the simulator. As Fig. 3.30(d) shows, again there is good match between steam pressure of proxy and simulator.

3.2.3 Realistic 3D Model 1 with Operating Strategy 2

Fig. 3.31 shows a comparison between the proxy and simulator results for the first model with the second operating strategy.

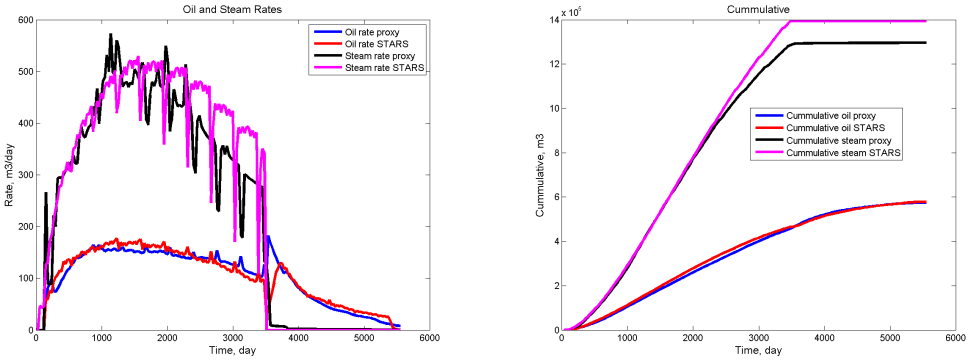

(a) Oil and steam rates

(b) Oil and steam cumulates

(c) Cumulative steam oil ratio

(d) Steam pressure

Figure 3.30: Comparison between results of proxy and simulator for model 2 with the first operating strategy

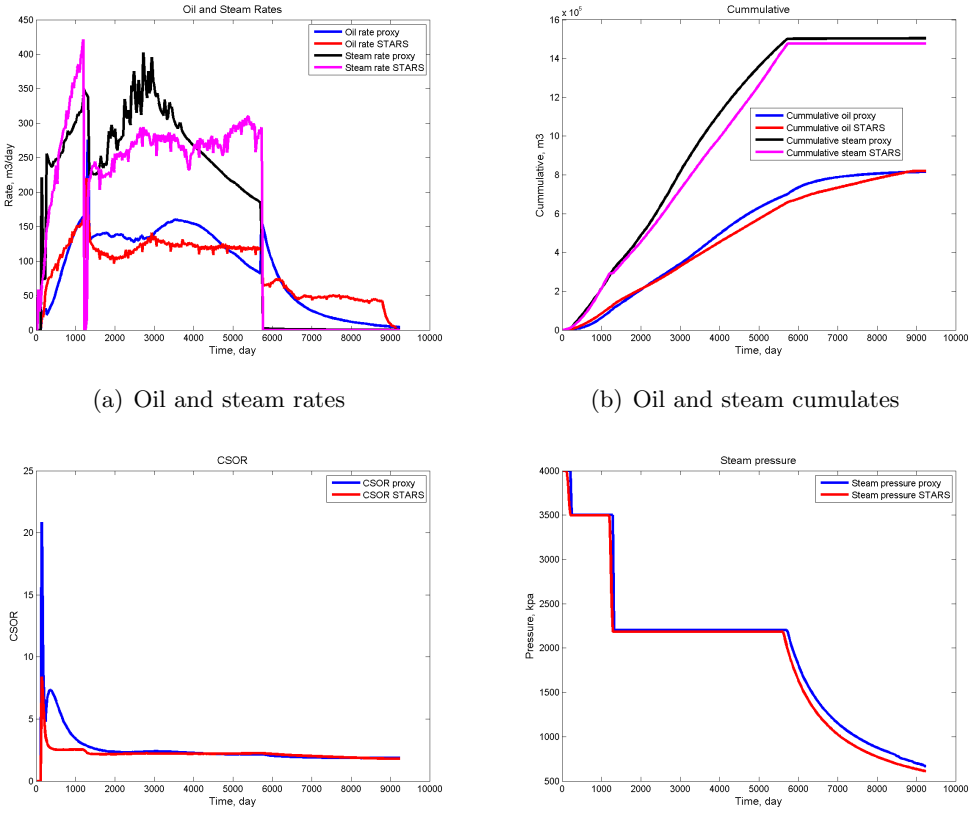

(a) Oil and steam rates

(b) Oil and steam cumulates

(c) Cumulative steam oil ratio

(d) Steam pressure

Figure 3.31: Comparison between results of proxy and simulator for model 1 with the second operating strategy

As Fig. 3.31 shows, the match between the rates is not as good as the first operating strategy and the trends of proxy and simulator rates (both oil and steam) are not completely the same. As a result, local mismatches between cumulative oil production and cumulative steam injection of the proxy and simulator can be observed, but final cumulative are very close to the each other. In this case, the final cumulative oil production of the proxy is about 1% less than the simulator and the final cumulative steam injection of the proxy is about 2% greater than the simulator. As a result, the final CSOR of the proxy is about 2% greater than the simulator. Again there is a little mismatch between CSOR results before 1000 days, but after that CSOR values are close to each other. As Fig. 3.31(d) shows, again there is good match between steam pressure of the proxy and simulator.

3.2.4 Realistic 3D Model 2 with Operating Strategy 2

Finally, Fig. 3.32 shows a comparison between the proxy and simulator results for the second model with the second operating strategy.

As Fig. 3.32 shows, the matches between rates are close and the trends of proxy and simulator rates (both oil and steam) are the same. The final cumulative oil production is close, but final cumulative steam injection is not particularly close. In this case, the final cumulative oil production of the proxy is about 3% greater than the simulator and the final cumulative steam injection of the proxy is about 5% less than the simulator. As a result, the final CSOR of the proxy is about 8% less than the simulator. As Fig. 3.32(d) shows, the match between the steam pressure of proxy and simulator before blow-down is very good, but there is a little difference between match of steam pressures after the blow-down.

As shown above, the comparison between the results of the proxy and simulator for different 2D and 3D models with different operating strategies were satisfactory and it seems that proxy is a reliable tool for forecasting SAGD performance.

This proxy assumes that all of producible oil inside a grid cell would be produced quickly if the steam front covers it. This assumption is not realistic. In reality, producible oil inside the steam chamber will decrease gradually by increasing the production time. By considering this effect, proxy can be used for other purposes such as history matching for finding a good match between proxy results and production data.

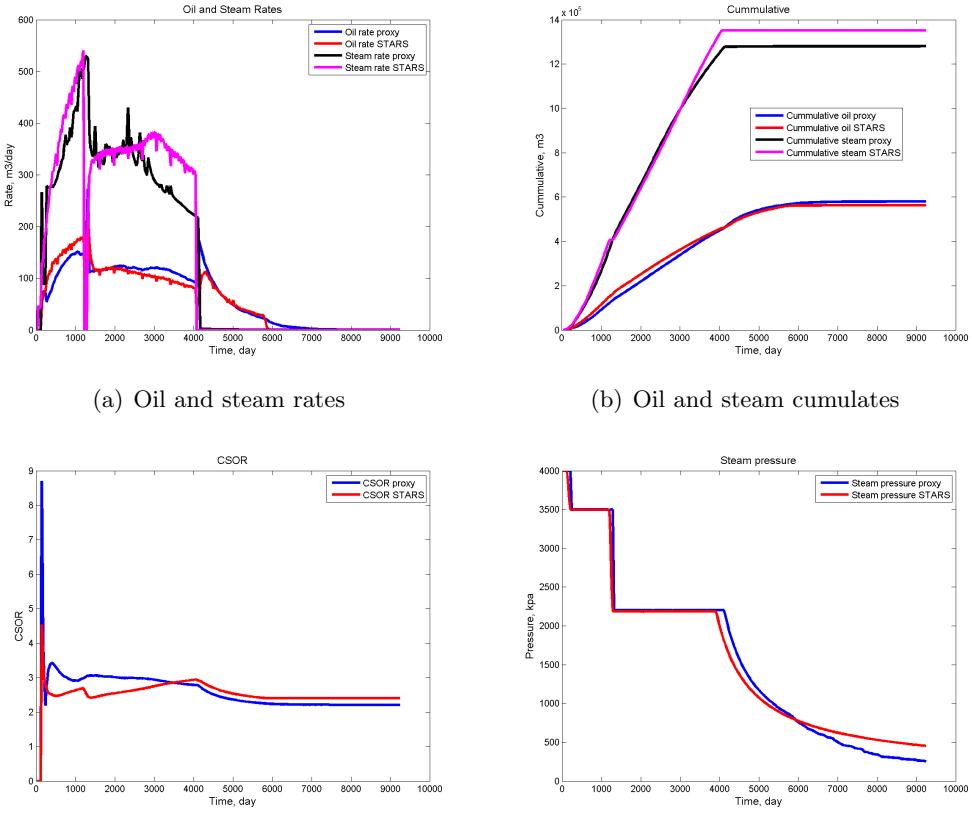

(a) Oil and steam rates

(b) Oil and steam cumulates

(c) Cumulative steam oil ratio

(d) Steam pressure

Figure 3.32: Comparison between results of proxy and simulator for model 2 with the second operating strategy

3.3 Comparison between Proxy and Simulator Run Time

The proxy developed in this work is a semi-analytical proxy based on Butler's SAGD theory. Butler's original theory has been modified significantly for considering effects of heterogeneity and different operating strategies. By adding these options, the proxy is still very fast and able to predict results close to the simulator results, but 1000 times faster than the reservoir simulator. The proxy run time depends on many factors including:

1. Proxy time step size
2. Operating strategy
3. Model size
4. Simulation time

By increasing the proxy time step size, the proxy run time decreases. For example, by increasing the time step size from 1 day to 10 days, the proxy would be approximately 10 times faster. Also by assuming unlimited steam availability, the proxy simulates faster than with a trigger operating strategy or other types of operating strategy. In the case of unlimited steam availability, there is no need for the proxy to change the steam injection pressure during the simulation. Also by increasing the model size or simulation time, the proxy run time increases too. The proxy run time for a large model with $\Delta t = 15$ days, a combination of different strategies and 30 years simulation on a machine with Intel® Core™ *i*7 CPU @2.80 GHz is about 15 seconds, which is very fast.

On the other hand, the simulator run time depends on many factors including:

1. Model size
2. Simulation time
3. Number of processors

Again by increasing the model size or simulation time, the simulator run time increases significantly. Also depending on the number of CPUs we are using for running the simulation models, the run time changes significantly. There are significant difference between simulator run time using 1 CPU or 4 CPUs for running a model. Simulator run time for a large model with 4 processors, combination of

different operating strategies and 30 years of simulation on a machine with Intel® Core™ *i*7 CPU @2.80 GHz is about 2 days.

3.4 Summary

Forecasting SAGD performance with multiple synthetic 2D and realistic history matched 3D models with different operating strategies was considered in this Chapter. Some conclusions from this Chapter:

- The comparison between the results of the proxy and simulator for different 2D and 3D models with different operating strategies is satisfactory and the proxy appears as a reliable tool for forecasting SAGD performance.
- The proxy is much faster than the flow simulator and results are reliable. The proxy can be used for other applications such as ranking, uncertainty transfer and well trajectory optimization in presence of multiple reservoir realizations.

Chapter 4

Forecasting Steam Chamber Location

Butler's model can be used for forecasting the steam interface location in homogeneous models at different time steps. Butler's model assumes three different periods for forecasting steam interface location. At first, the steam rises vertically during the rising period (Butler, 1987b, 1991), then spreads horizontally during the spreading period to reach to the reservoir boundary and finally moves downward during the confinement period (Fig. 1.8).

Based on Butler's model, the height of the steam chamber can be computed using Eq. 1.14 during the rising period. After the steam chamber contacts the top of the reservoir, the spreading period starts. The steam interface could be discretized by different planar segments. Then, as time increases, the steam interface location can be updated from the material balance equation assuming that the average flow of oil is related to how the planar segments move into the previously cold reservoir. Butler showed that Eq. 1.11 can be used for finding the interface location before confinement. Also, he showed that when the reservoir is not infinite, that is, when there is coalescence (contacting steam chambers of adjacent wells) or a reservoir boundary, the steam interface direction should be changed and it moves downward when it reaches the boundary. In this case, the planar segments move downward in y only according to Eq. 1.12. As a result, when adjacent wells exist, half of the spacing between them can be considered as the location of a no-flow boundary.

Butler's model is efficient for forecasting the steam chamber location of homogeneous models. Due to heterogeneity and existence of shale barriers in the model, the steam chamber location for heterogeneous models is not simply based on the idealized rising, spreading and confinement periods. Multiple rising and spreading

periods can be observed in the model and some of spreading periods can start before the rising periods are finished.

Many different options have been added in this dissertation to Butler's model to improve the estimation of SAGD performance from heterogeneous reservoir models with different operating strategies. One way of considering reservoir heterogeneity is by finding the connected net grids. The connected hydrocarbon volume (CHV) tool has been used (Wilde and Deutsch, 2012). This tool can compute production steps, angle between the original location of the bitumen and the production well and the distance of grids from the producer based on their step and angle. The proxy developed in this dissertation is efficient in estimating oil production and steam injection at different time steps, but forecasting the steam chamber location at different time steps for heterogeneous cases remains an important problem that is addressed in this Chapter. Finding the true location of the steam chamber will not change the proxy final cumulative oil production. It only changes the oil production rate at different time steps which is not very important for a quick tool such as proxy. Also, it will not change the proxy forecasted cumulate steam injection significantly. The only parameter that may change by finding the true steam chamber location is steam chamber size which does not have too much effect on the estimating the steam injection rate. Forecasting the steam chamber location can be very useful for considering the geomechanical effects and history matching. In these case, porosity and permeability of grid cells inside the steam chamber can be modified during the simulation which can be very useful for the history matching. Assume there is a thief zone on the top of the reservoir. Butler's theory converts the heterogeneous model to a homogeneous model and assumes that the steam chamber enters the thief zone. Although there is not any mobile oil inside of the thief zone and it will not change the amount of oil production rate at each time step, but the forecasted location of the steam chamber is completely different with reality and it may cause a problem during the history matching or considering the geomechanical effects.

The steam chamber location can be forecast by predicting the order of grid cells for production and knowing the cumulative oil production at each time step. This allows the grid cells inside the steam chamber (the produced grid cells) to be identified at each time step. The results of CHV can be used for forecasting order of grids for production. CHV provides the step, angle, and distance for each grid cell that can be used for defining the order of grid cells for production. For

finding a relationship between the CHV results and simulator order of grid cells for production, three 2D models are considered. By analyzing the CHV results and comparing them with the simulator results, the order of grid cells for production could be forecast by an empirical formula. The simulator order of grid cells for production can be identified based on the temperature of grid cells at different time steps. If the steam temperature is T_s, temperature $T_p = T_s - \Delta T$ can be selected for identifying the steam chamber location. ΔT is an arbitrary value and can be set to $10^{\circ c}$ or less. If the steam temperature is $240^{\circ c}$, by setting $T_p = 230^{\circ c}$, grid cells with the temperature greater or equal to the T_p are on the edge or inside of the steam chamber. For this reason, the grid cells temperatures at each time step should be monitored.

4.1 Analyzing the CHV Results

Three synthetic heterogeneous models are considered for finding a relationship between the CHV results and simulator order of grid cells for producing bitumen. Each model has a grid dimension of $1 \times 49 \times 83$. The grid size in the x, y and z directions are 25 m, 2.5 m and 1 m, respectively. A stratigraphic pinchout exists at the bottom of the reservoir. Top water and top gas exists above the pay zone. Five different facies and seven different thermal rock types are considered. Each facies has a separate relative permeability curve. For the operating strategy, unlimited steam is available for injection.

4.1.1 2D Synthetic Model 1

Figs. 4.1(a)–4.1(c) show CHV results such as step, angle, and distance for each grid for the first model. Dark blue grid cells in Fig. 4.1(a) show non-net grid cells with very low porosity or permeability. Three steps of production can be identified for this example, but the third step is only for a small number of grid cells. Dark blue grid cells in the Fig. 4.1(b) show rising periods for different steps. Fig. 4.1(c) shows distance of grid cells from the producer based on their steps and angles. Finally, Fig. 4.1(d) shows simulator order of grid cells for production. Darker areas show faster bitumen production. This map is obtained from the grid cells temperature.

On the top of the model thief zone existed. Usually thief zone contains cold water and steam cannot enter the thief zone. As Fig. 4.1(d) shows, steam did not enter the thief zone due to the excessive heat loss as a result of contact with the

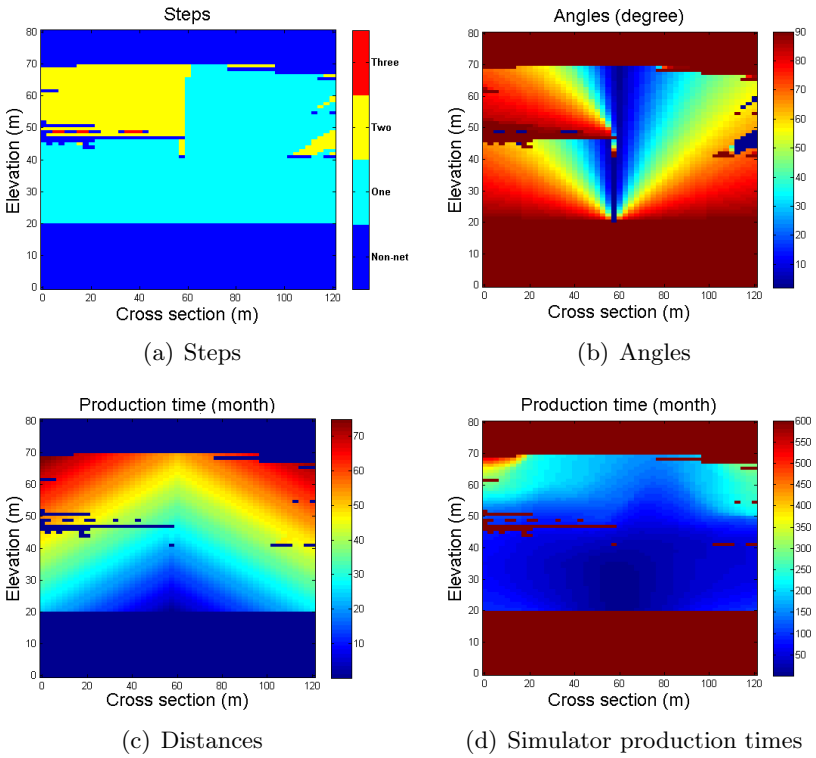

(a) Steps (b) Angles

(c) Distances (d) Simulator production times

Figure 4.1: Step, angle, distance and simulator production time maps for Model 1

cold water. There is little mobile oil in these grid cells and even entering the steam into these grid cells will not change the final cumulative oil production significantly, but due to the excessive heat loss to the overburden, the cumulative steam injection increases significantly.

For understanding the relation between the simulator order of grid cells for production, steps, angles, and distances, relationship between these parameters should be considered. Figs. 4.2(a)–4.2(b) show 2D plots of distance versus angle for different steps. Fig. 4.2(c) shows a 3D plot which is relationship between steps, angles, and distances. In these plots, the color shows the simulator production time for different distances and angles. Darker areas show the faster production. As Fig. 4.2 shows, bitumen of grids with smaller step, smaller angle and smaller distance can be produced faster.

It seems that the most important parameter is step. At each step by increasing the distance, production time increases too. At each time step, by increasing the angle production time increases for most of the grid cells. It seems that relationship between angle and distance is nonlinear. Fig. 4.1(a) and Fig. 4.1(c) show that grid cells with smaller steps and smaller distances are produced first. As Fig. 4.1(b)

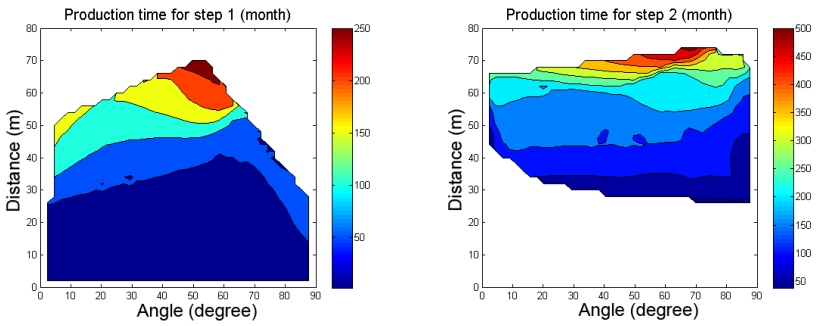

(a) Step 1

(b) Step 2

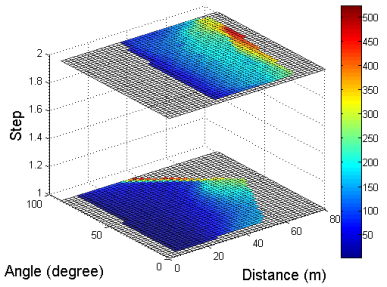

(c) 3D plot

Figure 4.2: Relationships between steps, angles and distances for example 1

shows, grid cells with smaller angles may not be produced earlier than other grid cells. It seems that angle depends on the elevation too. Only grid cells with small angle at low elevations can be produced at early time steps.

4.1.2 2D Synthetic Model 2

Figs. 4.3(a)–4.3(c) show CHV results such as step, angle, and distance for different grid cells of the second model. Fig. 4.3(d) shows simulator order of grid cells for production. Three steps with multiple rising periods can be identified for this model. The third step is for a larger number of grid cells respect to the first model. Larger step usually mean larger distance and longer production time. This can be seen in Figs. 4.3(c)–4.3(d).

Fig. 4.4 shows 2D and 3D relationships between the production time, steps, angles, and distances.

As with the first example, the most important parameter is the step. Then, distance is important followed by angle for the first two steps seems to be more uniform than distance at each step, but as mentioned before, the relation between angle and distance is nonlinear. One grid cell with a large step, but small distance

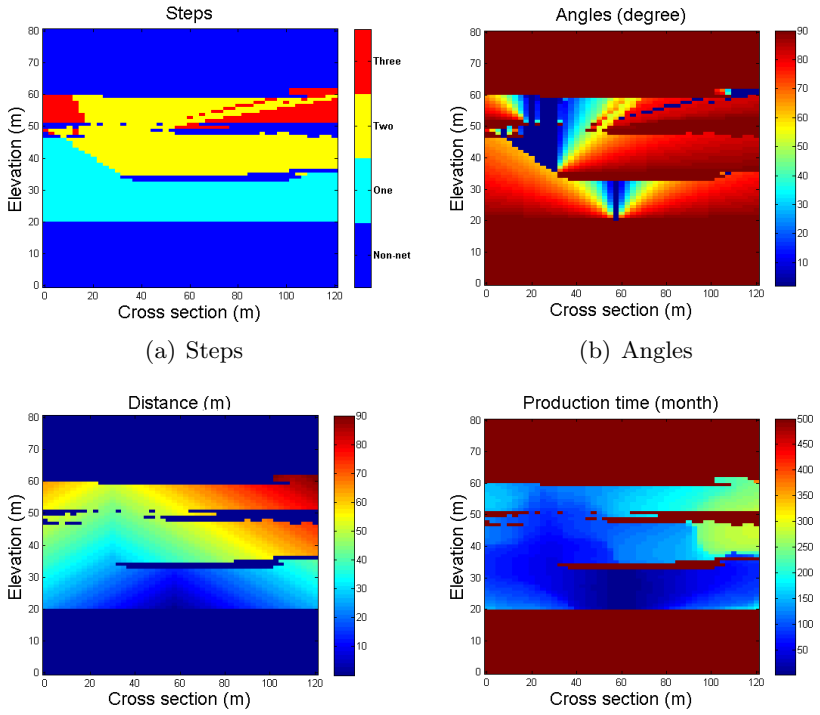

(a) Steps (b) Angles

(c) Distances (d) Simulator production times

Figure 4.3: Step, angle, distance and simulator production time maps for Model 2

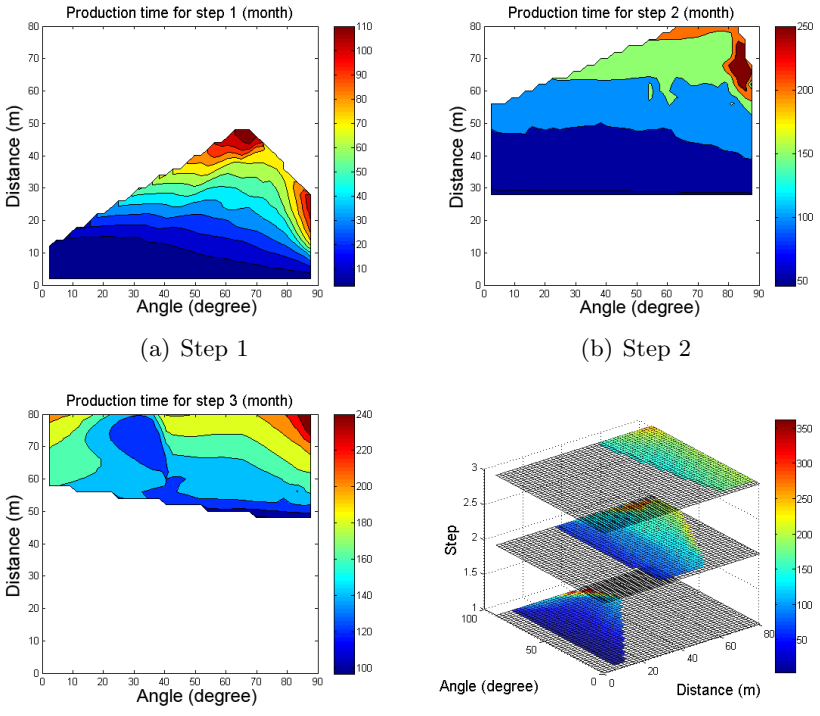

(a) Step 1 (b) Step 2

(c) Step 3 (d) 3D plot

Figure 4.4: Relationships between steps, angles and distances for example 2

or small angle can be produced earlier than most of grid cells with smaller steps. It shows that the relation between these three parameters are nonlinear and a nonlinear function should be defined for forecasting the order of grid cells for production. Similar to the first example, Fig. 4.3(a) and Fig. 4.3(c) show that grid cells with smaller steps and smaller distances are produced first. Fig. 4.3(b) shows that the angle parameter depends on the elevation and that grid cells with a small angle at low elevations can be produced at early time steps.

4.1.3 2D Synthetic Model 3

Figs. 4.5(a)–4.5(c) show CHV results such as step, angle, and distance for different grid cells of the third model. Fig. 4.5(d) shows simulator order of grid cells for production. Laminated shale barriers can be observed above the well at different elevations. Four steps with four rising periods can be identified for this model. By increasing the elevation, step increases continuously and as a result distance increases significantly which causes longer production time. This can be observed in Figs. 4.5(c)–4.5(d).

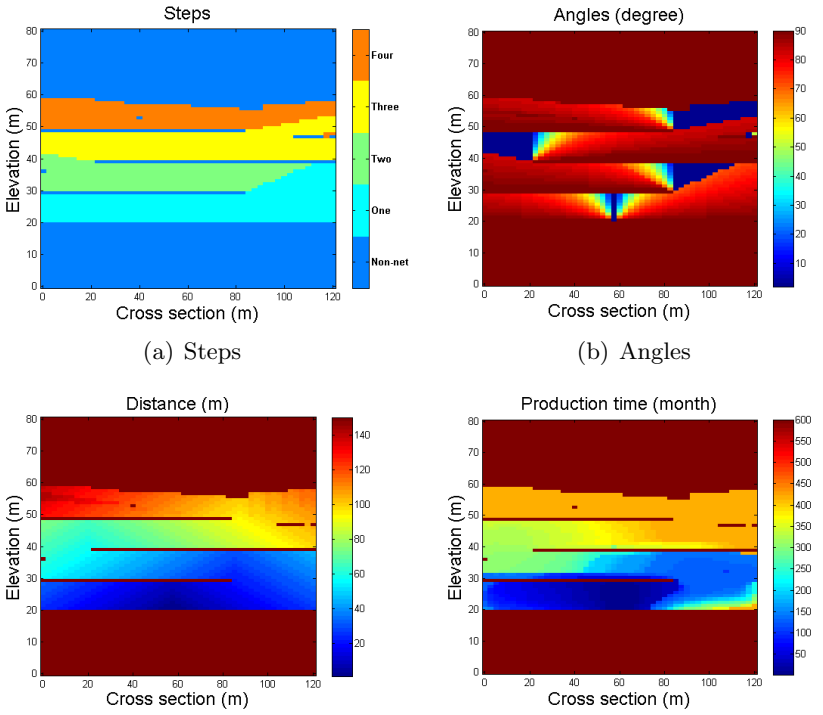

(a) Steps (b) Angles

(c) Distances (d) Simulator production times

Figure 4.5: Step, angle, distance and simulator production time maps for Model 3

Fig. 4.6 shows relations between production time, Steps, angles and distances.

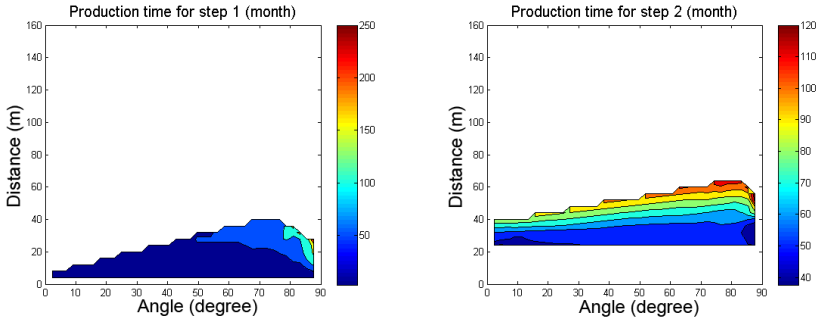

(a) Step 1

(b) Step 2

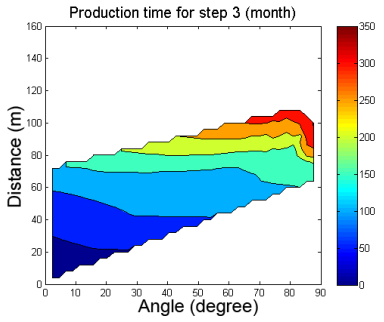

(c) Step 3

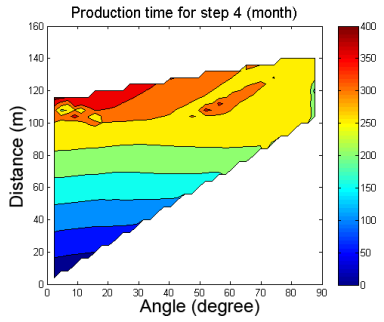

(d) Step 4

Figure 4.6: Relationships between steps, angles and distances for example 3

For the first two steps, the production time increases with increasing step. Also, for each of these steps, by increasing the distance, the production time increases. It seems that the effect of angle is not as important as distance for these steps. Results of the last two steps show that one grid cell with large step, but small distance or small angle can be produced earlier than most of grid cells with smaller steps. Again, this example shows that the relationship between these three parameters are nonlinear and a nonlinear function should be defined for forecasting the order of grid cells for production. Fig. 4.5(b) shows that grid cells with smaller angles may not be produced earlier than other grid cells and only grid cells with small angles at low elevations can be produced at early time steps.

4.2 Summary of Analyzing the CHV Results

By analyzing the CHV results of the last three models, the following points have been observed:

1. Relationship between these three parameters are not linear and a nonlinear function should be defined for forecasting the order of grid cells for production.

2. Step is the most important parameter, but one grid cell with large step with small distance and small angle can be produced earlier than most of grid cells with smaller steps.

3. At each step, by increasing the distance, the production time increases.

4. At each step, grid cells with smaller angles are candidates to be produced first. Grid cells with smaller steps and smaller distances produce first, but grid cells with smaller angles may not be produced earlier than other grid cells. It seems that the angle parameter depends on the elevation too and only grid cells with small angle at low elevations can be produced at early time steps.

Based on these results, an empirical equation can be defined for forecasting the order of grid cells for production.

4.3 Methodology

Based on the conclusions of the last section, an empirical equation is defined for forecasting the order of grid cells for production:

$$P_i = (1 + \frac{S_i}{S_{max}}) \times (1 + \frac{D_i}{D_{max}}) \times (1 + \frac{\tan\theta_i}{\tan\theta_{max}})^{(1+\frac{h_i}{H})} \tag{4.1}$$

S_i is the step of grid cell i, D_i is the distance of grid cell i, θ_i is the angle of grid cell i and h_i is the elevation of grid cell i. Also S_{max}, D_{max}, θ_{max} and H are the maximum step, maximum distance, maximum angle respect to the vertical and reservoir height, respectively.

Multiplication of terms is due to the nonlinear relationship between these three variables. One grid cell with large step, but small distance and small angle can be produced faster than the most of grid cells with smaller steps. Step is an integer variable and regardless of distance and angle, by increasing the step parameter P_i increases significantly. For decreasing the production time of grid cells which are producing during the rising period at low elevations and also increasing production time of grid cells with larger angle at high elevations, exponent of $(1 + \frac{h_i}{H})$ is selected for the angle parameter. Although grid cells with low angles can be produced fast, but it depends highly on the grid cells elevation. One grid may have a low production angle at the top of the reservoir. This grid cell cannot be produced in the early time steps. On the other hand, most of the times grid cells with smaller step or smaller

distance are at low elevations, for this reason an exponent for these two parameters is not selected.

The first grid for production is the grid at the producer. This grid has smallest step, angle, distance and elevation. As a result, the minimum value for this formula is approximately one and by increasing these parameters, P_i increases gradually. Smaller P_i means faster production of that grid. After finding P_i for all of grids, they should be ranked in the ascending order for finding order of grids for production.

For forecasting the steam chamber location, by predicting the order of grid cells for production and knowing the cumulative oil production at each time step, the grid cells inside the steam chamber (the produced grid cells) can be identified at each time step. The proxy estimates the cumulative oil production at each time step in a manner that closely matches flow simulation. The amount of oil inside each grid cell can be computed from Eq. 4.2:

$$\text{Oil}_i = V_i \phi_i (S_o - S_{or}) \tag{4.2}$$

where V_i is the volume of the grid i, S_o and S_{or} are oil saturation and residual oil saturation at the grid i, respectively.

The following algorithm can be used for estimating location of steam chamber in a 3D model.

1. Set $i = 1$
2. Compute amount of oil in each grid for 2D section i using Eq. 4.2
3. Run CHV for a 2D section and compute P_j for all grids using Eq. 4.1
4. Rank P_j vector in the ascending order for finding order of grids for production
5. Set $k = 1$
6. Run proxy for that 2D section and compute cumulative oil production for different time steps
7. Read the cumulative oil production at the time t_k
8. Based on the cumulative oil production at the time t_k, amount of the oil at each grid and rank of grids for production, grids inside the steam chamber at time t_k can be forecasted

9. Go to the step 11 if t_k is greater than the final simulation time

10. Set $k = k + 1$ and back to the step 7

11. Set $i = i + 1$ and stop the algorithm if i is greater than the number of 2D sections, otherwise back to the step 2

Based on this algorithm, the location of the steam chamber for each 2D section at each time step can be identified. This algorithm assumes that estimated cumulative oil production by the proxy at each time step is close to the simulator and there is no steam cross-over between adjacent slices.

4.4 Examples

In this Section, the three models have been considered in the Section 4.1 are used for testing the new proposed method.

4.4.1 Example 1 – 2D Synthetic Model 1

Fig. 4.7 shows a comparison between the Model 1 proxy and simulator order of grid cells for production. Proxy results have been obtained by running CHV and applying Eq. 4.1.

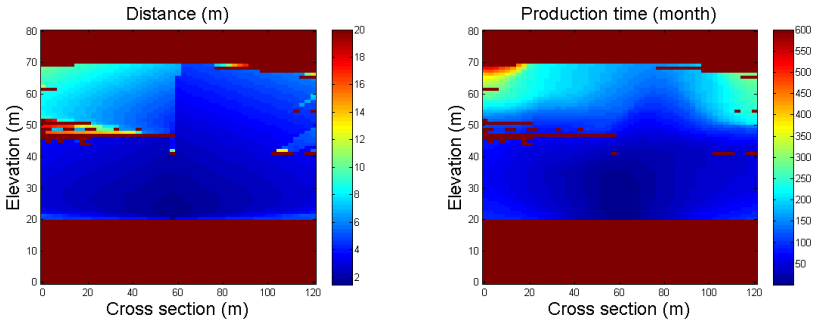

(a) Proxy order (b) Simulator order

Figure 4.7: Model 1 proxy and simulator order of grid cells for production

As Fig. 4.7 shows, dark areas in the both methods are around the same grid cells. Also light areas in the both methods are around the same grids. For better understanding of relationship between proxy and simulator results, result of each method is ranked in the ascending order and scatter plot of these two results is plotted and correlation coefficient between them is computed. Fig. 4.8 shows this scatter plot.

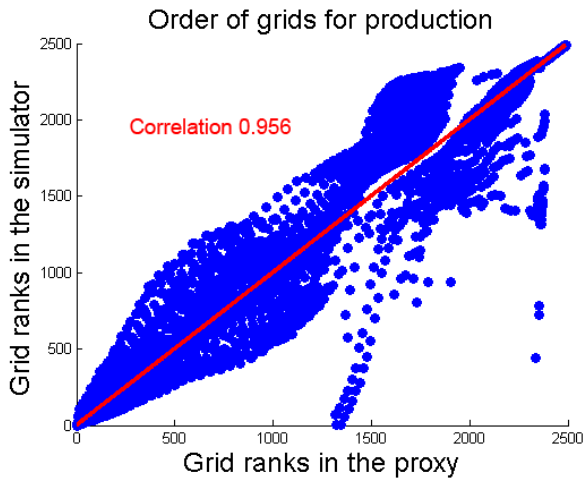

Figure 4.8: Scatter plot between proxy and simulator results of Model 1

As Fig. 4.8 shows, although there are some outliers around the 45 degree line, still correlation coefficient is about 0.96 which is very high. Eq. 4.1 is not precise and it sorts order of grid cells for production based on the static results. Reservoir simulator consider many parameters and by solving simulation equations location of the steam chamber can be identified. For this reason, some differences between results are expected. Next step is running the proxy for finding the cumulative oil production at each time step. Fig. 4.9 shows a comparison between the oil production and steam injection of the proxy and simulator for Model 1.

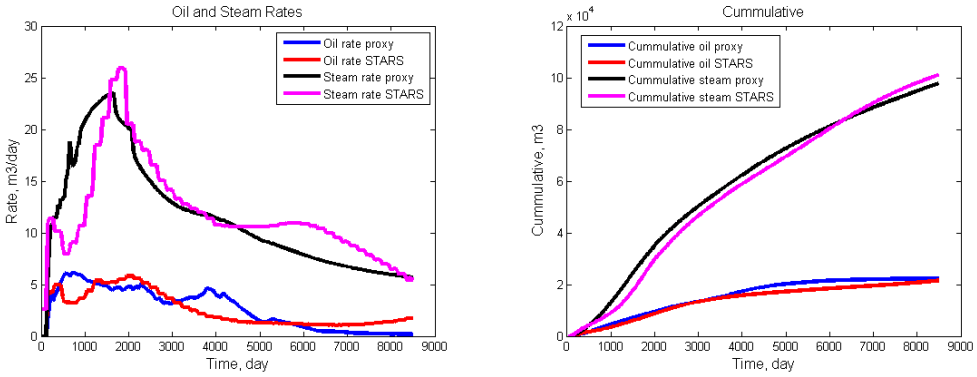

(a) Rates (b) Cumulates

Figure 4.9: Comparison between the proxy and simulator SAGD results for Model 1

As Fig. 4.9(a) shows, the oil production rates and steam injection rates of the proxy and simulator are close to the each other. There are local mismatches between the results which are due to the reservoir heterogeneity. Fig. 4.9(b) confirms that

matches between results are close. The final cumulative oil production of the proxy is 4% greater than the simulator and the final cumulative steam injection of the proxy is 3% less than the simulator, see Fig. 4.9(b). The order of grid cells for production are obtained using Eq. 4.1. Then, the amount of oil at each grid cell is computed using Eq. 4.2. By knowing the cumulative oil production at each time step (form proxy results), grids inside the steam chamber can be identified easily. Fig. 4.10 shows a comparison between the steam chamber location of the proxy, simulator and Butler theory for Model 1 after 1500, 5000 and 8500 days.

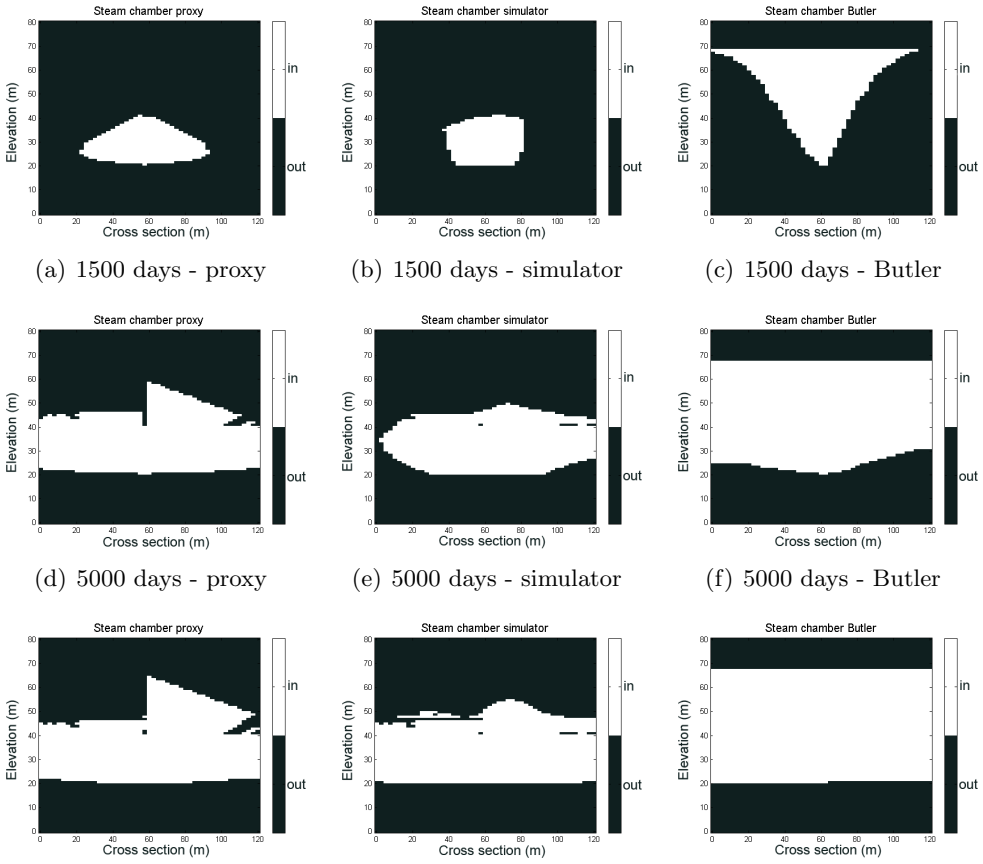

(a) 1500 days - proxy (b) 1500 days - simulator (c) 1500 days - Butler

(d) 5000 days - proxy (e) 5000 days - simulator (f) 5000 days - Butler

(g) 8500 days - proxy (h) 8500 days - simulator (i) 8500 days - Butler

Figure 4.10: Comparison between the steam chamber location of the proxy and simulator for Model 1 at different time steps

As Fig. 4.10 shows, the location of steam chamber using the proposed method at different time steps is close to the simulator. These results are much closer to the simulator than Butler's theory. Different reasons cause local differences between the proxy and simulator steam chamber location. First of all, Eq. 4.1 is an empirical correlation and cannot reproduce the order of grid cells for production exactly. the

cumulative oil productions of the proxy and simulator are not matched exactly, as a result, even by knowing correct order of grid cells for production, location of the steam chamber in the proxy and simulator would be different. For the first 4000 days, the cumulative oil production of the proxy is close to the simulator. As a result, shape of the proxy steam chamber is close to the simulator. But after that, the steam front in the proxy moves faster than the simulator. As a result, the size of the proxy steam chamber is bigger than the simulator.

Fig. 4.11 shows a comparison between the total error percentage for the forecasted steam chamber of Model 1 using the proposed method and the Butler's model. Total error percentage is summation of error type 1 and error type 2 ($E_T = E_I + E_{II}$). Error type one is the percentage of grid cells which are inside the steam chamber for the proposed method, but they are outside the simulator steam chamber. Error type two is percentage of grid cells which are outside the steam chamber for the proposed method, but they are inside the simulator steam chamber.

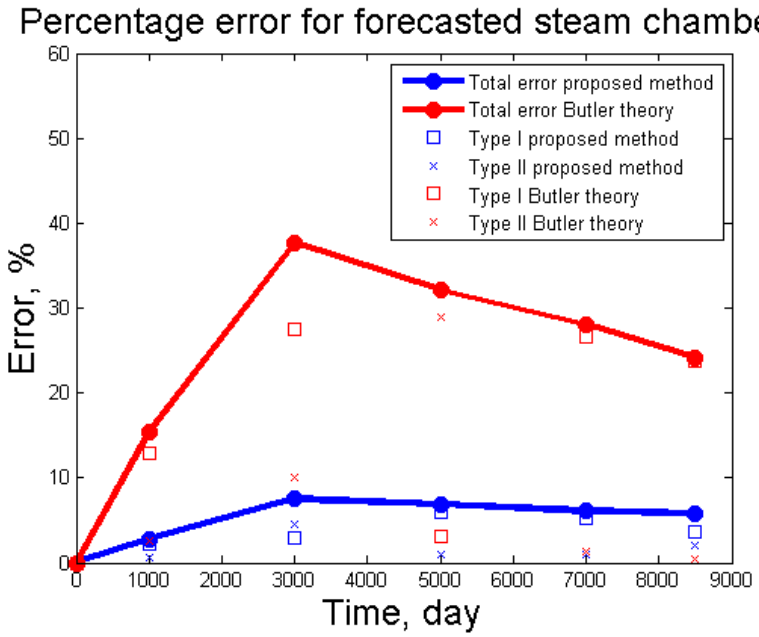

Figure 4.11: Total error percentage for the forecasted steam chamber of Model 1

Total error percentage for the proposed method is significantly lower than Butler's method at different time steps. The average of the total error percentage for the proposed method is about 5.8% and the average of the total error percentage for Butler's method is about 27.4%.

4.4.2 Example 2 – 2D Synthetic Model 2

Fig. 4.12 shows a comparison between the Model 2 proxy and simulator order of grid cells for production.

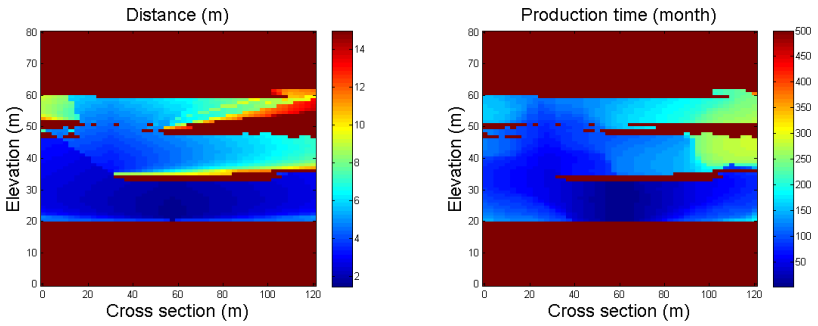

(a) Proxy order (b) Simulator order

Figure 4.12: Model 2 proxy and simulator order of grid cells for production

As Fig. 4.12 shows, again orders of production in both methods are close and dark area or light areas are relatively matched to each other. Scales of plots are different because parameters are different, but these two parameters have similar behavior. Fig. 4.13 shows a scatter plot between the ranked results.

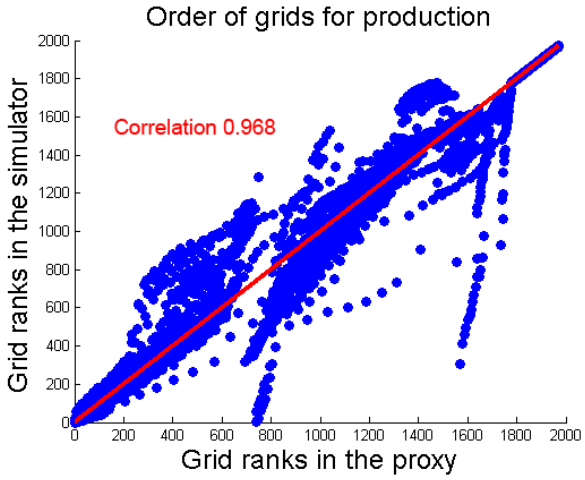

Figure 4.13: Scatter plot between proxy and simulator results of Model 2

Fig. 4.13 shows some outliers around the 45 degree line, but the correlation coefficient is about 0.97 which is very high. These outliers are due to the difference between the methods that proxy and simulator are using for forecasting the location of the steam chamber. Fig. 4.14 shows a comparison between the oil production and steam injection of the proxy and simulator for Model 2.

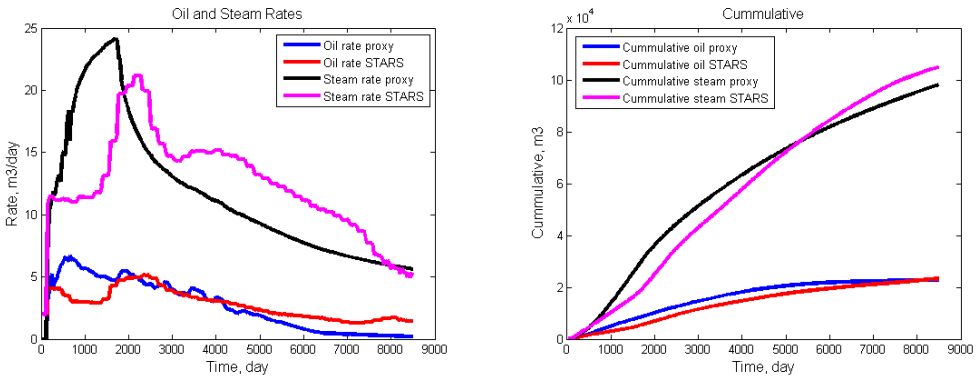

(a) Rates (b) Cumulates

Figure 4.14: Comparison between the proxy and simulator SAGD results for Model 2

The final cumulative oil production and steam injection of the proxy and simulator are close, but local mismatches are larger than the first model. The final cumulative oil of the proxy is 2% less than the simulator and the final cumulative steam injection of the proxy is 6% less than the simulator, see Fig. 4.14(b). For the forecasting the location of the steam chamber, the cumulative oil production results are needed and the mismatch between the steam injection results is not used. Fig. 4.15 shows a comparison between the proxy, simulator and Butler's model steam chamber location for Model 2 at three different time steps.

Fig. 4.15 shows that the shape of the proxy steam chamber is closer to the simulator than Butler's model at the different time steps. As Fig. 4.14 shows, the cumulative oil production of the proxy at different time steps are greater than the simulator. As a result, the steam front in the proxy moves faster than the simulator which causes a larger size of the proxy steam chamber compared to the simulator. Although the size of the proxy steam chamber is bigger than the simulator, the shape and size of the proxy steam chamber at different time steps is close to the simulator.

Fig. 4.16 shows a comparison between the total error percentage for forecasted steam chamber of Model 2 using the proposed method and the Butler's model.

Total error percentage for the proposed method is significantly less than the Butler's method at different time steps. The average of the total error percentage for the proposed method is about 4.6% and the average of the total error percentage for the Butler method is about 22%.

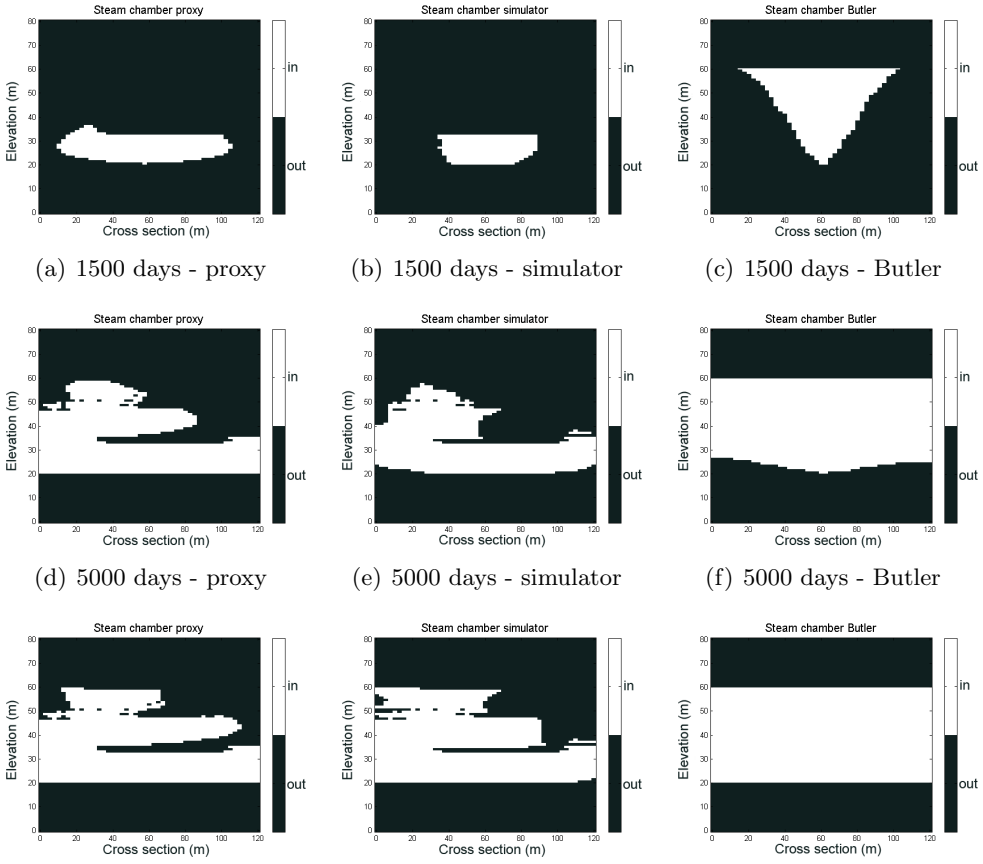

(a) 1500 days - proxy (b) 1500 days - simulator (c) 1500 days - Butler

(d) 5000 days - proxy (e) 5000 days - simulator (f) 5000 days - Butler

(g) 8500 days - proxy (h) 8500 days - simulator (i) 8500 days - Butler

Figure 4.15: Comparison between the steam chamber location of the proxy and simulator for Model 2 at different time steps

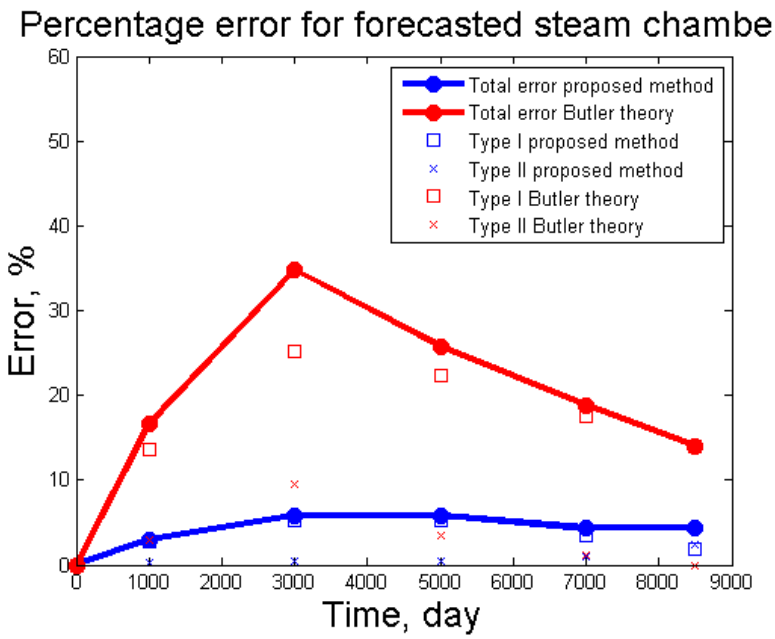

Figure 4.16: Total percentage error for the forecasted steam chamber of Model 2

4.4.3 Example 3 – 2D Synthetic Model 3

Fig. 4.17 shows a comparison between the Model 3 proxy and simulator order of grid cells for production.

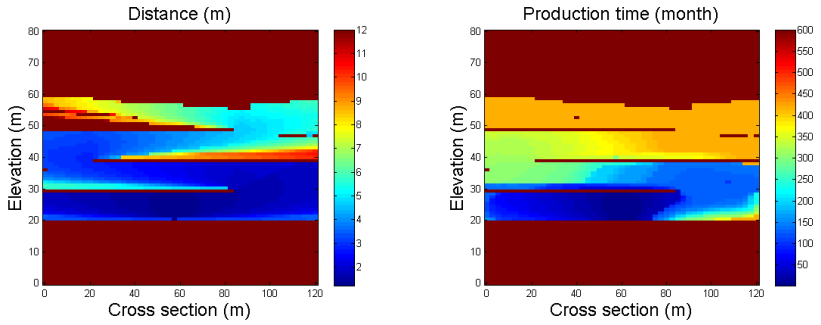

(a) Proxy order (b) Simulator order

Figure 4.17: Model 3 proxy and simulator order of grid cells for production

Fig. 4.17 shows order of grids for production in both of these methods are very close, although local differences can be observed. Fig. 4.18 shows a scatter plot between the results.

Fig. 4.18 shows some outliers around the 45 degree line, but the correlation coefficient is about 0.95 which is very high. Same as the first two examples, Fig. 4.19 shows a comparison between the oil production and steam injection of the proxy

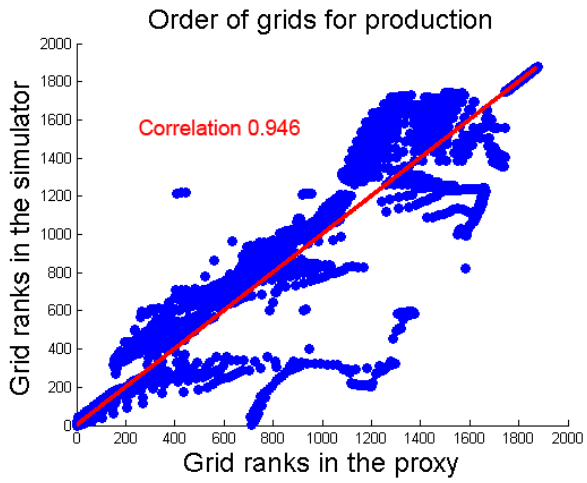

Figure 4.18: Scatter plot between proxy and simulator results of Model 3

and simulator for the Model 3.

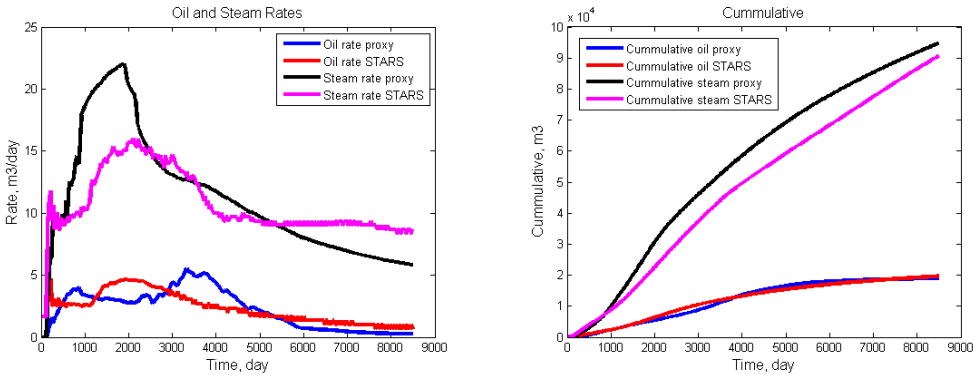

(a) Rates (b) Cumulates

Figure 4.19: Comparison between the proxy and simulator SAGD results for Model 3

Fig. 4.19 shows the final cumulative oil production and steam injection of the proxy and simulator. The mismatch between the oil production rates of the simulator and proxy is small and the final cumulative oil production of the proxy is only 3% less than the simulator which is not large. the mismatch between the steam injection rates is not important for finding location of the steam chamber. In this case, the final cumulative steam injection of the proxy is 4% greater than the simulator. Finally, Fig. 4.20 shows a comparison between the steam chamber location of the proxy, simulator and Butler's model for Model 3 at three different time steps.

As Fig. 4.20 shows, the shape of the proxy steam chambers are close to the simulator at different time steps. As Fig. 4.20 shows, the cumulative oil production

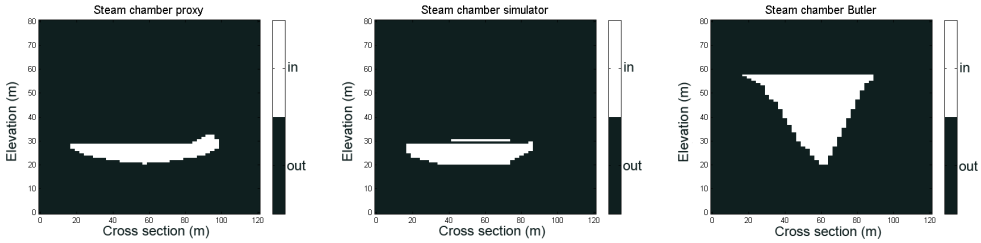

(a) 1500 days - proxy (b) 1500 days - simulator (c) 1500 days - Butler

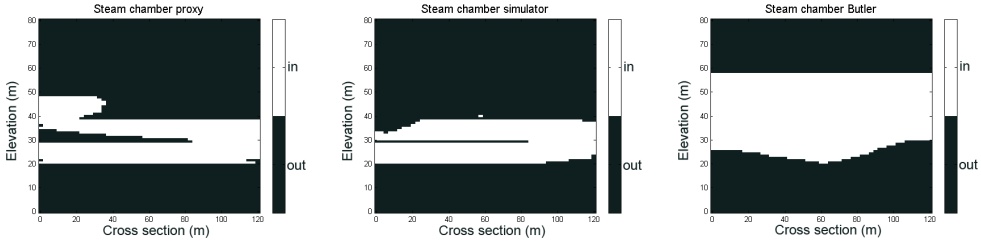

(d) 5000 days - proxy (e) 5000 days - simulator (f) 5000 days - Butler

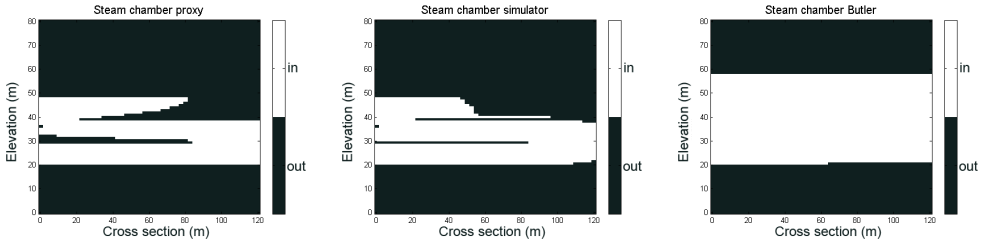

(g) 8500 days - proxy (h) 8500 days - simulator (i) 8500 days - Butler

Figure 4.20: Comparison between the steam chamber location of the proxy and simulator for Model 3 at different time steps

of the proxy after 4000 days is greater than the simulator, which causes faster move of the proxy steam chamber compared to the simulator and as a result, the bigger size of the proxy steam chamber compared to the simulator. Similar to the first two models, the shapes and sizes of proxy steam chamber are closer to the simulator results compared to Butler's model and it seems that this methodology works fine for forecasting the steam chamber location of heterogeneous models.

Fig. 4.21 shows a comparison between the total error percentage for forecasted steam chamber of Model 3 using new proposed method and Butler's model.

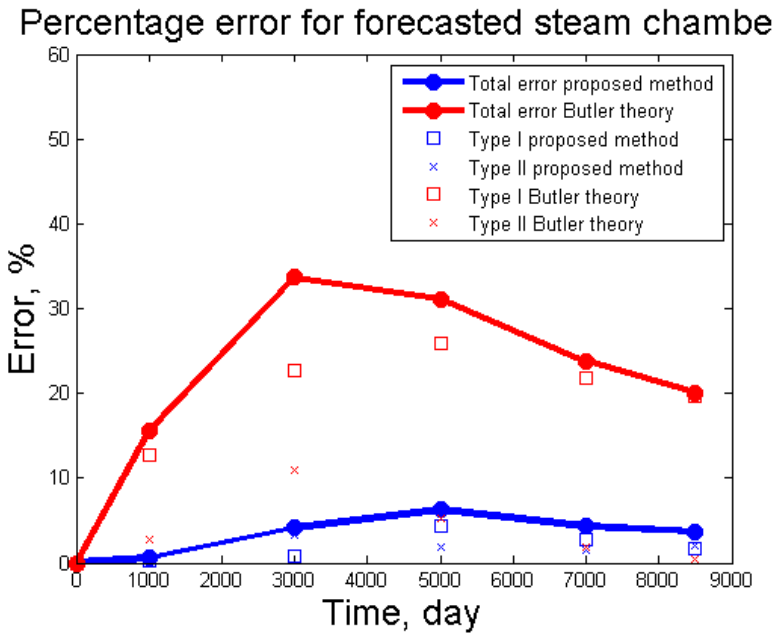

Figure 4.21: Total percentage error for the forecasted steam chamber of Model 3

The total error percentage for the proposed method is significantly less than Butler's method at different time steps. The average of the total error percentage for the proposed method is about 3.8% and the average of the total error percentage for Butler's method is about 24.8%.

4.5 Summary

In this Chapter, a new method for forecasting the steam chamber location is proposed. The results of CHV can be used for forecasting the order of grid cells for production. The CHV results are not time dependent and the proxy results can be used for finding the steam chamber location at different time steps. CHV finds the

order of grid cells for production. Also, the amount of oil inside each grid cell can be computed easily. By knowing the cumulative oil production at different time steps using the proxy, grid cells inside of the steam chamber at different time steps can be identified.

Different 2D heterogeneous models have been tested for forecasting the steam chamber location by the proposed method. Results show that the new method can predict the location of the steam chamber much better than Butler's theory. The following results can be concluded from this Chapter.

- Butler's method can be used for forecasting the steam chamber location of homogeneous model, but for heterogeneous models, the proposed method shows closer results to the simulator.

- For the proposed method, the steam chamber only covers grid cells that contain mobile oil. When there is no mobile oil in the grid cell, water is the mobile phase in those grid cells. As a result, steam loses its heat and cannot move through these grid cells. Butler's model covers all of the grid cells, including grid cells with mobile water.

- The forecasted steam chamber location can be used for considering the geomechanical effects to change the porosity and permeability of the grid cells inside the steam chamber at different time steps.

Chapter 5

Transferring Uncertainty and Ranking of Reservoir Realizations

Geostatistical methods are used to generate reservoir realizations for reservoir properties such as porosity, permeability and water saturation. Due to relatively widely spaced wells, there is always uncertainty in the reservoir properties. There are multiple realizations of each reservoir property at each location. These differences in the reservoir properties cause differences in the forecasted reservoir performance during simulation. The production uncertainty of the different reservoir realizations would be understood by running the flow simulator for each realization. An alternative is to rank the realizations based on a simpler ranking measure and then run the $P10$, $P50$ and $P90$ ranked realizations instead of all of them.

There are different ranking methods. Ranking can be done by the static OOIP or the connected hydrocarbon volume (CHV). These are statistical methods and in many cases the correlation between statistic and the flow simulation results may not be high. The true ranking could be obtained by running the flow simulator on all realizations and calculating the cumulative oil production or net present value (NPV) after a long production period. The NPV is perhaps the best ranking measurement, because it considers different factors such as oil price and injected steam costs, discount rate and amount of oil production and steam injection at different time steps. The run time for the reservoir simulator is very large. This is especially true with SAGD where a thermal simulator must be used due to temperature effects and changing fluids composition.

The semi-analytical SAGD proxy model developed in previous chapters could

be applied. This proxy is much faster than the flow simulator and it approximately estimates oil production and steam injection rates at different time steps. Geostatistical modeling of reservoir realizations are explained in Section 5.1. Then, Section 5.2 shows geological uncertainty of simulator results after applying the flow simulator to all realizations. The proxy results for ranking and uncertainty transferring are discussed in Sections 5.3 to 5.5. Experimental design for sensitivity analysis of ranking realizations are discussed in Section 5.6. Finally, conclusions are provided in Section 5.7.

5.1 Geostatistical Modeling of Reservoir Realizations

In this Chapter, a case study for ranking and uncertainty transferring of reservoir realizations has been considered. For this reason, 100 realizations similar to a realistic 3D model have been generated. The variogram has been fixed and 2 vertical wells were drilled were used for modeling reservoir properties. Top water and top gas exist in a thief zone at top of this model. There are two facies in this model. Wells are along the x direction. The grid dimensions are $26 \times 32 \times 83$ and grid sizes in x, y and z directions are 25 m, 2.5 m and 1 m respectively.

The first step is generating facies realizations. Non-stationary sequential indicator simulation has been used to account for the lower quality facies at the top of the reservoir. No significant horizontal trend has been observed in the model. Fig. 5.1 shows the vertical trend of the data by averaging within 3 m vertical increments using moving average method.

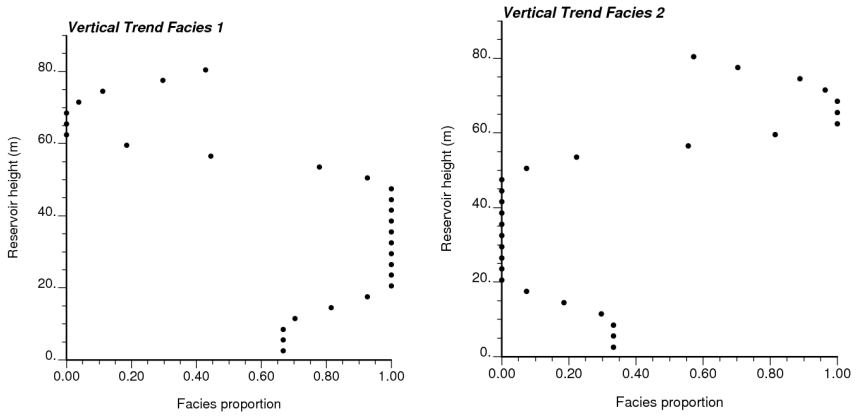

(a) Facies 1 (b) Facies 2

Figure 5.1: Vertical trend of simulation models

As Fig. 5.1 shows, facies 1 with high porosity and permeability has high probability between 15–50 m of the reservoir. The first 15 m of the model is below the well elevation. Most of the top portions of the reservoir belong to facies 2. The facies continuity in the horizontal plane is isotropic with a long range. Fig. 5.2 shows the horizontal and vertical indicator variogram.

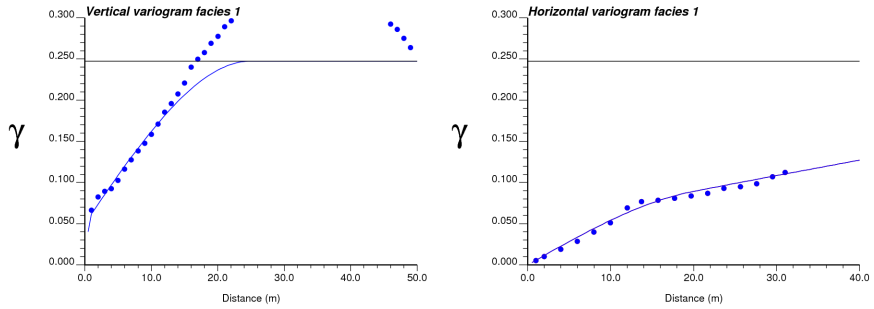

(a) Vertical (b) Horizontal

Figure 5.2: Vertical and horizontal variograms for rock type data of facies 1

As Fig. 5.2(a) shows, the vertical trend in the data is confirmed by the variogram points going above the variogram sill. After modeling the trend and fitting theoretical models to the experimental variograms, sequential indicator simulation has been used for generating 3D facies realizations (Deutsch and Journel, 1992). Fig. 5.3 shows slices of one of the generated realizations along the XZ and YZ planes. The XZ plane is along the well trajectory and the YZ plane is one of the 2D slices perpendicular to the well direction.

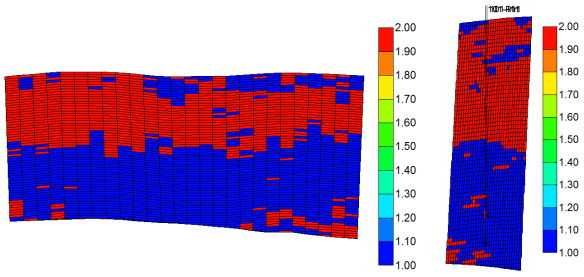

(a) XZ plane (b) YZ plane

Figure 5.3: Slices of one of the generated facies realizations at different directions – grid sizes in x, y and z directions are 25 m, 2.5 m and 1 m, respectively

As Fig. 5.3 shows, the low permeability formation above the sand formation is reproduced in the realization.

The next step is modeling porosity within each facies separately and then merg-

ing results of both facies based on the facies realizations. Porosity has been modeled using sequential Gaussian simulation method (Deutsch and Journel, 1992). Fig. 5.4 shows horizontal and vertical variograms of porosity data for facies 1 and facies 2.

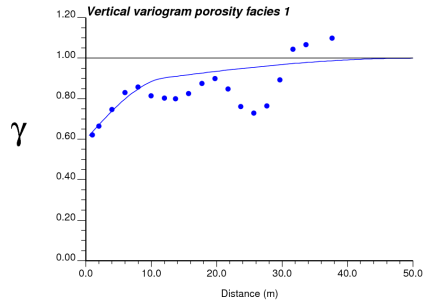

(a) Vertical variogram for porosity of facies 1

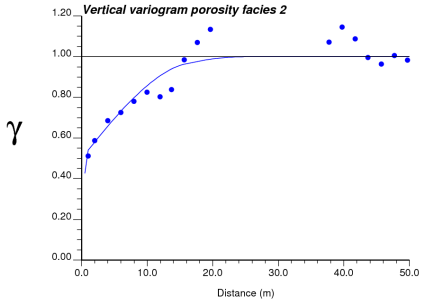

(b) Vertical variogram for porosity of facies 2

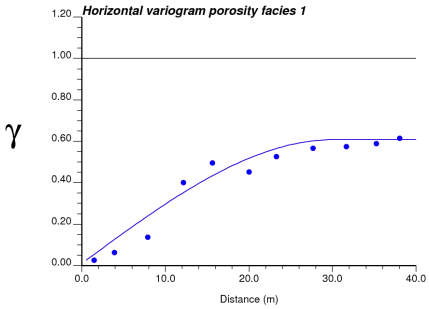

(c) Horizontal variogram for porosity of facies 1

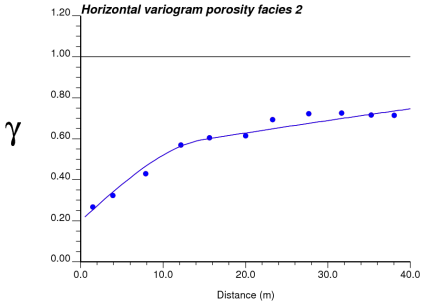

(d) Horizontal variogram for porosity of facies 2

Figure 5.4: Vertical and horizontal variograms of porosity data

As Fig. 5.4 shows, again horizontal range is much longer than the vertical range. Theoretical variograms were fit to these experimental variograms. Sequential Gaussian simulation was used for generating porosity realizations. Fig. 5.5 shows slices of one of the generated porosity realizations in the XZ and YZ planes.

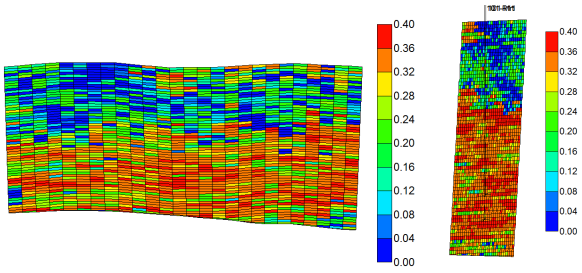

(a) XZ plane

(b) YZ plane

Figure 5.5: One slice of one of the generated porosity realizations at different directions – grid sizes in x, y and z directions are 25 m, 2.5 m and 1 m, respectively

The next step is generating horizontal permeability using the bi-model relationship with porosity and the cloud transform (Deutsch and Dose, 2005). Fig. 5.6 shows the relationship between porosity and horizontal permeability.

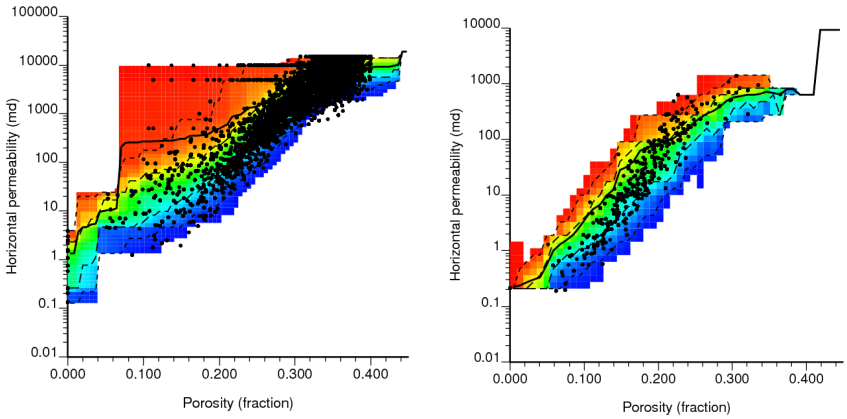

(a) Facies 1 (b) Facies 2

Figure 5.6: Bi-model relationship between porosity and horizontal permeability

The color in Fig. 5.6 represents the probability where blue is 0.0 and red is 1.0. Thus, the illustrated bivariate model is shown in cumulative conditional distribution functions (CCDF). The solid line is a series of the conditional mean of the horizontal permeability. The upper and lower dashed lines represent the $75th$ and $25th$ percentiles of the conditional distribution, respectively. Using this bi-variate CDF and the generated porosity realizations, the permeability realizations can be created.

Fig. 5.7 shows slices of one of the generated permeability realizations in the XZ and YZ planes.

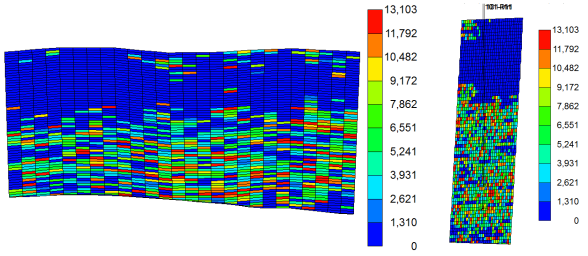

(a) XZ plane (b) YZ plane

Figure 5.7: One slice of one of the generated permeability realizations at different directions – grid sizes in x, y and z directions are 25 m, 2.5 m and 1 m, respectively

the vertical permeability realizations are generated from the horizontal perme-

ability realizations by multiplying them with a constant factor of 0.65.

Finally, the water saturation realizations have been generated using co-located co-kriging simulation with the porosity realizations (Deutsch and Journel, 1992). Water saturation of each facies has been modeled separately and then the results of both facies have been merged together based on the facies map. Fig. 5.8 shows these variograms.

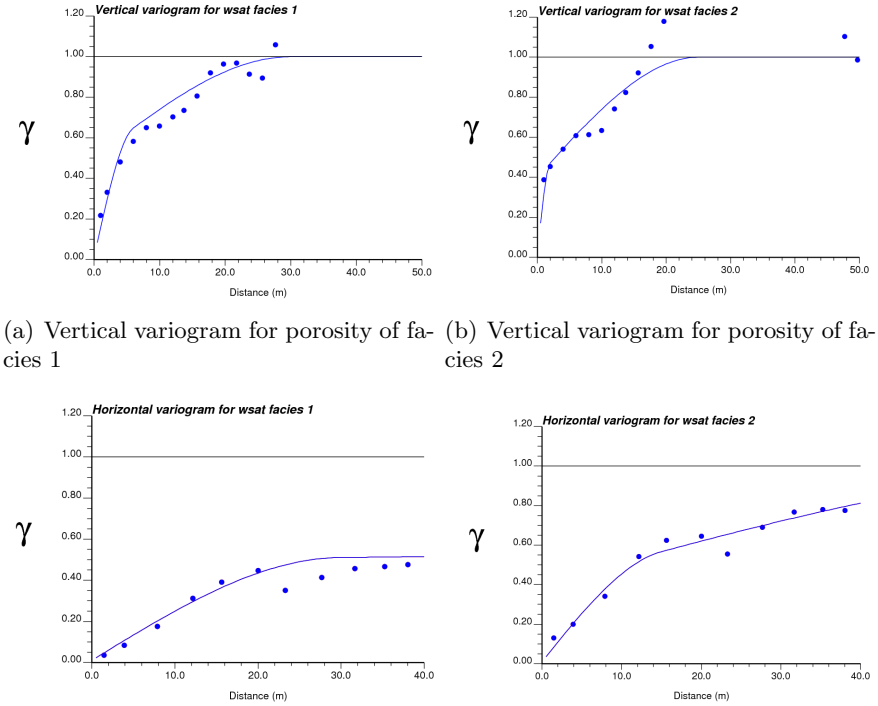

(a) Vertical variogram for porosity of facies 1

(b) Vertical variogram for porosity of facies 2

(c) Horizontal variogram for porosity of facies 1

(d) Horizontal variogram for porosity of facies 2

Figure 5.8: Vertical and horizontal variograms of water saturation data

As Fig. 5.8 shows, the horizontal ranges are much longer than the vertical ranges as expected. Water saturation realizations are cosimulated with the porosity realizations are generated for each facies. The results are merged together based on the facies realizations. Fig. 5.9 shows slices of one of the generated water saturation realizations in the XZ and YZ planes.

5.2 Simulator Results

100 realizations were simulated for facies, porosity, permeability and water saturation. This geological uncertainty can be transferred through simulation to understand uncertainty in cumulative oil production and cumulative steam injection. For

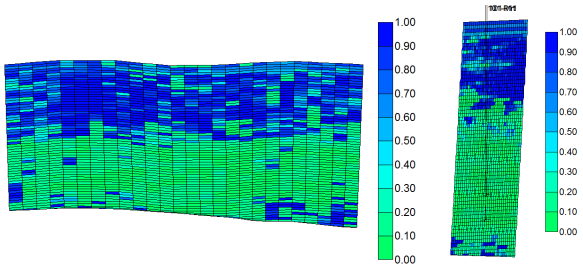

(a) XZ plane (b) YZ plane

Figure 5.9: Slices of one of the generated water saturation realizations in different directions – grid sizes in x, y and z directions are 25 m, 2.5 m and 1 m, respectively

this example, simulator the run time for each realization is about 20 hours. The STARS simulator, developed by CMG (Computer Modeling Group), is industry standard for thermal simulation (Computer Modeling Group Ltd., 2012) and has been applied to all realizations to establish a base case. To quantify the uncertainty with a limited number of realizations, realizations should be ranked for finding their orders based on NPV. The SAGD semi-analytical proxy developed in this dissertation can be used to run each realization in about 10 seconds compared to 20 hours for the flow simulator. For assessing ranking efficiency, the results can be compared with the results of the flow simulator.

The cumulative oil production and cumulative steam injection of the simulator are used to compute the NPV with a 10% discount rate per year. For this example, an oil production price of $\$500/m^3$ and a steam injection cost of $\$50/m^3$ were used. The realizations can be ranked based on the simulator NPV and results can be compared with other approximate ranking methods such as volumetric ranking by the OOIP, connected hydrocarbon volume ranking with various options and finally with proxy ranking based on the estimated NPV. Similar to the simulator, the proxy estimates both oil production and steam injection rates at different time steps. Other methods are unable to consider the effect of oil and steam prices, discount rate and amount of oil production and steam injection rates. It is desirable to find a quick method that gives a high correlation coefficient with the base case results of the simulator.

For setting the operating strategy of the simulation models, it is assumed that unlimited steam is available for injection into the reservoir and the maximum bottomhole pressure is 4000 kpa. The only difference between the realizations is reservoir properties. All of the models were run through STARS (Computer Modeling Group

Ltd., 2012) for finding base case oil production and steam injection for 15 years. Fig. 5.10 shows the results of simulated realizations after running them through STARS.

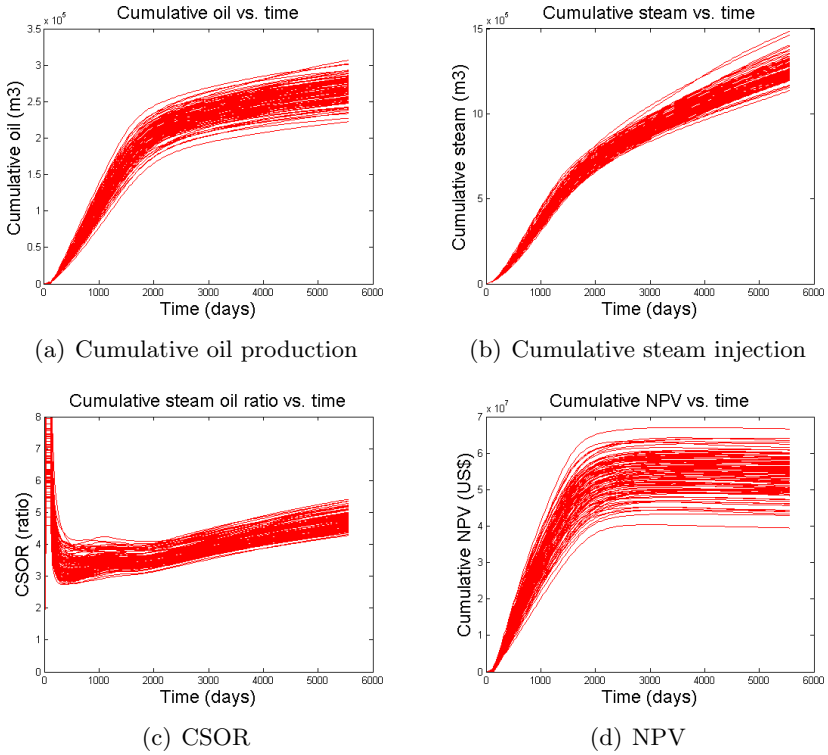

(a) Cumulative oil production

(b) Cumulative steam injection

(c) CSOR

(d) NPV

Figure 5.10: SAGD results of simulated realizations after running them by simulator

Fig. 5.10(a) shows the cumulative oil production of different realizations. The difference between the final cumulative oil productions of realizations is about 84000 m^3. This is a reasonable range of uncertainty; a very narrow range of uncertainty would make ranking of the realizations very difficult. Figs. 5.10(b)–5.10(c) show that the range of uncertainty for cumulative steam injection and CSOR are about 347000 m^3 and 1.1, respectively. The range of CSOR may be too narrow for a high correlation in the ranking results. Fig. 5.10(d) shows the cumulative simulator NPV. The NPV increases fast for the first 3000 days, then the rate is decreasing and for the last time steps NPV is negative. Decreasing cumulative NPV is due to steam injection into the reservoir without producing a significant amount of oil. As a result, the net income becomes negative. Fig. 5.11 shows the rate of NPV change versus time for all realizations.

Fig. 5.11 shows that the NPV rates are increasing for all realizations in the first 1000 days, then they start decreasing for the next 2000 days, but still they are all

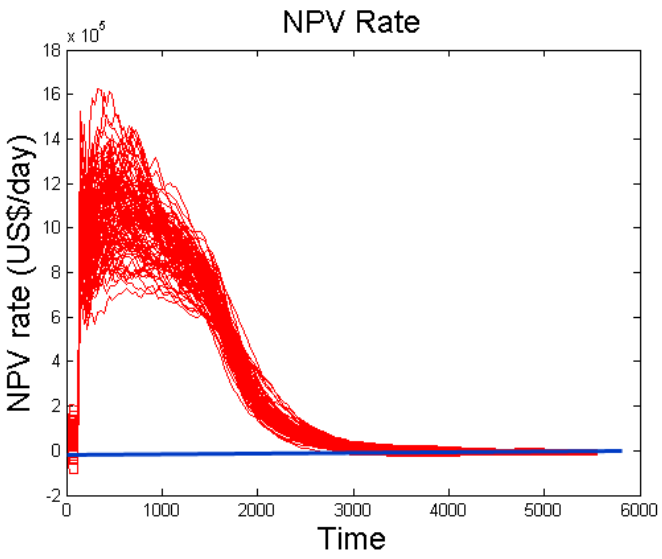

Figure 5.11: Rate of NPV change for different simulated realizations after running them in the reservoir simulator

positive. After 3000 days, the NPV rates are zero or negative. The blue line on Fig. 5.11 is the zero NPV line. The NPV can be computed for the proxy too. The ranked results of the simulator can be compared with the ranked results of the proxy as well as other ranking measures such as OOIP and CHV. There are two different versions for the CHV tool. The first older version is based on finding the connected net grids along lines of sight to the producer. The second newer version is based on the finding all of connected net cells in the model and tagging them with flow step, angle and distance.

Ranking has been repeated two times by selecting two different simulation periods. These periods are 1- Long-term ranking (15 years) and 2- Short-term ranking (5 years). Fig. 5.10 shows that the curves do not cross too much, but uncertainty ranges for the short-term production is too narrow. A very narrow range of uncertainty would make ranking of the realizations very difficult. For this reason, short-term ranking has been considered in this Chapter.

5.3 Long-term Ranking Results

Fig. 5.12 shows the comparison between ranking results of the simulator NPV and the ranking methods: the proxy NPV, the OOIP and the CHV (both versions) after 15 years of simulation. The vertical axes in all sub-figures are related to the simulator

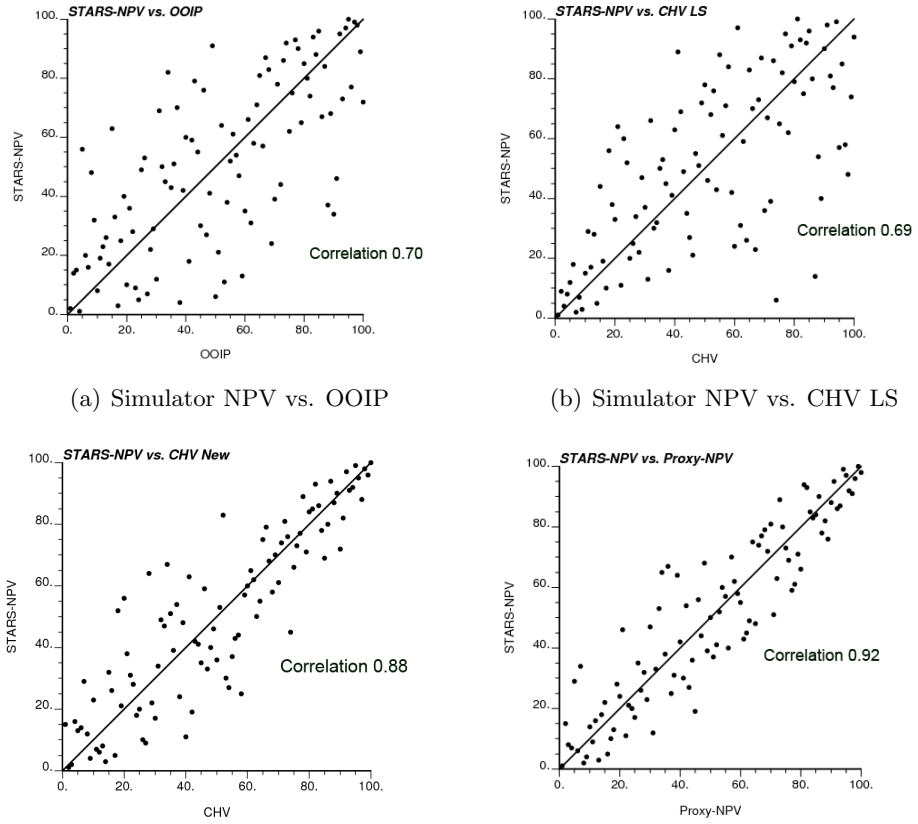

(a) Simulator NPV vs. OOIP

(b) Simulator NPV vs. CHV LS

(c) Simulator NPV vs. new CHV

(d) Simulator NPV vs. proxy NPV

Figure 5.12: Comparison between ranking results of simulator NPV and other methods such as proxy NPV, OOIP and also CHV after 15 years production using 23 slices

NPV ranking results. Horizontal axes are also related to the ranking results of other methods. In all of the methods, the results are ranked in descending order, that is, the order of results is from $P100$ (high) to $P1$ (low). The $P100$ realization has the best reservoir quality with the highest NPV. As discussed before, the proxy uses the new CHV tool internally to identify the producible amount of oil. For this reason, close results are expected for the proxy and the new CHV tool. Nevertheless, the proxy results should be better because the CHV cannot compute oil production rate and steam injection rates at each time step. As expected, the highest correlation coefficient is to the proxy NPV at 0.92. After that, the next highest correlation coefficient is between the simulator NPV and new CHV at 0.88. The OOIP and the old CHV show the lowest correlation coefficients at about 0.7 which is low and many outliers can be observed around the 45 degree line. It seems that the proxy is a reliable tool for forecasting NPV of different realizations. It can be interesting to look at correlation coefficient of ranking results of proxy and simulator for other parameters such as oil production, steam injection and CSOR. Fig. 5.13 shows the relationship between ranking results of proxy and simulator.

As Fig. 5.13(a) shows, the correlation coefficient between the simulator and proxy oil production is 0.89 which is quite high, but there are at least 6 outliers which that are shown within the red ellipse. In all of these cases, the proxy underestimated oil production compared to the simulator. Fig. 5.14 shows status of different slices along the well in the simulation model.

As Fig. 5.14 shows, the model has 26 cross sectional slices. 23 out of 26 of them have been completed and steam can be injected from them into the reservoir. These slices are identified by the dark blue color. There are no completions in the first two slices and the last slice of the simulation model. The simulator will permit, steam to enter these slices and produce oil from them. The proxy assumed that there are only 23 completions in the model and, as a result, may underestimate the cumulative oil production and cumulative steam injection. Steam cross-over to the non-completed slices will increase cumulative oil production and cumulative steam injection significantly. The correlation coefficient for the steam injection results decreased more than the oil production because these slices will take more steam.

Realization number 38 is one of the realizations within the red ellipse. Fig. 5.15 shows the location of the steam chamber in those three non-completed slices using ternary diagram of fluids. The steam chamber can be identified by the red color.

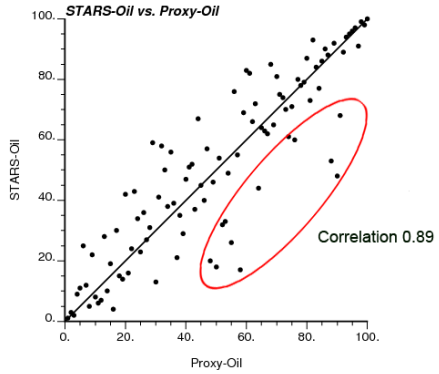

(a) Simulator oil vs. proxy oil

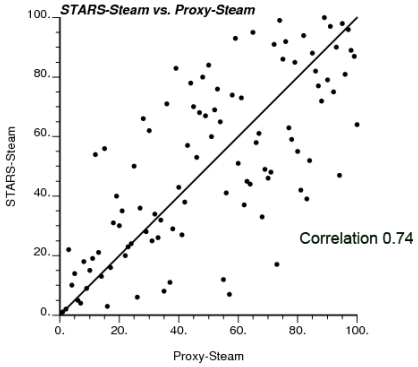

(b) Simulator steam vs. proxy steam

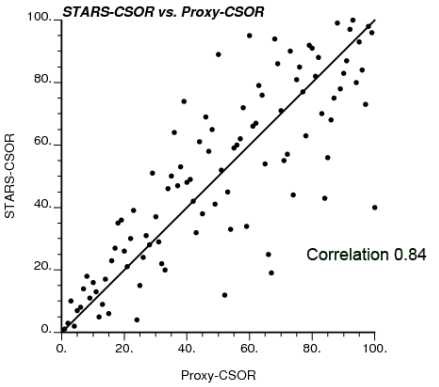

(c) Simulator CSOR vs. proxy CSOR

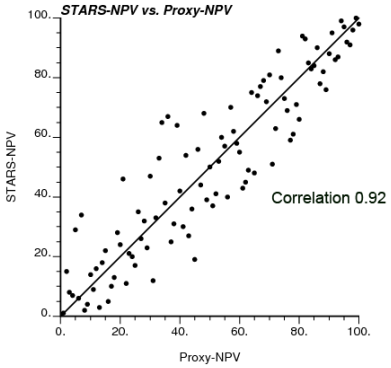

(d) Simulator NPV vs. proxy NPV

Figure 5.13: Relationship between ranking results of proxy and simulator after 15 years production

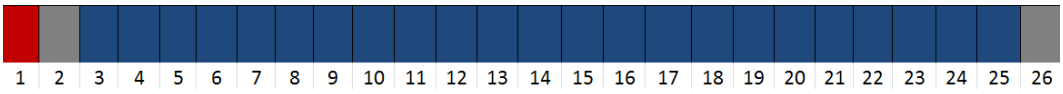

Figure 5.14: Status of different slices along the well in the simulation model

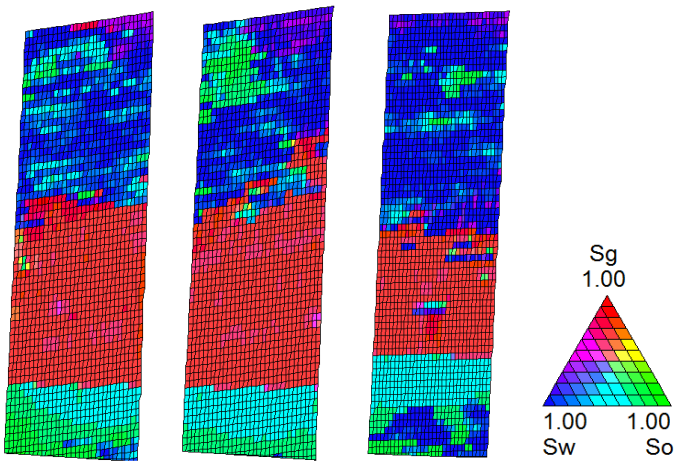

(a) Slice 1 (b) Slice 2 (c) Slice 3

Figure 5.15: Steam chamber at non-completed slices for realization number 38 – grid sizes in horizontal and vertical directions are 2.5 m and 1 m, respectively

As Fig. 5.15 shows, steam entered all of those three slices and oil was produced from those slices. As a result, both the cumulative oil production and cumulative steam injection have been increased significantly. By removing the 6 outliers in the Fig. 5.13(a), the correlation coefficient will increase to 0.94 which is very high. The cross-over of steam and oil between adjacent slices is an important limitation to be addressed. In any case, the correlation coefficient for NPV is about 0.92 which is very good. In the case of NPV, the effect of outliers with more oil production and steam injection would reduce because of the trade off between oil production price and steam injection cost.

The next step is to select the $P10$, $P50$ and $P90$ realizations by the proxy and compare them with the simulator results. The central idea of ranking is based on finding these realizations to limit uncertainty of the 100 realizations to 3. Table. 5.1 shows the corresponding simulator ranks for the chosen $P10$, $P50$ and $P90$ realizations of proxy after 15 years of simulation.

Table 5.1: Corresponding simulator ranks for $P10$, $P50$ and $P90$ realizations of proxy after 15 years production

Proxy	**Simulator**
P10	P12
P50	P50
P90	P86

As Table. 5.1 shows, the simulator $P50$ and proxy $P50$ are exactly the same which is a coincidence. The differences between the $P10$ and $P90$ of the simulator and the $P10$ and $P90$ of proxy are small. Fig. 5.16 shows a comparison between $P10$, $P50$ and $P90$ realizations of simulator NPV and proxy NPV after 15 years of production. Cumulative oil productions and cumulative steam injections for these realizations are compared. The proxy results are shown by the blue curves and the

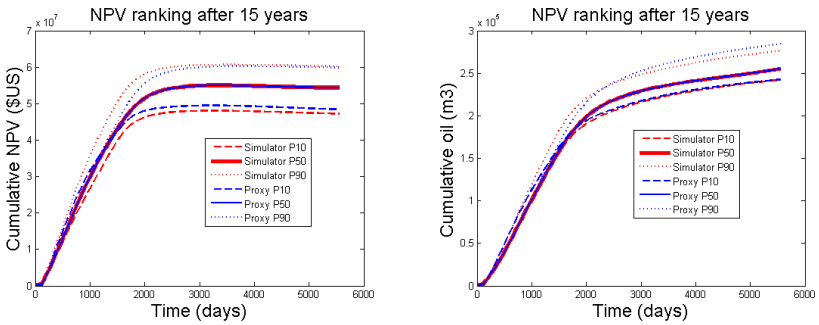

(a) Cumulative NPV vs. time

(b) Cumulative oil vs. time

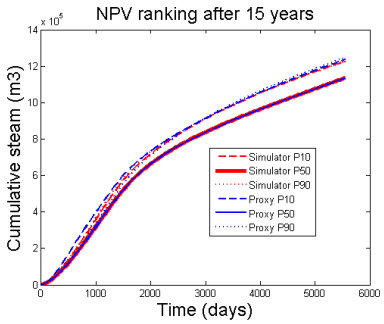

(c) Cumulative steam vs. time

Figure 5.16: Comparison between $P10$, $P50$ and $P90$ realizations of simulator NPV and proxy NPV after 15 years of simulation

simulator results are shown by the red curves. The $P50$ results overlay one another. The proxy $P10$ is the simulator $P12$; therefore, the proxy is slightly higher than the simulator, but difference is only about 2%. Also, the $P90$ of the proxy is the $P86$ of the simulator. As a result, the proxy $P90$ should be a little less than the proxy. In this case the difference is less than 1%. Based on these differences, the proxy computed the range of uncertainty very well. The cumulative steam injection of the $P10$ and $P90$ for both the proxy and simulator are very close to the each other.

Although the proxy $P50$ was the same as the simulator $P50$ in this case, it is not very common. There are scattered realizations around the $P50$ and any of them could have been selected instead of the one on the 45 degree line. It can be

interesting to find the range of uncertainty around each of the $P10$, $P50$ and $P90$ realizations. A large dispersion of points around the 45 degree line is not desirable. For finding uncertainty range around $P10$, $P50$ and $P90$ realizations, the interval could be divided into three groups and it is desirable to have a narrow distribution for each of these groups. These ranking indices do not necessarily predict oil and steam rates, but they can be standardized so that the results can be compared to each other. The following formula can be used for standardization:

$$y = \frac{z - \mu}{\sigma} \tag{5.1}$$

where z is value in original units, μ is the mean and σ is the standard deviation. Fig. 5.17 shows a comparison between the standardized simulator NPV and other methods based on their standardized values.

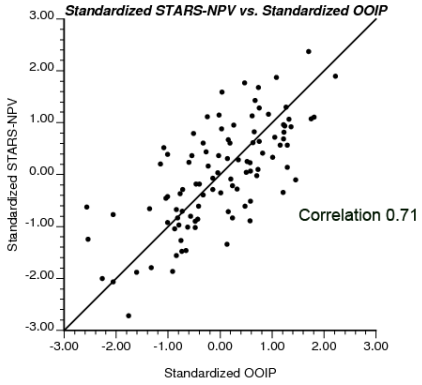

(a) Std. simulator NPV vs. Std. OOIP

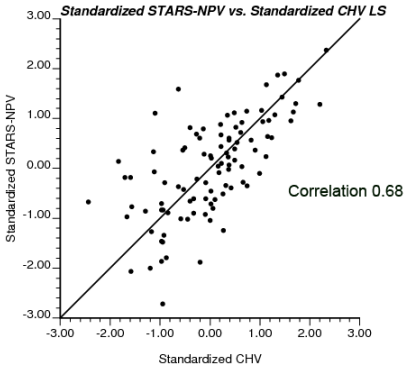

(b) Std. simulator NPV vs. Std. CHV LS

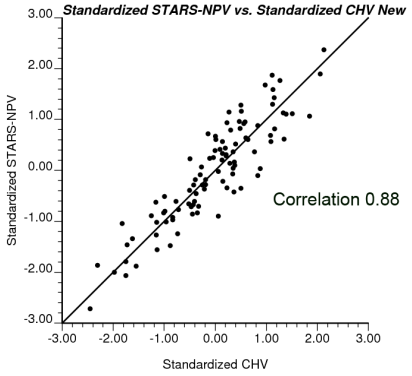

(c) Std. simulator NPV vs. Std. new CHV

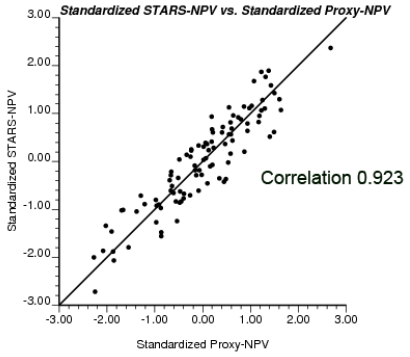

(d) Std. simulator NPV vs. Std. proxy NPV

Figure 5.17: Comparison between standardized simulator NPV and other methods based on their standardized values

Fig. 5.17 shows that the ranges of uncertainty around the $P10$, $P50$ and $P90$ for the proxy are very narrow. The ranges for new CHV are narrow too, but not as

narrow as the proxy. The ranges for the OOIP and old CHV ranking are worse.The mean absolute error (MAE) for identifying $P10$, $P50$ and $P90$ realizations using proxy NPV have been tabulated in Table. 5.2. These values have been obtained by averaging absolute errors between the simulator $P10$, $P50$ and $P90$ with the proxy $P10 \pm 5$, $P50 \pm 5$ and $P90 \pm 5$. As an example, all of values between $P45$ and $P55$ have been selected and the mean absolute error with the simulator $P50$ has been computed. In this case, effect of outliers around $P10$, $P50$ and $P90$ realizations can be studied.

Table 5.2: Maximum percentage errors for identifying $P10$, $P50$ and $P90$ using proxy

Rank	Maximum percentage of proxy error
P10	4.4%
P50	2.3%
P90	3.6%

Table. 5.2 shows that even in the worst case the errors are not very large.

5.4 Long-term Uncertainty Transferring

Fig. 5.18 shows the uncertainty in oil production, steam injection, CSOR and NPV computed by the proxy compared them with the simulator results. Both oil production and steam injection of the simulator may be higher because of the slices with no completions (cross over) and steam cross over between adjacent slices. In this case, effect of slices with no completions is mote than the effect of steam cross over between adjacent slices. Number of slices will completion is 23 and considering 2 non-completed slices on both sides may increase the cumulative oil production and steam injection significantly. For this reason, the simulator results have been compared with the proxy results by considering 23 completed slices, 25 slices (23 completed+2 non-completed slices on both sides) and 26 slices (23 completed+3 non-completed slices).

Fig. 5.18(a) shows that the proxy underestimates both the simulator oil production, that is, the uncertainty range is shifted down compared to the simulation results. In all of these 100 realizations, steam moved at least to one of those three slices. The proxy range of uncertainty for oil production considering 25 slices is close to the range of uncertainty from the simulator. In this case, the minimum oil

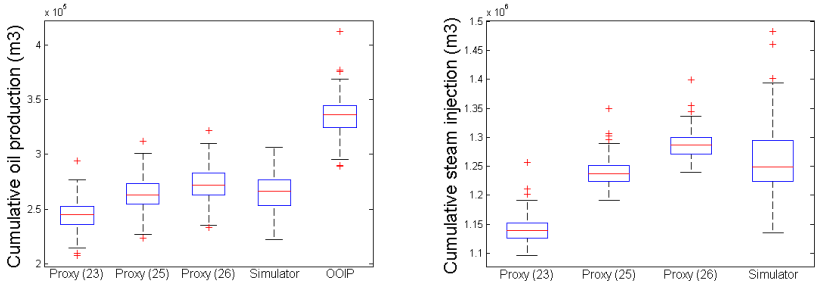

(a) Oil uncertainty range

(b) Steam uncertainty range

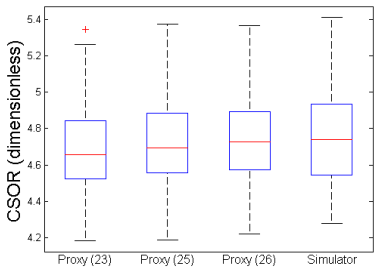

(c) CSOR uncertainty range

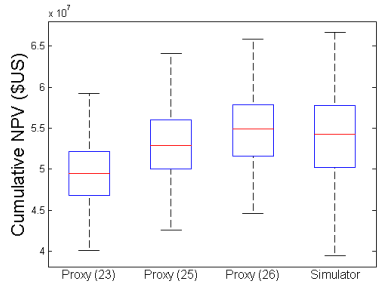

(d) NPV uncertainty range

Figure 5.18: Comparing proxy range of uncertainty with simulator

production in the proxy is about 1% greater than the simulator and the maximum oil production in the proxy is about 2% greater than the simulator. By considering all 26 slices, the oil production in some of the realizations would be overestimated. In most of the realizations, steam just moved to the slices left of the first completed slice and right of the last completed slice. The recovery factor for the different cases is around 70%-75% of recoverable oil above the producer. For this reason, the final cumulative oil production for the different cases are much less than the OOIP for those cases.

Also, Fig. 5.18(b) shows a comparison between the ranges of uncertainty for the cumulative steam injection for the proxy and simulator. The range of steam uncertainty for the proxy is much narrower than the simulator due the cross over discussed above. As discussed above, the steam of the first and last completed slices may enter other uncompleted slices. By considering only 23 slices, the proxy underestimates the cumulative steam injection of most realizations. Considering 25 slices provides results that are closer to the simulator.

Fig. 5.18(c) shows the CSOR ranges of uncertainty for the proxy and the simulator. As discussed before, when steam enters to the non-completed slices, both

oil production and steam injection are increased and the CSOR may not change significantly. For this reason, the range of uncertainty for cases with 23, 25 or 26 slices are very close to each other. By considering 25 slices, the minimum CSOR in the proxy is only about 2% less than simulator and the maximum CSOR in the proxy is about 1% less than the simulator. These differences are considered to be very small.

Finally, Fig. 5.18(d) shows the NPV ranges of uncertainty for the proxy and simulator. Again, the proxy NPV uncertainty range with 23, 25 and 26 slices cover the entire range of simulator uncertainty. Because the ranges of uncertainty for the cumulative oil production and cumulative steam injection are different, the range of uncertainty for NPV would be different too. As Fig. 5.18(d) shows, by considering 25 slices, the minimum NPV in the proxy is about 8% greater than the simulator and the maximum NPV in the proxy was about 3% less than the simulator.

Based on above discussions, non-completed slices in the model is an important cause of difference between the proxy and simulator results.

5.5 Short-term Ranking Results

Fig. 5.19 shows a comparison between the ranking results of simulator NPVs and other methods such as OOIP, new CHV and proxy NPV after 5 years of simulation.

In this case, the correlation coefficient between simulator NPV and proxy NPV is still high at 0.85. The correlation coefficient between the simulator NPV and new CHV ranking is about 0.83 which is less than the long-term ranking. OOIP and old CHV ranking show the lowest correlations with the simulator NPV at 0.62 and 0.67, respectively. In all cases the correlation coefficient decreased compared to the long term ranking. For short-term simulation, ranking of realizations is more difficult than long-term simulation. In this case, both the cumulative oil production and cumulative steam injection of different realizations at the end of 5 years are very close to each other. This can be observed in the Fig. 5.19. As a result, finding the correct rank order would be very difficult. The proxy can estimate oil production and steam injection at different time steps and, as a result, is able to rank the realizations quite well. Most of the deviations are around the $P50$ realization. As Fig. 5.19(d) shows, correlation coefficient between ranking result of simulator oil and proxy oil is still high which is 0.86. In this case, due to the short simulation period, steam did not enter to the other non-completed slices significantly, but because of

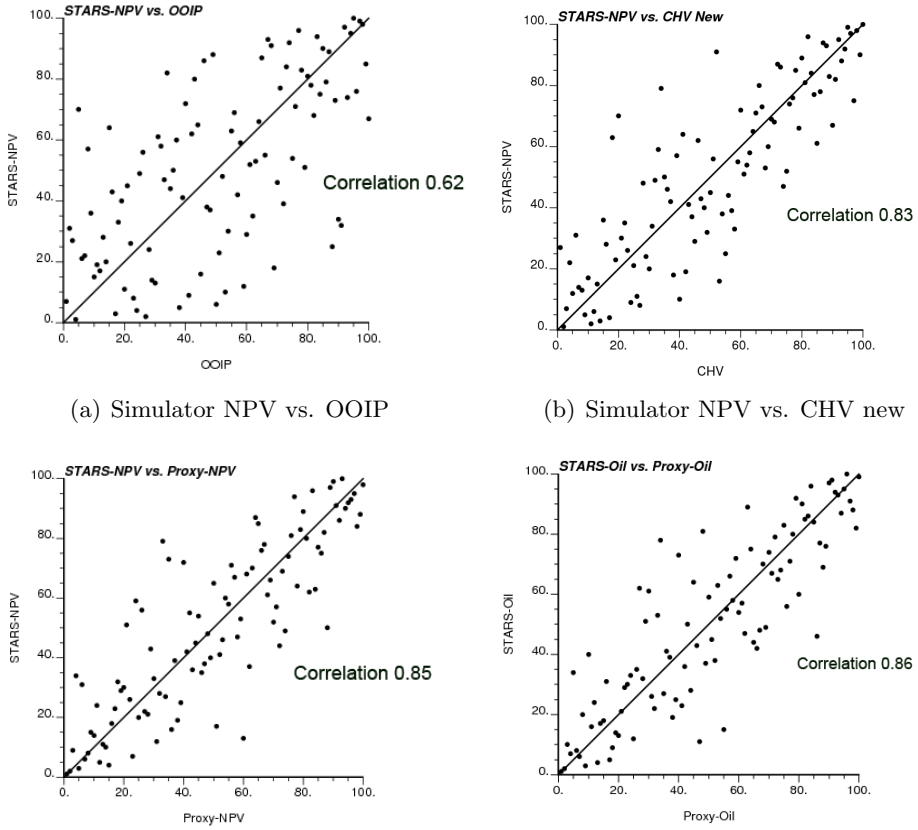

(a) Simulator NPV vs. OOIP

(b) Simulator NPV vs. CHV new

(c) Simulator NPV vs. proxy NPV

(d) Simulator oil vs. proxy oil

Figure 5.19: Comparison between ranking results of simulator NPV and other methods after 5 years production using 23 completed slices

short-term simulation, final cumulative oil productions of different realizations are close to the each other. Table. 5.3 shows the corresponding simulator rank for the $P10$, $P50$ and $P90$ realizations of the proxy after 5 years of simulation.

Table 5.3: Corresponding simulator rank for $P10$, $P50$ and $P90$ of proxy realizations after 5 years production using 23 completed slices

Proxy	Simulator
P10	P2
P50	P35
P90	P86

Table. 5.3 shows that the proxy overestimated the simulator rank $P10$, $P50$ and $P90$ realizations and proxy $P10$, $P50$ and $P90$ are less than the simulator $P10$, $P50$ and $P90$ realizations. Fig. 5.20 shows a comparison between $P10$, $P50$ and $P90$ realizations of simulator NPVs and proxy NPVs after 5 years of simulation. The oil production and steam injection for these realizations are also compared with each other.

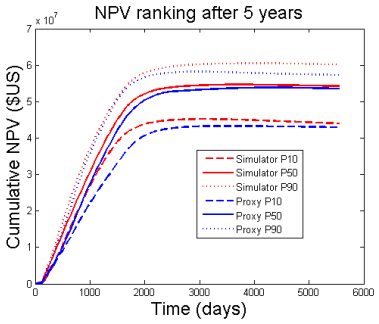

(a) Cumulative NPV vs. time

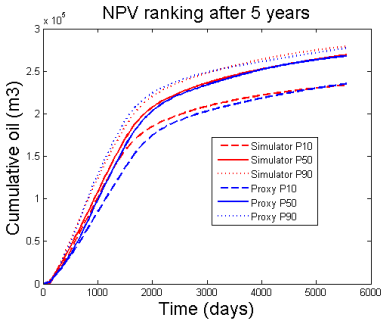

(b) Cumulative oil vs. time

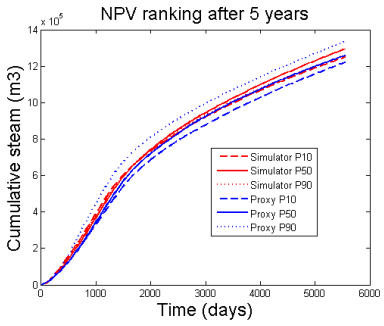

(c) Cumulative steam vs. time

Figure 5.20: Comparison between $P10$, $P50$ and $P90$ realizations of simulator NPV and proxy NPV after 5 years of simulation

Again, the proxy results have been shown by the blue curves and the simulator results have been shown by red curve. Fig. 5.20(a) shows that the proxy $P10$ is lower than the simulator $P10$ by about 2%. The proxy $P50$ and proxy $P90$ are about 1% and 4% less than the simulator $P50$ and $P90$ respectively. Figs. 5.20(b)–5.20(c) show that the final cumulative oil production of the proxy and simulator for each of $P10$, $P50$ and $P90$ are very close to each other. Also, the cumulative steam injection of each cases is close to each other.

5.6 Experimental Design for Sensitivity Analysis of Ranking Results

The correlation coefficient between the simulator and proxy results should be reasonably high, otherwise applying the proxy for different applications such as prediction, transferring uncertainty, ranking reservoir realizations and well trajectory optimization would may be unreliable. There are many parameters in the proxy parameter file, and most of them can be picked from the STARS simulation file, but some of them are uncertain and changing them may change the correlation coefficient and influence proxy accuracy. These uncertain parameters are the proxy time step size (Δt) and the maximum permeability (k_{max}). The duration of the simulation (t_f) can be important for some applications. Three levels have been selected for each of these factors. Reservoir realizations have been generated for the sensitivity analysis. These realizations have been run through the simulator. After that, they have been run by the proxy using different levels of parameters. For each case, realizations have been ranked based on their cumulative NPV. The correlation coefficients between the simulator and proxy have been computed. The sensitivity of changes in the correlation coefficient by changing these factors can be measured for finding significant factors.

5.6.1 Problem Statement

Although the proxy is very fast, some applications such as well trajectory optimization requires it to be run thousands of times. The time step size could be increased for faster run times but it may decrease the accuracy of prediction. The sensitivity of changing the results by changing the time step size should be considered. Also, the average permeability is a very important parameter for finding the steam front location at each time step. If the steam front moves very fast, all of oil in the

reservoir can be drained quickly. For computing the average permeability, a maximum value for permeability should be set in the proxy since a few high permeability values have a large influence on the results. For this reason, a maximum value for permeability is set in the proxy to keep the average permeability in a reasonable range. For this reason, a sensitivity of changing the maximum permeability should be considered as well. Also, the duration of simulation can be important. When the simulation period is short e.g. 1000 days, the effect of the steam front velocity would be important and it may affect the simulation results significantly. For all of these reasons, the important factors and their effects on changing production and injection results should be investigated. A full factorial experimental design with 3 levels for each factor has been selected for the sensitivity study. Using experimental design, important factors and their effects on changing the correlation coefficient between proxy and simulator results can be identified.

This experiment is called a three-way layout experiment. The proxy time step size, maximum permeability and duration of simulation are treated as setting parameters, that is three quantitative factors with three levels each are examined in the experiment. These factors and their levels are summarized in Table. 5.4. The response is the correlation coefficient between simulator and proxy results.

Table 5.4: Parameter settings for experimental design

Treatment effect	**Level 1**	**Level 2**	**Level 3**
Duration of simulation (t_f), $days$	1860	3720	5550
Proxy time step size (Δt), $days$	0.5	5	10
Maximum permeability (k_{max}), md	1500	2500	3500
Response	Correlation coefficient		

The three levels of time step size have been selected to assess increasing time step size and its effect on the ranking results. The base case maximum permeability is 2500 md.

5.6.2 Data Collection and Implementation of the Experiment

The realizations generated at the start of this chapter have been used. These 100 reservoir realizations have been randomly split into two groups of 50 realizations. Each group can be considered as one replicate. In this case, the variation between replicates can be computed. Then, each realization should be run with the simulator

and NPV should be computed based on the simulator oil productions and steam injection. As a result, 50 NPV values can be computed for each group from those 50 realizations. Then, these realizations should be run by the proxy for finding 50 NPV values based on the proxy results. Then, for each group, the correlation coefficient between the 50 NPV values from the simulator and the 50 NPV values from the proxy should be computed as the response variable. Only the simulation duration changes the simulator result, but by changing any of these parameters, the NPV values for the proxy can be changed. As a result, the correlation coefficient between simulator and proxy ranking result will change. By computing the response for all of these cases, analysis of results can be started using experimental design.

5.6.3 3^k Full Factorial Design

The experiment is analyzed using a three-way layout design with three levels for each factor (Montgomery, 2006; Wu and Hamada, 2000). The three-way layout model considers the influence of the main factor effects, the two factor interaction effects and the three factor interaction effect.

$$\begin{gathered} y_{ijk} = \eta + \alpha_i + \beta_j + \gamma_k + (\alpha\beta)_{ij} + (\alpha\gamma)_{ik} + (\beta\gamma)_{jk} + (\alpha\beta\gamma)_{ijk} + \varepsilon_{ijk} \\ i = 1,2,3 \quad j = 1,2,3 \quad k = 1,2,3 \end{gathered} \tag{5.2}$$

In this case, analysis of a 3^k factorial design is carried out where 3 is the number of levels and k is the number of factors. Because the number of factors in this example is three, the total number of cases would be $3^3 = 27$. Three levels for each factor permits consideration of two-factor interactions that are linear and quadratic effects. These three level are denoted by 0, 1 and 2. Assume two factors A and B, whose levels are denoted by x_1 and x_2. In this case, AB is contrasted among the response values whose x_1 and x_2 satisfy

$$x_1 + x_2 = 0, 1, 2 \text{ (mode 3)}$$

and AB^2 shows contrasts among the response values whose x_1 and x_2 satisfy

$$x_1 + 2x_2 = 0, 1, 2 \text{ (mode 3)}$$

As a result, $A \times B$ interaction can be decomposed into four components which are $(AB)_l$, $(AB)_q$, $(AB^2)_l$ and $(AB^2)_q$ (Montgomery, 2006; Wu and Hamada, 2000).

In the same way, $A \times B \times C$ can be decomposed to four components which are ABC, ABC^2, AB^2C and AB^2C^2 and same as before, each of them has two degrees

of freedom. In this case, 3^3 cases have 26 degrees of freedom (linear and quadratic effects) and they can be divided into 13 components where 3 of them are the main effects (A, B, C) and 10 of them are interactions.
These are: $(AB, AB^2, AC, AC^2, BC, BC^2, ABC, ABC^2, AB^2C, AB^2C^2)$. Other interactions are aliased with these 10 interactions and can be ignored.

Table. 5.5 shows the response for different factor-level combinations using a 27 factorial design.

Table 5.5: Response for different factor-level combinations

Simulation time (t_f)	**Time step size** (Δt)	**Maximum permeability** (K)	**Correlation coefficient**	
			Replicates 1	**Replicates 2**
1860	0.5	1500	0.720	0.777
		2500	0.884	0.909
		3500	0.904	0.935
	5	1500	0.723	0.780
		2500	0.885	0.910
		3500	0.904	0.936
	10	1500	0.726	0.783
		2500	0.885	0.910
		3500	0.906	0.936
3720	0.5	1500	0.934	0.927
		2500	0.945	0.940
		3500	0.949	0.945
	5	1500	0.934	0.928
		2500	0.945	0.940
		3500	0.949	0.945
	10	1500	0.933	0.928
		2500	0.945	0.940
		3500	0.949	0.945
5550	0.5	1500	0.912	0.926
		2500	0.918	0.931
		3500	0.921	0.932
	5	1500	0.913	0.927
		2500	0.919	0.931
		3500	0.921	0.933
	10	1500	0.913	0.927
		2500	0.921	0.932
		3500	0.924	0.934

As Table. 5.5 shows, the variation can be observed between the correlation coefficient of different replicates. For analyzing results, the average of replicates and variance of replicates for each case can be used for plotting location and dispersion half normal

plots. Fig. 5.21 shows different factors and their levels.

	t_f $(days)$
-1	1860
0	3720
1	5550

	Δt $(days)$
-1	0.5
0	5
1	10

	k_{max} (md)
-1	1500
0	2500
1	3500

Figure 5.21: Data configuration for DOE

As Fig. 5.21 shows, in this study, all factors are quantitative factors and the increment between levels for each factor is nearly the same.

5.6.4 Analysis for 3^k Full Factorial Design

In this section, the experimental design is evaluated with plots of main effects and factor interactions. To get the analysis of variance and compute half normal plots, the data from Table. 5.6 have been used.

Based on the above table, factorial and interaction effects can be computed. Fig. 5.22 shows a box plot of the different levels for each factor. The bounds of each box are the 25% and 75% percentiles, the whiskers are the extremes and line in the middle of box is the median.

These box plots provide rough idea of the significant factors. It seems that time step size did not change the correlation coefficient significantly. Also, it seems that lower levels of simulation time and maximum permeability changed the results significantly and these factors are significant.

Fig. 5.23 shows the interaction plots. From the interaction plots, it seems that the correlation coefficient only changes by changing simulation time or maximum permeability and time step size does not have any effect. The correlation coefficient for mid-term or long-term rankings are close to each other and it did not change significantly in the mid-level or high-level of maximum permeability. Also, the short-term ranking generally has lower correlation coefficient than the mid-term or long-term. This is especially true if the maximum permeability is low. During the short-term ranking, most of realizations have similar cumulative oil productions and steam injections, for this reason, ranking of realizations would be difficult. Especially when maximum permeability is low, the steam front moves very slow and a significant amount of oil cannot be drained during the simulation. For this reason, a lower

Table 5.6: Average response between replicates for different factor-level combinations

Run	Factor levels			Responses
	t_f	Δt	k_{max}	Mean replicates
1	-1	-1	-1	0.749
2	-1	-1	0	0.897
3	-1	-1	1	0.920
4	-1	0	-1	0.752
5	-1	0	0	0.898
6	-1	0	1	0.920
7	-1	1	-1	0.755
8	-1	1	0	0.898
9	-1	1	1	0.922
10	0	-1	-1	0.931
11	0	-1	0	0.943
12	0	-1	1	0.948
13	0	0	-1	0.932
14	0	0	0	0.943
15	0	0	1	0.948
16	0	1	-1	0.931
17	0	1	0	0.943
18	0	1	1	0.948
19	1	-1	-1	0.920
20	1	-1	0	0.925
21	1	-1	1	0.927
22	1	0	-1	0.920
23	1	0	0	0.926
24	1	0	1	0.928
25	1	1	-1	0.921
26	1	1	0	0.927
27	1	1	1	0.929

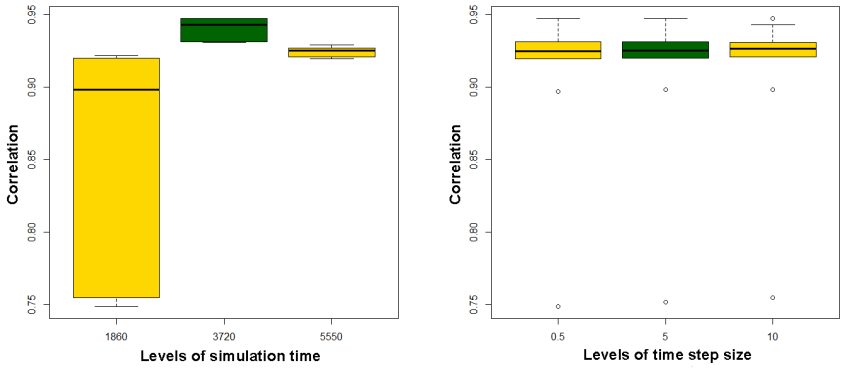

(a) Simulation time

(b) Time step size

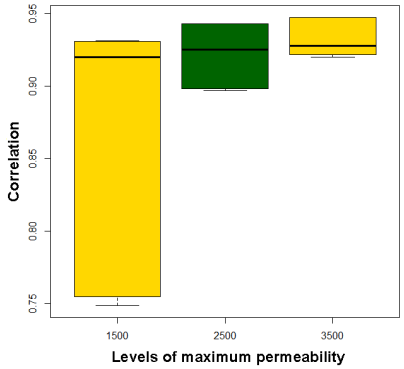

(c) Maximum permeability

Figure 5.22: Box plot for different levels of each factor

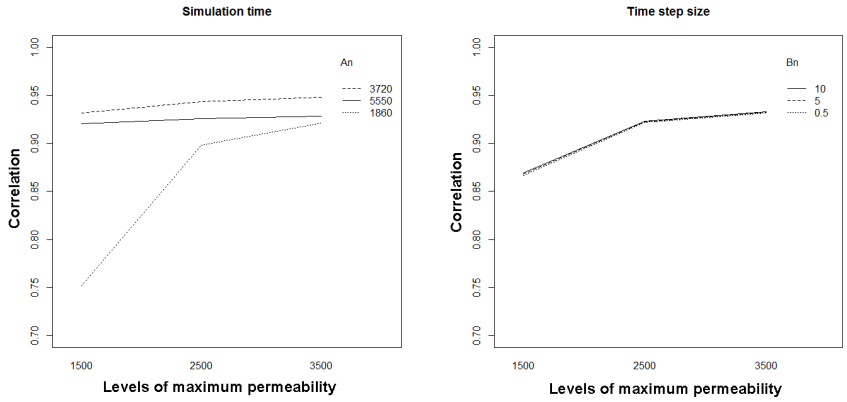

(a) Interaction between simulation time and maximum permeability

(b) Interaction time step size and maximum permeability

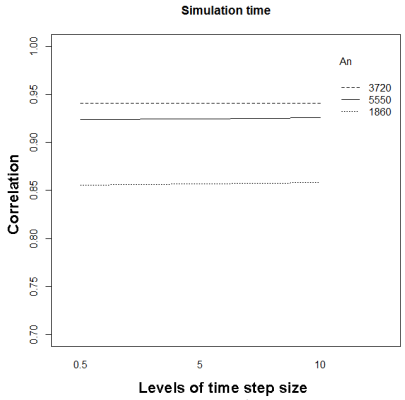

(c) Interaction between simulation time and time step size

Figure 5.23: Interaction effects between different factors

level of maximum permeability gives the lowest correlation coefficient, especially for short-term ranking.

As discussed before, for finding significant effects, the location and dispersion half normal plots can be used. A half normal plot is a plot of the absolute effects versus the positive axis of the normal distribution. By fitting a straight line (red line) to most of the points in the half normal plot, any effect whose corresponding point falls off the line is declared as significant (Daniel, 1959). Fig. 5.24 shows half normal plot for location and dispersion effects.

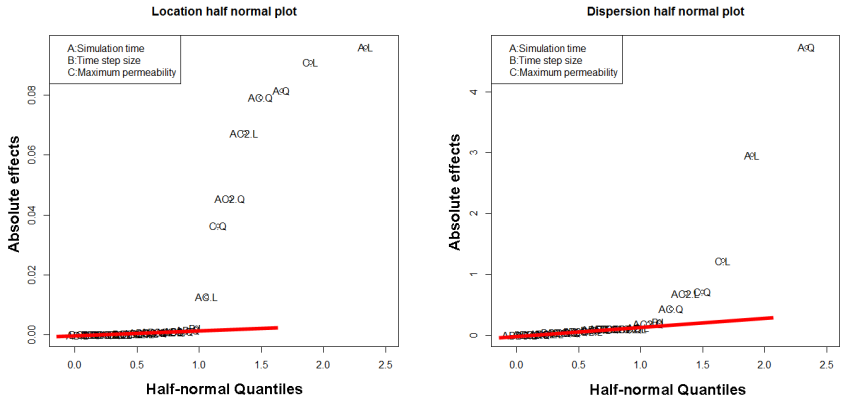

(a) Location (b) Dispersion

Figure 5.24: Half normal plots

The correlation coefficient can be maximized while minimizing dispersion between the replicates. For this reason, the important factors in both of location (correlation coefficient) and dispersion should be identified.

The half normal plot shows that factors A (simulation time), factor C (maximum permeability), and also interaction $A:C$ which has components (AC and AC^2) are significant (both linear and quadratic effects).

Also, the dispersion half normal plot shows that factors A (simulation time), factor C (maximum permeability), and also some components of interaction $A:C$ which are quadratic AC and linear AC^2 are significant.

After finding the significant factors for both location and dispersion, the model can be fitted to the significant factors. Final equations in terms of the coded factors are:

$$\hat{y} = 0.56 + 7.32 \times 10^{-5} x_{A_i} + 1.13 \times 10^{-4} x_{C_i} - 2.18 \times 10^{-8} x_{A_i C_i}$$

$$\ln s^2 = -5.26 - 8.22 \times 10^{-4} x_{A_i} - 8.05 \times 10^{-4} x_{C_i} + 1.004 \times 10^{-7} x_{A_i C_i}$$

For maximizing location and minimizing variance, a mid-level of factor A (simulation time) and a high level of factor C (maximum permeability) should be selected which gives the optimal correlation coefficient by selecting $A = 3750$ days and $C = 3500$ md.

This assumes that the residuals are normal. For these reason, a residual plot should be shown to check this assumption. The data should be normalized if necessary. Fig. 5.25 shows plots of residual vs. different levels of each significant factor.

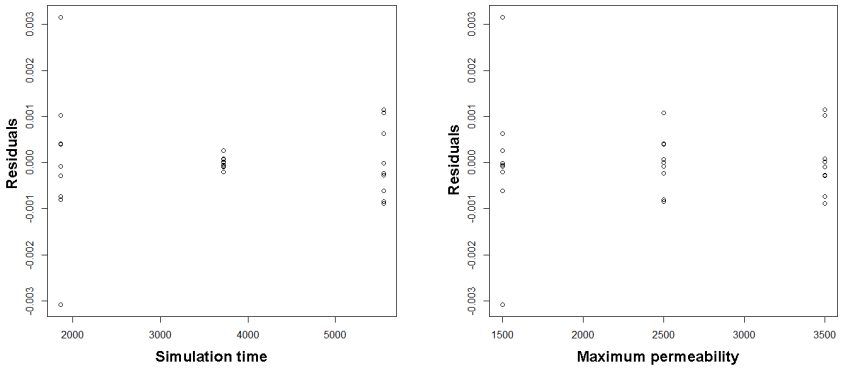

(a) Simulation time (b) Maximum permeability

Figure 5.25: Residual vs. different levels of each significant factor

If the model is correct and if the assumptions are satisfied, the residuals should be structureless. As Fig. 5.25 shows, in these cases the residuals are structureless. These plots also show that there is more variability in the low level of factor A (simulation time) and factor C (maximum permeability), but for other levels, the variability is less. Also, Fig. 5.26 shows a normal QQ plot as another check of normality.

As Fig. 5.26 shows, most of the data are on the straight line and the assumption of normality seems reasonable.

5.6.5 Response Surface Methodology

Although the factor B (time step size) is not significant, it is included in the response surface methodology. For considering the nonlinear effects in plotting response surfaces, the central composite design is used for finding the response surfaces, because it is a second order design and fit a second order model to capture the curvature effects (Wu and Hamada, 2000). Fig. 5.27 shows the response surfaces between each

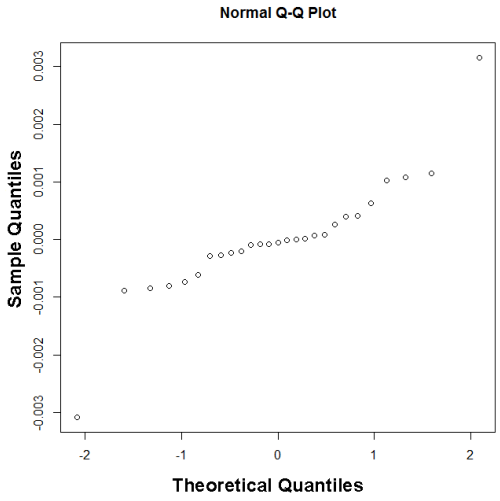

Figure 5.26: QQ plot for checking normality assumptions

two factors. As Fig. 5.27 shows, the time step size does not have any effect on changing the correlation coefficient. Also, lower values of simulation time and maximum permeability decrease the correlation coefficient significantly. As discussed before, mid-term ranking and high value of maximum permeability gives the highest correlation coefficient.

Obviously mid-term or long-term rankings are easier than short-term ranking. Also, by decreasing maximum permeability the steam front velocity will decrease significantly which causes underestimating the cumulative oil production. If we are uncertain about the optimal value of maximum permeability, a value around 2500 md can be a good choice.

5.7 Summary

Transferring uncertainty and ranking of reservoir realizations are discussed in this Chapter. At the start of this Chapter, Geostatistical modeling of $3D$ reservoir realizations was discussed. After that, long-term (15 years) transferring uncertainty and ranking of reservoir realizations for a set of realizations was performed. Ranking of reservoir realizations was also performed for short-term production to consider the proxy performance for a narrow range of uncertainty. Finally, experimental design was used for sensitivity analysis of ranking results. Some points can be concluded from this Chapter:

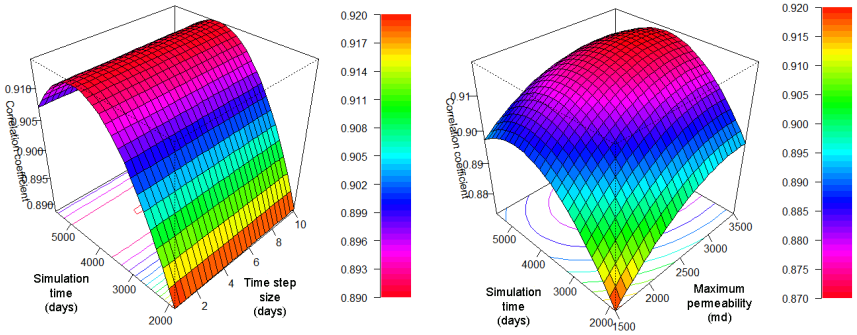

(a) Response of simulation time vs. time step size at $k = 3500$ md

(b) (b) Response of simulation time vs. maximum permeability at $\Delta t = 5$ days

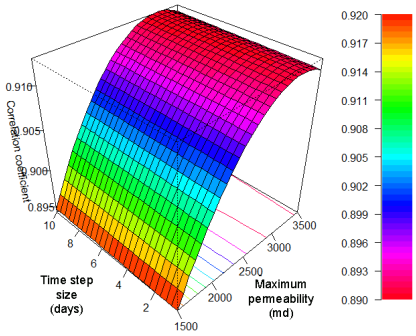

(c) (c) Response of time step size vs. maximum permeability at $t = 3750$ days

Figure 5.27: Response surfaces between different factors

- Ranking results show that the correlation coefficient between the simulator NPV and the proxy NPV is 0.92 for long-term ranking and 0.85 for short-term ranking. The proxy is a reliable tool for forecasting NPV of different realizations.

- Transferring uncertainty results show that the cumulative steam injection of the proxy is less than the simulator because of the slices with no completions (cross over) and steam cross over between adjacent slices. The oil, the CSOR and the NPV ranges of uncertainty for the proxy and simulator were close.

- Experimental design results show that by decreasing maximum permeability, the steam front velocity will decrease significantly which makes short-term ranking difficult because of underestimating the cumulative oil production. Also, short-term ranking is more difficult than mid-term or long-term rankings because of the narrow range of uncertainty of the simulator results.

Chapter 6

Well Trajectory Optimization

An important task before starting a SAGD operation is optimizing the location of the well trajectories. There are shale barriers and other heterogeneous features at different positions in these reservoir. Steam cannot pass a thick shale barrier. Also, if there is a shale barrier between the injector and producer, oil cannot drain to the producer. For these reasons, optimizing the injector and producer well trajectories is important. Running reservoir simulator is very time consuming and running trial and error cases to optimize the producer and injector trajectories is not practical. On the other hand, robust well trajectory optimization must consider uncertainty in the reservoir parameters. This optimization problem cannot be solved in a short time calling the simulator for many possible trajectories and geostatistical realizations. An approximate simulation of performance using the proxy is a practically important application.

In this Chapter, two methods are tested for well trajectory optimization. The first method is based on random sampling from a 3D box that has been selected for drilling wells. Then, the differential evolution (DE) optimization algorithm has been used for automatically improving the trajectory location. The second method is based on parameterizing the trajectory using a Hermite spline, then optimizing the parameters of the spline. The producer and injector trajectories of a realistic model have been optimized using these methods as a case study.

Section 6.1 explains details of the well trajectory optimization problem. Section 6.2 documents the methodology. Section 6.3 shows a case study based on a realistic 3D model. Finally, conclusions are provided in Section 6.4.

6.1 Problem Statement

It is desirable to drill production wells at or close to the bottom of the continuous bitumen interval, that is, the base of continuous bitumen (BCB). The BCB surface is not flat.

There are many constraints for the well trajectory. If the difference between the elevations of two adjacent completions is too great, there can be uneven growth of the steam chamber and steam cross-over between adjacent slices which increases heat losses and steam requirements (University of Alberta CCG Annual Meeting, 2013). The presence of bottom water (Doan et al., 2003) is very important and drilling a well too low into bottom water causes condensing steam production of mobile water. As a result, the SAGD operation would be inefficient. For these reasons, choosing the vertical position of the wells is a challenge. Fig. 6.1 shows a case that producer trajectory is above the BCB elevation and all of bitumen above producer can be produced during the SAGD operation. As Fig. 6.1 shows, the well

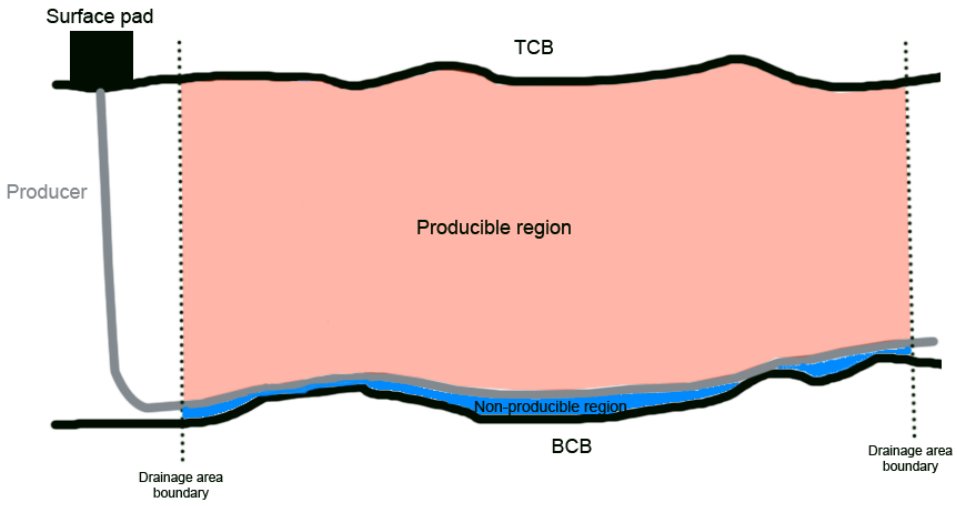

Figure 6.1: Drilling well trajectory close to the BCB elevation. Well length is 1 km, producible region thickness is 50 m, and the vertical exaggeration is $10\times$.

trajectory may be close to the BCB, but in some sections the trajectory is a little bit above the BCB elevation to permit a practically smooth well trajectory.

In certain cases it may be better to drill the well below the BCB elevation. In this case, although all of the oil of those slices may not be produced, other slices could be closer to the BCB and as a result, the cumulative NPV could be higher

than the case where all of the completions are above the BCB. A simple assumption is that a completion below the BCB, means that the oil of that slice cannot be produced. A sketch of this is shown in Fig. 6.2.

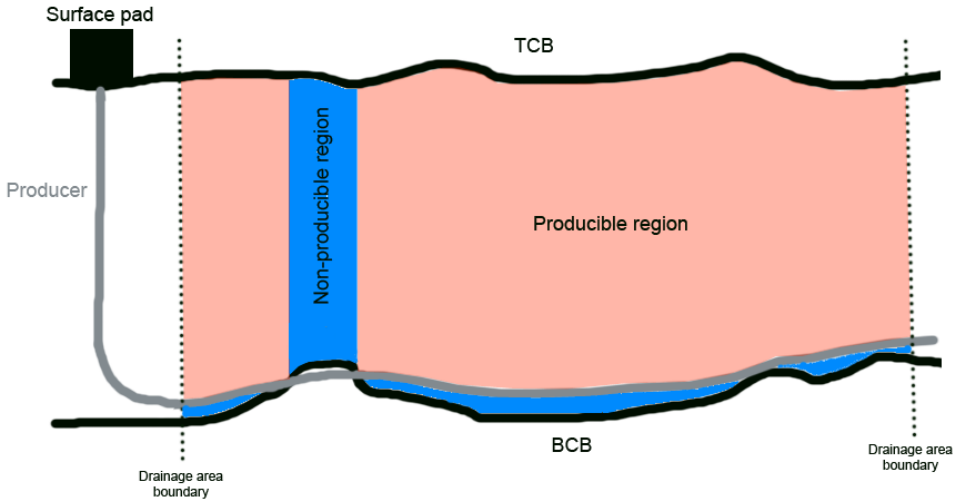

Figure 6.2: Drilling well trajectory below the BCB elevation. Well length is 1 km, producible region thickness is 50 m, and the vertical exaggeration is $10\times$.

Also the presence of shale barriers close to the bottom of the reservoir may cause different problems. Drilling a well through zones with very low porosity and/or permeability will reduce production from that completion. This is true for the injector too since steam cannot be injected into the reservoir and the bitumen not heated. Any shale barriers between the producer and injector may also prevent oil draining to the producer. In this case, even if the producer is drilled above the BCB elevation, the oil of those slices may not be produced. Fig. 6.3 shows an example with a shale barrier between the producer and injector. Fig. 6.3 illustrates that a shale barrier between the producer and injector will impede production. In this case, communication between injector and producer cannot be established to produce bitumen.

Robust well placement optimization should be done by considering uncertainty in the reservoir properties. True value of reservoir properties are never known and different realizations will have different BCB elevations. This uncertainty is very important for optimizing the well trajectory.

Running different models with trajectories chosen by trial and error is very time

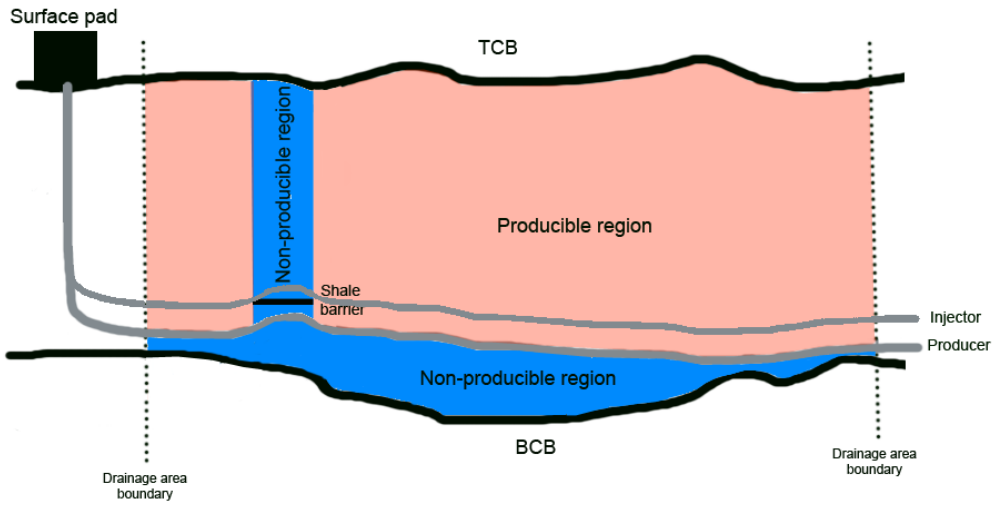

Figure 6.3: Shale barrier between producer and injector. Producer and injector lengths are 1 km, producible region thickness is 50 m, and the vertical exaggeration is $10\times$.

consuming and it is unlikely that optimal locations would be found. Average run time for a 3D model with 40 slices along the well (each 25 m thickness) and well spacing of 80 m is about 30 hours. For this reason, most of the well trajectory optimization is based on a static measure of recovery from the geological model (Manchuk and Deutsch, 2012; McLennan et al., 2006). Some authors screened the realizations and performed the optimization only on a few realizations with the flow simulator (Yang et al., 2011). Even with a few ranked realizations, the run time would be very large and uncertainty will not be considered completely. For this reason, using the proxy for well trajectory optimization can be very helpful.

6.2 Methodology

Two different methods for optimizing well trajectories have been implemented in this work. The optimal location of the injector is usually five meters above the producer. The only important factor about finding location of injector is to make sure that its location is not in or close to low porosity permeability grid cells, otherwise the injector will not be able to inject steam into the reservoir. During the calculation of the objective function based on the location of the producer, the proxy checks for shale barriers up to 5 meter above the producer. The porosity and permeability of all of grid cells inside a chamber with 64° (based on the angle of steam rising

chamber) above the producer for each layer should be checked for identifying shale barriers above the producer. If there is any shale barriers at these elevations, the proxy assumes that there is no connection between the producer and injector and, as a result, bitumen cannot be produced. Also, one meter above and one meter below the injector will be checked to avoid drilling the injector close to a shale barrier. The location of the producer and injector should be optimized simultaneously. Fig. 6.4 shows the procedure of checking the existence of a shale barriers around producer and injector. As Fig. 6.4 shows, the existence of shale barriers within a steam

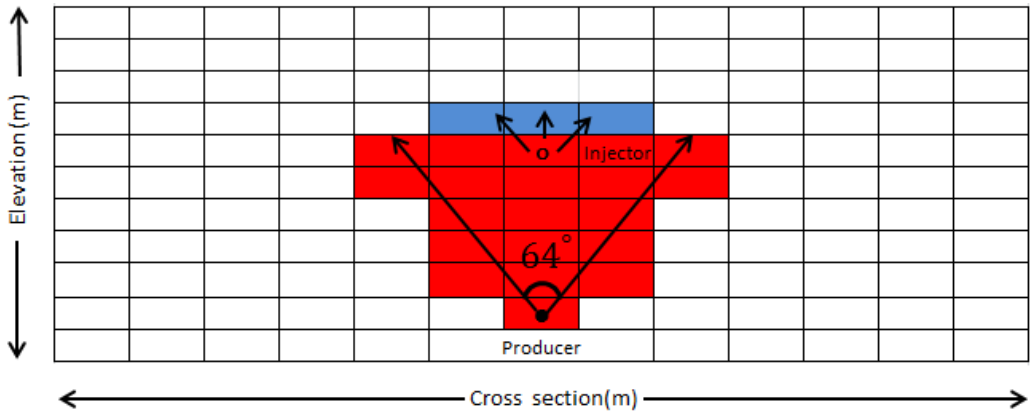

Figure 6.4: Checking the existence of shale barriers around the producer and injector

chamber with angle of 64 degree above the producer should be checked. If for any two successive rows, at least one grid cell for each slice inside the red steam chamber have low porosity or permeability, shale barrier can be identified and the proxy assumes that there is no connection between the producer and injector. Fig. 6.5 shows four different cases that shale barrier identified between the producer and injector or around each of them. In all of these cases, the proxy assumes that there is no connection between the producer and injector and bitumen cannot be produced.

6.2.1 Method 1: Undulate Trajectory Method (UTM)

The first method is based on the random repositioning of the well trajectory for different slices along the well. The differential evolution (DE) optimization algorithm has been used to automate this process. In this case, the objective function is to maximize the NPV. Constraints should be set to control the deviation of the well trajectory and avoid steep vertical or horizontal changes between adjacent slices.

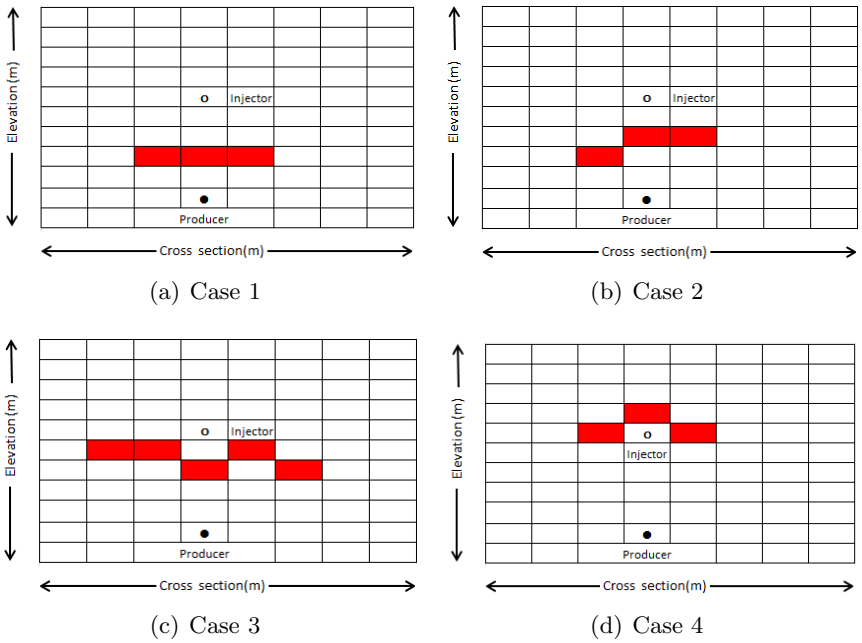

Figure 6.5: Identified shale barriers around the producer and injector

The grid size along the well, perpendicular to the well and in the vertical direction were 25 m, 2.5 m and 1 m, respectively for the cases presented in previous chapters. In this case, the vertical position on adjacent slices can be no more than one grid above or one grid below. This could be changed if desired. Also, the horizontal position can only change by one grid to the left or right for adjacent slices. In this case, to move from one slice to the next, only nine possibilities exist for the location of the well. Fig. 6.6 shows the nine possibilities of trajectory change from one slice to the adjacent slice. Cylinder shows the producer trajectory.

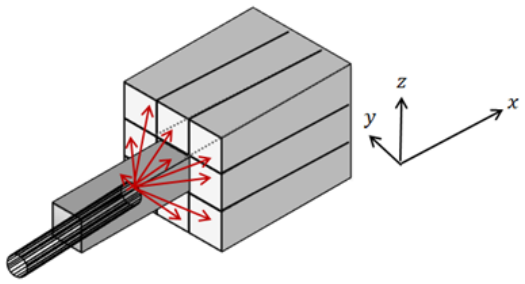

Figure 6.6: Nine possibilities (red arrows) of the location of well trajectory after moving from one slice to the other one. Cylinder shows producer trajectory.

Neglecting these constraints may cause two problems. First of all, an overly

complicated well trajectory could not be drilled and completed successfully. Also, steep undulations would cause uneven growth of the steam chambers. Even by considering these constraints, the difference between the minimum and maximum elevations along the well could be high which could cause uneven growth of the steam chamber along the well. If the well location for 10 consecutive slices increases 1 meter repeatedly, all of previous constraints would be satisfied, but changing 10 m elevation along 10 slices is large and may cause uneven growth of steam chamber along the well. For solving this problem, another constraint is set to control the maximum distance between the minimum and maximum elevations of the well. This constraint is shown in Fig. 6.7. As Fig. 6.7 shows, there should be a constraint for

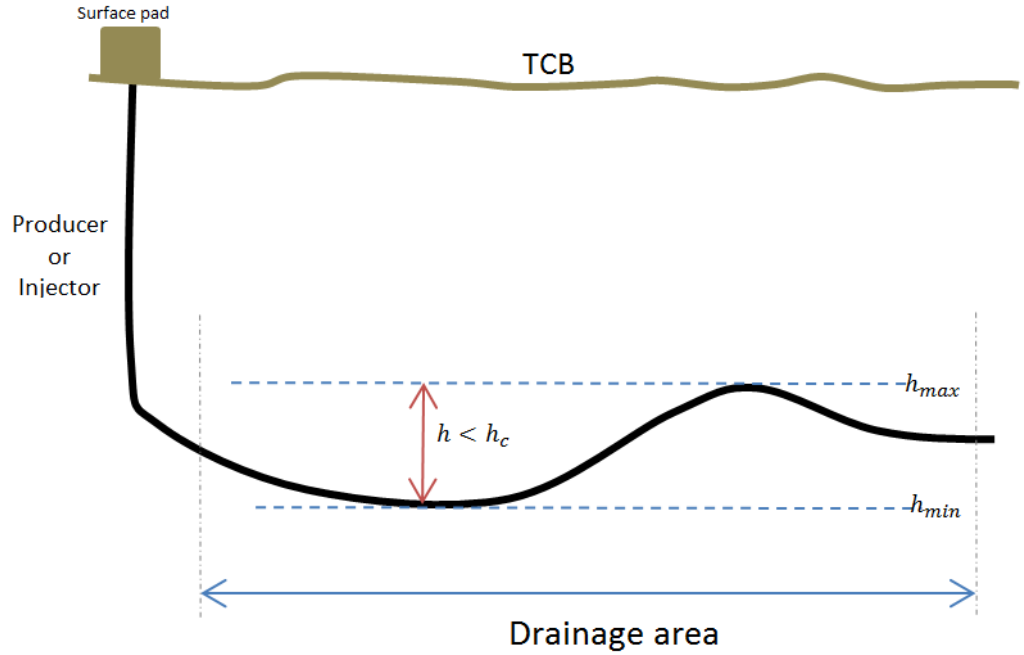

Figure 6.7: Maximum distance between minimum and maximum elevations of producer or injector. Well length is 1 km, well vertical thickness is 50 m, and the vertical exaggeration is $10\times$.

controlling the minimum and maximum elevation of the well along the trajectory.

In addition to all of these constraints a 3D box should be defined to constrain the well location. The starting and ending points of the box in the horizontal direction can be defined by two coordinate: (x_{min}, y_{min}) and (x_{max}, y_{max}). Without loss of generality, assume that the well trajectory is along the i or x direction. In this case, starting slice would be x_{min} and last slice would be x_{max}. Range of j or y direction

which is perpendicular to the well can be defined by setting n_1 grids right and n_2 grids left of the mid-point along the j or y axis. n_1 and n_2 are arbitrary values such as 2 or 3 grid cells. There is no limit for the minimum elevation of the well trajectory and it can pass below the BCB elevation, but the maximum elevation is about 20 m above the BCB. Also, the NPV below the BCB assumed to be zero. The maximum horizontal deviation in the trajectory can be controlled as well.

The BCB elevations should be computed automatically prior to the optimization. For finding BCB elevations, the bulk oil weight can be computed for all of grids between the (x_{min}, y_{min}) and (x_{max}, y_{max}) coordinates. The bulk oil weight is the ratio of oil weight to the total weight of the grid. If the bulk oil weight for at least 5 consecutive meters is above a threshold, e.g. 0.1, the start of BCB can be set at that elevation. The bulk oil weight can be computed by Eq. 6.1:

$$\text{BOW} = \frac{\rho_o \phi (1 - s_w)}{\rho_o \phi (1 - s_w) + \rho_w \phi s_w + \rho_m (1 - \phi)} \tag{6.1}$$

where ρ is density and o, w and m stand for oil, water and matrix, respectively. The constraints have been shown in Fig. 6.8.

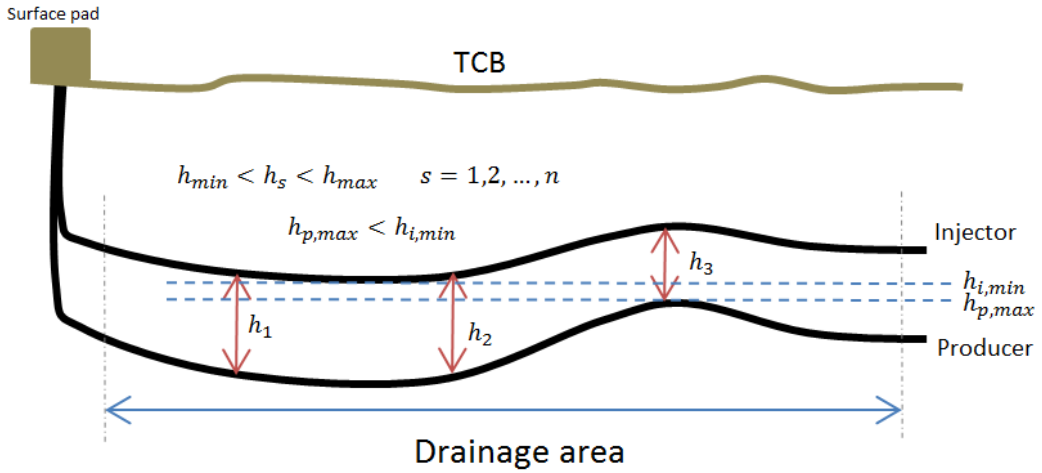

Figure 6.8: Injector constraints respect to the producer location. Producer and injector lengths are 1 km, the producer vertical thickness is 40 m, and the vertical exaggeration is $10\times$.

As mentioned, the distance between the minimum elevation of injector and the maximum elevation of the producer should be greater than zero, otherwise as Fig. 6.9 shows, steam by-pass can occur and steam can be produced through the producer.

The optimization algorithm forces the solution to stay in the feasible solution,

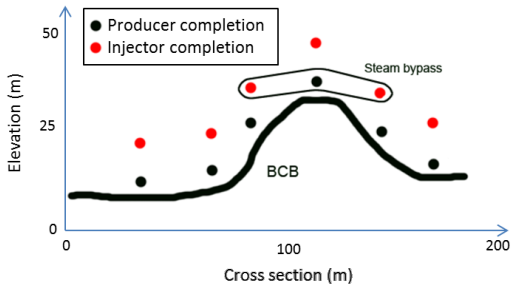

Figure 6.9: Steam bypass when elevation of injector is less than producer

that is, the specified 3-D box. For this reason, there is no need to set any constraint for minimum and maximum value of elevation or cross section grids. The objective function and constraints of the optimization problem are written as:

$$\text{maximize} \quad f(x, y, z) \tag{6.2a}$$

$$\text{Subject to}: \quad c_i(x, y, z) \leq 0 \qquad \text{for } i = 1, 2, \ldots, n \tag{6.2b}$$

where $c_i(x, y, z)$ are the constraints defined above and n is the number of constraints. Also $f(x, y, z)$ can be defined as:

$$f(x, y, z) = \sum_{j=1}^{s} \text{NPV}(x_j, y_j, z_j) \times P(x'_j, y'_j, z'_j) \tag{6.3}$$

where s is the number of 2D slices along the well and $P(x'_j, y'_j, z'_j)$ is an indicator which is zero if shale is around the injector of slice j, and it is 1 otherwise. This indicator considers the effect of shale barriers around the injector. As a result, the objective function is maximizing NPV subjects to above constraints. In this problem, the optimization variables are the x, y and z coordinates of the producer and injector completions for all of slices along the well.

For automatic optimization, the differential evolution (DE) algorithm has been used. DE is an unconstrained population-based optimization algorithm, as a result constraints must be implemented using a penalty method. For this reason, a new objective function will be used:

$$g(x, y, z) = f(x, y, z) - \mu[\sum_{i=1}^{n} \psi_i(x, y, z)] \tag{6.4}$$

where $\psi_i(x, y, z)$ is equal to the zero if constraint $c_i(x, y, z)$ satisfied and it is equal to $c_i(x, y, z)$ otherwise. Also μ is a positive large number.

In this case, the optimization algorithm forces all constraints to stay in the feasible region, otherwise, the penalty function would a large number and would decrease the objective function significantly. As a result, DE should maximize $g(x, y, z)$ instead of $f(x, y, z)$.

The proxy should be called for the objective function instead of the simulator which is thousands of times faster. Although the proxy is very fast, it will be called many times; otherwise, the final value would not be close to the global optimum. The DE optimization method is a population-based method and the rate of convergence to the optimal solution is not fast, but it is suitable for optimization problems with discrete variables. As discussed before, for finding cumulative oil and cumulative steam of a 3D models, Butler's method assumes each 2D slice separately and after finding cumulative oil and cumulative steam of each slice, all of them should be summed together for finding the performance of the 3D model. In DE optimization algorithm, thousands of 3D well trajectories should be considered and the total NPV using each trajectory must be computed. Although the proxy is very fast with an average run time for a 3D model of about 10 seconds, this can be slow when we want to compute the objective function thousands of times. Also, given uncertainty in the reservoir parameters, the proxy needs to be applied to all realizations. If DE needs to compute NPV for 1000 cases with 100 realizations, the total running time would be about 29 days. Usually there are about 40 2D slices in a 3D model which means the number of optimization variables are 160 (80 for producer and 80 for injector) and many different constraints should be considered during the optimization. Even for this case, 1000 runs (each for 100 realizations) may not be enough for finding the optimal solution. For solving this problem, a 3D array with the size of $(nx_{box}, ny_{box}, nz_{box})$ which nx_{box}, ny_{box} and nz_{box} are sizes of 3D box for finding the optimal path of well trajectory can be assumed. Then producer should be placed on each grid in that box and NPV should be computed for that producer location. Values of NPV's should be stored in a 3D array. Then, for finding the total NPV of the 3D model for one trajectory, the NPV value of different completions can be retrieved from this array without any need to run the proxy again. Using this method, the total number of pre-runs would be $nx_{box} \times ny_{box} \times nz_{box}$ runs of 2D models which can be done very fast. After that there is no need to run the proxy anymore. The following workflow summarizes the optimization of the well trajectory.

1. Define a horizontal box for the optimal location of the trajectory

2. Find 2D gridded BCB elevations and maximum allowable well elevation for all of grids along vertical direction inside of the 2D box of step 1. Using this method, a 3D box can be defined and the NPV for all of grids outside of this box are set to zero. This process should be repeated for all realizations. The horizontal box for all of realizations would be the same, but the vertical ranges would be different, which is due to the difference between BCB elevations

3. Calculate the objective function for all grids inside the 3D box for each realization and then calculate the average of NPV over all of realizations.

4. Sample different trajectories for the producer and injector randomly. If the injector completion in one slice is close to the shale barrier, regardless of producer location, the NPV for that slice would be reset to zero

5. Optimize the producer and injector trajectories simultaneously using the DE algorithm

6. Write the producer and injector trajectories in a file with GSLIB and STARS formats

The only time consuming step is step 3. All other steps are fast.

6.2.2 Method 2: Double Spline Method (DSM)

As discussed before, the undulate trajectory method can be very useful and reasonably constrained. The method works good when there are few drilling constraints. Another approach to parameterize a smoother trajectory would be to use a Hermite spline polynomial (Hearn and Baker, 2004). In this case, the well trajectory can be defined by four parameters. The starting point of the horizontal portion of the well is called the heel, and the end point of the well is called the toe. Using this method, by knowing the elevations of the toe and heel and also the slope of elevations at these two points, the location of the well trajectory for other slices between the heel and toe can be computed using the following formula:

$$z(u) = \begin{bmatrix} u^3 & u^2 & u & 1 \end{bmatrix} \begin{bmatrix} 2 & -2 & 1 & 1 \\ -3 & 3 & -2 & -1 \\ 0 & 0 & 1 & 0 \\ 1 & 0 & 0 & 0 \end{bmatrix} \begin{bmatrix} z(0) \\ z(1) \\ z'(0) \\ z'(1) \end{bmatrix} \tag{6.5}$$

where $z(0)$ is heel elevation, $z(1)$ is toe elevation, $z'(0)$ is slope of elevation at the heel and $z'(1)$ is slope of elevation at the toe. In this case, for any location u between 0 and 1, other elevations can be computed. For this reason, the horizontal position of heel should be assumed as 0 and horizontal position of toe should be assumed as 1. This method will lead to at most one inflection point in the well trajectory. Fig. 6.10 shows some example well trajectories defined by Hermite spline polynomials. The elevations of the trajectory at different slices can be optimized

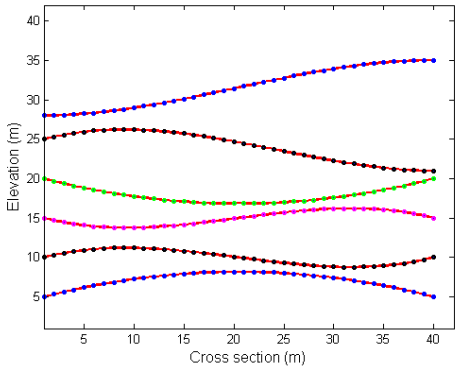

Figure 6.10: Well trajectories have been defined by Hermite spline method

with this parametrization but there would not be any horizontal deviation in the well. In 3D, the well trajectory might be deviated to the left or right for some slices to avoid the BCB elevations or shale barriers. Another spline in the horizontal direction can be considered. As a result, using such a double spline method, the well trajectory can be optimized in 3D space. This method gives smoother trajectories compared to the first method and drilling the well would be easier. The advantage of the first method is for complex BCB variations and flexible drilling.

The objective function and constraints are similar to the constraints that have been considered for the first method and they can be added to the objective function using the penalty method. There is no need to set any constraint for slopes at the heel and toe because the difference between the minimum and maximum distances would control the range of these slopes automatically. These constraints will force the optimal values of the slopes to have reasonable values.

DE can be used as an optimization algorithm for optimizing both producer and injector trajectories. In this case, the total number of variables for optimizing producer and injector trajectories would be 16 which is much less than the first

method and it does not depend on the number of 2D slices along the well. The optimization workflow is similar to the first method. The only difference between these two methods is related to the variables selected for optimization.

6.3 Case study – Single Realization of a Realistic 3D Model

In this section, a realistic 3D model has been tested. The model size is $57 \times 50 \times 74$ and the grid dimensions in the x,y and z directions are 25 m, 2.5 m and 1 m, respectively. Five facies and seven thermal rock types are present in the model. A thief zone exists at the top and a pinchout existed at the bottom of reservoir with very low permeability and low thickness.

The wells are oriented along the i or x direction between slices 16 to 51. A box perpendicular to the well direction between grids 22 and 28 has been considered for searching the optimal horizontal position. As discussed before, for finding minimum well elevations, a 2D BOW map should be computed and bulk oil weight for at least 5 consecutive meters above BCB should be above 0.10. This can be at or above the maximum pinchout elevation. Maximum well elevation at each 2D slice is 20 grid cells above the minimum well elevation. The 3D box of acceptable locations for drilling producer can be obtained. The NPV for all of cells outside of this 3D box is set to zero. Then, by setting producer location on each of grid cell in that 3D box and running the proxy for that 2D slice (along the well), the NPV for that cell can be computed. There is no need to call the proxy and calculate the NPV after that. In this case, the number of slices is 36, the number of horizontal grids perpendicular to the well trajectory is 7 and number of grids in the vertical direction is 20. As a result, a total number of cells in the box is 5040. Each 2D slice takes about 0.1 seconds using $\Delta t = 15$ days in the proxy. As a result, running all of these cases takes about 8 minutes which is quite fast. Fig. 6.11 shows a 3D NPV volume for all cells in the box. The NPV for all of grids outside the box have been set to zero and cannot be observed. Also NPV of some grids inside the box are zero which is due to the low permeability of that grid or existence of a shale barriers in short distance above of that grid. Fig. 6.12 shows low permeability cells (less than 20 md) in the reservoir model.

As Fig. 6.12 shows, continuity of permeability perpendicular to the well is high, for this reason the NPV of grid cells is not very different. The permeability along

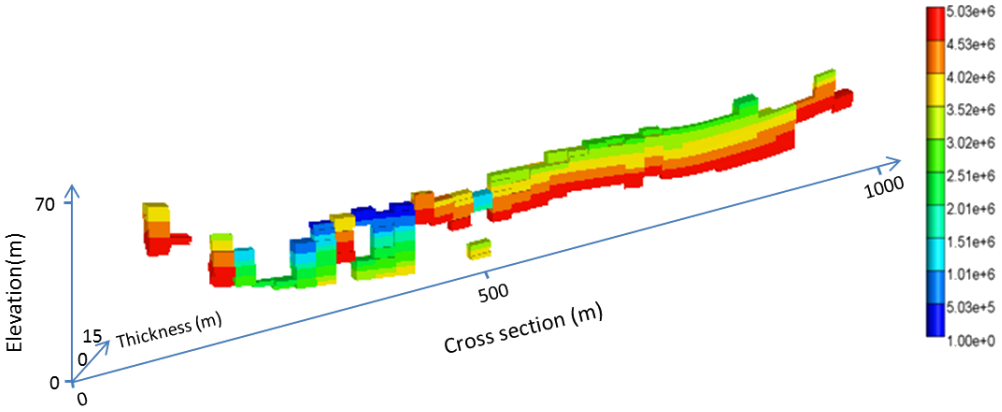

Figure 6.11: 3D NPV volume for all of grids in the box

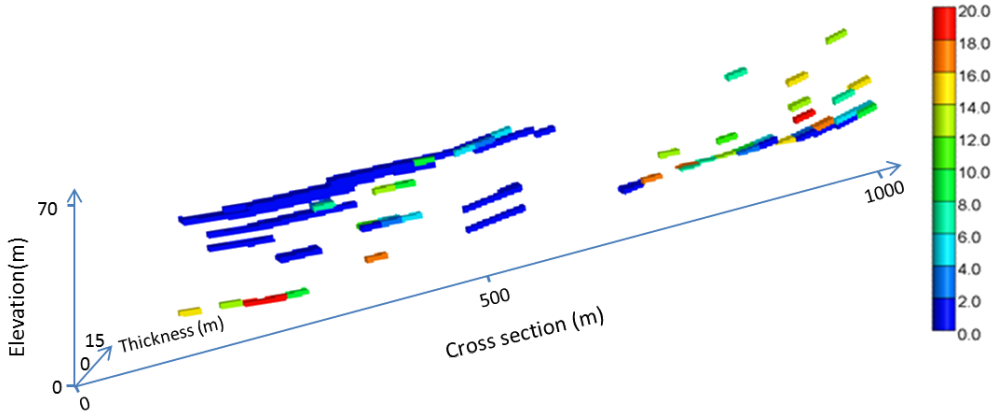

Figure 6.12: Low permeability cells (less than 20 md) in the reservoir model

the well will change significantly and as a result some cells close to the shale barriers cause a lack of communication between the producer and injector and, as a result, the NPV would be zero.

The NPV perpendicular to the well depends on the well location and usually the NPV is maximum if the well is at the center of the 2D slice. By moving the well to the boundaries, the NPV may decrease. The steam front will reach the close boundary faster and produce the oil from that side in a at shorter time. Steam injected beyond that time will increase the cumulative steam injection and decreases the cumulative NPV. Fig. 6.13 shows changing NPV in a 2D slice along the well by changing the producer location. As Fig. 6.13 shows, the NPV at lower depth is

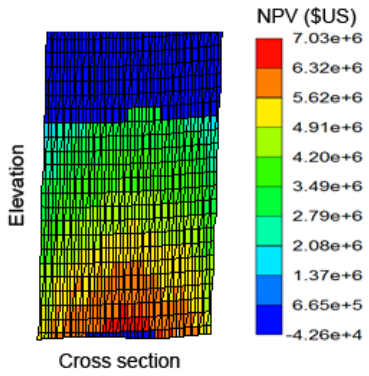

Figure 6.13: Changing NPV in a 2D slice along the well by changing the producer location

higher due to producing more bitumen. Also, by moving the location of the producer to the boundary, the NPV decreases gradually.

The NPV of each grid cell in each slice along the well and the total NPV of 3D well trajectory can be obtained by knowing the location of the well trajectory at each slice. The total NPV can be computed very fast.

The DE algorithm is a population based optimization algorithm that starts with a random population of producer and injector trajectories over the 3D box (based on the constraints). The NPV of all of them is computed and some of the higher NPV ones are selected by DE for optimization. This process should be continued until there is no improvement in the objective function.

The undulate trajectory method (UTM) and double spline method (DSM) have been used for finding optimal solution. Results of both of methods will be discussed.

Both methods find the optimum trajectory very fast. The initial objective function is about $1.59E+8$ and the trajectory assumed to be at the center of the box in the horizontal plane and above the maximum elevation of BCB. The UTM method found an optimal NPV of $1.99E+8$ \$US and DSM found the optimal NPV of $1.97E+8$ \$US. The optimal NPV of both methods are very close, but their trajectories are not the same because of how they are parameterized. Fig. 6.14 shows changing the NPV by changing the number of objective function computation in both of the methods. As Fig. 6.14 shows, the DSM method found the optimal value significantly faster,

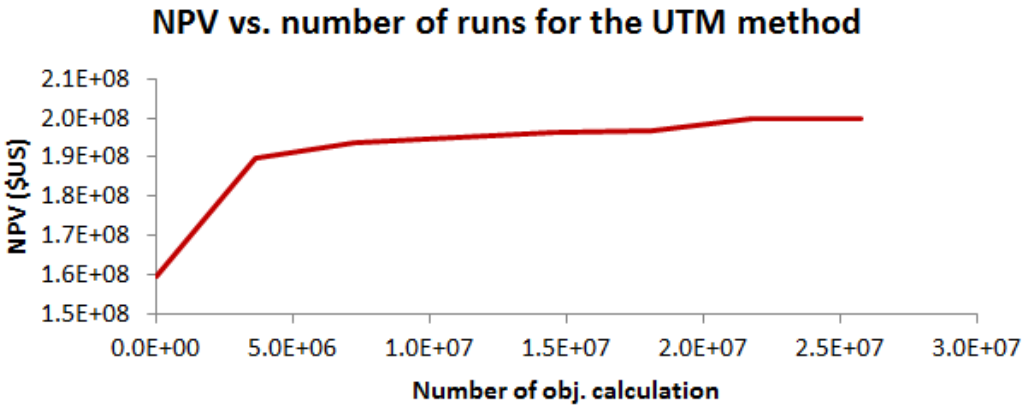

(a) Deviated well trajectory method

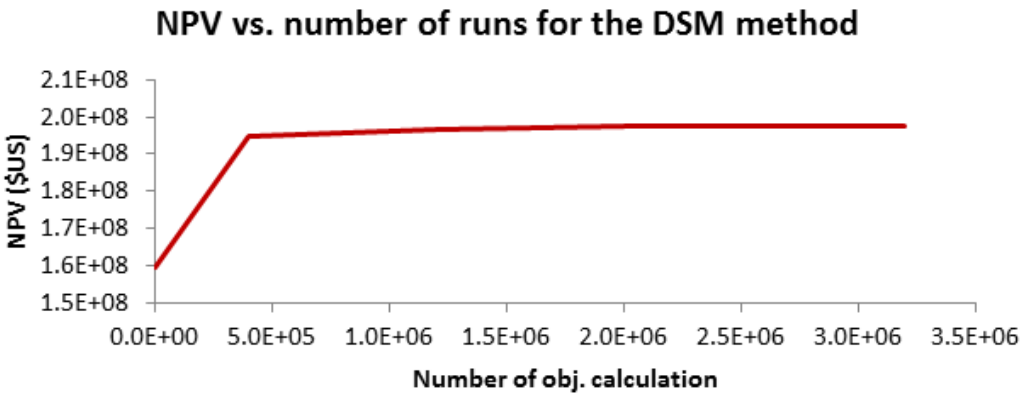

(b) Double spline method

Figure 6.14: Changing NPV by changing number of objective function computation

but both methods are fast (less than five minutes). The total number of variables in DSM method is sixteen (regardless of the number of slices in the model), but the total number of variables in UTM method is four times of the number of slices. As a result, the DSM parametrization can find optimal solution much faster than the UTM method, but UTM method is more flexible about the location of the well

trajectory and can find a higher NPV.

Fig. 6.15 shows 3D location of producer on the 2D BCB map for both methods. In this figure, the color shows the BCB elevation. As Fig. 6.15 shows, UTM method is more flexible and it is closer to the BCB than the DSM method.

Fig. 6.16 shows the horizontal and vertical NPV variations along the producer in both of these methods. The well trajectory finds a path that maximizes NPV by varying the trajectory in both the horizontal and vertical directions. In these case, the trajectories try to pass through hot colors that have greater NPV. It seems that these are global optimums (or near to it) for each cases. The location of the injector depends highly on the location of the producer, thus, the algorithm tries to optimize the producer trajectory in a way that maximizes the possibility of injecting steam into all of slices. In this case, the horizontal and vertical position of the injector should be optimized based the constraints defined above and the injector should not be around the shale barriers.

Fig. 6.17 shows a side view and top view of the producer and injector trajectories for both methods. As Figs. 6.17(a)–6.17(c) show, the vertical distance between the producer and injector is between 4-6 m to prevent steam by pass. Also as Fig. 6.17(b) shows the top view of trajectories in the UTM method, both injectors and producers are horizontally deviated, but the injector is exactly above the producer. Also as Fig. 6.17(d) shows the top view of the DSM trajectories, for all nodes, except one, the injector is exactly above the producer.

6.4 Summary

Well trajectory optimization was discussed in this Chapter. Two methods: the UTM (Undulate trajectory method) and the DSM (double spline method) were used for optimizing well trajectories. The differential evolution (DE) optimization algorithm was used to automate this process. Also, constraints were set to control the deviation of the well trajectory and avoid steep vertical or horizontal changes between adjacent slices. For testing the proposed methodology, trajectories of a 3D realistic model were computed using above methods. Some points can be concluded from this Chapter:

- By pre-computing the objective function for different positions, the optimal solution can be obtained fast.

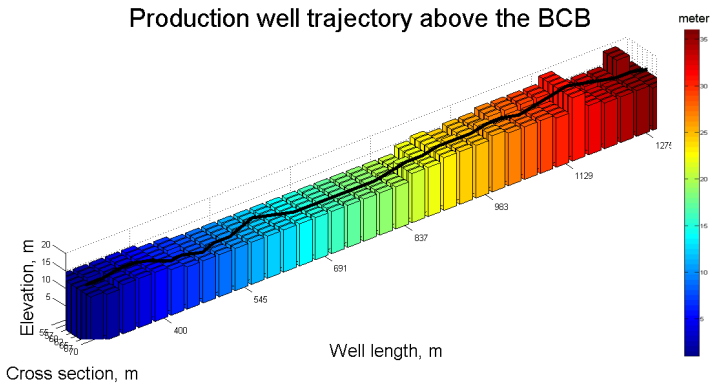

(a) 3D trajectory using undulate trajectory method

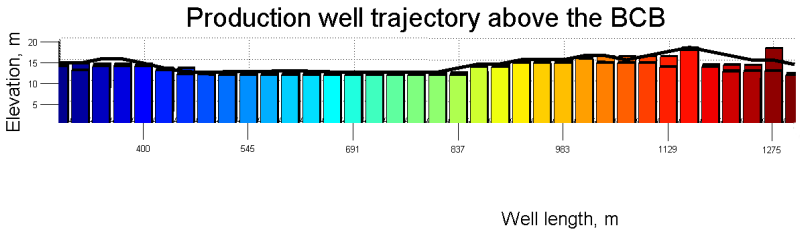

(b) 2D trajectory along the well using undulate trajectory method

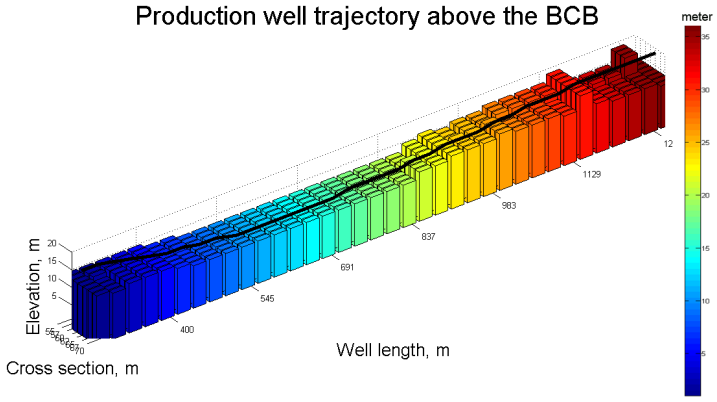

(c) 3D trajectory using double spline method

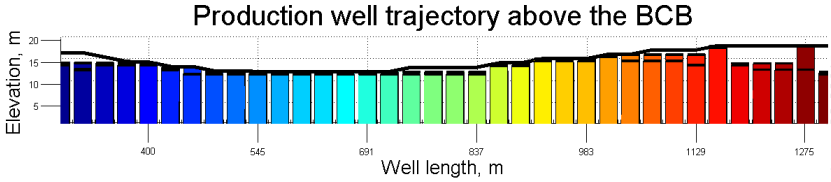

(d) 2D trajectory along the well using double spline method

Figure 6.15: 3D location of producer on the 2D BCB map for both methods

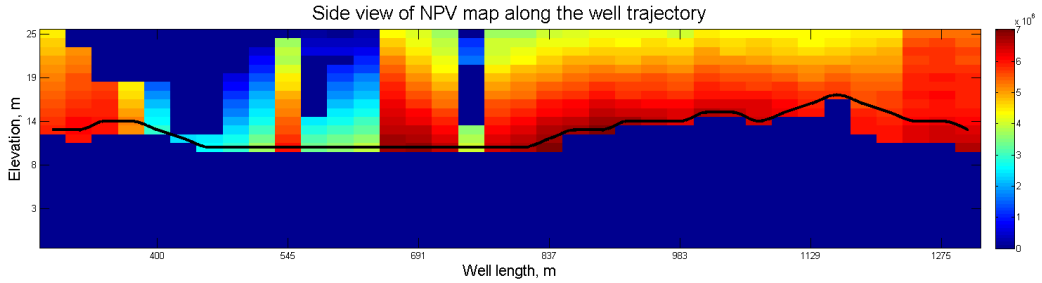

(a) Changing vertical NPV along the well using undulate trajectory method

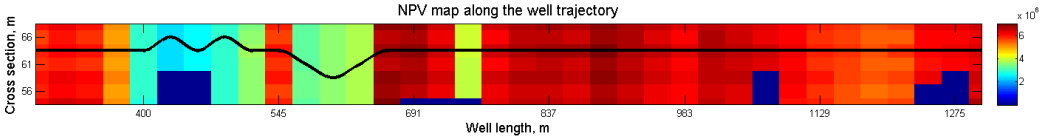

(b) Changing horizontal NPV along the well using undulate trajectory method

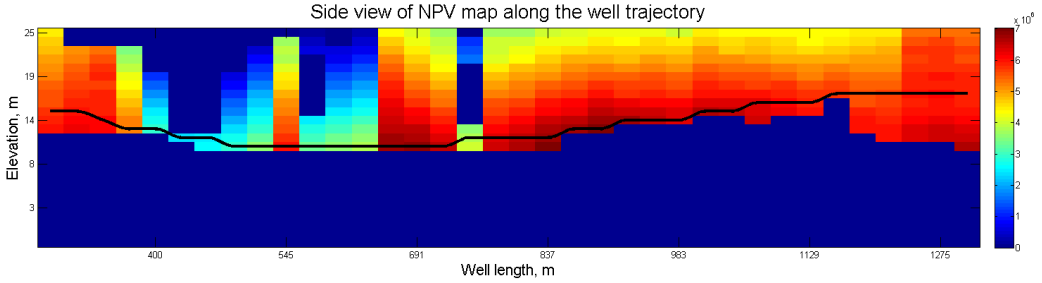

(c) Changing vertical NPV along the well using double spline method

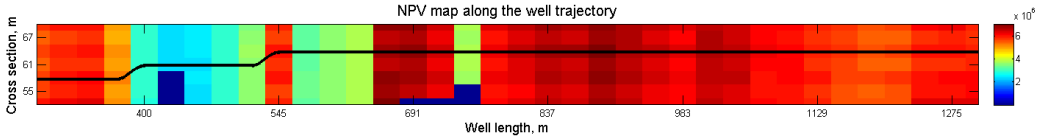

(d) Changing horizontal NPV along the well using double spline method

Figure 6.16: NPV map for both methods

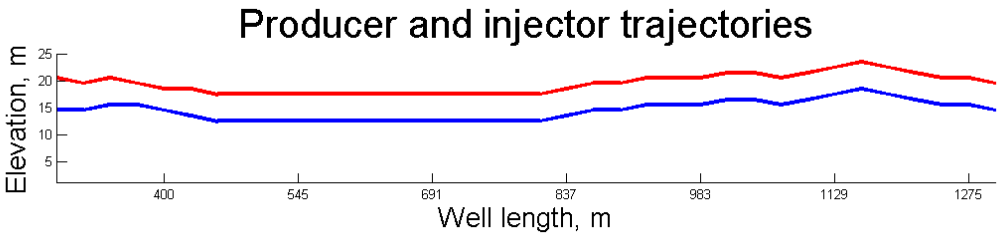

(a) Side view for undulate trajectory method (blue: producer, red: injector)

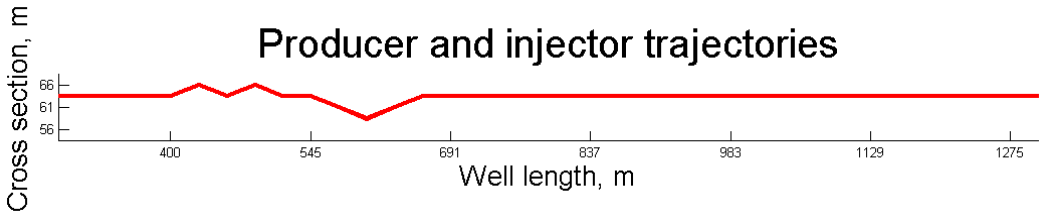

(b) Top view for undulate trajectory method (blue: producer, red: injector)

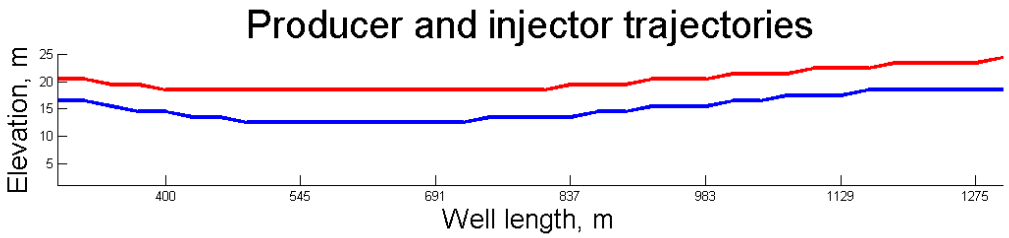

(c) Side view for double spline method (blue: producer, red: injector)

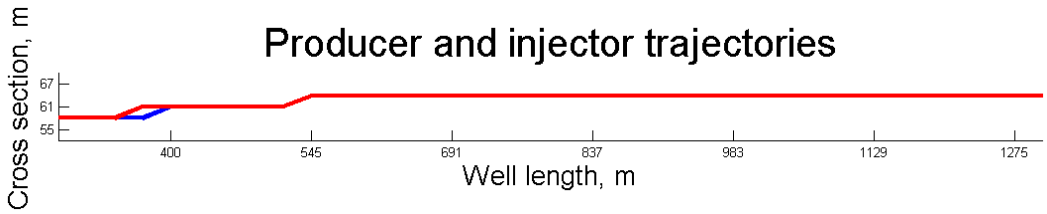

(d) Top view for double spline method (blue: producer, red: injector)

Figure 6.17: Producer and injector trajectories for both methods

- Both the UTM and DSM methods satisfy all constraints. The optimal trajectory of both methods are smooth and appear practical to drill.
- The DSM parametrization can find an optimal solution much faster than the UTM method, but the UTM method is more flexible about the location of the well trajectory and can find a higher NPV.
- In presence of a single realization, the optimal trajectory would be close to the BCB.

Chapter 7

Illustrative Case Study

A new semi-analytical proxy based on the Butler's theory has been developed that considers heterogeneity and different operating strategies. This proxy has been applied to different small examples in previous chapters. In this chapter, a more complete example will be presented. The realizations generated in Chapter 5 will be the starting point for a variety of applications. Traditional approach in the SAGD reservoir management is based on the ranking of reservoir realizations for the first step. Then, $P10$, $P50$ and $P90$ realizations will be selected for other applications such as transferring uncertainty and well trajectory optimization. Ranking results depend highly on the well trajectory and because of shale barriers around wells, by changing the well trajectory ranked results will change significantly. In this work, all of the realizations will be used for well trajectory optimization. Then, realizations will be used for ranking and transferring uncertainty using the optimal well trajectories in the first step. Finally, the $P10$, $P50$ and $P90$ realizations will be used for forecasting oil production and steam injection compared to flow simulation results.

Section 7.1 explains the settings and simulation model of the case study. Sections 7.2 to 7.4 documents details of the well trajectory optimization, ranking and transferring uncertainty and forecasting SAGD performance of the $P10$, $P50$ and $P90$ realizations. Section 7.5 shows a comparison between the current methodology and the traditional work-flow. Finally, conclusions are provided in Section 7.6.

7.1 About the Simulation Model

In this Chapter, 100 3D realizations with the trigger operating strategies have been tested. Geostatistical modeling of these realizations have been illustrated in Chapter

5. Three wells should be drilled in the model along the x direction. Grid size in the y direction is increased from 2.5 m to 5 m for increasing the spacing between the wells and testing the effect of changing the grid size on the proxy and simulator results. The grid dimensions are $26 \times 32 \times 83$ and the grid size in the x, y and z directions are 25 m, 5 m and 1 m, respectively. For all of examples in this Chapter only the reservoir property realizations are different. Two facies with seven different thermal rock types are considered. Top water and top gas are present in these models. For the operating strategy, the trigger starts working at 600 days and drops pressure 19 times by 100 kpa over 6 months. The trigger drops the pressure and causes a decreased steam injection rate. The simulator drops the pressure for three months and keeps the pressure constant for the next three months. This process has been simulated by the proxy too. Using this trigger, the final cumulative steam injection decreases significantly compared to the base case (no trigger case), but the final cumulative oil production remains close to the base case. All of the models were run through the STARS (Computer Modeling Group Ltd., 2012) and the proxy for finding the oil production and steam injection for 15 years.

In the next section, all of 100 realizations are used the first application that is well trajectory optimization for finding the optimal trajectory of the producer and injector by maximizing the expected NPV over all realizations. The proposed methodology is based on the drilling 3 well pairs with 50 m spacing along the x direction. 26 completions should be considered along the well (26 2D slices). Fig. 7.1 shows location of different well pairs in the model before optimizing their trajectories.

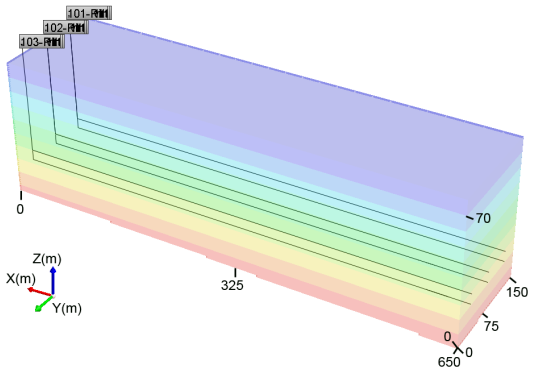

Figure 7.1: Location of different well pairs in the model before optimizing their trajectories

7.2 Well Trajectory Optimization

The proxy is very fast and the results are very close to the simulation results. Thus, all 100 realizations can be used for applications such as well trajectory optimization. As discussed in Chapter 6, when there is a single realization, the producer trajectory should be drilled close to the BCB. The BCB for each realization would be different. As a result, some of them could be at lower elevations compared to others. An optimal trajectory should maximize the expected NPV over all realizations after running them with the flow simulator or proxy. One of the differences between this case and the example of Chapter 6 is related to the elevation of adjacent well pairs. In this case, 3 well pairs are presented in the model. If elevations of different well pairs are significantly different, growth of the steam chamber would be uneven during the simulation. Thus, constraints should be set for the lower and upper elevations of different well pairs and optimal elevations of different well pairs should be computed simultaneously. Another difference between this case and the example of Chapter 6 relates to finding the NPV map. The NPV of all possible producer locations is computed for all 100 realizations. The average NPV over all realizations for all locations could be computed. Then, as before, the DE algorithm can be used for finding the optimal producer and injector trajectories by maximizing the average cumulative NPV using both UTM and DSM methods. The existence of shale barriers at or near the completions will be considered and the best trajectory should be found to maximize the possibility of injecting steam through most of realizations. Figs. 7.2–7.4 show the optimal producer trajectory of different well pairs in both of UTM and DSM methods on a side and top view.

As Figs. 7.2–7.4 show, the optimal trajectory depends on the parametrization of the trajectory. The UTM method has more flexibility and can find a higher NPV compared to the DSM method. Optimal cumulative NPV for both methods are close to each other. The final cumulative NPV of UTM method is $1.51E+8$ \$US and the final cumulative NPV of the DSM method is $1.50E+8$ \$US. As Figs. 7.2–7.4 show, it seems that DE optimization algorithm found the best trajectories based on the method and problem constraints by passing the trajectory through hot colors which have higher NPV. Below the minimum elevation of all of the realizations, the NPV for all the grid cells would be zero. Also, above the maximum elevation of all of realizations, the NPV for all the grid cells would be zero. As Fig. 7.2 shows,

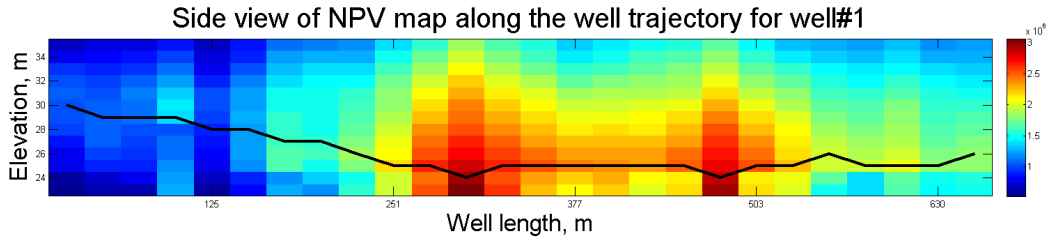

(a) Changing vertical NPV along the well using undulate trajectory method

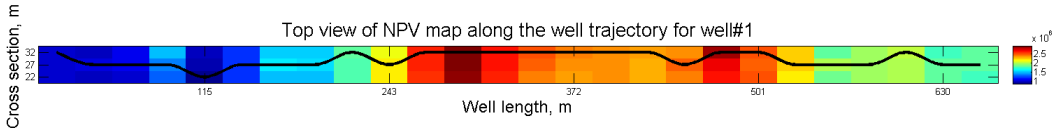

(b) Changing horizontal NPV along the well using undulate trajectory method

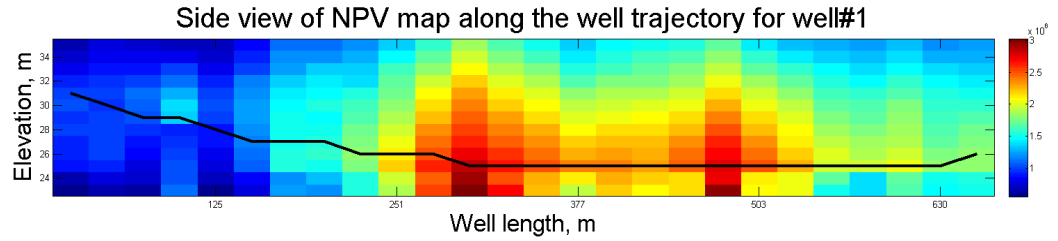

(c) Changing vertical NPV along the well using double spline method

(d) Changing horizontal NPV along the well using double spline method

Figure 7.2: Optimal producer trajectory of well pair 1 over NPV map for both of methods

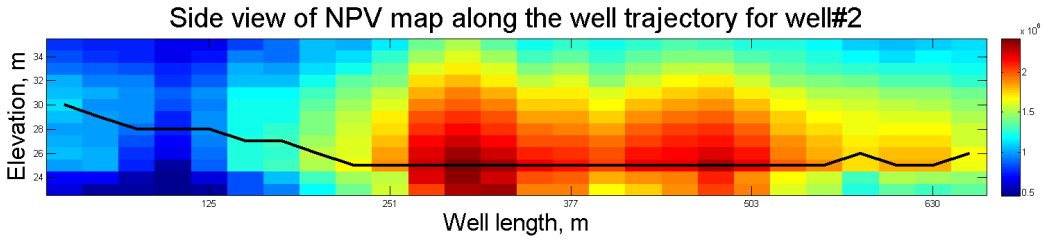

(a) Changing vertical NPV along the well using undulate trajectory method

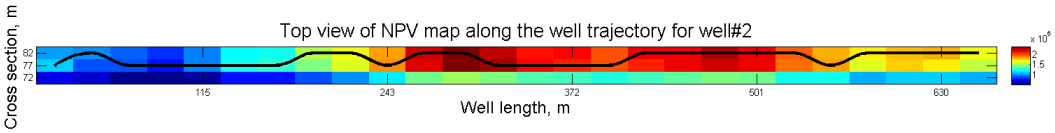

(b) Changing horizontal NPV along the well using undulate trajectory method

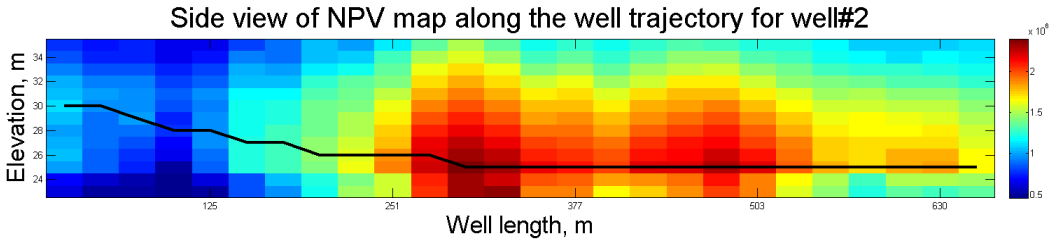

(c) Changing vertical NPV along the well using double spline method

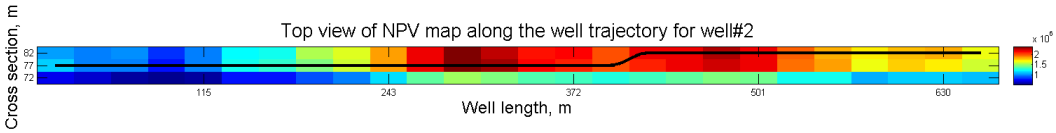

(d) Changing horizontal NPV along the well using double spline method

Figure 7.3: Optimal producer trajectory of well pair 2 over NPV map for both of methods

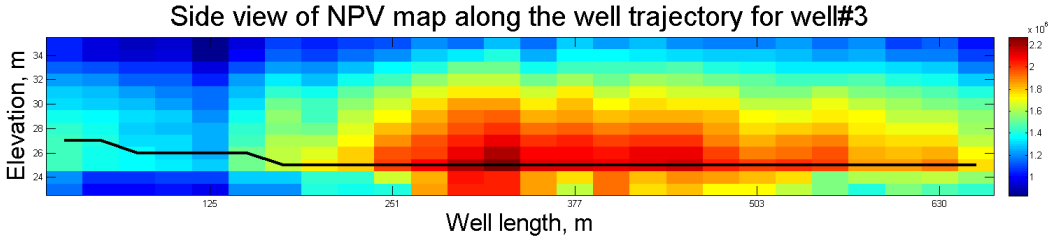

(a) Changing vertical NPV along the well using undulate trajectory method

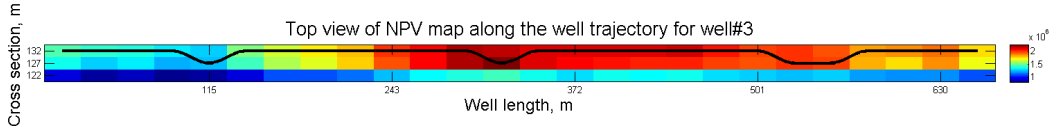

(b) Changing horizontal NPV along the well using undulate trajectory method

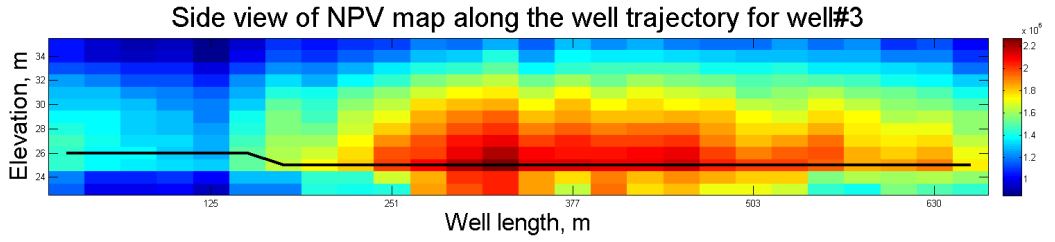

(c) Changing vertical NPV along the well using double spline method

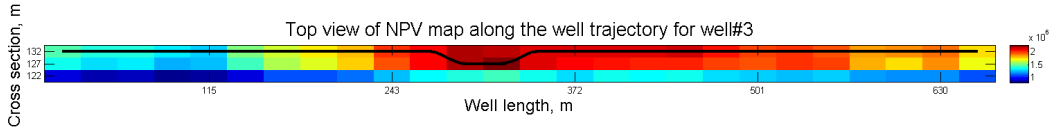

(d) Changing horizontal NPV along the well using double spline method

Figure 7.4: Optimal producer trajectory of well pair 3 over NPV map for both of methods

shale barriers are present at different elevations of different slices, and both UTM and DSM methods, placed the optimal location of producer above these barriers to maximize the NPV.

Figs. 7.5–7.7 show the side view and top view of the producer and injector trajectories of different wells for both methods. Figs. 7.5–7.7 show the trajectories in both of these methods. The injectors are between 4 to 6 meters above the producers and also the minimum elevations of injectors are higher than the maximum elevations of producers to avoid steam by-pass. Also, as the top views show, the location of the injector at each slice can be moved at most one grid left or one grid right of the producer locations for each slice. Also, the constraints on the horizontal and vertical differences between grid cells elevations and horizontal positions have been satisfied in both of these methods. When the trajectories are optimized with more than one realization, the possibility of placing injector completions between shale barriers would be increase – at least on some realizations. For this reason, the optimal injector may moves left or right of the producer location.

In the next section, all of these realizations with the optimal well trajectories by the UTM method will be used for ranking and transferring uncertainty of the reservoir realizations.

7.3 Uncertainty Transferring and Ranking of the Reservoir Realizations

In the examples of Chapter 5, unlimited steam was available and the injection pressure was constant at 4000 kpa. This increases the CSOR especially in the last years. When a thief zone exists at the top of the reservoir, the pressure trigger operating strategy can be a good solution to reduce CSOR. In this case, for each well the trigger starts at 600 days and drops pressure $n = 19$ times by 100 kpa during 6 months. As a result, the final cumulative oil production of different realizations would be close to the no trigger case, but the cumulative steam injection and CSOR would decrease significantly. The producer and injector trajectories of the wells in the model are selected from the optimized well trajectories of the last section by the UTM method.

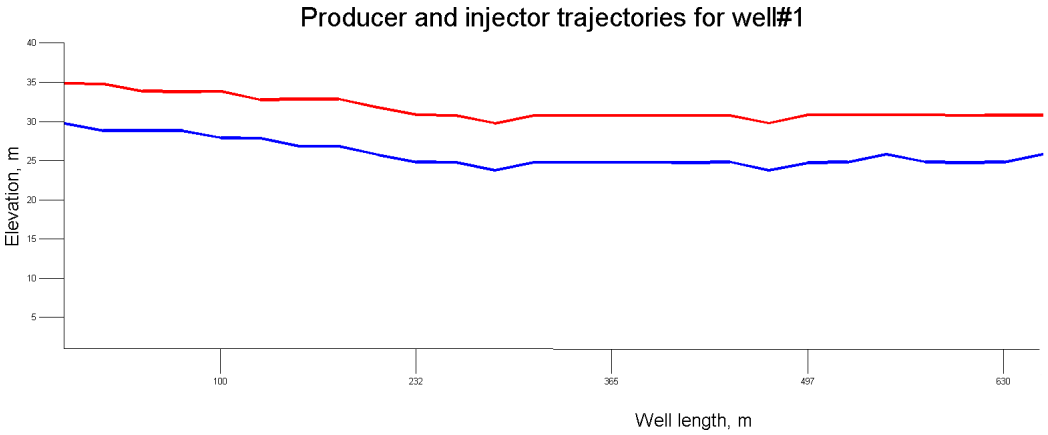

(a) Side view for undulate trajectory method (blue: producer, red: injector)

(b) Top view for undulate trajectory method (blue: producer, red: injector)

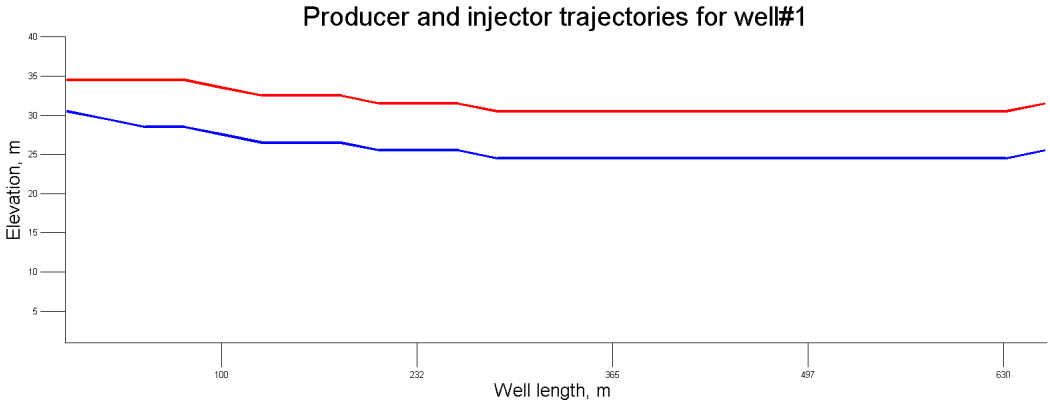

(c) Side view for double spline method (blue: producer, red: injector)

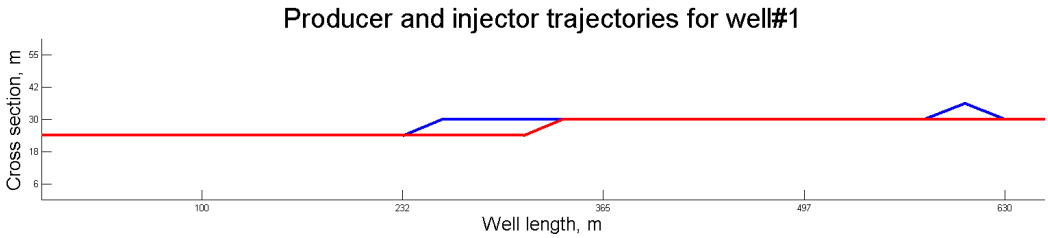

(d) Top view for double spline method (blue: producer, red: injector)

Figure 7.5: Producer and injector trajectories of well pair 1 for both of methods

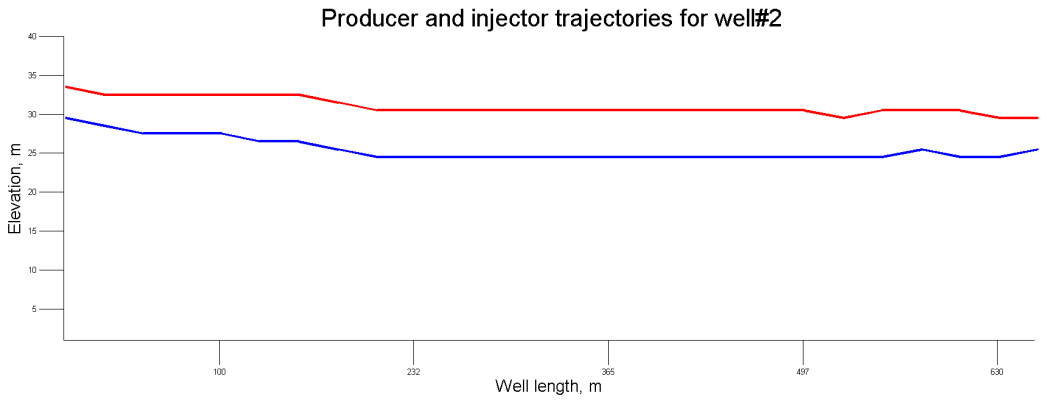

(a) Side view for undulate trajectory method (blue: producer, red: injector)

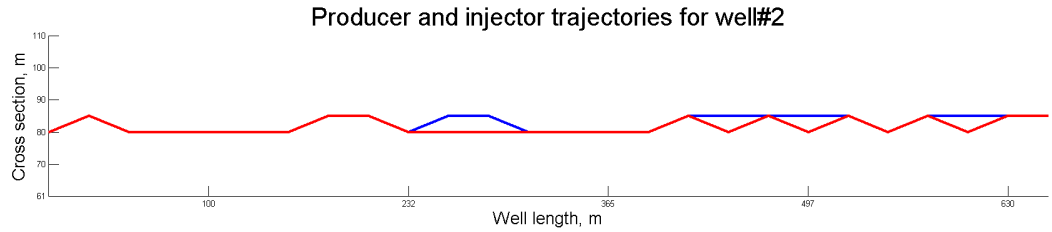

(b) Top view for undulate trajectory method (blue: producer, red: injector)

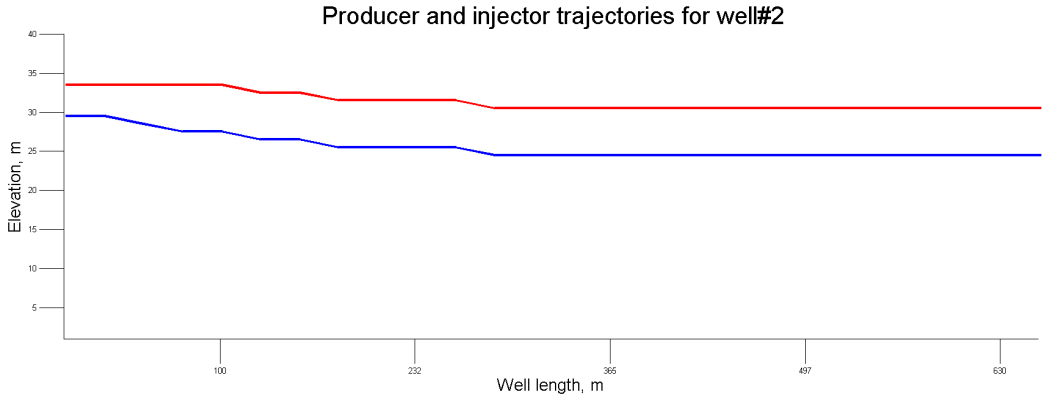

(c) Side view for double spline method (blue: producer, red: injector)

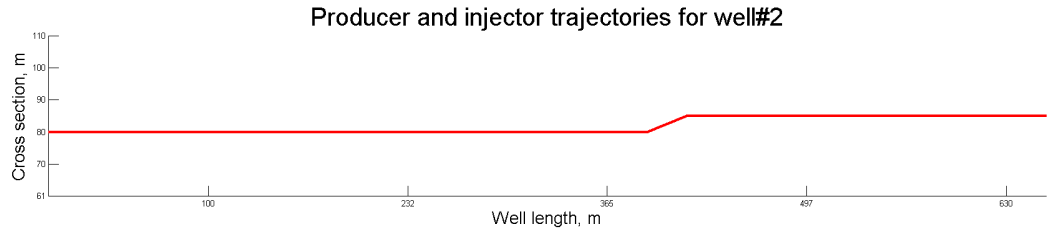

(d) Top view for double spline method (blue: producer, red: injector)

Figure 7.6: Producer and injector trajectories of well pair 2 for both of methods

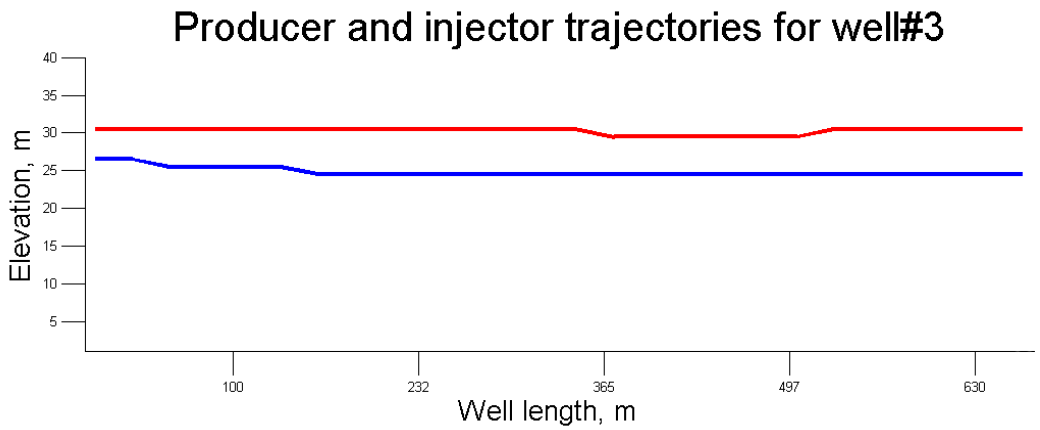

(a) Side view for undulate trajectory method (blue: producer, red: injector)

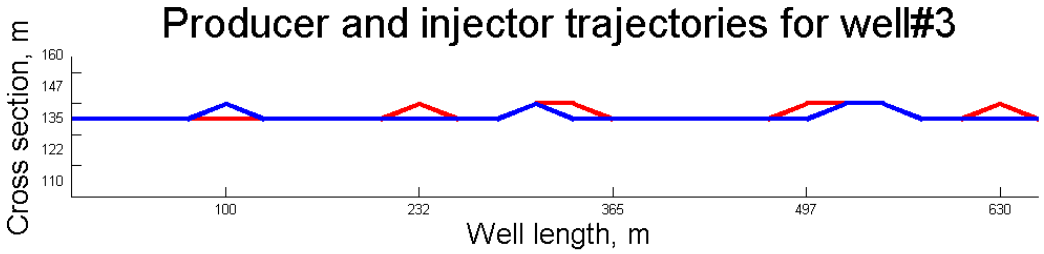

(b) Top view for undulate trajectory method (blue: producer, red: injector)

(c) Side view for double spline method (blue: producer, red: injector)

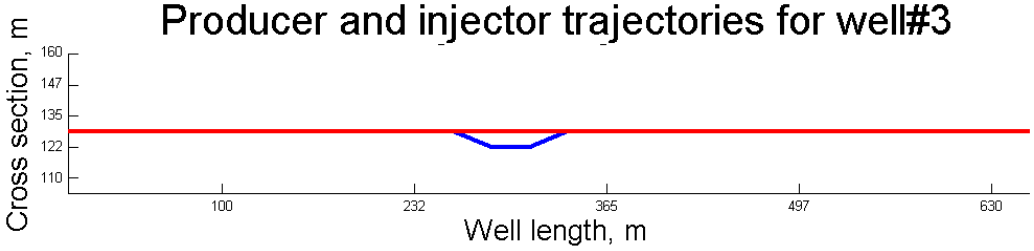

(d) Top view for double spline method (blue: producer, red: injector)

Figure 7.7: Producer and injector trajectories of well pair 3 for both of methods

7.3.1 Simulator Results

Fig. 7.8 shows the results of simulated realizations after running them through STARS after 15 years of production.

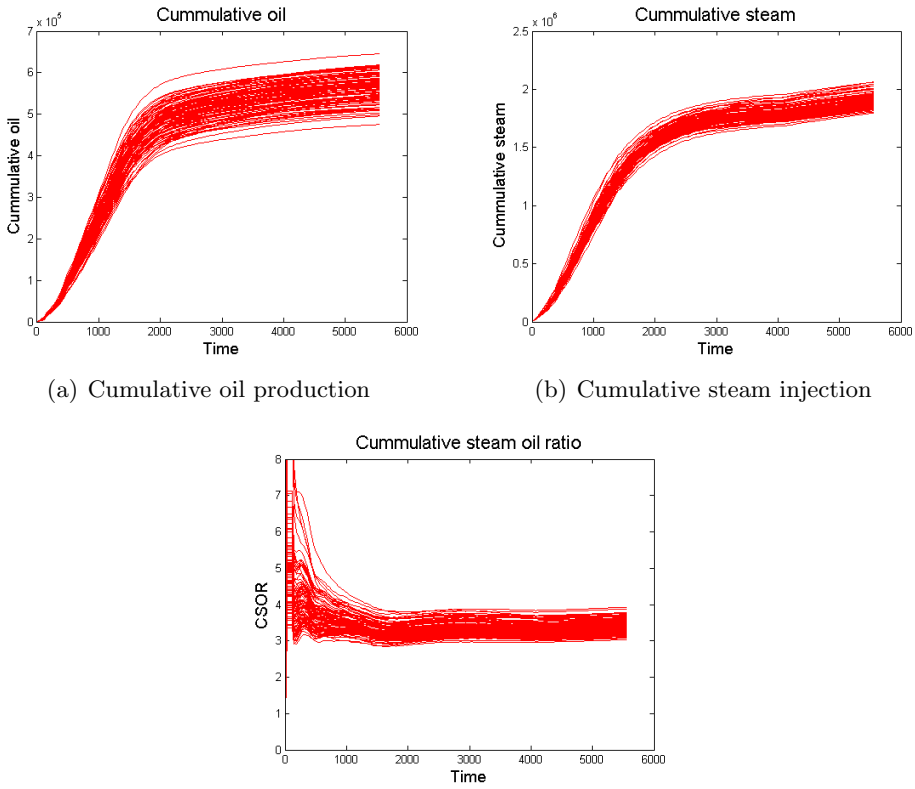

(a) Cumulative oil production

(b) Cumulative steam injection

(c) CSOR

Figure 7.8: SAGD results of simulated realizations after running them by simulator

Figs. 7.8(a)–7.8(b) show the cumulative oil production and the cumulative steam injection of different realizations. The differences between the final cumulative oil productions and final cumulative steam injections of realizations are about 170000 m^3 and 265000 m^3, respectively. These are reasonable ranges of uncertainty. Fig. 7.8(c) shows that the range of uncertainty for CSOR is about 0.9. This range of CSOR variation may be too narrow for a high correlation in the ranking results. After finding the simulation results, the cumulative NPV and rate of NPV change can be computed from the simulation results. In this case, the oil price and steam cost are assumed to be 500 \$US/m^3 and 50 \$US/m^3, respectively. Also, the discount rate is 10% per year.

Fig. 7.9(a) shows the cumulative simulator NPV. The difference between the final cumulative NPV of realizations is about $6.1E+7$ \$US. As Fig. 7.9(b) shows,

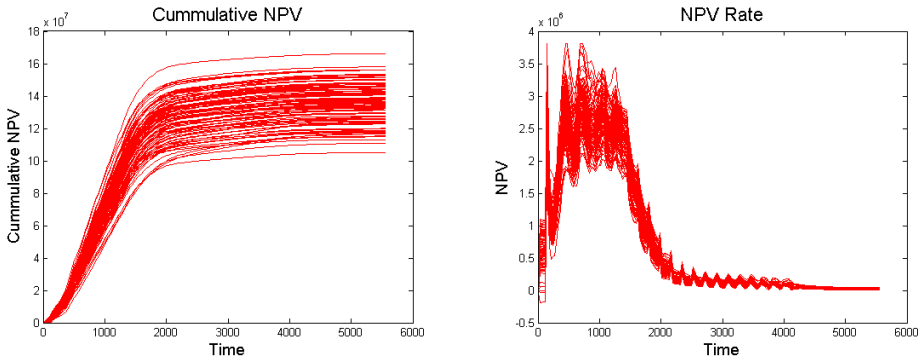

(a) Cumulative NPV (b) Rate of NPV change

Figure 7.9: Cumulative NPV and rate of NPV change for different simulated realizations after running them in the reservoir simulator

the NPV increases fast for the first 1000 days, then rate is decreasing and for the last time steps NPV is close to the zero. Decreasing cumulative NPV is due to the steam injection into the reservoir without producing a significant amount of oil. As a result, the net income becomes zero.

7.3.2 Uncertainty Transferring

Fig. 7.10 shows a comparison between the ranges of uncertainty in the proxy results with the simulator results after 15 years of production.

The minimum and maximum cumulative oil production of the proxy results are very close to the simulator results (less than 0.01%) and proxy forecasted the simulator results with very good accuracy. On the other hand, the maximum cumulative steam injection of the proxy results is about 6% lower than the maximum cumulative steam injection of the simulator results. Also the minimum cumulative steam injection of the proxy results is about 1% greater than the minimum cumulative steam injection of the simulator results. These differences are not significant, but it seems that the proxy cumulative steam injections of different realizations decreased compared to the simulator results which is due to the steam cross over between the adjacent slices. Proxy cannot account for this additional steam injection and as a result additional oil production. The maximum CSOR of the proxy results is about 2% less than the maximum CSOR of the simulator results. The minimum CSOR of the proxy results is about 2% less than the minimum CSOR of the simulator results. These differences are not significant as well. Although the cumulative oil production and the cumulative steam injection of the proxy results is less than the simulator

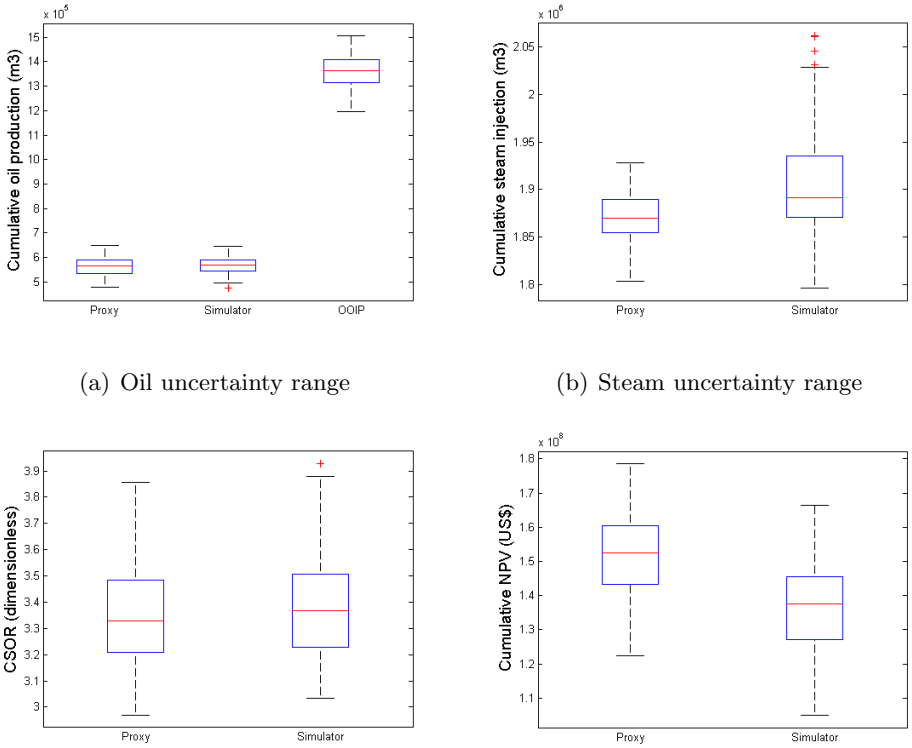

(a) Oil uncertainty range

(b) Steam uncertainty range

(c) CSOR uncertainty range

(d) NPV uncertainty range

Figure 7.10: Comparison between ranges of uncertainty of proxy results with the simulator results using trigger operating strategy after 15 years of production

results, but the CSOR which is the ratio of these results did not change significantly. As a result, the CSOR range of the proxy is very close to the simulator. Finally, the maximum cumulative NPV of the proxy results is 7% higher than the maximum cumulative NPV of the simulator results. The minimum cumulative NPV of the proxy results is 15% higher than the minimum cumulative NPV of the simulator results. These differences are due to underestimating the cumulative steam injection of the simulator results.

7.3.3 Ranking Results

Fig. 7.11 shows a comparison between ranking the reservoir models using the simulator and the other methods after 15 years of production. The lowest correlation

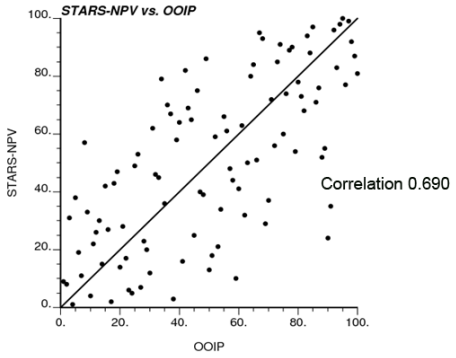

(a) Simulator NPV vs. OOIP

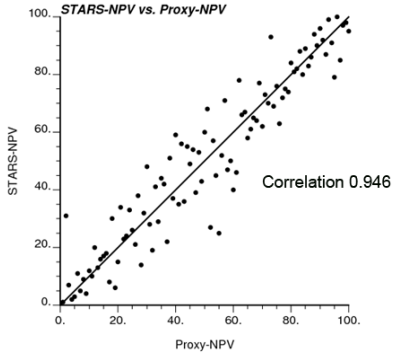

(b) Simulator NPV vs. proxy NPV

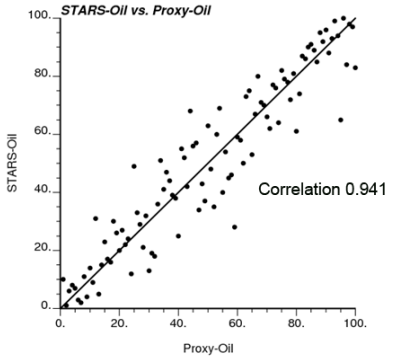

(c) Simulator oil vs. proxy oil

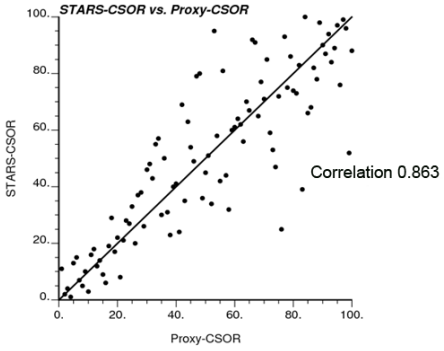

(d) Simulator CSOR vs. proxy CSOR

Figure 7.11: Comparison between ranking the reservoir models using the simulator and the other methods after 15 years of production

coefficient is related to the ranking with OOIP which is 0.69. The correlation coefficient between the ranked results of the simulator NPV and the proxy NPV is 0.95 which is very good. The correlation coefficient between the ranked results of the

simulator oil and the proxy oil is 0.94 which is very good too. Finally, the correlation coefficient between the ranked results of the simulator CSOR and the proxy CSOR is 0.86 which is lower than the oil and NPV cases. This is due to the simulator range of uncertainty for CSOR which is about 0.9. The range of CSOR is too narrow for a high correlation in the ranking results.

The next step is finding the $P10$, $P50$ and $P90$ realizations by the proxy to compare them with the simulator. The central idea of ranking is based on finding these realizations to limit uncertainty of the 100 realizations to 3. Table. 7.1 shows the corresponding simulator ranks for the chosen $P10$, $P50$ and $P90$ realizations based on the proxy after 15 years of simulation.

Table 7.1: Corresponding simulator ranks for $P10$, $P50$ and $P90$ realizations of proxy after 15 years production

Proxy	**Simulator**
P10	P4
P50	P40
P90	P88

Table. 7.1 shows that the proxy overestimated the simulator rank $P10$, $P50$ and $P90$ realizations and proxy $P10$, $P50$ and $P90$ are less than the simulator $P10$, $P50$ and $P90$ realizations. Fig. 7.12 shows a comparison between $P10$, $P50$ and $P90$ realizations of simulator NPVs and proxy NPVs after 15 years of simulation. The

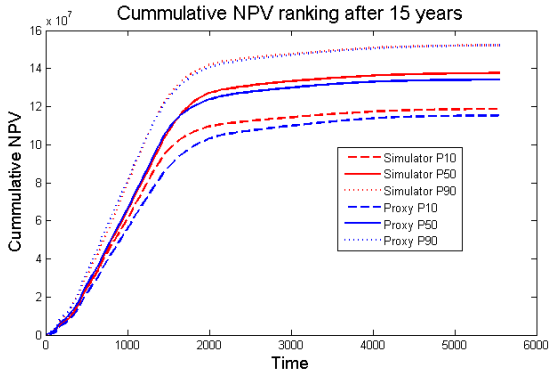

Figure 7.12: Comparison between $P10$, $P50$ and $P90$ realizations of simulator NPV and proxy NPV after 15 years of simulation

proxy results have been shown by the blue curves and the simulator results have been shown by the red curves. Fig. 7.12 shows that the proxy $P10$ is lower than

the simulator $P10$ by about 3%. The proxy $P50$ and proxy $P90$ are about 2% and 0.1% less than the simulator $P50$ and $P90$ respectively. These differences are not significant.

For finding the range of uncertainty around each of the $P10$, $P50$ and $P90$ realizations, the interval could be divided into three groups and it is desirable to have a narrow distribution for each of these groups. These results can be standardized so that the results can be compared to each other. Eq. 5.1 can be used to standardize results. Fig. 7.13 shows a comparison between the standardized simulator results and other methods based on their standardized values.

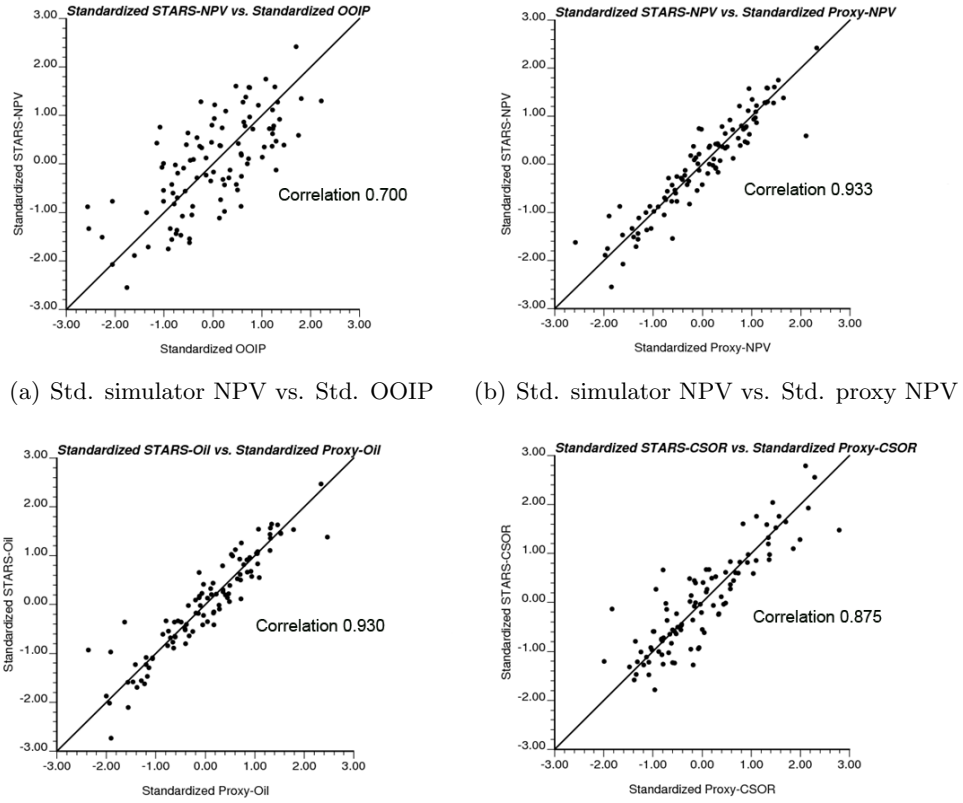

(a) Std. simulator NPV vs. Std. OOIP

(b) Std. simulator NPV vs. Std. proxy NPV

(c) Std. simulator oil vs. Std. proxy oil

(d) Std. simulator CSOR vs. Std. proxy CSOR

Figure 7.13: Comparison between standardized simulator results and other methods based on their standardized values

Fig. 7.13 shows that the ranges of uncertainty around the $P10$, $P50$ and $P90$ realizations for the proxy NPV and proxy oil are very narrow. The ranges for the proxy CSOR are narrow too, but not as narrow as the proxy NPV and proxy oil. The ranges for the OOIP are worse. The mean absolute error (MAE) for identifying

$P10$, $P50$ and $P90$ realizations using proxy NPV have been tabulated in Table. 7.2. These values have been obtained by averaging absolute errors between the simulator $P10$, $P50$ and $P90$ with the proxy $P10 \pm 5$, $P50 \pm 5$ and $P90 \pm 5$. As an example, all of values between $P45$ and $P55$ have been selected and the mean absolute error with the simulator $P50$ has been computed. In this case, effect of outliers around $P10$, $P50$ and $P90$ realizations can be studied.

Table 7.2: Maximum percentage errors for identifying $P10$, $P50$ and $P90$ using proxy NPV

Rank	**Proxy NPV mean absolute error (MAE)**
P10	3.4%
P50	2.6%
P90	1.4%

Table. 7.2 shows that even in the worst case, errors are not very large. The largest error is around $P10$ were there is more scatter compared to the $P50$ and $P90$.

After finding the $P10$, $P50$ and $P90$ realizations, these realization will be used in the next section for forecasting oil production and steam injection compared to flow simulation results.

7.4 Forecasting SAGD Performance

The amount of injected steam can be computed based on the heat loss to the steam chamber and produced oil, the heat loss to the reservoir, and the heat loss to the overburden. By combining these heat losses and using the steam enthalpy, steam injection rate can be computed. In reality, the steam from one slice could help to produce bitumen in the adjacent slices. In this case, the cumulative oil production and cumulative steam injection would be higher. Due to the long variogram range in the horizontal direction compared to the vertical direction, this effect may not be significant. If the variogram range in the horizontal direction is long and elevations of different completions are not significantly different, this effect can be ignored and steam cross-over between adjacent slices would not be significant. If the steam chamber in one slice growths quickly to the top of the reservoir in one slice, then steam will enter to the adjacent slices and lose heat to them too. This will increase heat loss for that slice, and as a result, increase the steam injection rate to that slice. This would also decrease the steam injection rate to the adjacent slices. In

this case, the steam injection rate of different slices may not be matched, but the predicted cumulative steam injection should be close to the simulator. The proxy can consider the interaction between adjacent slices only when one slice is not able to inject steam or produce the oil of that slice.

7.4.1 The $P10$ Realization

Fig. 7.14 shows a comparison between the proxy and simulator for the $P10$ realization.

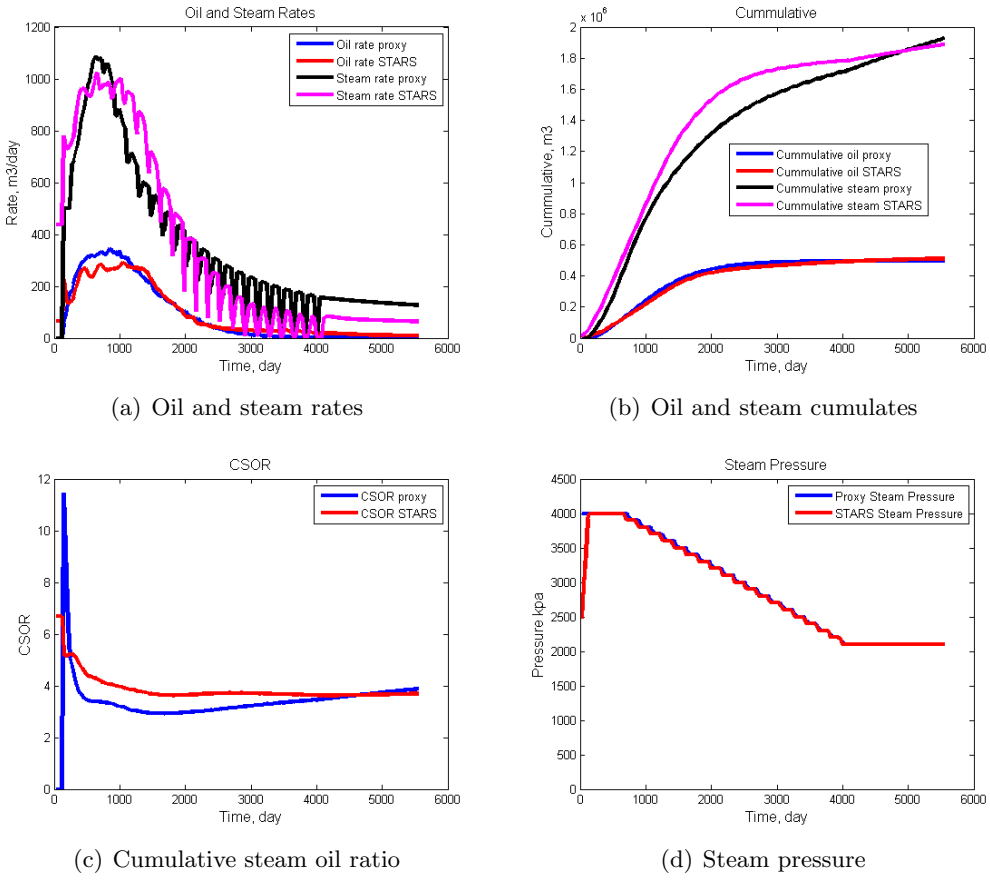

(a) Oil and steam rates

(b) Oil and steam cumulates

(c) Cumulative steam oil ratio

(d) Steam pressure

Figure 7.14: Comparison between results of proxy and simulator for the $P10$ realization

As Fig. 7.14 shows, the match between the simulator and proxy is good. The final cumulative oil production of the proxy is about 3% less than the simulator result, and the final cumulative steam injection of the proxy is about 2% greater than the simulator result. As a result, the final CSOR of the proxy is about 5% greater than the simulator. There is a peak in the proxy CSOR results at the start of estimation which is due to the slower proxy steam front velocity during the rising

period. In this case, the steam injection pressures of the proxy and simulator are the same. Using the trigger, the steam injection pressure is dropped continuously and steam does not move into the thief zone and adjacent slices. As Fig. 7.14 shows, the results are very close to each other.

7.4.2 The $P50$ Realization

For testing proxy efficiency and also considering effect of heterogeneity on the results, another model has been tested by the simulator. Fig. 7.15 shows a comparison between the simulator and proxy for the $P50$ realization as another 3D example.

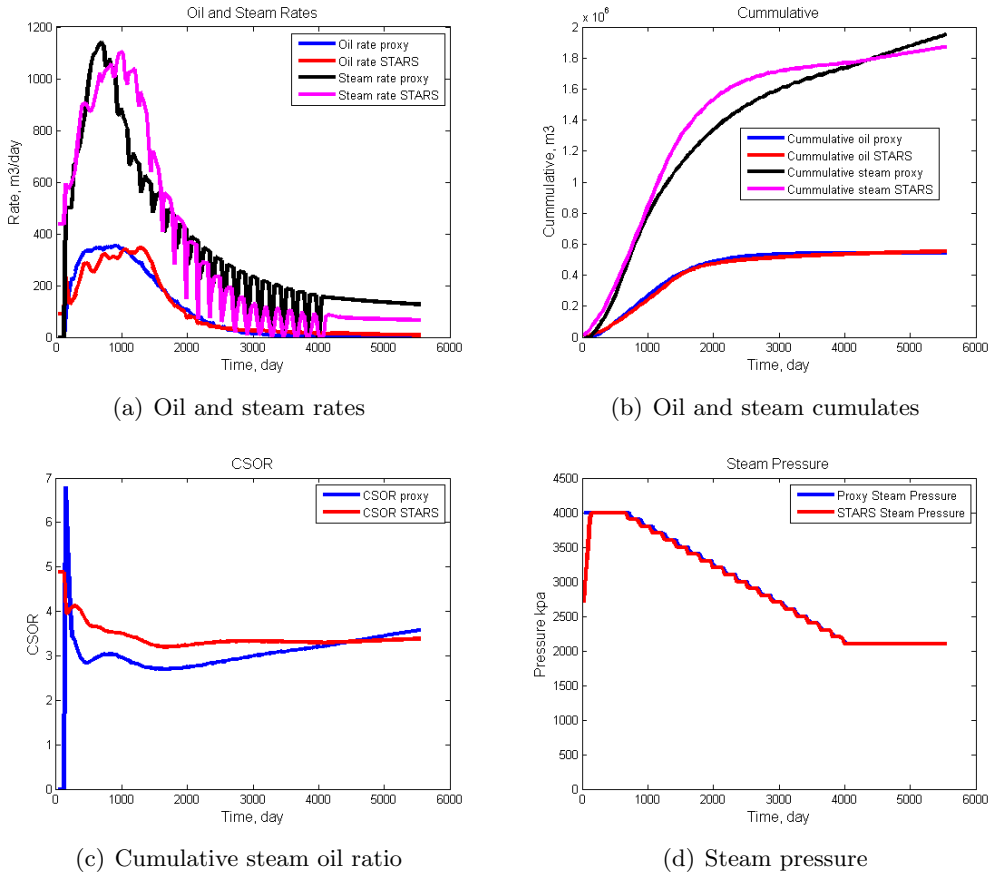

(a) Oil and steam rates

(b) Oil and steam cumulates

(c) Cumulative steam oil ratio

(d) Steam pressure

Figure 7.15: Comparison between results of proxy and simulator for the $P50$ realization

As Fig. 7.15 shows, the proxy final cumulative oil production and cumulative steam injection are close to the simulator. In this case, the final cumulative oil production of the proxy is about 2% less than the simulator result, and the final cumulative steam injection of the proxy is about 4% greater than the simulator result. Also, the oil production and steam injection profiles of the simulator and

proxy are close to each other. Again, except for the first year, the match between the proxy and simulator CSOR is close. The final CSOR of proxy is about 6% greater than the simulator result. The steam injection pressures are matched completely.

7.4.3 The $P90$ Realization

For the last 3D example, the third realization which is the $P90$ realization has been considered for testing the proxy. Fig. 7.16 shows a comparison between results of proxy and simulator.

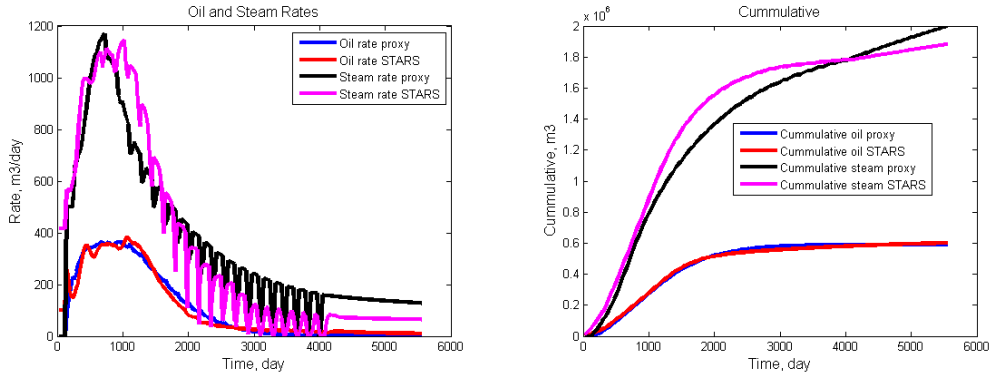

(a) Oil and steam rates

(b) Oil and steam cumulates

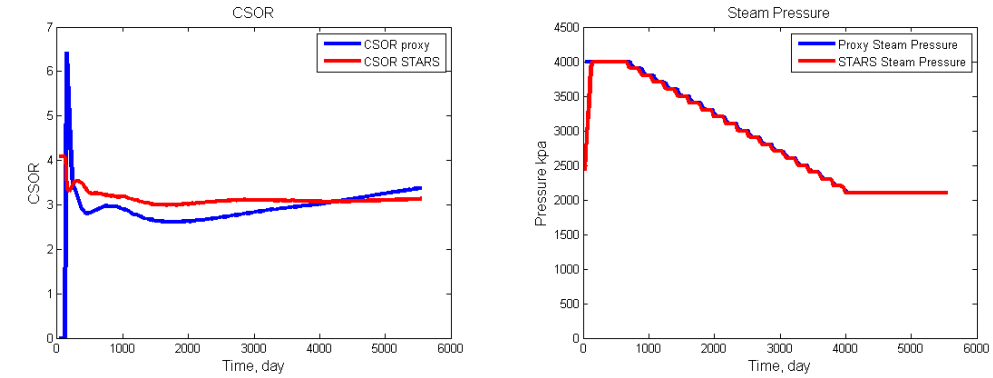

(c) Cumulative steam oil ratio

(d) Steam pressure

Figure 7.16: Comparison between results of proxy and simulator for the $P90$ realization

As Fig. 7.16 shows, the proxy final cumulative oil production and cumulative steam injection are close to the simulator results. The difference between the final cumulative oil production of the proxy and simulator is about 2%. The final cumulative steam injection of the proxy is about 6% greater than the simulator result, and the final CSOR of the proxy is about 8% greater than the simulator result. In all three models, the match between cumulative oil production of the simulator and

proxy are close, but in some of them, match between cumulative steam injections are not close due to the difference in heterogeneity. These results can be improved by calibrating the proxy with the simulation results.

Calibrating Results of the $P90$ Realization with the Simulator

The SQP optimization algorithm has been used as a calibration engine to calibrate the results of the the $P90$ realization. All of calibration parameters have been calibrated at the same time. Eq. 2.24 has been used as the objective function to minimize mismatch between the rates. Fig. 7.17 shows the calibration results.

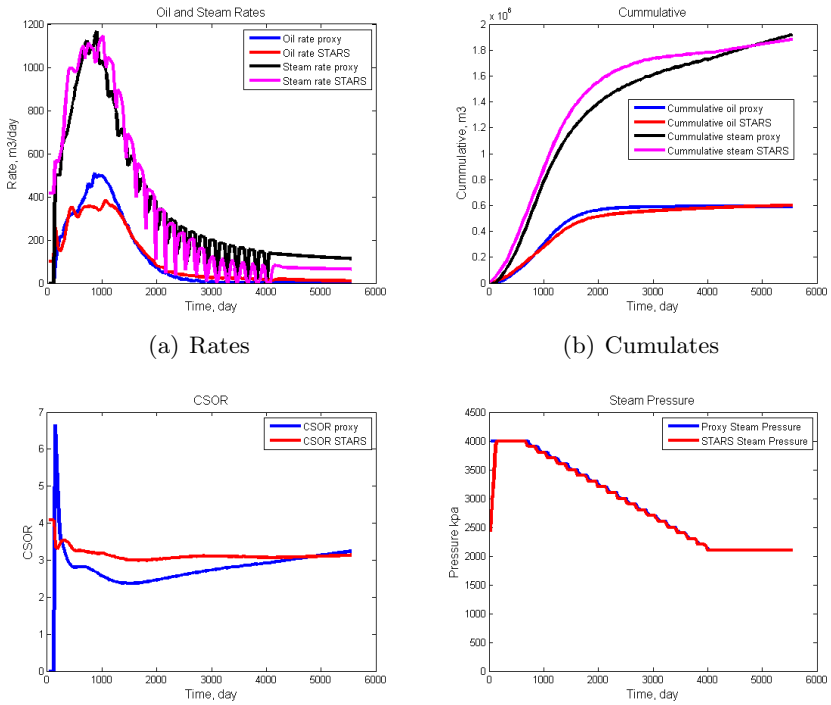

(a) Rates (b) Cumulates

(c) Cumulative steam oil ratio (d) Steam pressure

Figure 7.17: Calibrating results of the proxy for the $P90$ realization

The final match between the cumulative steam injection, steam injection rate and CSOR of the simulator and proxy are better than the base case, but still local match between rates are not satisfactory. Match between the cumulative oil production and oil production rate did not change significantly. Table. 7.3 shows values of the calibrated oil and steam parameters.

As Table. 7.1 shows, the steam chamber velocity has been decreased during the rising and spreading, and has been increased during the confinement. Also, the

Table 7.3: Calibrating parameters of the proxy for the $P90$ realization using SQP method as optimization algorithm

	V_r **mult.**	V_s **mult.**	V_c **mult.**	α_{ob} **mult.**	VHC **mult.**
Initial	1.0	1.0	1.0	1.0	1.0
Final	0.97	0.85	1.60	1.00	1.47

overburden thermal diffusivity has been increased and the volumetric heat capacity did not change to calibrate heat losses and the steam injection rate at different periods of simulation. It seems that all of these changes are for improving estimation of the total heat losses and steam injection rates at different periods. In this case, the final cumulative oil production of the proxy is about 1% less than the simulator and the final cumulative steam injection of the proxy is about 2% greater than the simulator. Also, the final CSOR of the proxy is about 3% greater than the simulator. These results are much better than the uncalibrated results.

The proxy run time is about 10 seconds. Fig. 7.18 shows changes to the objective function by increasing the number of proxy runs in the optimization algorithms.

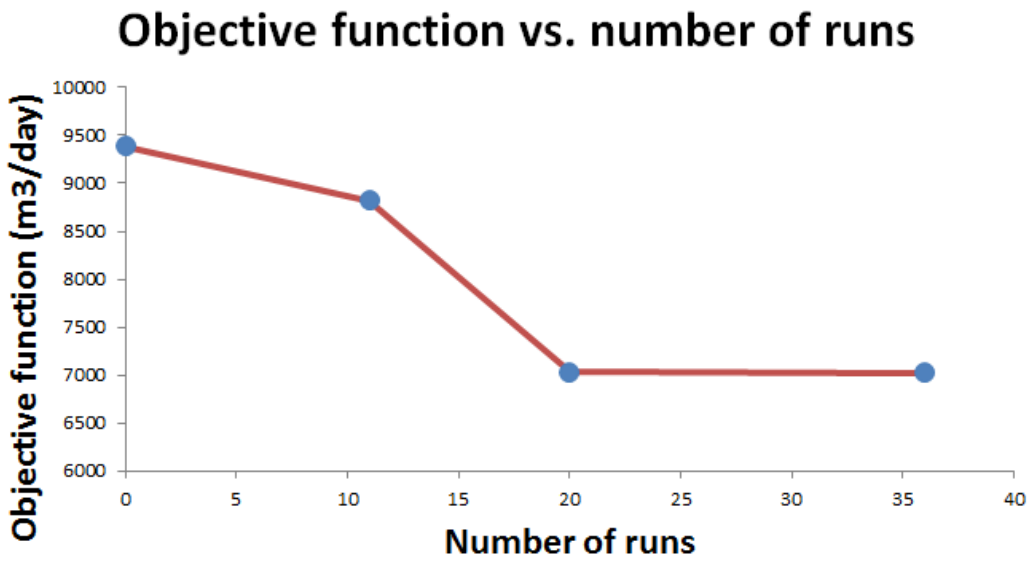

Figure 7.18: Objective function vs. number of runs for calibrating parameters of the $P90$ realization

The objective function drops significantly after 20 runs (two iterations in optimization algorithm) and after 36 runs, the objective function is reasonably small and does not change significantly. This takes about 6 minutes.

7.5 Comparison between the Proposed Work-flow and the Traditional Work-flow

As discussed before, the traditional approach in the SAGD reservoir management is based on the ranking of the reservoir realizations based on the visually optimized well trajectories. For traditional approach, both producer and injector are on the horizontal lines. The producer elevation is 26 m above the base of the reservoir and the injector elevation is 5 m above of the producer. Then, $P10$, $P50$ and $P90$ realizations will be selected for other applications such as transferring uncertainty and well trajectory optimization. Ranking results depends highly on the well trajectory and because of shale barriers around wells, by changing well trajectory ranked results will change significantly. In this work, all of the realizations have been used for well trajectory optimization. Then, all realizations have been used for ranking and transferring uncertainty using the optimal well trajectories in the first step. Using this approach, the expected NPV of realizations would be higher than the traditional approach. Fig. 7.19 shows a comparison between the NPV of proposed work-flow and the traditional work-flow. Using the proposed methodology, the expected NPV of the realizations is 16% greater than the expected NPV of the realizations using the traditional work-flow. Also, the $P10$, $P50$ and $P90$ NPV of realizations in the proposed methodology are 16%, 17% and 15%, respectively. Results show increase in the NPV compared to the traditional approach. Although the producer elevation for traditional approach is below the optimal trajectory for the proposed approach for many slices, but the final NPV of the traditional approach is less than the proposed approach.

7.6 Summary

An illustrative case study was performed on a synthetic model with 3 well pairs. This dissertation proposes new methodology for SAGD reservoir management. Based on this method, optimal well trajectories have been computed using all of the realizations. After that, all other applications such as, ranking, transferring uncertainty and forecasting SAGD performance have been done using the optimal well trajectories. Some points can be concluded from this case study.

- The optimal producer trajectory is close to the averaged BCB for different realizations. In this case, most of the BCBs are below the optimal producer

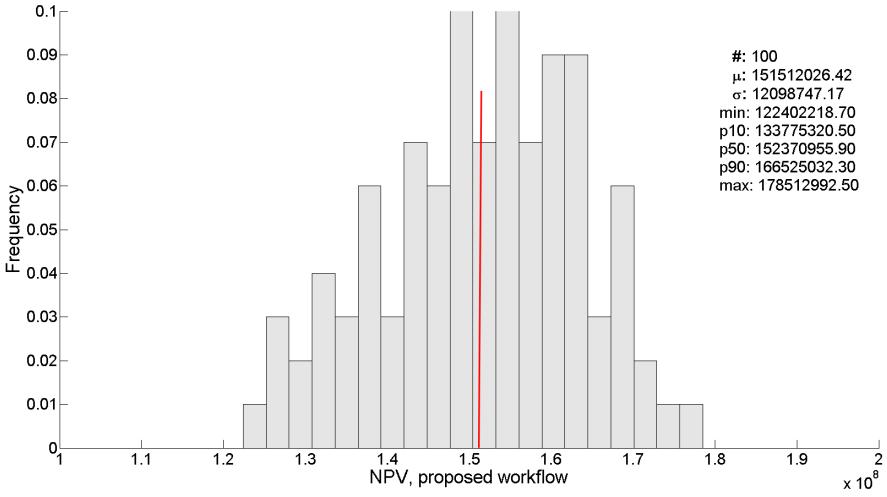

(a) Proposed work-flow

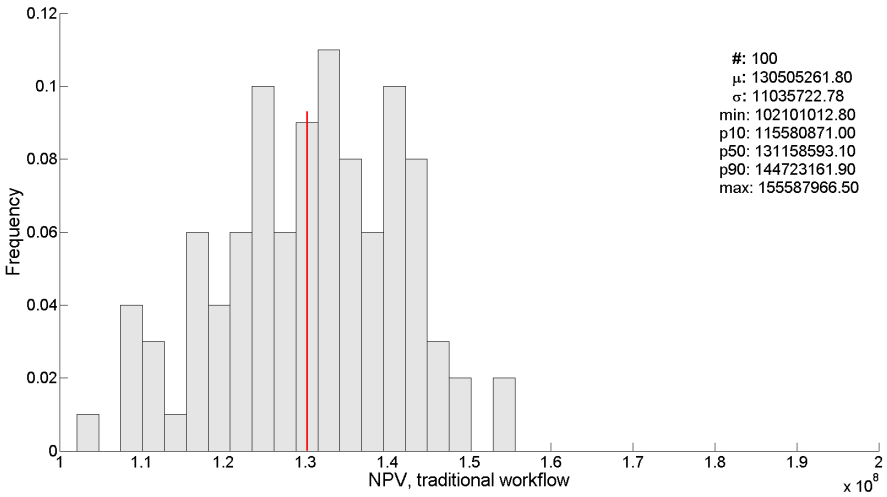

(b) Traditional work-flow

Figure 7.19: Comparison between the NPV of proposed work-flow and the traditional work-flow

which maximized the expected NPV.

- The proxy transfers the simulator cumulative oil production and CSOR very quickly and reliably, but the transferred cumulative steam injection of different realizations are less than the simulator which is due to neglecting steam cross over between adjacent slices. As a result, the transferred NPVs are less than the simulator results.
- Using the proposed methodology, the expected NPV of the proposed reservoir development with the realizations is significantly higher than the expected NPV of the realizations using the traditional work-flow.

Chapter 8

Summary and Conclusions

A new semi-analytical approximate thermal simulator based on the Butler's theory (a proxy) has been developed and tested on different synthetic and realistic history matched 2D and 3D models. Many modifications, extensions and improvements have been made to Butler's original model.

Different types of reservoir heterogeneity have been tested with different operating strategies including changes to the steam injection rate, maximum bottom-hole pressure, time varying pressure, ISOR and blow-down trigger. In general, the oil production and steam injection rates and cumulative amounts have been forecast with high accuracy.

Ideally, the proxy results should be matched with real production data. Reservoir parameters are uncertain. As a result, geostatistical models are uncertain and different than the true reservoir model. In this dissertation, the proxy results have been compared with the simulator results. This is reasonable since the flow simulation results are history matched to production data; therefore, matching the flow simulator is close to matching to real production data. This has been shown by comparing the proxy results with the realistic history matched 3D models.

This proxy or approximate simulator can be used for different applications such as forecasting the location of the steam chamber, ranking the reservoir realizations, transferring or roll-up of uncertainty and well trajectory optimization. These applications have been demonstrated and results have been compared with simulator results.

The proxy run time for a large model (130 m spacing and 1 km length) with $\Delta t = 15$ days, a combination of different strategies and 30 years of simulation time takes about 15 seconds. The simulator run time for this model is about 2 days which

is thousands of times slower than the proxy.

Not only is the proxy much faster than the reservoir simulator, setting up the input parameters to the proxy is much easier than building a simulation model and it does not have numerical convergence issues common to commercial simulation.

The proxy assumes different assumptions. Based on the Butler's original theory, only conduction heat transfer mechanism is assumed for oil production. Also, it is assumed that the temperature distribution beyond a steam interface is steady state for a moving front with constant velocity. Butler assumed that the steam chamber pressure is uniform and it is equal to the steam injection pressure. One limitation of the proxy is related to the changing grid cell oil saturation during the SAGD operation. This proxy assumes that all of producible oil inside a grid cell would be produced quickly if the steam front covers it. This assumption is not realistic. In reality, producible oil inside the steam chamber will decrease gradually by increasing the production time. By considering this effect, proxy can be used for other purposes such as history matching for finding a good match between proxy results and production data.

8.1 Summary of Contributions

Other analytical methods have been developed, but they cannot consider heterogeneity in an efficient way. Also, none of them can consider different operating strategies related to limited steam injection rate or pressure constraints. Other methods require many training cases that can be very time consuming and limit the range of applicability of the results. For this reason, a new proxy based on other a Butler's theory has been developed that can consider reservoir heterogeneity and different operating strategies in an efficient way. Chapter 1 summarized recent works on thermal proxy models.

8.1.1 New Rising Model

Butler rising model assumes a cone shaped steam chamber above the producer that is applicable to homogeneous models. In this work, a new analytical rising model based on a trapezoid shape above the well has been developed that is suitable for heterogeneous models. This model can forecast the end of the rising period more accurately than Butler's rising model. The derivation of this new model has been explained in the Chapter 2.

8.1.2 Reservoir Heterogeneity

Butler's theory only works for homogeneous models. For considering heterogeneity, the proxy has been linked to the CHV (connected hydrocarbon volume) tool for finding net connected grids in the model. In this case, only producible oil will be considered. As a result, the final cumulative oil production of the proxy is very close to the simulator.

Different methods for considering heterogeneity have been explained in Chapter 2 of this dissertation. Chapter 3 shows a number of 2D and 3D examples with different types of heterogeneity. All results have been compared to simulator results.

8.1.3 Operating Strategies

Butler's model assumes unlimited steam availability. This is not a good assumption and in most of the simulation models, different constraints such as maximum steam injection rate and maximum bottom-hole pressure are set for injection. For considering these constraints, the proxy is able to change the steam injection pressure during the simulation based on these constraints.

This ability permits consideration of using other operating strategies such as a pressure trigger, ISOR trigger or blow-down trigger that are needed for realistic simulation models.

The methodology of considering different operating strategies has been explained in Chapter 2. Also Chapter 3 considers a number of 2D and 3D heterogeneous models with different operating strategies compared with the simulator. Results show a very good match between the proxy and simulator results.

8.1.4 Calibrating the Proxy with Flow Simulator

The differences between the proxy and simulator are small, but some parameters of the proxy are uncertain and can cause differences in forecasted production and injection. An efficient gradient based optimization algorithm (SQP) has been used for automatic calibration of these parameters and minimizing the mismatch between the proxy and simulator results. Chapter 2 discussed the calibration methods and Chapter 3 showed successful examples for calibrating the proxy results.

8.1.5 Forecasting the Location of the Steam Chamber

Butler's model forecasts the location of the steam chamber based on the rising, spreading and confinement periods. This estimation only works for homogeneous models. For heterogeneous models, the steam chamber location is completely different. In this work, the results of CHV and the proxy provide a new method for finding the location of the steam chamber at different time steps. This methodology has been explained in Chapter 4 and different examples have been considered for testing this methodology. Then results have been compared with simulator result with a very good match.

8.1.6 Ranking and Transferring Uncertainty

This proxy can be used for other applications such as ranking of reservoir realizations and transferring uncertainty of realizations. In Chapter 5, 100 realizations have been generated and used for long-term, and short-term rankings. These realizations have been run with both the proxy and flow simulator and they have been ranked based on their NPV. Then, the results of proxy have been compared with the simulator. The results show a high correlation coefficient. Also, the sensitivity of different proxy parameters can be understood. Instead on running all of realizations with flow simulator, they can be run with the proxy for transferring uncertainty of realizations through to production forecasts shown in Chapter 5.

8.1.7 Well Trajectory Optimization by Considering Reservoir Uncertainty

The proxy has also been applied to well trajectory optimization (both producer and injector locations) in Chapter 6. Two methods were considered for optimization using the DE optimization algorithm. Many constraints on the trajectories can be considered and multiple reservoir realizations can be used for maximizing the NPV over all realizations.

Finally, Chapter 7 considers a case study for testing all of the applications including ranking, transferring uncertainty, prediction, calibration, and well trajectory optimization. Results are compared with the simulator which show that the proxy model is an efficient and effective alternative.

8.2 Future Work

There are many ideas to improve the results of the proxy.

The geometric average of permeability used for the connected net grid cells could be refined. The relative permeability at each time step could be estimated better to control the steam front velocity.

In this work a new method has been developed for forecasting location of steam chamber for heterogeneous models. This model could be used for correcting heat losses to different parts of the reservoir.

In reality, producible oil inside the steam chamber will decrease gradually by increasing the production time. By considering this effect, proxy can be used for other purposes such as history matching for finding a good match between proxy results and production data.

For well trajectory optimization, multiple well pairs should be optimized simultaneously to prevent uneven growth of the steam chamber.

The proxy could also be applied for optimizing the operating strategy using different optimization techniques such as SQP. For example, steam injection pressure can be optimized during the simulation for maximizing NPV. It can be a very interesting research especially if multiple reservoir realizations are used.

The proxy could also be used for field scale optimization of drainage area locations. All of these parameters should be optimized at the same time for finding a global optimum for reservoir development planning.

Appendix

Appendix A

SAGD Proxy Manual

SAATS (Semi Analytical Approximate Thermal Simulator) is a new program for quick simulation of the SAGD process. This program forecasts simulation results using a semi-analytical model based on the Butler's SAGD theory. Butler's SAGD theory is a method for forecasting the SAGD performance of homogeneous reservoir models. Different modifications have been done on this theory to improve its results for predicting the SAGD performance of heterogeneous reservoir models by simulating different operating strategies. This tool can be used for different applications such as prediction, ranking reservoir realizations, and well trajectory optimization. Some parameters in the proxy can be calibrated automatically for finding a better match between the proxy and simulator results. Although the proxy parameter file is simpler than the STARS data file, but still there are many keywords in that, and this paper describe all of them with illustrative examples.

A.1 Parameter File Sections

The parameter file of this proxy is similar to the STARS. Double star ** at any place of parameter file means starting a comment and software will not read the remaining characters of that line. Each parameter can be identified by a keyword. The order of keywords is not important, although it is better to keep the order same as the template. Input data files format is the same as the GSLIB format. Origin for gridded data files is the same as all of the GSLIB data files that is close left of the bottom layer. The parameter file has been divided into 10 different sections. These sections are:

1. Program mode and basic information

2. Static model specifications
3. Static reservoir properties
4. PVT data
5. Relative permeability data
6. Thermal and rock properties
7. Steam properties
8. Calibrating parameters using the SQP optimization algorithm
9. Ranking reservoir realizations
10. Well trajectory optimization

Keywords should be started at the start of each line and space is not allowed before the keywords or in writing the file paths. In the following sections, format and application of all keywords are explained.

A.1.1 Section 1: Program Modes and Basic Information

```
****************************************
**
** Program mode and basic information
**
****************************************

**
** Program mode
**
PROXYMODE    1            ** Proxy mode (1:Prediction  2:Ranking  3:Calibration  4:Well trajectory optimization)

FILEPRE      test         ** prefix used for result files
PRTMODE      1 1          ** Option for writing a) calculation details and b) heat losses (0:No 1:Yes)
NSETS        1            ** Number of realizations should be used for ranking, calibrations or well trajectory optimization
NWELLS       1            ** Number of well pairs in the model

**
** Time specifications for results and criteria to stop the runs
**
DELT         5            ** Time step increment during simulation, days
TIMEFREQ     30.0         ** Frequency for reporting results, days
ENDTIME      5550.0       ** Simulation time, days
```

The first section is for setting program mode and the basic information. The first keyword is **PROXYMODE** that specifies the program mode. By setting it to one, proxy can be used for prediction. For other applications such as ranking, calibration or well trajectory optimization, it should be set to 2, 3 and 4, respectively. Any of these applications has a separate section and they will be explained later. Keyword **FILEPRE** specifies a prefix for the result files. Keyword **PRTMODE** is related to writing the calculation details. It follows by two different values. The first one is for writing the computation details of the proxy for each time step in the debug file. For writing this file, its value should be set to 1, otherwise it should be set to

zero. The second one is for writing details of the heat losses at each time step in a separate file. Keyword **NSETS** specifies number of reservoir realizations. Number of realizations should be set to one for prediction mode, but for other modes such as ranking, calibration or well trajectory optimization larger number can be set for this keyword. Keyword **NWELLS** specifies number of well pairs in the model. If user would like to simulate the SAGD performance of a DA, performance of all wells can be forecasted simultaneously. **DELT** specifies the time step size during the simulation and **TIMEFREQ** specifies the frequency of writing results in the result file. Finally, keyword **ENDTIME** specifies duration of the simulation.

A.1.2 Section 2: Static Model Specifications

```
**************************************
**
** Static model specifications
**
**************************************

**
** Number of grids and size of grids
**
NX        26              ** Number of grids in X direction
XSIZ      25.0            ** Size of grids in X direction (meters)
NY        32              ** Number of grids in Y direction
YSIZ      2.5             ** Size of grids in Y direction (meters)
NZ        83              ** Number of grids in Z direction
ZSIZ      1.0             ** Size of grids in Z direction (meters)
WELLCOORD_1   1 26  1 32  1 83   ** Simulation box of each well in the model (Xmin,Xmax,Ymin,Ymax,Zmin,Zmax)

NDISC     0               ** Number of grids in proxy (0=default value)
WELLDIR   1               ** well direction (1=i direction    2=j direction)
DIRSIM   -1  1  -1        ** Direction of simulator coordinates compare to the proxy (diri dirj dirk). 1:Same  -1:Reverse


NODESI_1    23            ** number of slices along the injector based on the CMG format (if PROXYMODE not equal to 4)
24 16 50                  ** X, Y and Z coordinates (each node at one row - number of rows=number of slices
23 16 50

NODESP_1    23            ** number of slices along the well based on the CMG format (if PROXYMODE not equal to 4)
24 16 55                  ** X, Y and Z coordinates (each node at one row - number of rows=number of slices
23 16 55
```

Second section specifies the model size and well trajectories. Keywords **NX**, **NY** and **NZ** specify number of grids in the x, y and z directions. Keywords **XSIZ**, **YSIZ** and **ZSIZ** specify grid sizes in the x, y and z directions as well. Keyword **WELLCOORD** specifies coordinates of the simulation box for each well. _1 after this keyword means well number one. If there are multiple well pairs in the model (NWELSS>1), for each well user should define these coordinates in a separate line. For example, coordinates of the well number two can be defined using keyword WELLCOORD_2. Keyword **NDISC** sets number of grids in the proxy model. During the spreading and confinement periods, the proxy divides the vertical reservoir thickness into NDISC grid cells. In this case, number of grids in the horizontal direction would be the same as the vertical direction, but grid cell sizes along different directions are variable are not the same. On the other hand, during the confinement, NDISC would be number of proxy grid cells in the horizontal directions and vertical locations of grid cells would be specified based on the location

of the steam front. If user is not sure about this value, value 0 can be set for this parameter. In this case NDISC would be the minimum of model grid cells sizes in the horizontal and vertical directions.

Keyword **WELLDIR** specifies the well direction. One means I direction and two means J direction. In the GSLIB format, reference grid is the close left grid of the bottom layer, but in the simulation model, the reference grid could be different. For this reason, **DIRSIM** defines the direction of simulator coordinates respect to the proxy direction in the I, J and K directions. In this case, 1 means the same direction and value -1 means the reverse direction. Assume that the reference grid in the simulator is the close right grid in the top layer. In this case I and K directions in the simulator are not the same as the GSLIB format. For this reason, DIRSIM for the I, J and K directions would be -1, 1 and -1.

Keywords **NODESI** and **NODSP** specify the injector and producer well trajectories, respectively. Again, _1 after these keywords means well number one. If there are multiple well pairs in the model (NWELSS>1), for each well user should define these keywords separately. Number of nodes should be written in front of these keywords and in the next rows, the I, J and K coordinates of each node should be specified. These trajectories can be copied from the simulator data file. Proxy converts coordinates to the GSLIB format based on the DIRSIM keywords.

A.1.3 Section 3: Static Reservoir Properties

```
****************************************
**
** Static reservoir properties
**
****************************************

** Each property can be in a seperate file or all of them should be in different column of a single file
** multiple realizations should be in the same file (one after each other)


** Facies, column number and file name
Rockval   1    D:\proxy_code\Manual\proxy\Geology\datafile_All.out

** Horizontal permeability (md), column number and file name
Khval     2    D:\proxy_code\Manual\proxy\Geology\datafile_All.out

** Vertical permeability (md), column number and file name
Kvval     3    D:\proxy_code\Manual\proxy\Geology\datafile_All.out

** Porosity (frac), column number and file name
Phival    4    D:\proxy_code\Manual\proxy\Geology\datafile_All.out

** Water saturation (frac), column number and file name
Wsatkval  5    D:\proxy_code\Manual\proxy\Geology\datafile_All.out


**
** STARS results file
**

** Number of STARS files for calibration should be equal to NSETS
STARSCOMP   0    ** Do you want to compare proxy results with STARS results  (1: Yes   0:No)
TRUEFL      D:\proxy_code\Trajectory\proxy2\Geology\stars.dat      ** STARS results file (if STARSCOMP=1)
```

Section 3 specifies the static reservoir properties for all of grid cells. Keywords **Rockval**, **Khval**, **Kvval**, **Phival** and **Wsatval** are for specifying paths of the gridded data files for the facies, horizontal permeability, vertical permeability, porosity and water saturation, respectively. Each of these properties should be in a separate data file or all of them should be in the different columns of a single data file. Format of data files are based on the GSLIB format and the reference grid is the close left grid of the bottom layer. For calibration, proxy results can be compared with the simulator results. For this reason, path of STARS result file should be specified in front of the keyword **TRUEFL**. For prediction application, proxy results can be compared with the simulator results. If user would like to compare them, **STARSCOMP** should be set to one and TRUEFL should be specified, otherwise STARSCOMP should be set to zero.

A.1.4 Section 4: PVT Data

```
*****************************************
**
** PVT data
**
*****************************************

VISFLG      0           ** Flag to use viscosity table file (VISCFL). if 0 it uses correlations
VISCNUM     28          ** Number of lines in viscosity tablae
10      0       9645716.11      ** Temperature (C), Water viscosity (cp) and Oil viscosity (cp) respectiviely
20      0       1366301.91
30      0       259053.13
40      0       62471.47
50      0       18393.83
60      0       6398.06
70      0       2559.73
80      0       1152.46
90      0       573.51
100     0       310.83
110     0       181.21
120     0       112.49
130     0       73.71
140     0       50.61
150     0       36.20
160     0       26.83
170     0       20.51
180     0       16.11
190     0       12.96
200     0       10.65
210     0       8.91
220     0       7.59
230     0       6.56
240     0       5.74
250     0       5.08
260     0       4.55
270     0       4.11
280     0       3.74
```

Section 4 specifies the PVT properties in the proxy model. Keyword **VSIFLG** specifies that correlations or the PVT table should be used for computing the PVT properties. If VISFLG is equal to zero, different correlations internally calculate the PVT properties, but if VISFLG is equal to one, the PVT table should be inserted after the **VISCNUM** keyword. Number after VISCNUM specifies number of rows in the PVT table. PVT table has three columns. The first column is the temperature (c), the second and third columns are water viscosity (cp) and oil viscosity (cp), respectively. Only one PVT table is allowed for inserting in the proxy parameter

file.

A.1.5 Section 5: Relative Permeability Data

```
****************************************
**
** Relative permeability data
**
****************************************
RELPERMFLG    1          ** Relative permeability flag (0:do not use kperm, 1: use kperm)
RELPERMTYPE   1          ** Relative permeability calculation (1:use correlation   2:use table)
RELPTABLE     19         ** Number of lines in table (in the next lines write Sw, krw and krow respectively)
0.07     0.000000   1.000000
0.116    0.000106   0.878905
0.161    0.000851   0.765625
0.207    0.002873   0.660155
0.253    0.006809   0.562500
0.298    0.013300   0.472655
0.344    0.022982   0.390625
0.389    0.036494   0.316405
0.435    0.054475   0.250000
0.481    0.077563   0.191406
0.526    0.106396   0.140625
0.572    0.141614   0.097656
0.618    0.183853   0.062500
0.663    0.233753   0.035156
0.709    0.291951   0.015625
0.754    0.359088   0.003906
0.800    0.435799   0.000000
0.9      0.679339   0.000000
1.0      1.000000   0.000000
```

Section 5 specifies the oil relative permeability information. If user would like to convert the average permeability to the oil effective permeability, keyword **RELPERMFLG** should be set to one, otherwise it should be set to zero. The oil effective permeability can be obtained by multiplying the average permeability by the oil relative permeability. For this reason, the oil relative permeability should be computed. If RELPERMFLG is equal to one, keyword **RELPERMTYPE** should be specified as well. If user would like to use correlations for calculating the relative permeability, it should be set equal to 1, but if user would like to use the relative permeability table, this keyword should be set to 2 and the relative permeability table should be inserted after the **RELPTABLE** keyword. Number of rows in the table should be set after RELPTABLE keyword. Relative permeability table has three different columns. These columns are the water saturation, the water relative permeability and the oil relative permeability, respectively.

A.1.6 Section 6: Thermal and Rock Properties

```
****************************************
**
** Thermal and rock properties
**
****************************************

**
** Rock properties
**

FANUM       2              ** Number of facies
RESOS       0.20  0.20     ** Residual oil saturation for different facies, fraction
RESWS       0.07  0.60     ** Residual water saturation for different facies, fraction
THIEFZONE   1              ** Existence of thief zone on the top (0:No   1:Yes)

NNET     1   1          ** Number of net facies - numbers of net facis
PERMCUT  20             ** Permeability cutoff for computing connected net cells (md)
PERMMAX  1800           ** Max permeability for computing CHV and average permeability

TEMPR    11.0           ** Initial reservoir temperature, deg C
API      9.08           ** Oil API density, deg  8.5
AVGMODE  1              ** Averaging method (1:Based on CHV  2:Based on line of sights)

**
** Thermal properties
**

THNUM    7              ** Number of thermal rock types
THRESH   0.05  0.2  0.4  0.6  0.8  0.95     ** Shale volume thresholds (should be THNUM-1 values)
THCONR   6.56E+05 5.99E+05 4.85E+05 3.71E+05 2.57E+05 1.44E+05 8.67E+04   ** Thermal conductivity of different rock types (start from rocktype=1) J/m.d.C
THCONW   5.68E+04       ** Water thermal conductivity, J/m.d.C
THCONO   9.27E+03       ** Oil thermal conductivity, J/m.d.C
THCOB    2.22E+05       ** Overburden thermal conductivity, J/m.d.C

ROCKCP   1.94E+06 1.96E+06 1.99E+06 2.02E+06 2.05E+06 2.08E+06 2.09E+06 ** Heat capacity of different rock types (start from rocktype=1) J/m3-C
CPOIL    2442.611       ** Oil fluid heat capacity, J/Kg-C   true=2442.0
CPOB     2.01E+06       ** Heat capacity of overburden, volumetric, J/m3-C
```

Section 6 specifies the thermal and rock properties. The first keyword in this section is **FANUM** that specifies the number of facies in the model. Keywords **RESOS** and **RESWS** specify the residual oil saturation and residual water saturation for different facies, respectively. Number of values after each of these keywords should be equal to the FANUM. If thief zone exists on the top of the reservoir, **THIEFZONE** keyword should be set 1. In this case, heat loss to the overburden would be computed based on the thief zone properties such as the porosity and water saturation, for modifying the overburden thermal diffusivity. Otherwise, it should be set zero.

Keyword **NNET** specifies number of net facies and numeric values of the net facies. As an example, if there are 5 facies in the model and 3 of them with numbers 1, 2 and 3 are good quality facies (net facies) the first value after NNET keyword would be 3 and after that numeric values of these net facies should be written. As a result, four numbers after NNET would be 3, 1, 2 and 3. **PERMCUT** is the permeability threshold for specifying the net connected grid cells. If PERMCUT is 20 *md* and permeability of a grid cell is less that this value, this grid would be recognized as non-net grid cell. **PERMMAX** is the maximum allowable value for permeability. For finding the steam front location, proxy calculates the average reservoir permeability. For computing the average permeability, a maximum value for the permeability values should be assumed to keep the average permeability in a reasonable range, otherwise the steam front moves very fast.

TEMPR is the average reservoir temperature before starting the simulation and **API** is the oil API density. **AVGMODE** specifies the method for computing

the average of reservoir properties. If it is one, average porosity and water saturation would be arithmetic average of all of connected net grid cells, and average permeability would be geometric average of all of connected net grid cells. If the AVGMODE is 2, the averages would be computed based on the location of the steam front at each time step. In this case, the average of porosity and water saturation would be arithmetic average of porosity or water saturation of all of grid cells on the edge of the steam chamber. For computing the permeability average, at first the harmonic average of all of grid cells at each segment of the edge of the steam chamber should be computed, then the final average of the permeability would be the arithmetic average of permeability of all of these segments.

Number of thermal rock types specifies by keyword **THNUM**. Thermal rock types can be identified based on the shale volume (Paradigm Ltd., 2012). For this reason, shale volume can be computed for each block from the effective porosity. By setting different thresholds, thermal rock type can be identified. If 7 different thermal rock types exists in the model, 6 thresholds should be defined. For example, if the shale volume is less than 5%, that grid has thermal rock type 1 and if the shale volume is between 5%–20%, the thermal rock type is 2. Shale volume thresholds should be specified with keyword **THRESH**. Number of values after THRESH should be equal to THNUM-1. Keyword **THCONR** specifies the thermal conductivity for each of these thermal rock types. Number of values after this keyword is equal to the THNUM. Keywords **THCONW**, **THCONO** and **THCOB** specify the water, oil and overburden thermal conductivities, respectively. Keyword **ROCKCP** specifies the heat capacity of different thermal rock types. Number of values after this keyword should be equal to the THNUM. Finally, the oil fluid heat capacity and overburden heat capacity should be specified by keywords **CPOIL** and **CPOB**, respectively.

A.1.7 Section 7: Steam Properties

```
****************************************
**
** Steam properties
**
****************************************

**
** Steam injection mode
**
PRMODE   2    ** 0=variable pressure  1=Trigger    2=both
RISING   2    ** Rising model for computing steam rate (1:Butler model    2:Vahid model)
TDIFFER  50   ** Approximate difference between steam temperature and average chamber temperature
TINTFC   100  ** Difference between steam temperature at injector and temperature at steam interface

**
** Steam injection pressure
**
PRESS    2  60  ** Number of changes in steam chamber pressure, duration of change (days)
0.0   4000       ** Time (days), Pressure (kPa) -- each changes in one line
120   3500

**
** Trigger settings (only if PRMODE=1 or PRMODE=2)
**
TRIGS     450        ** start time for trigger
TRIGTIME  360        ** Frequency of applying trigger (only for pressure trigger)
TRIGCP    100        ** change in pressure for trigger
TRIGISOR  0.0        ** isor limit for trigger (only for isor trigger)
TRIGMINP  1600       ** minimum pressure for applying trigger

**
** Blow-down setting - It starrts working after a certain time or after producing specific amount of oil)
**
BLOWDOWN    1        ** Blow-down trigger (0: No   1: Yes)
BLTIMEMAX   4000     ** Maximum time to start blow down
BLLIMIT     1403284  ** Cum oil limit for starting blow-down
BHPMAXP     500      ** Maximum BHP for shut-in the producer

**
** Steam injection conditions:
**
STEAMQL    0.90      ** Quality of injected steam, fraction
MAXSTEAM   10000     ** Maximum field steam injection rate (m3/day)

**
** Start up time
**
STUPTIME  120.0      ** Start up time, days
PRODCIRC   1         ** Producer status during circulation (0: only injects   1: injects and producees)
```

Section 7 specifies the steam properties. **PRMODE** specifies the program mode for changing the steam pressure. Zero means the operating strategy is based on changing the steam pressure multiple times during the simulation. One means trigger (pressure or ISOR) should be used as an operating strategy and 2 means the operating strategy is combination of the first two modes. Keyword **RISING** specifies the type of the rising model during the rising period. One means, the Butler cone shape model, and 2 means the trapezoid shape new rising model. Usually, the steam temperature at the injector is higher than the average temperature of the steam chamber. By increasing the distance from the injector, the steam chamber temperature decreases. Keyword **TDIFFER** specifies an approximate difference between the steam temperature at the injector and the average temperature of the steam chamber. Also, the temperature at the steam interface is less than the steam temperature at the injector, but it is higher than the reservoir temperature. A linear average between the steam temperature and the reservoir temperature can be assumed for the steam temperature at interface. As an example, if the steam injection temperature is 190 C and reservoir temperature is 10 C, temperature at

the steam interface would be around 100 C. Keyword **TINTFC** specifies the difference between the steam temperature at the injector and temperature at the steam interface.

Keyword **PRESS** specifies number of changes in the steam injection pressure and duration of change (days). If the steam pressure changes only one time for 6 months, values after PRESS would be 1 and 180. Each change in the steam injection pressure should be specified in a separate line with two parameters. The first one is duration of pressure change and the second one is the steam injection pressure (kpa). If PRMODE=1, only initial pressure should be specified with the PRESS keyword.

If PRMODE=1, the trigger keywords should be specified. The pressure trigger drops the pressure after a specific time and can be repeated multiple times. ISOR trigger drops the steam pressure each time that ISOR is greater than a specific limit. **TRIGS** specifies the starting time for applying the trigger, **TRIGTIME** specifies the frequency of dropping pressure if trigger is the pressure trigger, **TRIGCP** specifies the amount of pressure drop after each time trigger is applied. **TRIGISOR** specifies the ISOR (instantaneous steam oil ration) limit for dropping the pressure if trigger is ISOR trigger. If user is using pressure trigger, this value should be set zero. **TRIGMINP** specifies the minimum pressure for applying the trigger. If the steam injection pressure is less than this value, trigger cannot drop the steam pressure anymore and it would be stopped.

Setting a blow-down trigger can be useful for controlling the amount of steam injection at the end of the well pair productive life. Blow-down trigger starts after a certain amount of oil recovery (e.g. 55%) or cumulative oil production. At this time, steam injection should be stopped, but oil production will continue for a time. In this case, the steam injection rate is zero and the CSOR will decrease significantly. Neglecting this operating strategy may overstate the CSOR significantly. This operating strategy has been simulated in the proxy and can be used along other operating strategies such as the trigger or variable steam injection pressure. If user would like to simulate this process, keyword **BLOWDOWN** should be set one, otherwise it should be set zero. Maximum time to start the blow-down can be specified by **BLTIMEMAX** keyword. The cumulative oil limit for starting the blow-down can be set by **BLLIMIT** keyword. If time is greater than **BLTIMEMAX**, or cumulative oil production is greater than the BLLIMIT, the blow-down would be

started. If user would like to use only one of these limits, the other one should be set to a very large number. The maximum bottom-hole pressure for the injector can be set by **BHPMAXP** keyword. If the BHP is less than the BHPMAXP, producer will be shut-in and simulation will be stopped.

Steam quality of the injected steam can be specified by **STEAMQL** keyword. The maximum field steam injection rate can be specified by **MAXSTEAM**. If the field steam injection rate is above this limit, proxy starts decreasing the steam pressure to keep this value below or equal to the limit.

Before starting the SAGD operation, during the start-up, producer can inject steam into the reservoir. Duration of steam circulation before starting the SAGD operation can be specified by **STUPTIME** keyword. Producer status during the start-up can be specified by **PRODCIRC** keyword. If producer only injects steam, this value should be set zero. If the producer both injects and produces the bitumen simultaneously, this value should be set one.

A.1.8 Section 8: Calibrating Parameters Using SQP Optimization Algorithm

```
**********************************************
**
** Calibrating parameters using SQP optimization
**
**********************************************

**
** Parameters for optimization
**
AFR         1.0  0.5   2.0    ** Calibrating factor for changing steam front velocity during rising period
AFS1        1.0  0.5   2.0    ** Calibrating factor for changing steam front velocity during spreading period (before confinement)
AFS2        1.0  0.5   2.0    ** Calibrating factor for changing steam front velocity during spreading period (after confinement)
AFCSOR1     1.0  0.3   2.0    ** Calibrating factor for modifying volumetric heat capacity of steam chamber
AFCSOR2     1.0  0.3   2.0    ** Calibrating factor for modifying overburden thermal diffusivity

**
** Objective function setting
**
RATEMODE   2      ** optimize rates (RATEMODE=1) or cumulates (RATEMODE=2) or only CSOR (RATEMODE=3)
NUMSTEPS   1      ** number of steps in optimization (1=optimize oil and steam parameters simultaneously
                  ** 2=first optimize oil parameters and then optimize steam parameters)
**
** Optimization settings for SQP method
**
PERTURBS   0.001  0.001  0.001   0.001   0.001      ** perturbations for gradient computation (AFR,AFS1,AFS2,AFCSOR1,AFCSOR2)
OPTINDEX   1 1 1 1 1    ** Select calibration parameters (AFR,AFS1,AFS2,AFCSOR1,AFCSOR2) -- 0:No, 1:Yes
```

Section 8 specifies the calibration parameters. Five parameters have been selected for calibration. These parameters are the steam interface velocity at the rising (**AFR**), steam interface velocity at the spreading (**AFS1**), steam interface velocity at the confinement (**AFS2**), overburden thermal diffusivity (**ASCSOR1**) and reservoir volumetric heat capacity (**ASCSOR2**), respectively. Three values should be specified for each of them. The first value is initial value for that parameter and the next two values specify the lower and upper bounds for that parameter. For prediction, ranking or well trajectory optimization, only the first values are important, but for calibration specifying the lower and upper bounds of each 6pa-

rameter is important and the SQP optimization algorithm searches between these bounds.

The objective function is minimizing the mismatch between the proxy and simulator oil production results plus the steam injection results. Keyword **RATEMODE** specifies the type of objective function parameters. User can select to minimize the mismatch between the rates (RATEMODE=1), cumulative (RATEMODE=2) or CSOR (RATEMODE=3). Keyword **NUMSTEPS** specifies the number of steps in the optimization. If user would like to first minimizes the mismatch between oil results and then, in the second step minimizes the mismatch between steam results, NUMSTEPS should be set to two, otherwise it should be set to one for simultaneous calibration of all parameters.

PERTURBES keyword specifies the perturbation for each parameter during gradient calculations. The SQP computes gradients based on the forward finite difference method.

$$g_{x_i} = \frac{f(x_i + \Delta x_i) - f(x_i)}{\Delta x_i}$$

In this case, gradient of parameter x_i can be computed by adding a small perturbation to parameter x_i for computing the objective function. This perturbation should not be very small to prevent changing the objective function, and it should not be large to compute the gradient without enough accuracy. User can specifies the perturbation of each parameter in the parameter file. Keyword **OPTINDEX** specifies the effective parameters in the optimization. One means that parameter should be optimized and zero means it should not be optimized. Values in front of OPTINDEX keyword are for five parameters AFS, AFR1, AFR2, AFCSOR1 and AFCSOR2, respectively.

A.1.9 Section 9: Ranking Reservoir Realizations

```
*******************************************
**
** Ranking of reservoir realizations
**
*******************************************

OILP      500          ** Oil price per m3
WATERP    30           ** Steam cost per m3
DISCOUNT  0.1          ** Discount rate per year
```

Section 9 specifies keywords for ranking reservoir realizations. The oil price per m^3, steam cost per m^3 and discount rate per year should be specified by **OILP**, **WATERP** and **DISCOUNT** keywords, respectively.

A.1.10 Section 10: Well Trajectory Optimization

```
*******************************************
**
** Well trajectory optimization
**
*******************************************

BOXRG          2   24   15  20    ** Horizontal box range for finding optimal trajectory path in each slice  (xmin,xmax,ymin,ymax)
LIMVERELEV     10  45             ** Minimum depth for dirilling wells (if PINCHOUT=1) (zmin,zmax)
INJHORLOC      1   1              ** Minimum and maximum number of grids in each side of producer in horizontal direction for drilling injector
INJVERLOC      4   6              ** Minimum and maximum number of grids above the producer for drilling injector
MAXVERDIST     4   7              ** Maximum distance between minimum and maximum elevations of injector or producer
PINCHOUT       1                  ** Is pinchout existed at the bottom of the reservoir (0:No  1:Yes)
PINCHARRAY     26                 ** Pinchout elevation for each slice along the well (if PINCHOUT=1)
23
22
22
22
22
22
22
22
22
22
22
22
22
21
21
20
19
18
18
18
17
17
17
16
16
16
```

Section 10 specifies parameters for optimizing wells trajectories. For optimizing wells trajectories, a box in the horizontal plane should be specified and horizontal location of wells should be optimized inside this box. Keyword **BOXRG** specifies the x_{min}, x_{max}, y_{min} and y_{max} for this box. If well direction is in the I direction, x_{min} and x_{max} would be the initial section and last section for drilling the well, otherwise y_{min} and y_{max} specify these sections. Keyword **LIMVERELEV** specifies the minimum and maximum depths for drilling the producer. Producer should be drilled at the bottom of the reservoir, but three different factors may affect the minimum elevation for drilling the well: 1- The bottom continuous bitumen (BCB) 2- The pinchout at the bottom of the reservoir 3- The minimum elevation that has been defined by the keyword LIMVERELEV. The BCB can be automatically identified in the proxy by computing the bulk oil weight of grid cells. If pinchout exists at the bottom of the reservoir, **PINCHOUT** keyword should be set 1 and Pinchout arrays should be specified in the parameter file with the keyword **PINCHARRAY**. The minimum depth for each slice along the well would be a maximum value among all of these three factors.

Optimal location of the injector can be left or right of the horizontal position of the producer and its elevation can be between t_1 to t_2 grid cells above the producer. These ranges can be specified by keywords **INJHORLOC** and **INJVERLOC**, respectively. INJHORLOC specifies the minimum and maximum number of grid cells in each side of producer in the horizontal direction. INJVERLOC specifies the minimum and maximum number of grid cells above the producer for drilling the

injector.

During the optimization, distance between the minimum and maximum elevations of the producer or injector should not be very high. If they are high, drilling well would be very difficult and also growth of the steam chambers at different slices would be uneven which causes increasing the heat losses and steam cross-over. For preventing this problem, the maximum distance between the minimum and maximum elevations of the injector or producer can be controlled by **MAXVERDIST** keyword. The first value specifies the maximum distance for the injector and the second value specifies the maximum distance for the producer.

A.2 Examples

For the case study, 100 synthetic reservoir realizations based on a realistic model have been generated. The grid dimensions are $26 \times 32 \times 83$ and the grid sizes in x, y and z directions are 25 m, 2.5 m and 1 m, respectively. A pinchout exists at the bottom of the reservoir. Top water and top gas exist in a thief zone at top of this model. There are two facies and 7 different thermal rock types in the model. Facies one is net and facies two is non-net. Wells are along the x direction. Correlations have been used for calculating the oil relative permeability and PVT properties. Permeability cutoff is 20 md and CHV has been used for averaging different properties. The new rising model has been used for forecasting the SAGD performance during the rising period. Operating strategy is combination of the pressure trigger strategy and blow-down trigger. The initial steam pressure is 4000 kpa and at the end of the start-up period after 120 days, pressure drops to 3500 kpa. After 450 days trigger start working and drops pressure 100 kpa for a year. Blow-down trigger starts working after 4000 days. Simulation stops after 5550 days and the time step size during the simulation is 5 days.

After running the proxy, it generates some result files. The name of these files depends on the prefix name that should be defined by the keyword PRTMODE in the first section. These files are:

1. Prefix_debug.out: This file contains basic information and if PRTMODE for debug file is one, it prints the calculation details for all time steps.

2. Prefix_heat.out: If PRTMODE for heat losses is one, proxy prints the calculation for the heat losses at each time step (if second value of PRTMODE is

equal to one).

3. Prefix_summary.out: This file contains information about the overburden thermal diffusivity, producible oil, the final cumulative oil production, the average of reservoir properties and etc. for each half slice.

4. Prefix_connectivity.out: This file contains gridded CHV results about steps, angles and distances for each slice in the 3D model.

5. Prefix_location.csv: It prints location of the steam chamber at different time steps for each half slice in an excel file.

6. Prefix_results.csv: This file contains the time, oil and steam rates, oil and steam cumulative, steam temperature and steam pressure at different time steps with frequency of TIMEFREQ in an excel file. Also if STARSCOMP is equal to one, it prints simulator results too.

7. Prefix_rank.out: This file contains the ranking results (only if PROXYMODE is equal to two).

8. Prefix_obj.csv: This file contains objective function values, calibrated parameters values, and number of the proxy calls during the calibration using the SQP optimization algorithm (only if PROXYMODE is equal to three).

9. Prefix_Welltraj_UTM.out: This file contains the optimal trajectory for both of the producer and injector using the undulate trajectory method (UTM) with two different formats which are the GSLIB and STARS format (only if PROXYMODE is equal to four).

10. Prefix_Welltraj_DSM.out: This file contains optimal trajectory for both of the producer and injector using the double spline method (DSM) with two different formats which are the GSLIB and STARS format (only if PROXYMODE is equal to four).

11. Prefix_valobjs.out: This file contains the objective values for all cases during the well trajectory optimization (only if PROXYMODE is equal to four).

Different examples have been tested by the proxy. For all examples, most of the keywords in the first 7 sections of parameter file are the same and they are similar to the sections have been shown in the manual. Only small changes such as

number of realizations should be changed. For prediction, there is no need to change the remaining sections, but section 8 for calibration, section 9 for the ranking, and section 10 for the well trajectory optimization should be completed. Four different examples have been tested by the proxy. These examples are: 1- prediction 2- calibration 3- ranking reservoir realizations 4- well trajectory optimization.

A.2.1 Example 1: Prediction

The first example is about predicting the SAGD performance of the first realization out of those 100 realizations. In this example, number of realizations should be set to one and initial calibration parameters in the calibration section should be set one. This example has 23 slices along the well and because time step size is 5 days, proxy run would be very short and the total run time is 10 seconds. In this case, prefix name is "test", as a result calculation details and heat losses can be seen in the test_debug.out and test_heat.out files, respectively. The main result file is the test_results.csv and all of important results can be seen in this file. Fig. A.1 shows prediction results for this case. Fig. A.1(a) shows the proxy oil and steam rates, Fig. A.1(b) shows the cumulative oil production and steam injection, Fig. A.1(c) shows the proxy CSOR and finally, Fig. A.1(d) shows changing the steam injection pressure. Fig. A.1(d) shows that the initial steam pressure is 4000 *kpa* and after 120 days it drops to 3500 *kpa*. After 450 days, the trigger starts working and drops pressure 100 *kpa* for a year. Finally, blow-down trigger starts working after 4000 days. During the blow-down, rate of the steam injection is zero and rate of the oil production is very low. The steam pressure decreases gradually up to the end of simulation.

A.2.2 Example 2: Ranking Reservoir Realizations

In this example the oil price, steam cost and discount rate should be set in the ranking section. Number of realizations is 100 and NSETS should be set to 100. Fig. A.2 shows upper part of the result file. Based on these results, realizations can be ranked easily. Results of all of realizations would be saved in the test_rank.out file. Total run time by selecting time step size equal to 20 days would be about 4:30 minutes which is quick.

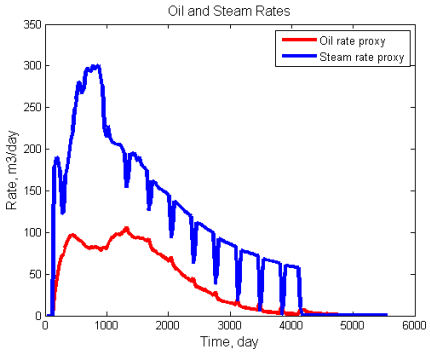

(a) Oil and steam rates

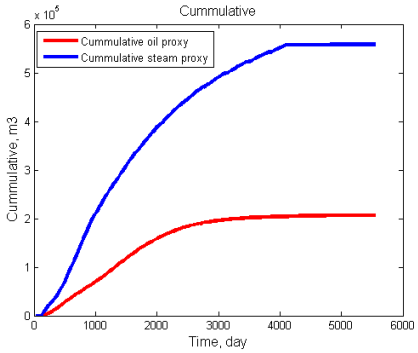

(b) Oil and steam cumulates

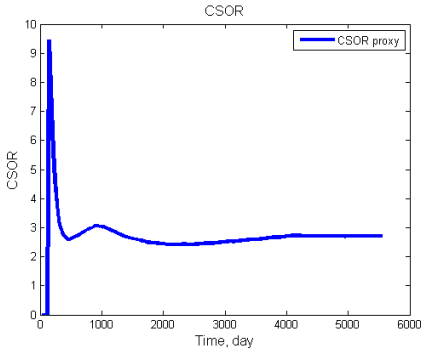

(c) Cumulative steam oil ratio

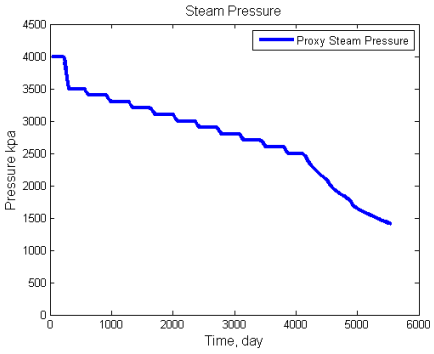

(d) Steam pressure

Figure A.1: Prediction results of proxy for model

Realization #	OOIP all	OOIP up	RF	Qo m3	Qw m3	CSOR	NPV	Rank Qo	Rank Qw	Rank CSOR	Rank NPV
1	685884.781	279234.891	0.733	204602.370	574757.887	2.809	73943669.050	42	48	57	44
2	672494.383	271245.090	0.721	195657.704	540249.935	2.761	69657132.943	35	28	39	32
3	674385.754	315005.284	0.731	230367.565	627992.384	2.726	82419643.190	85	83	23	84
4	690967.571	281143.771	0.740	208094.362	580720.274	2.829	74573607.323	52	59	63	49
5	700628.800	326068.718	0.731	238223.748	639067.136	2.683	86261156.433	94	90	12	92
6	665376.633	290627.709	0.732	212638.579	606000.625	2.850	75937570.397	62	74	70	60
7	661599.536	314519.075	0.742	233273.630	652287.174	2.796	83840003.508	90	95	51	87
8	684206.961	289904.027	0.735	213086.743	592986.838	2.783	76838487.224	63	62	45	65
9	659254.262	250083.385	0.729	182191.385	544816.531	2.990	64517940.997	19	30	92	17
10	675065.315	287505.050	0.732	210310.734	620708.341	2.951	75861829.004	58	80	87	59

Figure A.2: Ranking results

A.2.3 Example 3: Calibration

Most of the times, uncalibrated results are acceptable, but for finding a better match between the simulator and proxy results, calibration helps to calibrate some of the proxy parameters. Manually changing the calibration parameters is very tedious and time consuming. The SQP optimization algorithm has been used as calibration engine. In this case, all of calibration parameters have been calibrated at the same time. Fig. A.3 shows the proxy results before and after the calibration. As Fig. A.3

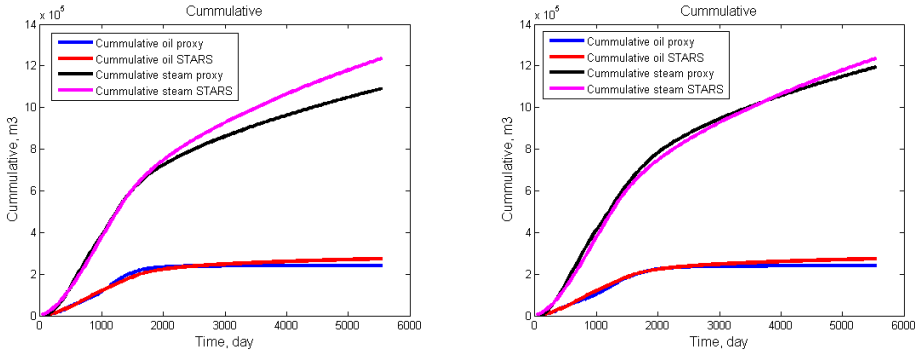

(a) Uncalibrated (b) Calibrated

Figure A.3: Cumulative oil and steam before and after calibration

shows, the cumulative steam injection of the proxy before calibration is less than the simulator, but after calibration, the cumulative steam injection of the proxy and simulator are very close. Table. A.1 shows values of calibration parameters before and after calibration.

Table A.1: Calibrating proxy parameters using SQP method as optimization algorithm

	V_r **mult.**	V_s **mult.**	V_c **mult.**	α_{ob} **mult.**	VHC **mult.**
Initial	1.0	1.0	1.0	1.0	1.0
Final	1.05	0.92	0.94	1.2	0.82

As Table. A.1 shows, before calibration all of calibration parameters are equal to one. After calibration, SQP increased the steam front velocity during the rising and decreased the steam front velocity during the spreading and confinement periods. On the other hand, for improving the cumulative steam injection results, it increased the overburden thermal diffusivity and decreased the volumetric heat capacity to obtain a better match between the proxy and simulator results.

In this case, total run time by selecting the time step size of 15 days is 3 minutes which is quick. Total number of objective calls is 59 times.

A.2.4 Example 4: Well Trajectory Optimization

In this example, all 100 realizations are used for well trajectory optimization. For this reason, PROXYMODE should be set equal to 4, number of realizations NSETS should be equal to 100 and NODESI and NODESP keywords are not important and these sections can be skipped. Finally, the last section of the parameter file which is for the well trajectory optimization should be completed. In this case, there is a pinchout at bottom of the reservoir and PINCHARRAY should be imported to the parameter file. All parameters for this section are explained in the manual.

Program internally computes the optimal wells trajectories using two methods. The first method is called the undulate trajectory method (UTM) and the second method is called the double spline method (DSM). In the UTM method, multiple undulations can be observed for the well trajectories and undulations slopes can be controlled by the MAXVERDIST keyword.

Fig. A.4 shows a side view of the optimal producer and injector trajectories for both methods. As Figs. A.4(a)–A.4(b) show, the vertical distance between the

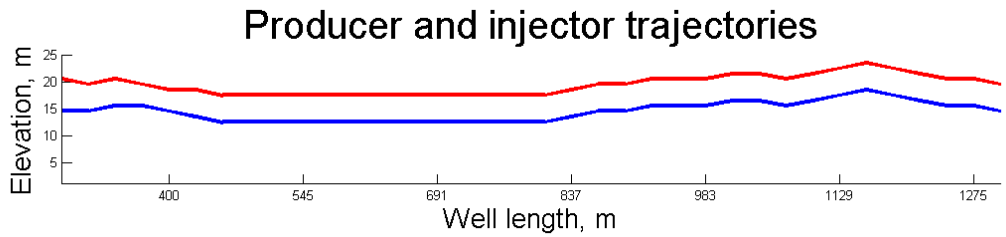

(a) Side view for undulate trajectory method (blue: producer, red: injector)

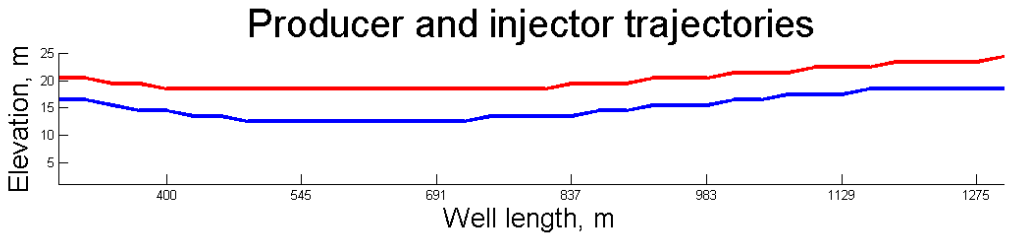

(b) Side view for double spline method (blue: producer, red: injector)

Figure A.4: Producer and injector trajectories for both of methods

producer and injector is between 4-6 m. In this case, the objective function should be computed many times. By selecting time step size equal to 20 days, the total run time for finding the optimized trajectories using both methods would be about 6:30 hours.

Bibliography

Ahmed, T., 2006. Reservoir engineering handbook.

Akin, S., 2005. Mathematical modeling of steam assisted gravity drainage. SPE Reservoir Evaluation & Engineering 8 (5), 372–376.

Alberta Energy Regulator, 2013 and before. Resource management reports. Tech. rep., accessed November 2013.
URL `http://www.aer.ca`

Antoniou, A., Lu, W., 2007. Practical Optimization: Algorithms and Engineering Applications. Springer-Verlag New York Inc.

Azad, A., Chalaturnyk, R., 2010. A mathematical improvement to sagd using geomechanical modelling. Journal of Canadian Petroleum Technology 49 (10), 53–64.

Azad, A., Chalaturnyk, R., 2013. Application of analytical proxy models in reservoir estimation for sagd process: Utf-project case study. Journal of Canadian Petroleum Technology 52 (3), 219–232.

Butler, R., 1987a. A new approach to the modelling of steam-assisted gravity drainage. Journal of Canadian Petroleum Technology 24 (3).

Butler, R., 1987b. Rise of interfering steam chambers. Journal of Canadian Petroleum Technology 26 (3).

Butler, R., 1991. Thermal recovery of oil and bitumen.

Butler, R., Dargie, B., 1994. Horizontal wells for the recovery of oil, gas, and bitumen (No.2). No. 2. Gulf Pub Co.

Cardwell, W., Parsons, R., 1949. Gravity drainage theory. trans. AIME 179 (199), 1–215.

Computer Modeling Group Ltd., 2012. Stars user manual. Tech. rep., accessed January 2012.
URL `http://www.cmgl.ca/software/soft-stars`

Daniel, C., 1959. Use of half-normal plots in interpreting factorial two-level experiments. Technometrics 1 (4), 311–341.

Dehdari, V., 2011. Class notes of min e 615 course. Tech. rep., University of Alberta.

Dehdari, V., Oliver, D., 2012. Sequential quadratic programming for solving constrained production optimization–case study from brugge field. SPE Journal 17 (3), 874–884.

Dehdari, V., Oliver, D., Deutsch, C., 2012. Comparison of optimization algorithms for reservoir management with constraints – a case study. Journal of petroleum science & engineering 100, 41–49.

Deutsch, C., Dose, T., 2005. Programs for debiasing and cloud transformation: bimodel and cltrans. CCG Anual Report 7 404, University of Alberta.

Deutsch, C., Journel, A., 1992. Geostatistical software library and user&s guide. Vol. 1996. Oxford university press New York.

Doan, L., Baird, H., Doan, Q., Farouq Ali, S., 2003. Performance of the sagd process in the presence of a water sand-a preliminary investigation. Journal of Canadian Petroleum Technology 42 (1).

Edmunds, N., Peterson, J., 2007. A unified model for prediction of csor in steam-based bitumen recovery. In: Canadian International Petroleum Conference.

Energy Resources Conservation Board, 2012. Resource management reports. Tech. rep., accessed March 2012.
URL `http://www.ercb.ca/data-and-publications/activity-and-data`

Farouq-Ali, S., 1997. Is there life after sagd? Journal of Canadian Petroleum Technology 36 (6).

Fenik, D., Nouri, A., Deutsch, C., 2009. Criteria for ranking realizations in the investigation of sagd reservoir performance. In: Canadian International Petroleum Conference.

Government of Alberta, 2011. Talk about oil sands, oil sands publications. Tech. rep., accessed April 2011.
URL `http://www.oilsands.alberta.ca`

Gupta, S., Gittins, S., 2012. An investigation into optimal solvent use and the nature of vapor/liquid interface in solvent-aided sagd process with a semianalytical approach. SPE Journal 17 (4), 1255–1264.

Hampton, T., Kumar, D., Azom, P., Srinivasan, S., 2013. Analysis of impact of thermal and permeability heterogeneity on sagd performance using a semi-analytical approach. In: 2013 SPE Heavy Oil Conference-Canada.

Hearn, D., Baker, M., 2004. Computer Graphics with OpenGL. Pearson prentice hall.

Ito, Y., Suzuki, S., Yamada, H., 1998. Effect of reservoir parameter on oil rates and steam oil ratios in sagd projects. In: 7th UNITAR International Conference on Heavy Crude and Tar Sands, Beijing, China. pp. 27–31.

Manchuk, J., Deutsch, C., 2012. Well trajectory optimization for sagd. CCG Anual Report 14 208, University of Alberta.

McLennan, J., Deutsch, C., 2005. Ranking geostatistical realizations by measures of connectivity. In: SPE International Thermal Operations and Heavy Oil Symposium, 98168, Alberta, Canada.

McLennan, J., Ren, W., Leuangthong, O., Deutsch, C., 2006. Optimization of sagd well elevation. Natural Resources Research 15 (2), 119–127.

Miura, K., Wang, J., 2012. An analytical model to predict cumulative steam/oil ratio (csor) in thermal-recovery sagd process. Journal of Canadian Petroleum Technology 51 (4), 268–275.

Montgomery, D., 2006. Design and analysis of experiments.

Nocedal, J., Wright, S., 2006. Numerical Optimization. Springer.

Nukhaev, M., Pimenov, V., Shandrygin, A., Tertychnyi, V., 2006. A new analytical model for the sagd production phase. In: SPE Annual Technical Conference and Exhibition.

Oliver, D., Reynolds, A., Liu, N., 2008. Inverse Theory for Petroleum Reservoir Characterization and History Matching, 1st Edition. Cambridge University Press, Cambridge.

Paradigm Ltd., 2012. Gocad user manual. Tech. rep., accessed January 2012. URL http://www.pdgm.com/products/GOCAD

Reis, J., 1992. A steam-assisted gravity drainage model for tar sands: linear geometry. Journal of Canadian Petroleum Technology 31 (10).

Sharma, J., Gates, I., 2011. Convection at the edge of a steam-assisted-gravity-drainage steam chamber. SPE Journal 16 (3), 503–512.

Storn, R., Price, K., 1997. Differential evolution–a simple and efficient heuristic for global optimization over continuous spaces. Journal of global optimization 11 (4), 341–359.

University of Alberta CCG Annual Meeting, 2013. personal communication.

Upstream Dialogue, 2012. The facts on: oil sands, canadian association of petroleum producers. Tech. rep., accessed June 2012. URL http://www.capp.ca/upstreamdialogue

Vanegas, J., Deutsch, C., Cunha, L., 2008. Uncertainty assessment of sagd performance using a proxy model based on butler's theory. In: SPE Annual Technical Conference and Exhibition.

Vanegas, J., Deutsch, C., Cunha, L., 2009. Transference of reservoir uncertainty in multi sagd well pairs. In: SPE Annual Technical Conference and Exhibition.

Wilde, B., Deutsch, C., 2012. Calculating an improved connected hydrocarbon volume with line-of-sight for ranking realizations by sagd performance. CCG Anual Report 14 205, University of Alberta.

Wu, C., Hamada, M., 2000. Experiments: planning, analysis, and parameter design optimization.

Yang, C., Card, C., Nghiem, L., Fedutenko, E., 2011. Robust optimization of sagd operations under geological uncertainties. In: SPE Reservoir Simulation Symposium.

Zanon, S., Zabel, F., Deutsch, C., 2005. Improvement of realizations through ranking for oil reservoir performance prediction. CCG Anual Report 7 112, University of Alberta.